1-1-2010

Development Of Lower Extremity Injury Criteria And Biomechanical Surrogate To Evaluate Military Vehicle Occupant Injury During An Explosive Blast Event

Brian J. Mckay
Wayne State University

DEVELOPMENT OF LOWER EXTREMITY INJURY CRITERIA AND BIOMECHANICAL SURROGATE TO EVALUATE MILITARY VEHICLE OCCUPANT INJURY DURING AN EXPLOSIVE BLAST EVENT

by

BRIAN J. MCKAY

DISSERTATION

Submitted to the Graduate School

of Wayne State University,

Detroit, Michigan

in partial fulfillment of the requirements

for the degree of

DOCTOR OF PHILOSOPHY

2010

MAJOR: BIOMEDICAL ENGINEERING

Approved by:

_____
Advisor Date

_____

_____

_____

_____

ACKNOWLEDGEMENTS

This work was supported in part by U.S. Army Tank-Automotive and Armaments Command (TACOM) and Tank-Automotive Research, Development and Engineering Center (TARDEC). The author acknowledges his colleagues within the U.S. Army who helped spearhead and support the research.

The author gratefully acknowledges his advisor Dr. Cynthia Bir. Her endless patience and encouragement were critical to the completion of this research. More importantly, the author wishes to thank Dr. Bir for her mentoring, which will have an everlasting effect on the author's academic, professional and personal life. It has been a privilege working alongside her.

The author gratefully acknowledges the guidance and encouragement of his committee members: Dr. Paul Begeman, Dr. Paul Dougherty, and Dr. Albert King. The time and expertise they have dedicated to the author were generous and essential to completion of this research.

The author wishes to thank the Wayne State University Sports and Ballistics group for their assistance in test preparation, data collection and processing. Specifically, the author would like to thank Nathan Dau, Samantha Staley and James Kopacz for their assistance with the experimental testing. Special thanks to Dr. Paul Dougherty and Dr. Todd Frush for conducting autopsy evaluations.

The author gratefully acknowledges the NATO HFM-090 and HFM-148 task groups for their collaboration, insights and data contribution. Their support and encouragement throughout the research process was endearing and greatly appreciated. Thank you to Denton ATD/Humanetics for their support in surrogate

development. Specifically, the author would like to thank Craig Foster and Paul Depinet for their collaboration in designing and experimental testing.

Finally, the author lovingly acknowledges his family for their endless support. Thank you to my Mom and Dad for their unconditional love and encouragement. Thank you to my brothers, sister, nephews and niece for making my life so enjoyable.

TABLE OF CONTENTS

LIST OF TABLES

LIST OF FIGURES

CHAPTER 1

INTRODUCTION

1.1 Statement of Problem

The lower extremity is the foremost injured body region in modern warfare (Owens, 2007). Military vehicle occupants, or mounted soldiers, face the ubiquitous threat of anti-vehicular (AV) explosive devices. Detonations occurring under a vehicle produce localized floorboard deformation and transmit high axial loads onto the foot/ankle/tibia complex of the occupant causing injuries to the lower leg. Military tactical and combat vehicles are being up-armored to defeat axial threats and mitigate injuries to vehicle occupants. Vehicle protection systems are evaluated in full-scale landmine blast tests using anthropometric test devices (ATD) to simulate the biomechanical response of vehicle occupants. Vehicle protection levels are determined by comparing the biomechanical response measured by an ATD to established human injury tolerances.

In order to define the optimal level of protection required to neutralize a given axial blast magnitude, a fundamental understanding of lower extremity injury tolerance must be established for impact conditions representative of AV blast impacts. Lower limb injury risk models established by the automotive community for axial loading have critical shortcomings that prevent their application in blast impacts. Currently available ATD developed by the automotive industry have been shown to be insensitive at measuring high amplitude, short duration acceleration pulses characteristic of blast impacts (Barbir, 2005). Therefore, there is an urgent need to develop lower extremity injury criteria for military vehicle occupants involved in explosive blast events.

Secondly, there is a need to develop an ATD capable of simulating the biomechanical response of a human occupant under blast impact conditions.

1.2 Background and Significance

The rise of the mechanized infantry battalion in World War I propelled the landmine to the forefront of combat warfare. AV landmines are utilized to immobilize or destroy armored vehicles and their occupants. The landmine has inflicted more catastrophic damage to United States (U.S.) military vehicles than any other weaponry agent in modern armed conflicts (Bird, 2001). Their devastation and lethality have increased rapidly with time. From World War II to the Korean War, U.S. military vehicle losses attributed to landmines grew from 22 to 55 percent (Bird, 2001). In the most recent U.S. military armed conflicts, Operation Iraqi Freedom (OIF) and Operation Enduring Freedom (OEF), over 44 percent of all U.S. military hostile casualties and wounded were attributed to a weaponry explosive device (which includes landmines and improvised explosive devices and excludes artillery, mortar, or rocket fire) (Department of Defense Personnel & Procurement Statistics, 2008).

In the classical scenario, an AV explosive device is detonated under a vehicle emitting an explosive shock wave. The amount of energy absorbed by the vehicle depends on its location relative to the AV explosive device position when detonation occurs. The vehicle hull absorbs the reflected energy emitted by the shock wave and transmits local mechanical accelerations through the vehicle structure. This scenario is commonly described as an underbelly blast as the hull is typically the most vulnerable impact location due to its lack of armor.

The foot-ankle-tibia region is the primary impact point of an occupant in an underbelly blast event. Wang et al. (2001) noted that the average velocity of a medium sized armored vehicle floorplate exceeded 12 m/s and 100 g following an AV mine blast. As a result of the high rate of mechanical compressive loading, the lower extremity of the occupant is susceptible to severe injury following an underbelly blast event (North Atlantic Treaty Organization TR-HFM-090, 2007).

Since World War I, U.S. Servicemen have endured more lower extremity injuries in armed conflicts than any other combat wound (Champion, 2003). Although lower extremity injuries may not be an immediate threat to life, many are immediately incapacitating. As such, targeting the protection of the lower extremity is critical. Much research has been conducted to protect dismounted soldiers from anti-personnel (AP) mines. This research fostered the development of mine protective footwear currently used by soldiers (Bergeron, 2001). Similarly, vast efforts and funding have been dedicated to develop vehicle blast mitigation technologies to protect mounted soldiers during blast events (Feickert, 2006).

Internationally recognized procedures have been established to evaluate the protection levels of a military vehicle against a mine threat. These procedures specify the test methodology, threat conditions, and crew casualty/injury criteria of vehicle occupants (North Atlantic Treaty Organization AEP 55, 2005). Injury criteria serve as the principal metric for determining the level of protection afforded to military vehicle occupants when subjected to a specific blast threat. Although widely accepted, these procedures are not without critical shortcomings. The injury criteria and ATD adopted into military specifications were developed primarily by the automotive and aviation

industry for impact conditions generally less severe than explosive blast events. In response to the North Atlantic Treaty Organization (NATO) Research and Technology Organization Human Factors and Medicine (RTO/HFM) Panel Exploratory Team (ET) 007 identification of the lack of data surrounding AV landmine injury assessment, the NATO RTO/HFM 090 Task Group 25 was formed. This task group was initiated to establish blast-specific injury criteria for vehicle occupants when Federal Motor Vehicle Safety Standard (FMVSS) are not appropriate or inadequate (North Atlantic Treaty Organization TR-HFM-090, 2007).

With respect to lower extremity, the NATO HFM task group determined the Yoganandan et al. (1996) injury model was the most suitable injury criterion available for axial loading noting the model's large post mortem human specimen (PMHS) sample size and wide age range (North Atlantic Treaty Organization TR-HFM-090, 2007). However, the task group cautioned the application of the PMHS criteria to an ATD is problematic considering the biomechanical response of the ATD tibia (both the THOR-Lx and Hybrid III lower extremity surrogate) is significantly stiffer than a human tibia. Barbir (2005) stated the tibia compression measured by a biomechanical lower extremity surrogate exceeds the tibia compression of a PMHS by as much as 50 percent at high rate impacts (Barbir, 2005). The inability of an ATD to produce a biofidelic response at high rate impacts, typical of blast impacts, severely limits the effectiveness of utilizing currently available biomechanical surrogates in military vehicle evaluations. Similarly, the impact severity utilized by Yoganandan et al. (1996) to establish a PMHS injury criterion fall well short of blast loading rates described by Wang et al. (2001) for AV blast impacts.

Lower extremity injury criteria developed using typical AV blast loading severities and a biofidelic biomechanical surrogate capable of reproducing human response are needed to accurately and repeatability assess the probability of lower extremity injury to vehicle occupants under various blast threats. Ultimately, the accuracy of the established criteria and sensitivity of a biomechanical lower extremity surrogate are critical to quantifying the protection provided by military vehicle occupant safety systems.

1.3 Specific Aims

The research presented in this study aims to provide the international blast community with the critical information and data needed to develop improved occupant protection and blast mitigation systems capable of protecting mounted soldiers from axial AV landmine and explosive device threats. The following aims are offered:

- A description of the lower extremity anatomy focusing on foot/ankle/tibia complex.
- An investigation of lower extremity injury patterns in modern warfare.
- A review of currently available lower extremity injury criteria.
- The establishment of lower extremity injury criteria for axial blast impacts using PMHS impact data.
- The design, development, and validation of a biofidelic biomechanical lower extremity surrogate for axial blast impacts.
- The evaluation of the protective capability of military footwear to reduce occupant injury in axial blast impacts.

- The evaluation of kinetic energy attenuating materials to reduce occupant injury in axial blast impacts.

CHAPTER 2

UNDERBELLY BLAST MECHANISM AND LOWER EXTREMITY INJURY

2.1 Introduction

Tanks and armored fighting vehicles were utilized in World War I to break the stalemate imposed by trench warfare. Vehicle armor provided protection against small arm fire and tracks provided improved mobility to maneuver through coarse terrain and barbed trenches. In order to neutralize armored tanks and vehicles, the opposition developed and deployed anti-tank (AT) and AV mines. The explosive energy emitted by an AT or AV mine dwarfed the less powerful AP mine, which is utilized to deter dismounted infantry soldiers. An AT/AV mine is strategically buried beneath roads and trails and detonates upon sensing the weight or seismic activity of a vehicle (Schneck, 1998). An AT/AV explosive blast produces high amplitude mechanical loads capable of damaging vehicle tracks, penetrating vehicle armor and compromising the vehicle's structural integrity resulting in immobilization or complete catastrophic damage.

As armor protection improved in tanks, the explosive content of mines escalated and became more devastating. Since its inception, AT and AV mines have become considerably more lethal. From World War I to World War II a typical AT/AV mine increased from one to five kilograms of trinitrotoluene (TNT) (Schneck, 1998). Contemporary AT/AV mines contain a net explosive weight ranging from one to 12 kilograms of TNT (North Atlantic Treaty Organization TR-HFM-090, 2007). AT/AV mines may be specially designed with shaped charges to maximize the emission of axial energy (perpendicular to the vehicle underbelly; along the positive Z-axis) and minimize radial energy (X and Y-axis) losses to more effectively immobilize armored

vehicles. This ability to focus blast energy in a specific direction is referred to as the Munroe effect (Schneck, 1998).

An improvised explosive device (IED), the signature weapon of enemy combatants during OIF and OEF, may utilize conventional military ordnances, such as an artillery round or bomb, in a non-conventional service. An IED may be utilized as an AP or AV explosive device. When used as an AV explosive device an IED is very similar to a conventional AV landmine. An IED may be automatically or remotely detonated as opposed to landmines, which detonate automatically due to pressure or seismic activity. Due to their unconventional nature, the net explosive weight of IED widely varies. Reports have described 226 kg (500-pound) bombs converted into AV IED in OIF (U.S. Army 25th Infantry Division, 2004). Unlike conventional landmines, most IED radiate energy uniformly in all directions. Therefore, although an IED may contain a larger net explosive weight it may not necessarily exceed the axial energy emission of a smaller AV landmine. Considering their many similarities, landmines and IED may be (mistakenly) used interchangeably in medical reports, literature and in conversation.

The devastation and lethality of an AV mine or IED increases exponentially when shrapnel is incorporated into the design. Similar to the AP Claymore mine, an explosively formed projectile (EFP) AV mine fires molten hot projectiles capable of piercing the most robust vehicle armor systems available. Unlike the Munroe effect, an EFP produces a fan-shaped blast wave to maximize the distribution of fragments to threaten a larger area—known as the Misznay-Schardin effect (Schneck, 1998).

2.2 Effects of an Explosive Device Detonation

An explosive device detonation may be described as a series of effects that transfer potential energy into kinetic energy to both the vehicle and occupants. In the classical scenario, an AV explosive device is detonated under a vehicle emitting an explosive shock wave. This scenario is often described as an underbelly blast because it is considered the most vulnerable impact location. An explosive device detonation produces four effects: local, global, drop down and subsequent effects (North Atlantic Treaty Organization TR-HFM-090, 2007).

2.2.1 Local Effects

A blast shock wave is formed and rapidly emitted following the detonation of an explosive device. The shock wave accelerates rapidly until it reaches the vehicle hull less than 0.5 milliseconds later. Upon contacting the hull, the shock wave is either deflected or reflected. The vehicle hull absorbs the reflected energy emitted by the shock wave and transmits local mechanical accelerations through the vehicle structure. The portion of the vehicle closest to the detonation is characterized as the primary impact point. The primary impact point will reflect the largest local peak pressures and mechanical loads. The surface surrounding the primary impact point will experience attenuated pressures and loads.

The vehicle floorplate (also known as the floorboard or toe pan) is the interface location connecting the vehicle hull to the interior compartment. Vehicle occupants rest their feet and manipulate pedals at this location. Figure 1 portrays the relative position of these interfaces. The floorplate is one of the primary structures loaded in an axial AV blast impact. Within five milliseconds following detonation, the vehicle hull and

floorplate deform elastically and plastically depending on the mechanical energy transmitted and attenuated, and material properties used in the vehicle. Wang et al. (2001) noted that the average velocity of a medium sized armored vehicle floorplate exceeded 12 m/s following an AV mine blast. Very high amplitude and short duration axial compressive forces are transmitted through the floorboard to the occupant feet and through the seat to the occupant pelvis. Figure 2 showcases the violent transmission of energy from the floorboard onto an occupant. The occupant lower extremity reaches peak compressive loading within ten milliseconds at which point the lumbar spine and upper neck are loaded. Local effect loading typically terminates within 50 milliseconds of the initial detonation (North Atlantic Treaty Organization TR-HFM-090, 2007).

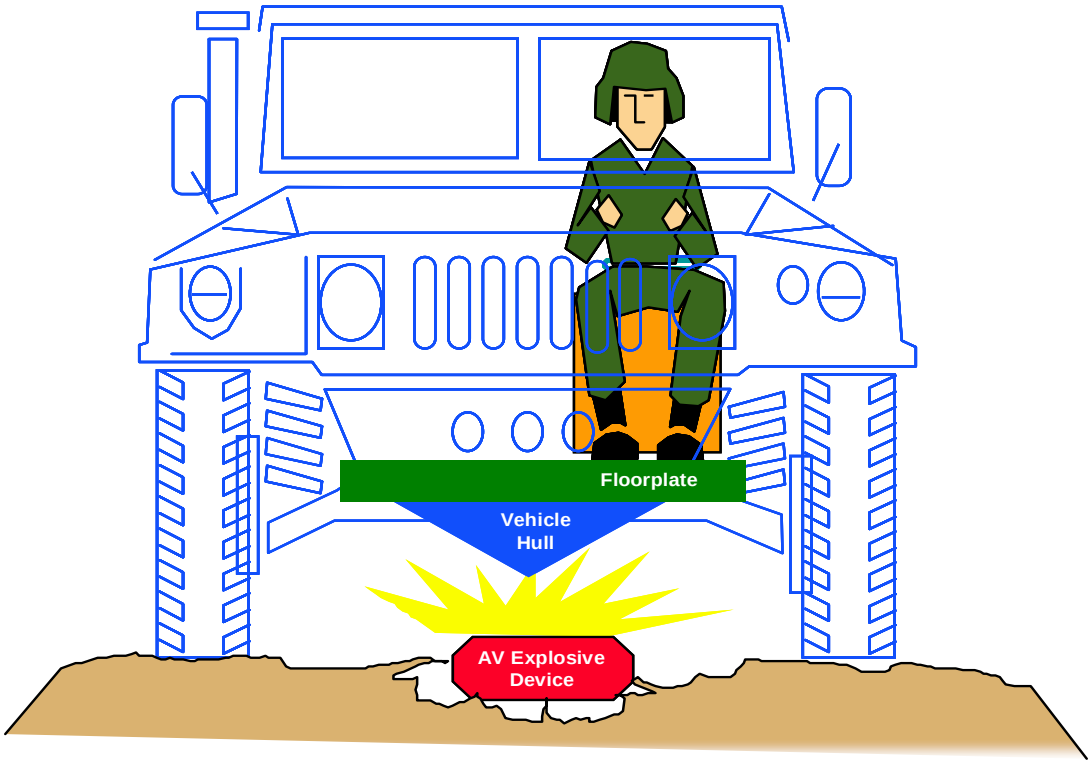

Figure 1: Relative Position of Vehicle and Passenger Interfaces.

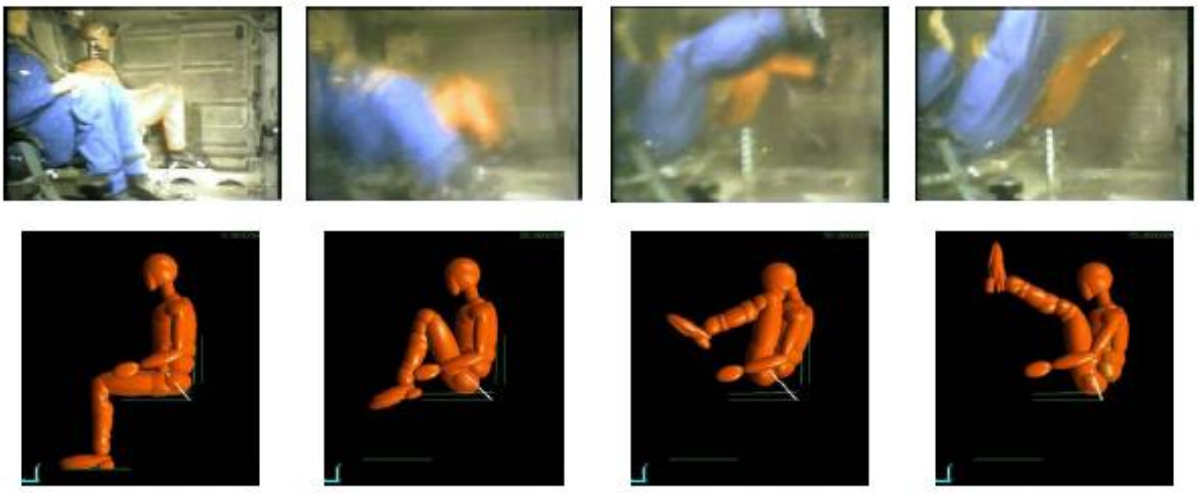

Figure 2: Experimental and Simulation of Axial Blast Loading (reprinted from North Atlantic Treaty Organization TR-HFM-090, 2007).

2.2.2 Global Effects

As the vehicle hull absorbs the reflected energy emitted by the shock wave, the vehicle weight may be offset causing the complete or partial vehicle to leap from the ground. The vehicle begins moving vertically after ten to 20 milliseconds following detonation and reaches peak height between 100 and 300 milliseconds. The vertical height achieved is proportional to the explosive blast magnitude and the weight of the vehicle. An unrestrained vehicle occupant is more susceptible to accelerative loading than a restrained occupant (North Atlantic Treaty Organization TR-HFM-090, 2007). A summary of local and global effect loading is presented in Figure 3.

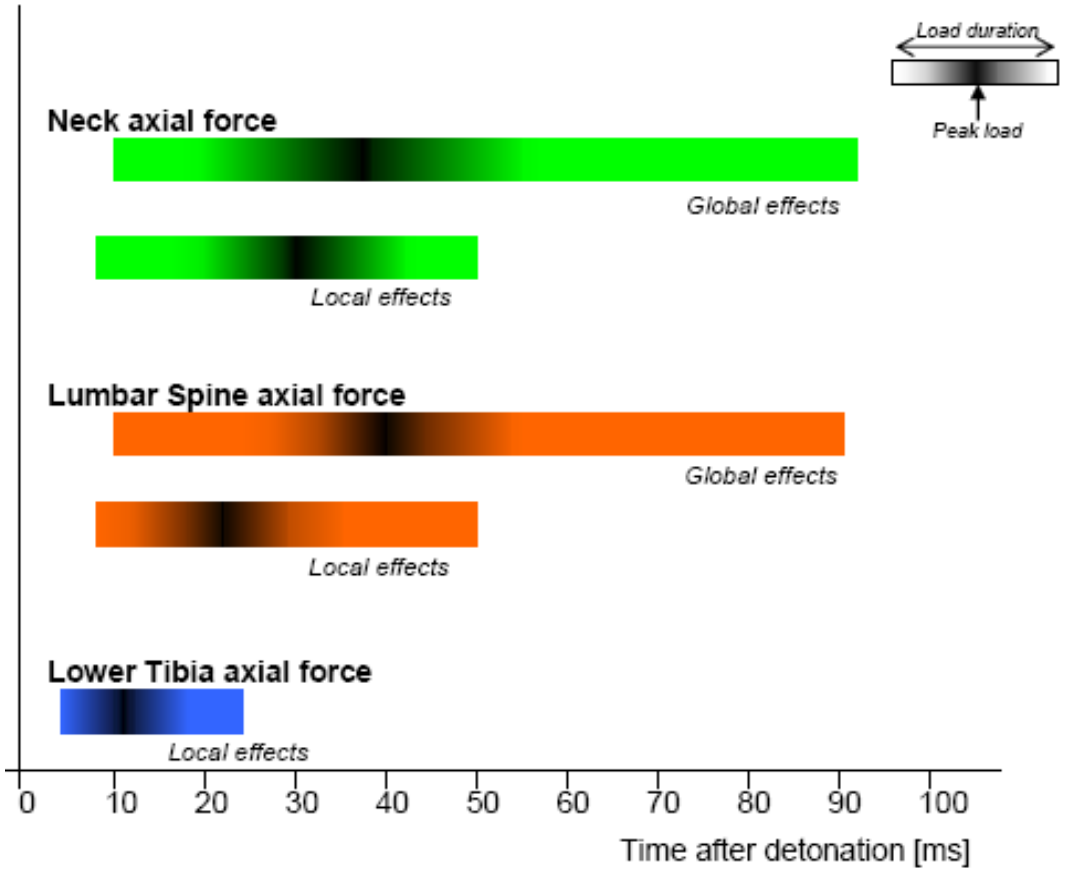

Figure 3: Loading Effects Following a Blast Detonation (reprinted from North Atlantic Treaty Organization TR-HFM-090, 2007).

2.2.3 Drop Down Effects

After the vehicle reaches peak height, the vehicle will fall due to gravity. The accelerative loads produced by gravity are also transmitted to the occupant; however, these loads are typically insignificant compared to the initial local mechanical effect. One second after detonation the impacted vehicle and occupants return to steady state (North Atlantic Treaty Organization TR-HFM-090, 2007).

2.2.4 Subsequent Effects

An impacted vehicle is susceptible to other events that may injure vehicle occupants—particularly if structural integrity is not maintained. These effects include vehicle rollover, toxic fumes, fire, heat effects, blast overpressure, and fragment projectiles.

2.2.5 Occupant Loading and Injury

Vehicle occupants are initially exposed to acceleration and mechanical loading during the local effect stage. Depending on the occupant's proximity to the primary impact point and the geometry of the vehicle structure, the occupant may see peak or attenuated forces. Loading direction is also dependant on the occupant's location relative to the primary impact point. The occupant may experience pure axial loading if the primary impact point is directly beneath the occupant, as in the classical AV underbelly blast scenario, or a combination of axial and lateral loading if the detonation is offset. Therefore, an occupant may encounter a range of loading magnitudes depending on their relative position within the crew cabin and its proximity to the blast.

Similarly, the various body regions of an occupant encounter a range of compressive peak forces based on its proximity to the blast. The foot-ankle-tibia region is the primary impact point of an occupant in an underbelly blast event. In addition to being the first region to receive high rate mechanical compressive loading, the lower extremity will experience the most severe peak axial force of any other body region. Figure 4 highlights the relative magnitude of compressive loading experienced by the lower extremity compared to the lumbar spine and upper neck for an underbelly blast event.

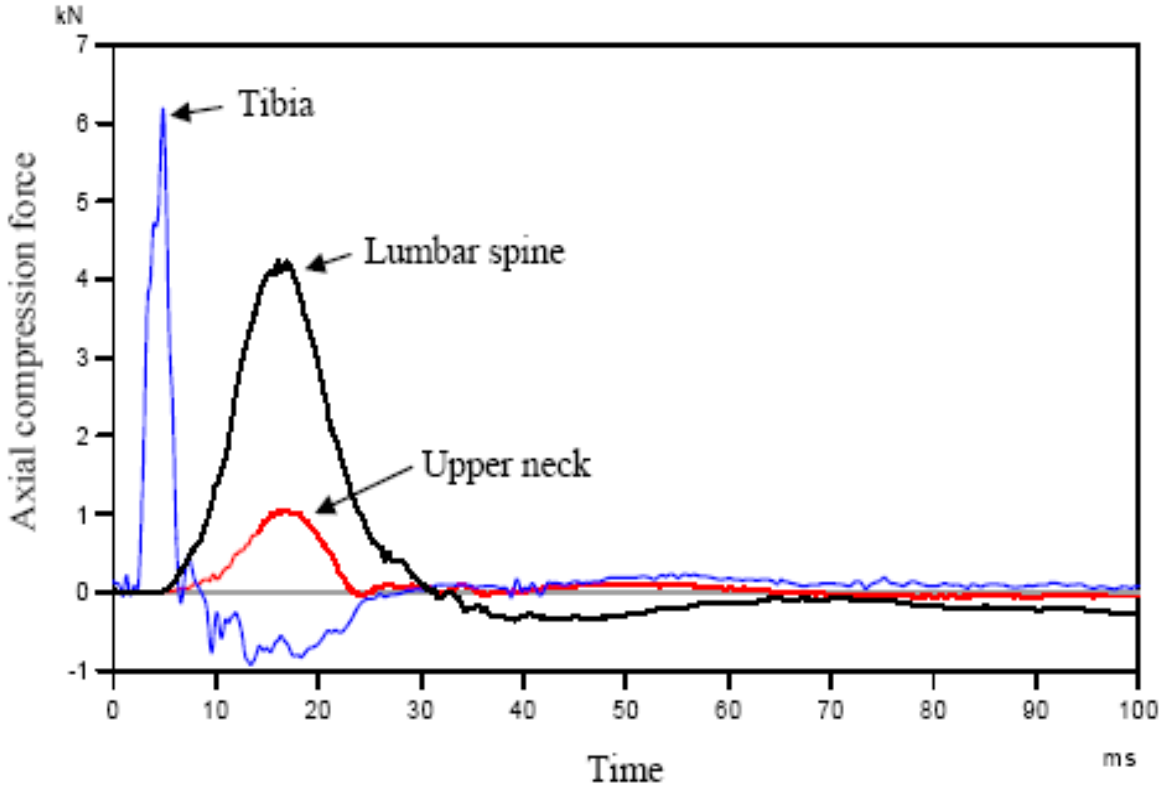

Figure 4: Relative Magnitude of Compressive Loading in an Underbelly Blast Event (reprinted from North Atlantic Treaty Organization TR-HFM-090, 2007).

2.3 Modern Warfare Statistics

Considering the lower extremity experiences the highest peak axial force of any other body region in an AV underbelly blast, it can be expected that mounted soldiers experience a high level of lower extremity injuries. A review of modern warfare casualty statistics reveals the most injured body region is the lower extremity. Unfortunately often lost in war time statistics is the distinction of wound patterns experienced by mounted and dismounted soldier. Despite these shortcomings, deciphering casualty statistics provides an in-depth snapshot of wound patterns and, more recently, mechanism of injury. Combining detailed statistics with informative field reports regarding mounted soldiers/civilians who have experienced lower extremity trauma

provides a better understanding of the frequency and severity of the threat. In the future, more detailed U.S. soldier casualty information will become available. The U.S. Department of Defense developed the Joint Theatre Trauma Registry (JTTR), a database which aggregates medical treatment information of U.S. soldiers. The database combines soldier injury information with forensic information from the battlefield ("crime scene investigation"). The database records information specific to the incident including the type/size of causative agent, soldier positions, soldier personal protective equipment (PPE) and injuries sustained (Galarneau, 2004).

The effectiveness and widespread use of body armor by has significantly reduced the percentage of penetrating thoracic and abdominal injuries in U.S. Servicemen (Zouris, 2006). Unprotected anatomical regions are the most susceptible to injury. In each armed conflict since World War II, greater than 54 percent of all U.S. military combat wounds were extremity wounds (Owens, 2007). Lower extremity injuries accounted for 26 to 48 percent of all combat injuries sustained during this time period (Table 1). Despite the vast technological advancements from conflict to conflict, which have exponentially increased the destructive power of weapons and improvements to protection systems, the distribution of lower extremity injuries remain consistently high.

While the majority of extremity wounds were soft tissue injuries, a large proportion, ranging from 23 to 39 percent in recent armed conflicts, resulted in fractures (Owens, 2007). Historically, greater than 80 percent of combat fractures are classified as open (Owens, 2007). Although most extremity injuries are not an immediate threat

to life, complex open fractures are associated with high infection and complication rates leading to long term health issues, financial and functionality costs.

Table 1: Extremity Wounds as a Percentage of all U.S. Servicemen Combat Wounds (Owens, 2007).

Extremity Wounds as Percent of All Wounds

Extremity	WWII	Korea	Vietnam	Desert Storm	OIF/OEF
Upper	23%	29%	27%	23%	28%
Lower	35%	36%	34%	48%	26%
Total	58%	65%	61%	71%	54%

Owens (2007) et al. reviewed the medical treatment information of 1,566 U.S. soldiers that suffered 6,609 combat wounds during OIF and OEF. He determined the most common fracture of the lower extremity was to the leg followed by fractures to the femur and foot. Greater than 75 percent of all lower extremity fractures were classified as open fractures.

Table 2: Distribution of Lower Extremity Injuries in OIF & OEF (Owens, 2007).

Fracture	% of Lower Extremity Fractures	% with Open Fractures
Femur	27%	87%
Leg	48%	79%
Foot	25%	76%

Zouris et al. (2006) studied combat injuries to U.S. Marines and Sailors during the initial combat phase of OIF (OIF-I). The study examined the wounds incurred by 270 Marines and nine Sailors. Of the 454 wounds suffered, Zouris et al. (2006) determined that 35 percent of wounds were lower extremity injuries. The leading diagnoses for injury were open wounds (42 percent) and fracture (18 percent). The amputation rate was 2.4 percent (Zouris, 2006).

Radonic et al. (2004) evaluated 26 incidences of AV landmine blast impacts in Southern Croatia from 1991 to 1995. The vehicles destroyed in the blasts included 15 civilian cars, three lorries, two buses, two jeeps, a transporter, an excavator, an ambulance, and a tractor. The civilian vehicles were unarmored.

Forty-two people were injured in the blast: 29 armed forces personnel and 13 civilians. Twelve (29 percent) sustained fatal injuries, ten of which were pronounced dead at the scene. Brain injury (50 percent) was the leading cause of death followed by exsanguinating hemorrhage (33 percent). Of the 39 survivors, 27 (69 percent) required surgery. Twenty-one of the 27 survivors required more than one surgery to repair wounds.

Seven traumatic amputations were performed on six subjects. One subject with massive tissue destruction had traumatic amputation of both upper legs, but later died of exsanguinating hemorrhage. Three other subjects with massive tissue destruction received traumatic amputations of an upper leg. Two subjects with lower leg traumatic amputations also suffered a calcaneus fracture in the opposite limb. Five other subjects suffered from six calcaneus fractures—many displaced. In two cases, the tibia was also fractured. The subject with two calcaneus fractures also suffered from a fractured

femur. Three additional subjects required surgery to repair fractured lower legs (Radonic, 2004).

Gondusky et al. (2005) evaluated the battle injuries suffered by a mechanized battalion operating in Iraq during OIF-II (post combat phase). The 1st Light Armored Reconnaissance (LAR) was lead by 950 U.S. Marines driving approximately 75 light armored vehicles (LAV) and numerous up-armored high mobility multipurpose wheeled vehicles (HMMWV) and trucks.

Over a six month period beginning March 2004, 120 Marines were injured in 32 separate attacks causing 188 injuries. Five Marines were fatality injured. 115 Marines were injured while riding in a LAV. Ninety-seven percent of injuries were caused by landmine (32 percent) or IED (65 percent). Three percent were injured from direct fire.

The ears and head were the most often injured anatomical region sustaining 23 and 16 percent of all injuries respectively. The upper and lower extremities were the third and fourth most injured anatomical regions sustaining 13 and 11 percent of all injuries respectively. Nine percent of the lower extremity injuries were to the legs and two percent to the ankle. The foot was not injured. The lower extremity injuries that occurred were primarily soft tissue injuries caused by the Marine's impact with the interior of the vehicle. This data suggest the LAV provided satisfactory protection to the lower extremity against the anti-vehicular landmine and explosive devices utilized in the attacks. In addition, occupant footwear may have decreased injury risk to the foot and lower leg to some degree.

The reports from Radonic and Gondusky illustrate the dichotomy between unarmored and armored vehicle protection, and stresses the need for adequately designed vehicle protection systems.

2.4 Mechanism of Extremity Injury

Defining the causative agent of lower extremity injury is critical due to the distinct differences in injury mechanism, trauma pattern, and severity. The mechanism suggests a biomechanical loading direction and magnitude that perpetrated the injury. For the purposes of this study, injuries resulting from landmines suggest the injuries occurred to mounted soldiers from axial loading. Injuries from IED, the signature weapon of enemy combatants during OIF and OEF, can be utilized as an AP or AV explosive device. Because the term IED is used so extensively in media and literature to describe all ground blast events in OIF and OEF it is difficult to distinguish whether statistics attributed to “IED” blasts refer to an AV or AP, axial (underbelly) or axial and lateral (roadside) blast threat. However, certain general conclusions can be inferred from this data regarding the specific modern threat of blast related injuries.

According to Owens et al. (2007), explosive munitions accounted for 75 percent of extremity injuries (Figure 5) to U.S. soldiers in OIF and OEF. Approximately 38 percent of the extremity injuries were the result of an IED or landmine. Conventional landmines caused only two percent of extremity injuries. Rocket propelled grenade (RPG), gunshot, and mortar each contributed 16 percent.

Similarly, Zouris et al. (2006) determined that landmines and IED combined accounted for 34 percent of all lower extremity injuries during OIF-I. Zouris et al. (2006) specifies landmines caused 24 percent of injuries while IED caused 10 percent

of lower extremity injuries notably behind small arms, mortar and shrapnel (Figure 6). In this survey of 297 Marines and Sailors, landmine blasts caused significantly more lower extremity injuries (79 percent) than upper extremity injuries (12 percent). The landmine caused fractures and amputations at a devastating rate of 14 percent. The IED caused more upper extremity injuries (36 percent) than lower extremity injuries (28 percent). The IED produced fractures at a rate of 11 percent and amputations at 3.2 percent. The IED was more efficient at causing open wounds (53 percent) than the landmine (43 percent).

U.S. Soldiers remain susceptible to lower extremity injuries. Based on several studies of historical and ongoing armed conflicts, it appears mounted soldiers are frequently injured by landmine and IED blasts. Injuries resulting from high energy explosive blasts create severe open fractures and soft tissue injuries resulting in high incapacitation rates and alarming amputation rates.

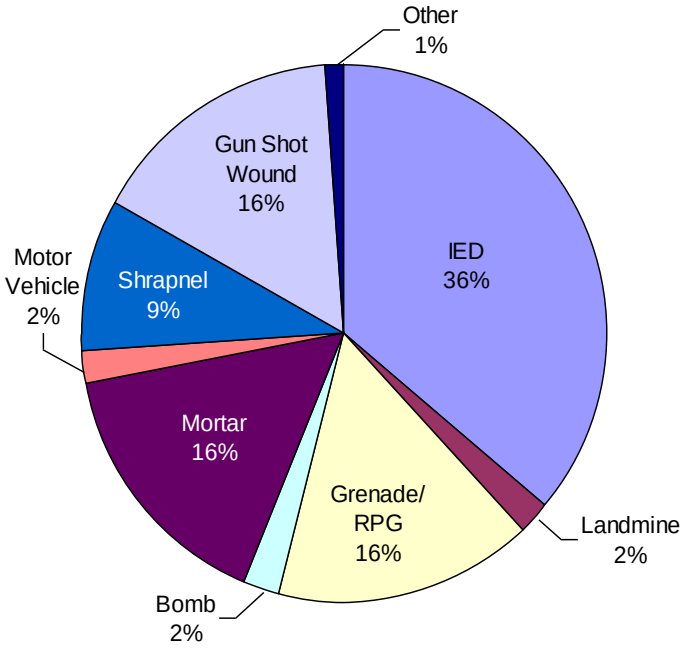

Figure 5: Causative Agent for Extremity Injuries during OIF & OEF (Owens, 2007).

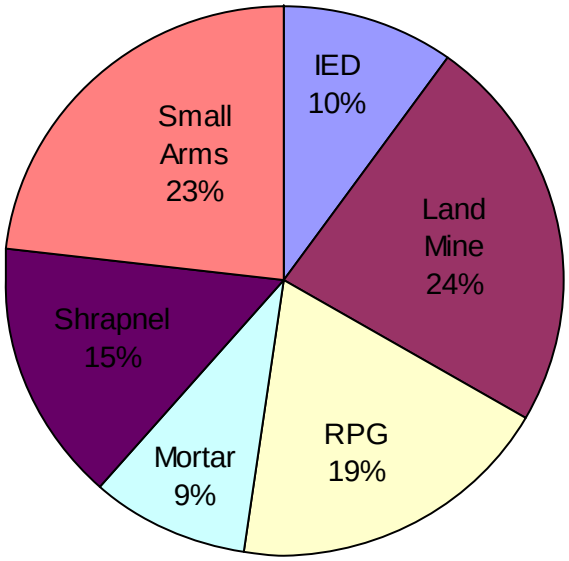

Figure 6: Causative Agent for Lower Extremity Injuries during OIF-I (Zouris, 2006).

CHAPTER 3

RISK OF LOWER EXTREMITY INJURY FROM AXIAL BLAST LOADING

3.1 Occupant Orientation and Anatomy

The orientation, location, and biomechanics of a mounted soldier are dependent on the duty assignments. It is often convenient to subdivide these duties into three categories based on their seating position: driver, passenger and gunner. Regardless of the seating arrangement (facing the front or the side of vehicle) or seating system (standard fastened seating or suspended seating) used in a particular vehicle build, the driver and passenger rest their feet directly on the vehicle floorboard. The driver will maneuver a foot to operate the pedals. The gunner(s) is positioned on an elevated rotating platform above the main floorboard. The gunner may assume one of two positions depending on the situation. The gunner may stand, particularly during combat operations, or may sit in a sling or seat during non combat operations. The gunner's feet rest on an elevated platform, which is not in direct contact with the vehicle floorboard. For the framework of this research study, the anatomy and biomechanics of the standing gunner position will be disregarded.

In an underbelly AV blast event the lower extremity of a vehicle occupant is most susceptible to injury because of its proximity to the primary impact point and the magnitude and rate of axial compressive loading. The lower extremity can be divided into four regions: pelvic, thigh, leg, foot, and ankle (Huelke, 1986). In the seated position, the pelvis and thighs rest on the seat while the feet rest on the floorboard. During an AV blast impact, the foot is the first anatomical structure loaded in a classical AV landmine explosive impact scenario because of its immediate vicinity to the blast.

Subsequently, loading is transferred from the foot through the ankle and onto the leg, which contains the tibia and fibula. The foot, ankle, and leg region are commonly referred to as the lower leg while the knee, thigh, and pelvis region is referred to as the upper leg. Overloading the lower leg structure will result in skeletal injury. As such, the skeletal integrity of the lower extremity is of particular importance in this research study.

3.1.1 Pelvis

The pelvic bone transfers the body weight from the vertebral column to the pelvic girdle. From the pelvic girdle, weight is transferred to the femur. As shown in Figure 7 the pelvis is comprised of three fused bones: ilium, ischium and pubis (Moore, 2002). This fusion forms a socket cavity, or acetabulum, on the lateral aspect for articulation with the head of the femur (Huelke, 1986).

Three gluteal muscles, gluteus maximus, medius and minimus, reside posteriorly on the pelvis and act to rotate the thigh region. The gluteal muscles originate from the ischium and ilium and attach to the proximal femur. The muscles are supplied by the internal iliac arteries and are innervated by the superior and inferior gluteal nerve (Moore, 2002).

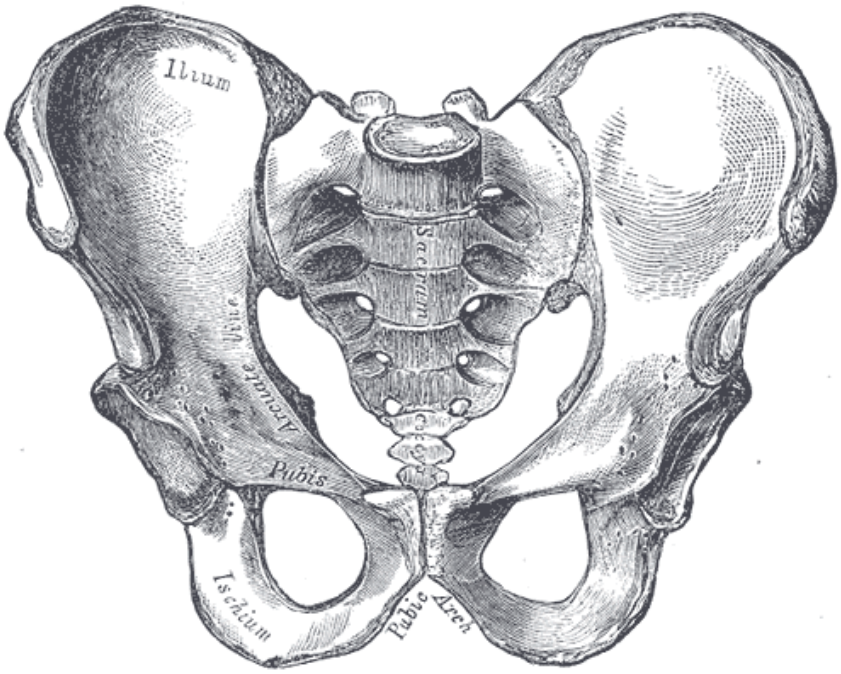

Figure 7: Bones of the Pelvis (reprinted from Gray, 2000).

3.1.2 Thigh

The thigh encompasses the area between the pelvic bone and the knee. The femur, the largest and heaviest bone of the body, resides in the thigh and transmits the body weight from the pelvis to the tibia. The cylindrical shaped femoral head, which lies at the proximal end of the femur, articulates with the acetabulum. The articulation is illustrated in Figure 8. The femoral head is connected to the femoral shaft by a narrow neck, which lies at an approximate angle of 125 degrees with the shaft (Moore, 2002). The distal portion of the femur diverges into a medial and lateral condyle. The femoral condyles articulate with the proximal tibia condyles to form the knee joint.

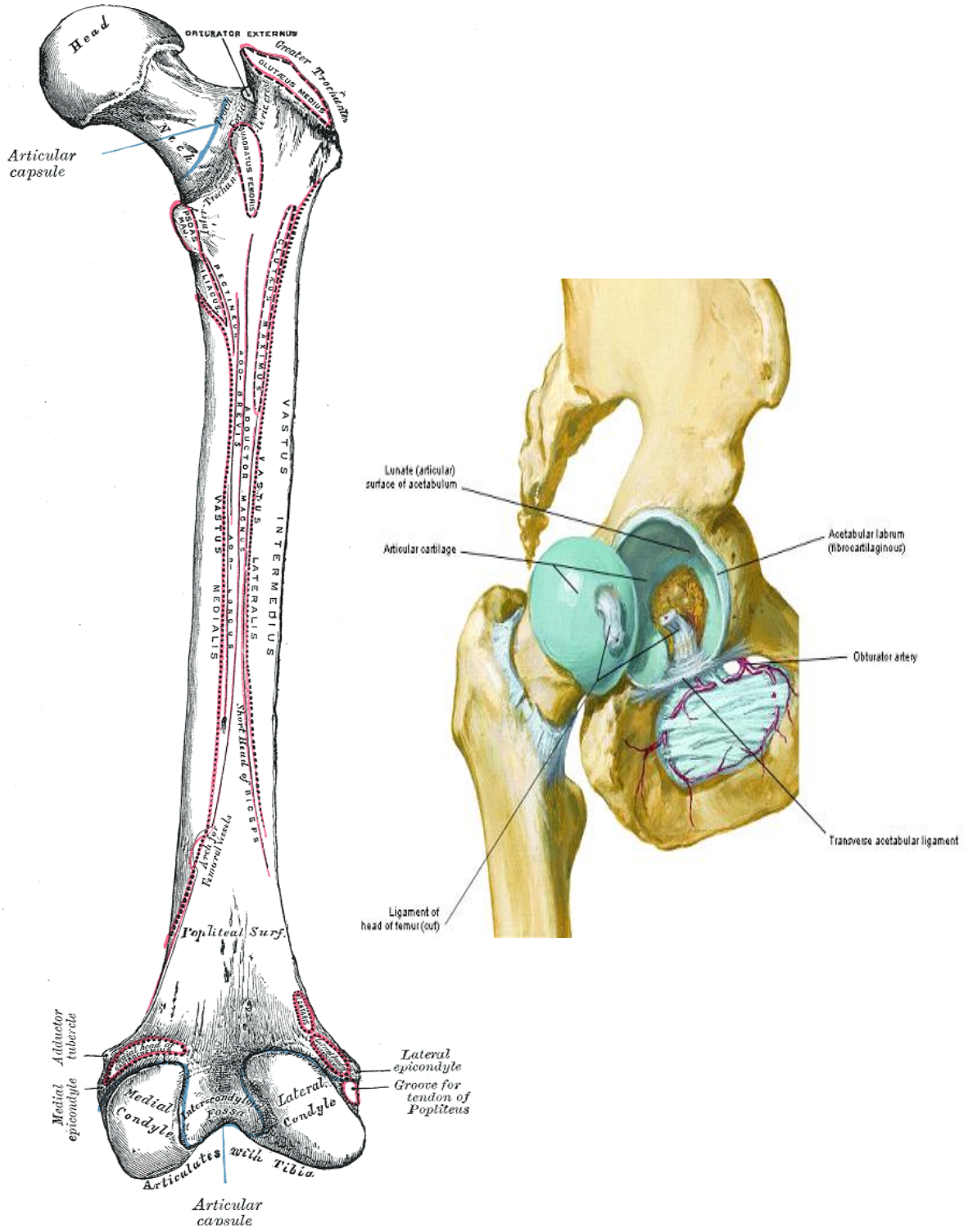

Figure 8: Left - Anterior View of the Left Femur Bone (reprinted from Gray, 2000). Right – Lateral View of the Hip Joint (reprinted from Netter, 2006).

The musculature of the thigh can be divided into three compartments: anterior, medial, and posterior (Huelke, 1986). The anterior compartment consists of hip flexors and knee extensors. The quadriceps femoris, which includes the rectus femoris, vastus lateralis, vastus medialis, and vastus intermedius, are the most powerful extensors of the knee joint. The medial compartment features a heavy group of adductor muscles including the adductor longis, adductor brevis, adductor magnus, gracilis, and obturator externus. The hamstrings, located in the posterior compartment, are responsible for flexing the knee and extending the hip and thigh. The hamstrings consist of the semitendinosus, semimembranosus, and bicep femoris (Moore, 2002).

The patella, or knee cap, is a large sesamoid bone that is formed intratendinously after birth. The patella is positioned anterior to the knee joint and serves as a fulcrum giving the quadriceps more power when extending the leg (Huelke, 1986). The knee joint, as shown in Figure 9, is a hinge type of synovial joint that allows flexion and extension the leg. The knee joint consists of two joints forming three articulations. The femoro-patellar joint is the articulation between the patella and femur. The femoro-tibial joint links the lateral and medial articulations between the femoral and tibial condyles. The knee joint is held intact by ligaments connecting the tibia and femur as well as surrounding muscles and tendons (Moore, 2002).

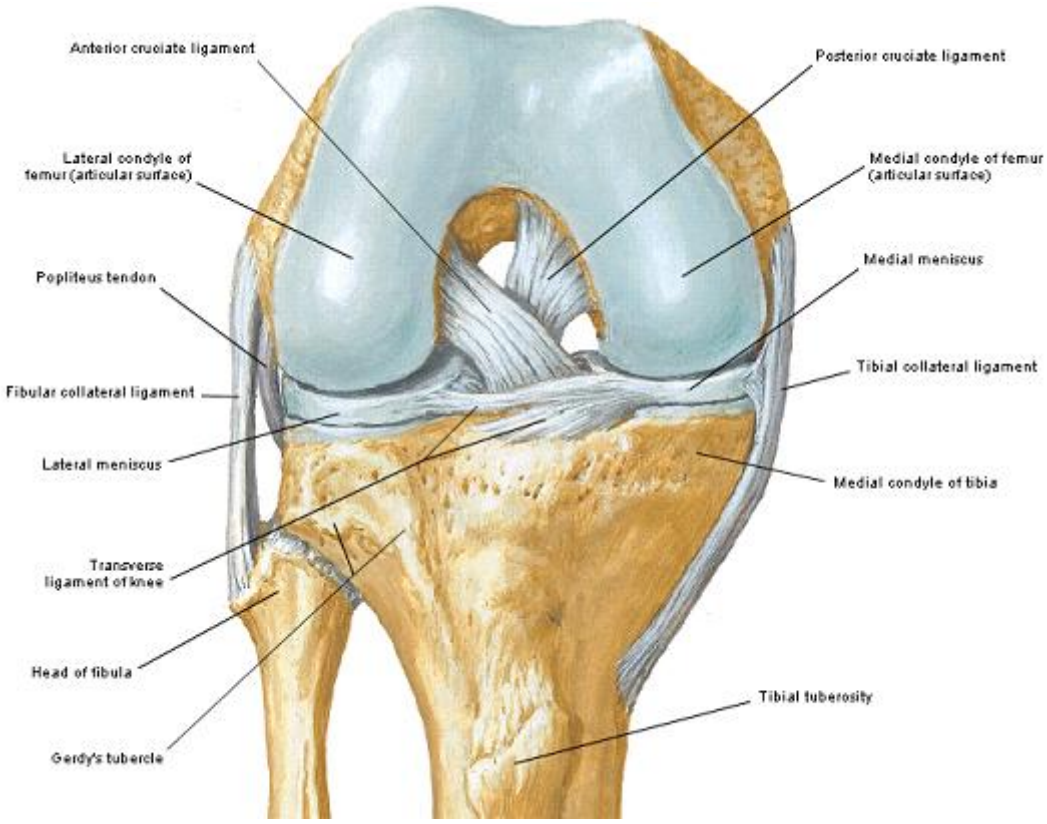

Figure 9: Anterior View of the Right Knee in Flexion (reprinted from Netter, 2006).

3.1.3 Leg

The leg is supported by two bones: tibia and fibula. The tibia and fibula are shown in Figure 10. The tibia, the second longest bone of the body, resides in the medial portion of the leg while the fibula resides in the lateral portion of the leg and posterolateral of the tibia. The tibia is longer, larger in diameter and stronger than the fibula. The tibia is the primary weight-bearing bone of the leg accounting for 85 to 90 percent of weight transfer depending on the position of the foot and ankle (Moore, 2002). The tibia articulates with the medial and lateral femoral condyles superiorly, talus inferiorly and laterally, and with the fibula at its proximal and distal ends (Moore,

2002). The distal portion of the tibia and fibula diverge into medial malleolus of the tibia and lateral malleolus of the fibula.

The tibia forms two joints with the fibula. The proximal tibiofibular joint is an arthodial joint that links a facet located on the posterolateral portion of the lateral tibia condyle with a facet located on fibular head (Huelke, 1986). This proximal joint enables slight gliding movements during plantar flexion and dorsiflexion of the foot. The distal tibiofibular joint is a fibrous joint linking the medial distal fibula to the lateral malleolus of the tibia. The distal joint accommodates the talus during dorsiflexion of the foot, which is critical to ensuring ankle stability. Both joints are strengthened by anterior and posterior tibiofibular ligaments (Moore, 2002).

Similar to the thigh, the musculature of the leg can be divided into three compartments. The anterior compartment, responsible for extending the ankle and phalanges, includes the tibialis anterior, extensor hallicis longus, and extensor digitorum longus. The lateral or peroneal compartment is responsible for everting the ankle and includes the peroneus longus and peroneus brevis. The posterior compartment, responsible for flexing the ankle and phalanges, includes the gastrocnemius, soleus, tibialis posterior, flexor hallicis longus, and flexor digitorum longus (Huelke, 1986).

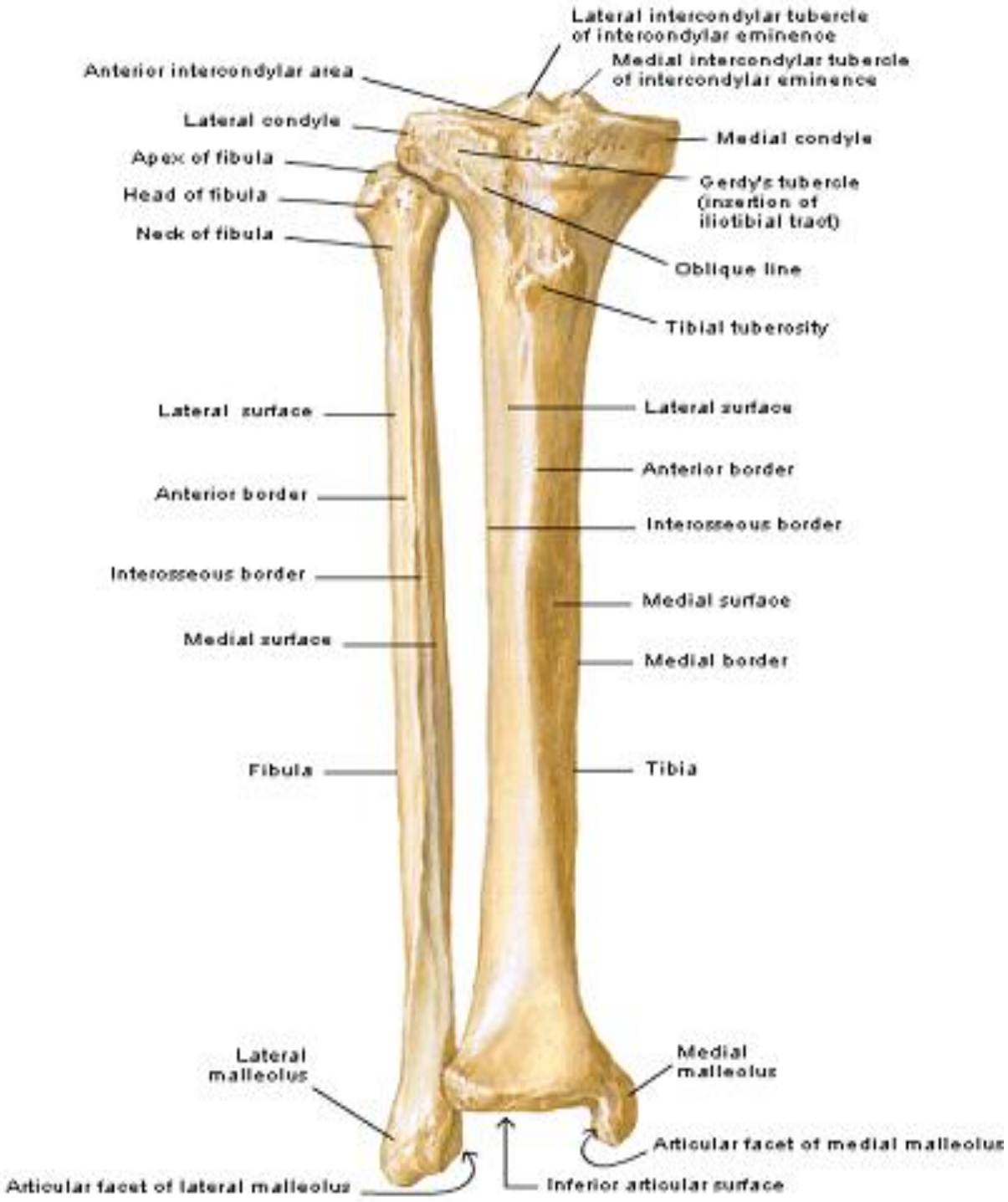

Figure 10: Anterior View of the Right Tibia and Fibula (reprinted from Netter, 2006).

3.1.4 Foot

The foot, located distal to the leg, is comprised of three main parts: hindfoot, midfoot and forefoot. These parts work in harmony to support the body weight transferred from the leg and facilitate locomotion. The hindfoot includes talus and the calcaneus. The midfoot includes navicular, cuboid, and three medial cuneiforms. The forefoot includes the five metatarsals and fourteen phalanges (Figure 11) (Moore, 2002).

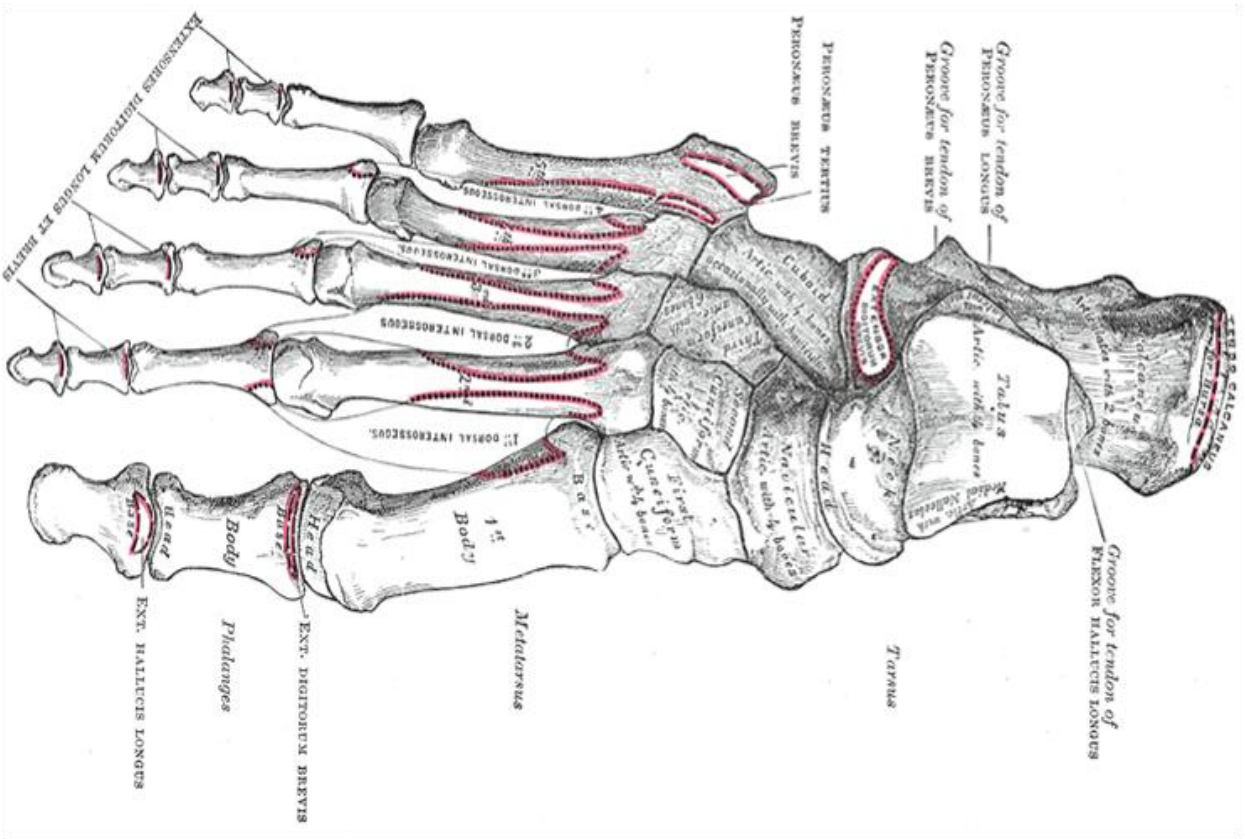

Figure 11: Anterior View of the Left Foot (reprinted from Gray, 2000).

The talocrural joint, or ankle joint, is a synovial joint that links the distal tibia and fibula to the proximal articular surfaces of the talus. The talus, the second largest bone

in the foot, resides distal to the tibia and fibula and proximal to the calcaneus (or heel). The talus is the only bone in the foot that articulates with bones of the leg (Figure 12). The talus articulates with the tibia in two locations: (1) medial malloeus articulates with medial aspect of the talus; (2) inferior surface of the distal tibia articulate with the superior surface, or trochlea, of the talus (Moore, 2002). The lateral malleous of the fibula articulates with the lateral aspect of the talus. The articulation between talus and tibia supports more weight than smaller talus and fibula articulation (Moore, 2002). The fibrous capsule of the ankle joint is strengthened laterally and medially by multiple ligaments (Moore, 2002).

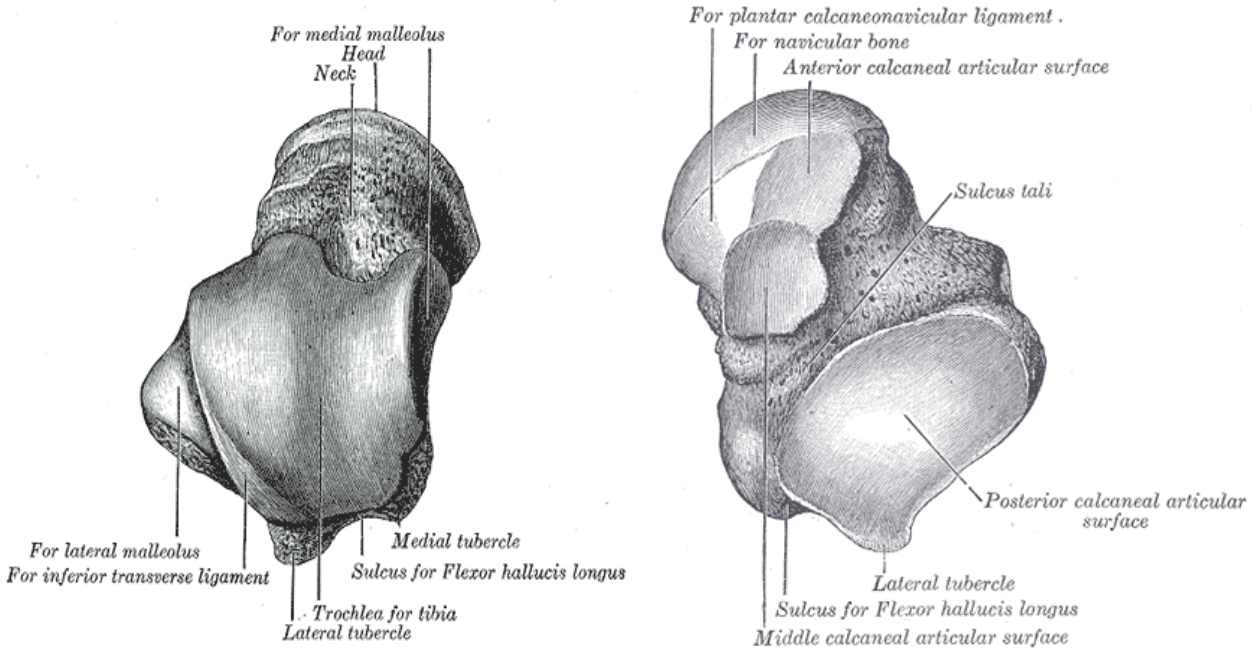

Figure 12: Left – Left Talus, Superior View. Right – Left Talus, Inferior View (reprinted from Gray, 2000).

The talus rests on the anterior two-thirds of the calcaneus (Moore, 2002). The calcaneus is the largest and strongest bone of the foot and transmits the majority of the

body weight from the talus to the ground (Figure 13). The posterior portion of the calcaneus serves as the insertion point for the Achilles tendon. The head of the talus is supported by the talar shelf (L. sustentaculum tali) of the calcaneus. The head of the talus also articulates with the navicular. The navicular bone resides on the medial side of the foot and has three strongly concave proximal articular surfaces for each of the three cuneiform bones. The medial, middle, and lateral cuneiform articulate with the first, second, and third metarsal bones respectively via a tarsometatarsal joint. Residing medial of the cuneiform is the cuboid bone. The lateral cuneiform and navicular bones articulate with the medial surface of the cuboid bone. The cuboid bone also articulates with the fourth and fifth metatarsal bones forming the tarsometatarsal joint and with the calcaneus proximally at the calcaneocuboid joint. The metatarsals connect the tarsus to the fourteen phalanges. Each phalange is constructed of the three bones except the first phalange, which is consists of two bones (Moore, 2002).

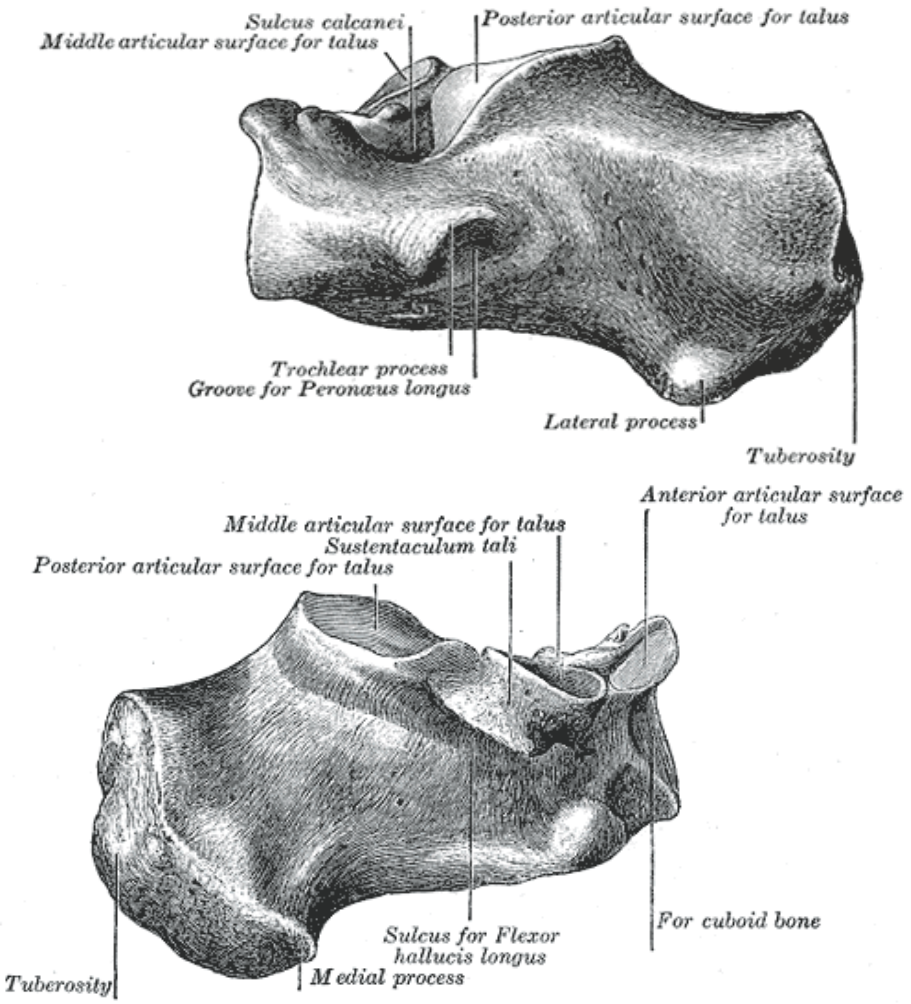

Figure 13: Top – Left Calcaneus, Lateral Surface. Bottom – Left Calcaneus, Medial Surface (reprinted from Gray, 2000).

3.2 Lower Extremity Injury Classification and Scaling

The lower extremity is composed of bone matter, epithelium, connective, muscle, and neural tissue. Significant damage to any component may result in an incapacitating injury or the catastrophic loss of a limb. The objective of military vehicle protection systems is to protect all occupants from injuries that may "cause complete and immediate incapacitation for military tasks" (Walter Reed Army Institute of Research, 1989). In practice the aforementioned requirement asserts an occupant must have

sufficient physical capacity to escape a defeated vehicle in ample time to avoid further injury. Following an explosive blast event the lower extremity of a military vehicle occupant is subject to a wide range of injuries. An injury may occur to one or more components. A lower extremity injury criterion for military vehicle occupants must be sensitive to distinguish a non severe injury from an incapacitating injury. Generally, the type and severity of injury is a function of the loading mechanism, loading energy, and the occupant's physical condition. The following sections will discuss the common types of lower extremity injuries and present several injury scaling systems used to classify injury severity and level of impairment.

3.2.1 Fracture

A fracture is a medical term for a break in bone continuity (Levine, 2003). Fractures are the result of high stress or impact forces projected on a bone. The potential for a particular bone to fracture is a function of its biomechanical properties, which are largely dependent on bone density, age, and health. Furthermore, certain components of a bone may be more prone to fracture than others (Levine, 2003).

A fracture is classified as either open or closed. A closed fracture is contained within epithelium tissue. In contrast, an open fracture breeches the epithelium tissue thereby exposing internal tissue and bone to the outside environment. Environmental exposure significantly increases the risk of contamination or infection of the wound (Levine, 2003). Open fractures may also lacerate underlying muscle, arterial, and neural tissue.

All fractures are also categorized as being undisplaced or displaced. A fracture is defined as undisplaced when all bone fragments are contained within the normal

anatomical position. In contrast, a displaced fracture occurs when one or more bone fragments shift from normal anatomical position. The presence and level of displacement indicate the magnitude of forces involved. Undisplaced fractures usually indicate a relatively low energy input force while a displaced fracture indicates a higher energy input (Levine, 2003).

All fractures are also categorized as being non-comminuted or comminuted. A non-comminuted fracture is defined as a bone broken into only two fragments while a comminuted bone is broken into more than two fragments. The level of comminution indicates the magnitude of forces involved; a higher energy input correlates with more comminution. Weaker bones are more prone to comminution than relatively stronger bones (Levine, 2003).

3.2.2 Other Tissue Injuries

Epithelium, connective, muscle, and neural tissue may be injured with or without incidence of fracture. Tissue may be injured from penetrating fragments—a signature injury of explosive blasts—impact with the crew cabin resulting in contusion or laceration, or internally from displaced bones and fractures.

The majority of extremity amputations in modern warfare are associated with vascular injury (Owens, 2007). Vascular injuries may result from internal bone displacement or external forces including high energy projectiles. Similarly, significant loss of epithelium, connective, and muscle tissue may result in the catastrophic loss of a limb.

3.2.3 Abbreviated Injury Scale

Injury scales are utilized by the medical, automotive, and military community to standardize injury assessment. An injury scale assigns a particular injury a metric or score, which correlates with a relative rank. The rank may refer to the probability of survival, probability of amputation, injury severity, or long term impairment. Several injury scales are commonly used to rank lower extremity injuries.

The Association for the Advancement of Automotive Medicine (AAAM) employs the Abbreviated Injury Scale (AIS) to standardize the classification of injury level to a body region or organ (Cavanaugh, 2003). The AIS utilizes a seven-point numerical rating system to describe the threat to life (Table 3). Although AIS is an excellent tool for measuring injury severity, it is insufficient at distinguishing the severity of skeletal injuries and predicting impairment (Levine, 2003).

Levine et al. (2003) noted that a displaced medial malleolus fracture and an articular-displaced calcaneal fracture both receive an AIS score of two. However, the subject with a medial malleolus fracture is expected to make a full recovery with no long term impairment while the subject with an articular-displaced calcaneal fracture will suffer severe lifetime impairment. Due to the insensitive nature of AIS for lower limb injuries, AIS scaling is not the most appropriate injury assessment system for determining occupant lower extremity incapacitation.

Table 3: Application of the Abbreviated Injury Scale for the Lower Extremity (Association for the Advancement of Automotive Medicine, 1990).

AIS Code	Injury Description	Example of Injury
0	No Injury	No Injury
1	Minor	Ankle sprain
2	Moderate	Simple or comminuted fracture of the tibia, talus, or calcaneus
3	Serious	Open fracture of the tibia. Fracture of the fibula with artery or nerve damage
4	Severe	Traumatic amputation
5	Critical	Not applicable
6	Maximum	Not applicable

3.2.4 Mangled Extremity Severity Score

Three injury scales are employed to predict the salvageability of a mangled extremity: Triage-Revised Trauma Score (T-RTS), Mangled Extremity Syndrome Index (MESI), and Mangled Extremity Severity Score (MESS) (Levine, 2003). The ability to accurately assess whether a mangled extremity should be salvaged or amputated impacts the subject's survival rate and the triage center's allocation of medical resources (Levine, 2003).

The T-RTS is utilized in civilian and military triage centers to predict the probability of survival from very severe injuries (Rush, 2007). T-RTS is a 13-point scale that incorporates the Glasgow coma scale, blood pressure, and respiratory rate (Levine, 2003).

In military combat settings the T-RTS and MESS are utilized to assess whether a mangled extremity should be salvaged or amputated (Rush, 2007). MESS is based on

the MESI developed by Gregory (1985). MESI incorporates an injury severity score (ISS), skin injury, nerve injury, vascular injury, bone injury, time since injury, and shock (Levine, 2003). A MESI score greater than 20 results in an unsalvageable limb. MESS was developed to simplify MESI so it can be quickly and easily applied when time is critical. MESS relies on four criteria: skeletal/soft tissue injury, limb ischemia, shock, and patient age. MESS assigns a score to each criterion in order of increasing severity or risk. A MESS score of seven or greater indicates a limb should be amputated.

Rush et al. (2007) applied the T-RTS and MESS prospectively to 26 lower extremity injuries sustained in OIF during a 12-month period at two military trauma centers. Each lower extremity injury comprised of an open fracture and vascular injury. Rush et al. (2007) found a significant difference in the mean MESS score for amputated and salvaged limbs. A MESS score greater than seven predicted amputation with 100 percent accuracy.

3.2.5 Ankle and Foot Injury Scale

In 1995, the American Orthopaedic Foot and Ankle Society Trauma Society issued the Ankle and Foot Injury Scales (AFIS). AFIS is divided into an injury severity and long term impairment scale. Similar to AIS, AFIS is a seven-point numerical rating system. AFIS evaluates a comprehensive list of lower limb injuries and describes the relative severity (AFIS-S) and long term impairment (AFIS-I) (Table 4).

AFIS is able to distinguish the severity and impairment of lower limb injuries. Utilizing the aforementioned example, a displaced medial malleolus fracture would receive an AFIS-S score of two (mild injury) and an AFIS-I score of one (slightly limited). In contrast, an articular-displaced calcaneal fracture would receive in AFIS-S score of

five (very severe injury) and an AFIS-I score of three (moderate impairment). A subject sustaining a displaced medial malleolus fracture would suffer minor impairment while a subject sustaining an articular-displaced calcaneal fracture would have some trouble with weight bearing activities.

Table 4: Ankle and Foot Injury Scale (Ankle and Foot Injury Scales, 1995).

AFIS Code	AFIS-S	AFIS-I	AFIS-I: Description of Functional Limitations	AFIS-I: Description of Assistance Required
0	No Injury	No Impairment	None	None
1	Minimal Injury	Minimal Impairment	Slightly limited	Occasional pain controlled by OTC medication
2	Mild Injury	Mild Impairment	Some limitations	Recurring pain controlled by OTC medication
3	Moderate Injury	Moderate Impairment	Limited weight bearing activity	Prescription pain relief medication; requires orthotics device
4	Severe Injury	Severe Impairment	Weight bearing with aid	Regular use of non-opoid pain medication; requires walking aid
5	Very Severe Injury	Very Severe Impairment	Very limited weight bearing	Regular use of non-narcotic pain medication; requires walking aid or wheelchair
6	Currently Untreatable	Total Impairment	Unable to bear weight	Pain poorly controlled by opoid medication; requires walking aid

An occupant with an AFIS-S score of four (severe injury) is unable to complete weight bearing activities and are relatively immobile at the time of injury. Therefore, an AFIS-S score of four or greater (abbreviated 4^{+}) is, by description, an appropriate measure for incapacitation as this value specifically addresses limited weight bearing and mobility.

3.3 Lower Extremity Injury Risk Models for Axial Loading

Numerous lower extremity injury risk models have been developed to establish protection requirements for automotive collisions. The military vehicle manufacturers and blast testing community have attempted to leverage injury models that utilize PMHS and pure axial impact conditions in order to establish lower extremity protection criteria for AV mine blast events.

An AV landmine and explosive blast device exert a mechanical load onto the lower limb of vehicle occupants. The lower limb will experience an axial compressive force that is proportional to the magnitude of the blast and its attenuation through the vehicle hull and floorplate (Wang, 2001). A similar axial loading mechanism is generated in frontal motor vehicle collisions and projected to the lower extremity of vehicle occupants (Dischinger, 1994). In frontal collisions, the exterior structural framework of the automobile absorbs the kinetic energy resulting from the collision. As the vehicle exterior structure deforms and crushes kinetic energy is dissipated. The resultant energy is transmitted to the interior compartment of the vehicle, which produces localized direct and indirect accelerative loads on the occupant. The lower extremity of vehicle occupants may be axially loaded by the intruding footplate (footwell or toepan) or pedals (Pilkey, 1994). Similar to the AV blast, the magnitude of the axial load is a function of the initial kinetic energy generated minus its attenuation through the vehicle structure and floorplate.

The following sections will discuss risk models that are most applicable to the AV blast loading mechanism.

3.3.1 Injury Risk Model for the Upper Leg

With the advancement and successful implementation of safety belts and active restraint systems, the number of fatal or serious injuries was substantially decreased. Non-fatal injuries, particularly the lower extremity, became the focus of occupant protection research and development. Early automotive lower extremity injury research focused on the impact tolerance of the upper leg. In frontal collisions, the interior dashboard of a vehicle may impact the flexed knee of an unrestrained or restrained occupant. The longitudinal impact would produce axial loading of the knee and femur. Melvin et al. (1975) conducted knee impacts on 31 instrumented unembalmed human cadavers using a transfer piston. Seven fractures were observed. No injuries to the patella, femur or pelvis were recorded at peak loads less than 13,340 N. Powell et al. (1975) impacted the knees of nine seated cadavers with a pendulum. The cadavers were instrumented with femur strain gages. Impactor velocity and force were measured. Femur fractures were produced in seven of the 15 legs impacted. The femur fracture forces ranged from 7.1 kN to 12.5 kN with an average value of 10.0 kN. Patella fractures were observed in 80 percent of the legs seated and occurred at forces below the force levels of the femur. The National Highway Traffic Safety Administration (NHTSA) FMVSS 208 specifies a 10.0 kN maximum axial femur force in automotive vehicles.

Mertz (1994) developed time-dependent injury threshold curves for axial compressive femur force for utilization with the Hybrid III ATD. The curves were generated based on bone properties gathered in dynamic compression testing. The threshold predicted the potential for fracture of the patella, femur or pelvis based on

short (less than ten milliseconds) and long duration (greater than ten milliseconds) characteristic pulse durations (Figure 14).

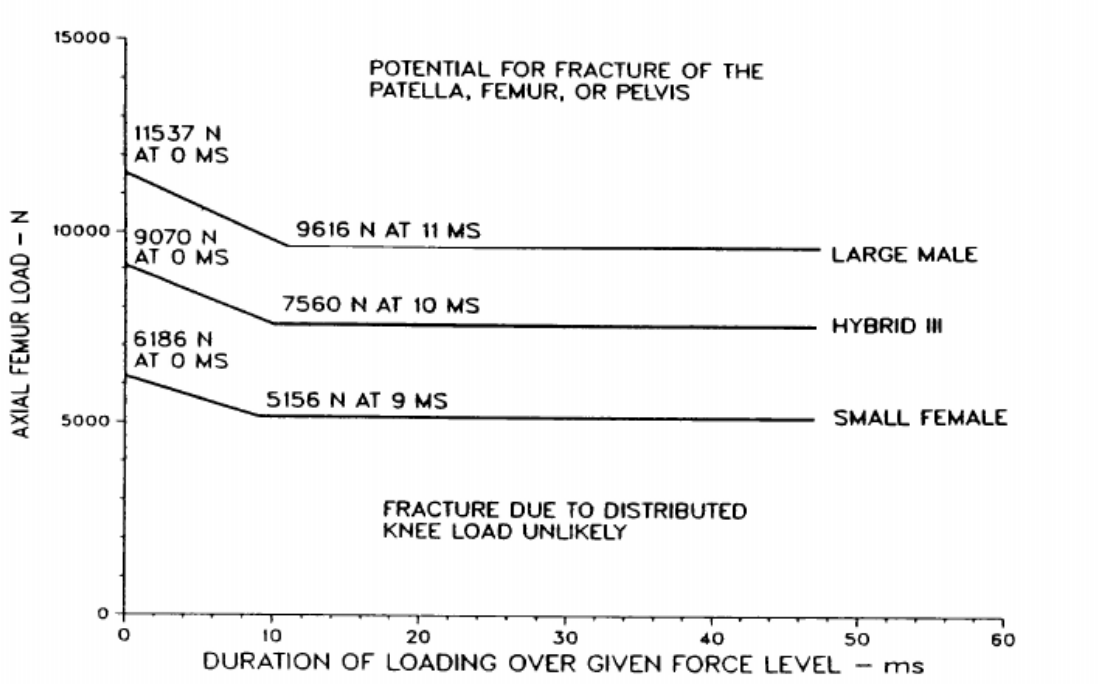

Figure 14: Axial Compressive Force Criterion for the Upper Leg (reprinted from Mertz 1994).

3.3.2 Injury Risk Model for the Lower Leg

As lower extremity research progressed the lower limb increasingly became the subject of concern. The lower limb experienced increasing rates of foot and ankle injuries in automobile frontal collisions including malleolar and bimalleolar fractures, displaced joints, ruptured ligaments, fractured talus, calcaneus, cuboid, and metatarsals (Begeman, 1990). In 1979, Glyons attributed approximately 75 percent of lower limb injuries among restrained occupants to footwell intrusion impact. The footwell intrusion produced high axial loads to the occupant foot-ankle-tibia complex. Tibia and fibula fractures could be produced by axial compression alone or by a combination of

compression and torsion, bending, and tension (Ziedler, 1981). As such, two primary lower limb injury mechanisms were established: (1) axial loading with rotational bending moments; and (2) pure axial loading. The later is the primary injury mechanism resulting from an AV mine blast (North Atlantic Treaty Organization TR-HFM-090, 2007).

3.3.3 Rotational Injury Risk Models

In an effort to quantify the foot and ankle tolerance, Culver et al. (1984) axially loaded the lower limbs of PMHS pseudostatically using an Instron (material testing machine). Axial loads were applied to the plantar portion of the foot while the foot was held in a fixed dorsiflexion state to simulate a driver's foot on a pedal. The PMHS ankle joint failure occurred at approximately 5.5 kN resulting in fractures of the anterior calcaneus. The fractures were caused by the medial rotation of the foot with respect to the tibia.

Begeman et al. (1990) attempted to define the impact response of axial loads with dorsiflexion. Eighteen PMHS lower limbs were impacted. The proximal end of the tibia was restrained in a box instrumented with load cell. Additional load cells were mounted on an aluminum plate and located near the ball and heel of the foot. A 16.3 kg pneumatic linear impactor was propelled at velocities ranging from 3.0 to 8.1 m/s into the instrumented aluminum plate and PMHS foot. The targeted impact point was approximately 62.5 mm above the ankle joint to cause axial load and dorsiflexion. PMHS range of motion was noted before and after the test. Six of 18 specimens sustained fractures. Five of six female specimens tested sustained fracture while only one of twelve male specimens was fractured. The author suggested female tolerance

limits may be less than their male counterparts. The peak fracture force measured at the proximal end of the tibia ranged from 1.4 kN to 3.9 kN and between 1.9 kN to 3.6 kN for those sustaining injury. Load data concluded the heel bone absorbed greater than twice the force loading than the ball of the foot. Multiple AIS 2 injuries were observed including malleolar and bimalleolar fractures, torn muscles, and stretched and torn ligaments.

In 1994, Mertz proposed the tibia index (TI) criterion for tibia and fibula shaft fractures. The criterion is an injury tolerance for the combined tibia axial force and bending moment. The criterion was developed using PMHS leg specimens excised at the proximal and distal tibia. Each leg specimen was simultaneously axially compressed and impacted at the tibia shaft. TI is presented in Equation 1.

$$TI = (M_R/M_c) + (F/F_c) \qquad \textbf{(Equation 1)}$$

- M_R is the resultant tibia moment $(M_x^2 + M_y^2)^{1/2}$, Nm
- M_c is equal to 225 Nm
- F is the tibia axial force, N
- F_c is equal to 35.9 kN for a 50-percentile male.

The TI utilizes critical values for tibia axial force and bending moment. The critical axial force value is based on the compressive failure strength of a tibia compact bone short specimen, and critical bending moment is based on the work of Nyquist et al. (1985). A TI value less than 1.0 represents a 10 percent risk of an AIS 2 tibia and fibula shaft fracture. The Revised Tibia Index (RTI), developed by Kuppa et al. (2001), amended the critical force and moment values proposed by Mertz. Kuppa et al. (2001)

evaluated experimental data from Schuster et al. (2000) and established a critical moment (M_c) equal to 240 Nm and critical force (F_c) equal to 12 kN for a 50 percentile male subject. A RTI value less than 0.75 represents a 10 percent risk of an AIS two tibia and fibula shaft fracture.

3.4 Pure Axial Loading Injury Risk Models

Numerous axial loading injury risk models have been developed using PMHS. In general, these models can be subdivided into two classes based on the techniques used for harvesting the specimen: (1) below knee; and (2) mid-femur or whole lower extremity. Below knee models utilize PMHS specimen disarticulated at the knee joint leaving the tibia intact. The specimen consists of a foot, ankle, fibula, and tibia. Specimens harvested at the mid femur leave the knee joint intact. The distinction between these models is important to understanding the fundamental human response of axial loading and the ability for a biomechanical surrogate to reproduce the loading response.

3.4.1 Below Knee Models

Yoganandan et al. (1996) conducted 26 dynamic axial impact tests on below knee PMHS lower limbs at the Medical College of Wisconsin. The ankle of each specimen was positioned in neutral position for each test. The proximal tibia was potted and ballasted to 16.8 kg in order to simulate the mass of the thigh. A 25 kg pendulum was launched at loading rates ranging from 3.4 to 7.6 m/s (145 to 722 J) into the plantar surface of the specimen. Load cells were positioned at the ballast and pendulum. An accelerometer was attached to the pendulum. The fracture forces, as measured by the

load cell located at the proximal tibia, ranged from 4.3 to 11.4 kN. The injuries sustained included extra/intra-articular fractures of the distal tibia and calcaneus.

Begeman et al. (1996) subjected 20 below knee PMHS lower limbs to a series of static and dynamic axial loading tests. The tibia and fibula were excised at the mid-shaft and inserted the remaining bone into a custom pot device. Three of the specimens were tested without the foot. The ankle was positioned in neutral position for each test. The proximal end of the tibia was restrained in a box instrumented with load cell. A 16.3 kg pneumatic linear impactor was propelled at velocities ranging from 4.0 to 9.2 m/s (130 to 690 J) into the plantar surface of the specimen. The average failure load was 7.8 kN and ranged from 6.9 to 8.7 kN. The failure load was found to be higher with the foot than without. The injuries sustained included calcaneus, talus, and plafond (also called a tibial pilon) fractures. The plafond fractures were sustained in the lower limbs without the foot.

Roberts et al. (1993) conducted nine static and dynamic axial impact tests on below knee PMHS lower limbs at Calspan Corporation. The proximal end of the tibia was restrained in a box instrumented with load cell. Unlike Yoganandan et al. (1996) and Begeman et al. (1996), the foot was impacted at 20 degrees dorsiflexion. The impactor loading rate was held constant at 4.6 m/s. The average failure load was 12.2 kN and ranged from 7.8 to 13.0 kN. The injuries sustained included calcaneus, talus, and tibia fractures.

Yoganandan et al. (1996) compiled 52 lower limb axial impacts from the Medical College of Wisconsin, Wayne State University (WSU), and Calpan Corporation. The three specimens without a foot from Begeman et al. (1996) were excluded. The average

specimen age was 59. The sample ranged from 27 to 85 years old. The compilation of data was utilized to develop “more definitive and quantitative relationship between biomechanical parameters such as specimen age, axial force, and injury” (Yoganandan, 1996). A statistical analysis using Weibull techniques was utilized to analyze the data. Dynamic axial force and age were found to be the most significant discriminant variables for an injury risk model. Two equations were developed to predict the probability of foot and ankle fracture. The first equation describes the probability of injury as a function of tibia axial force, and the second equation described the probability of injury as a function of tibia axial force and age (Equation 2). Figure 15 shows the probability distribution for foot and ankle injury for three age groups: 25, 45, and 65. According to Figure 15, for a 50 percentile male subject of age 45, a 10 percent and 50 percent probability of foot and ankle injury correlates with a tibia axial force of 5.4 and 7.8 kN respectively.

$$P = 1 - \left[\exp\left\{ -\left(\frac{0.0348 * A + 0.415 * F}{5.13076} \right)^{7.42582} \right\} \right] \quad \textbf{(Equation 2)}$$

where P is the probability of foot and ankle fracture; F is the peak tibia axial force, N; and A is the subject’s age.

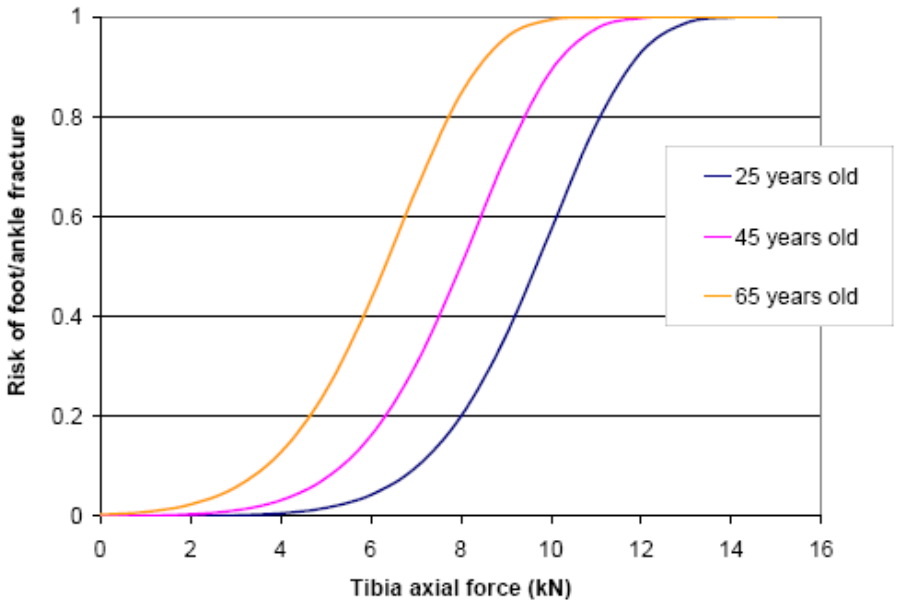

Figure 15: Yoganandan Age-Dependent Below Knee Risk Curve (reprinted from North Atlantic Treaty Organization TR-HFM-090, 2007).

Kitagawa et al. (1998) subjected 16 below knee PMHS lower limbs ranging from 59 to 83 years to dynamic axial impacts to study the effect of lower extremity entrapment in automotive frontal collisions. The tibia and fibula of each PMHS were excised at the proximal end so that the length of the specimen was 300 mm. The tibia and fibula were inserted into a custom pot device. The pot was attached to load cell, which was fixed against a table to simulate a knee that is captured by a dashboard. The Achilles tendon was placed into a tendon catcher to simulate occupant panic braking. The tendon catcher administered 1.8 to 2.0 kN of force. Precautions were taken to ensure the Achilles tendon did not slip from the catcher during the testing. An 18 kg rigid pendulum was used to impact the plantar surface of the specimen. The peak velocity ranged from 2.37 to 3.99 m/s (51 to 143 J). The centerline of the impactor

was slightly offset compared to the centerline of the tibia to cause a degree of rotational compression. Fifteen of the 16 specimen sustained a skeletal injury. The average failure load was 7.6 kN and ranged from 5.7 to 9.1 kN. Five of the 15 specimens sustained a plafond fracture and had an average failure load of 7.3 kN. Ten sustained calcaneus fractures and had an average failure load of 8.1. However, when accounting for the nearly 2.0 kN tendon preload force, the external tolerance of the tibia was approximately 5.6 kN.

3.4.2 Mid-Femur or Whole Lower Extremity Models

Schueler et al. (1995) subjected 12 full body PMHS to a series of plantar axial foot impacts. The specimens ranged from 24 to 67 years of age. The ankle was positioned in neutral position for each test. Accelerometers were mounted to each tibia. In addition, a specially designed ‘shoe’ was worn by the specimens. The shoe contained six force transducers and two accelerometers located at the sole and heel of the foot. A total of 24 plantar foot impacts (two per specimen) were conducted using a 38 kg pneumatic coaxial impactor at impact velocities ranging from 6.7 to 12.5 m/s (853 to 2969 J). The impact velocities were selected to simulate a 24 to 45 km/hr (15 to 28 mph) automotive impact. Fourteen of the 24 specimens were injured. The injuries sustained included calcaneus and talus fractures. Impact velocity, sole acceleration, sole force, and body index were found to be the most significant discriminant variables for an injury risk model. The proposed threshold for impact velocity was 9.7 m/s.

Funk et al. (2000) conducted dynamic axial impact tests on 92 PMHS lower limbs harvested at the mid femur. The functional anatomy of the knee joint and associated musculature was left intact. A piston driven pendulum impactor delivered axial impact

loads to the plantar surface of the foot. The mass and height of the pendulum were varied to produce a particular loading pulse. A 5-axis load cell and tri-axial accelerometer were mounted to the impacting footplate. A gap osteotomy was performed at the mid-tibia of each specimen removing approximately 9.0 cm from the tibia diaphysis. Each end of the removed tibia was potted with customized cups and sealed with an epoxy. An implantable tibia load cell was installed between the pots at the mid-tibia. A tri-axial angular rate sensor and accelerometer assembly was mounted to the tibia and foot. The proximal end of the mid femur was potted and attached to a bar to reproduce the original hip to knee length of the specimen.

The PMHS impacts were divided into two phases. Seventy-one instrumented specimens were positioned to simulate typical driver geometry in phase one. Occupant bracing was simulated using a spring loaded harness attached to the knee, which was activated just prior to impact. The foot position was variable and ranged from dorsi/plantarflexion and eversion/inversion angles. The impactor velocity ranged from 2.0 to 7.0 m/s (100 to 809 J).

Phase two focused on direct pure axial loading using simplified kinematics. Twenty-one PMHS were impacted with each ankle in neutral position. The specimen leg was placed horizontal and the knee was constrained to eliminate flexion upon impact. The impactor weight velocity was fixed 33 kg and 7.0 m/s (809 J) respectively. Initially, 11 tests were conducted with 16 cm of footplate intrusion. However, the intrusion length was deemed high after producing artificial fractures at the bone-pot interface. Footplate intrusion was reduced to 6.0 cm for the final ten tests. Upon plantar impact, the tibia was loaded for approximately 50 milliseconds with peak force

occurring at approximately 15 to 20 milliseconds. Fractures were produced in 32 of the 92 specimens tested. The injuries sustained included 23 calcaneus fractures, 11 malleolar fractures, ten talar fractures, four fibular fractures and three tibia plafond fractures. Twenty-nine of 32 specimens sustained an injury commonly associated with axial loading (calcaneus fractures, plafond, or talar fractures). Twelve of 32 specimens sustained an injury commonly associated with excessive rotation (malleolar or fibular fractures). Specimens sustaining malleolar or fibular fractures produced an average peak axial tibia force of 5.2 kN ranging from 2.7 to 7.9 kN. Funk et al. (2000) concluded that malleolar and fibula fractures may occur at very low ankle rotation moments when a large axial load is present.

In order to determine the impacts of occupant bracing in axial impacts, Funk et al. (2002) evaluated the effect of the Achilles tension on the fracture mode of the lower limb. Forty-three PMHS lower limbs harvested at the mid femur. The specimens had an average age of 62 and ranged from 41 to 74 years of age. The specimens were impacted using a modified experimental setup utilized in phase two of Funk et al. (2000). A piston driven pendulum impactor delivered axial impact loads to the plantar surface of the foot. A 5-axis load cell and tri-axial accelerometer were mounted to the impacting footplate. An implantable tibia load cell was installed between the pots located at the mid-tibia. Acoustic sensors were mounted to the anterior distal tibia and/or medial calcaneus to monitor time of fracture. The proximal end of the mid femur was potted and attached to a bar to reproduce the original hip to knee length of the specimen. The specimen leg was placed horizontal and the knee was constrained to eliminate flexion upon impact. Active triceps surae muscle tension was simulated in

twenty-two specimen by applying tension to the Achilles tendon using an Achilles pretension system. The plantar aspect of the foot was impacted at an approximate velocity of 5.0 m/s. Upon plantar impact, the tibia was loaded for approximately 25 milliseconds with peak force occurring at approximately eight to ten milliseconds.

Thirty specimens sustained fractures; 15 with and without Achilles pretension. The foot and ankle injuries sustained included 25 calcaneus fractures, nine talar fractures, eight lateral malleolar fractures, seven tibia plafond fractures, four medial malleolar fractures, two distal fibula fractures, and two navicular fractures. In addition, specimens also sustained 12 tibial plateau fractures, five fibular neck fractures, and two femoral condyle fractures. Among non-injured specimens, the average peak tibia fracture force was 5.2 kN and ranged from 2.2 to 9.6 kN. Among injured specimens, the average peak tibia fracture force was 5.7 kN and ranged from 2.6 to 10.8 kN. A multivariate Weibull model was developed to predict peak axial tibia force using age, gender, body mass, and Achilles force. The probability of injury model is shown in Equation 3. Figure 16 shows the probability distribution for foot and ankle injury for two age groups and genders: 45 and 65. According to Figure 16, a 50 percentile male subject of age 45, for a 10 percent and 50 percent probability of foot and ankle injury correlate with a tibia axial force of 5.9 and 8.2 kN respectively.

$$P = 1 - \left[\exp\left\{ -\exp\left[\begin{matrix} 4.99\ln(F) - 43.7 - 0.964G + 0.0793A \\ -0.0552W - 0.473AT \end{matrix} \right] \right\} \right] \quad \textbf{(Equation 3)}$$

where P is the probability of foot and ankle fracture; F is the peak tibia axial force, N; A is the subjects age; G is gender; equals zero for female and one for male; W is the body weight, kg; and AT is the Achilles tension, N.

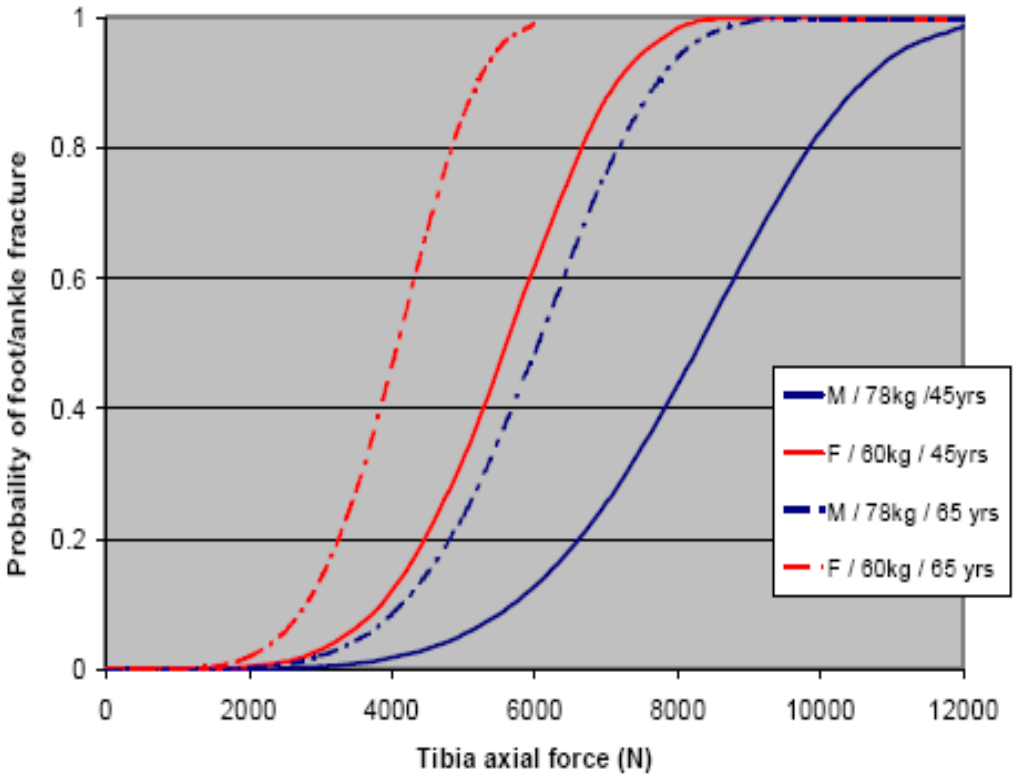

Figure 16: Funk Age-Dependent Axial Loading Risk Curve (reprinted from North Atlantic Treaty Organization TR-HFM-090, 2007).

3.4.3 Low Energy AV Landmine Lower Limb Impacts

A coordinated research effort was initiated by the NATO HFM task group (090/TG-25) to strictly define an AV landmine blast loading event for lower limb impacts (Horst, 2005). Initially, full-scale vehicle blast tests were simulated in a controlled test rig using scaled detonations (Dosquet, 2004). The Test Rig for Occupant Safety Systems (TROSS™) utilizes scaled charges to produce reproducible blast loads that propel an elastic deformable floorplate towards the lower limb of a biomechanical surrogate (Dosquet, 2004). The interior of the TROSS™ is representative of a military vehicle crew cabin. An occupant, as simulated by a full body ATD biomechanical

surrogate, is seated and belted. The lower limbs of the surrogate are set on the moveable floorplate. A series of tests were conducted to characterize three relatively low energy AV landmine blast events. Each event was characterized using floorplate acceleration, velocity, and dynamic displacement measurements. The effect on the vehicle occupant was measured using the tibia axial force measured by a Hybrid III and THOR-Lx biomechanical lower extremity surrogate. A summary of the Hybrid III test results are shown in Table 5.

Table 5: Simulated Low Energy AV Landmine Loading Characteristics (reprinted from Barbir 2005).

Condition	Explosive mass (g)	Boot/Foot	Plate displacement (mm)	Tibia Force (N)
1	100	Foot	12.3	5,970
1	100	Boot	12.6	3,709
2	200	Foot	21.8	10,740
2	200	Boot	20.5	7,000
3	300	Boot	27.1	9,984

The three parametric floorplate impact conditions were carefully replicated and validated in a laboratory-scale setup using a Hybrid III (Barbir, 2005). Specifically, force-time trajectories measured by the Hybrid III lower limb in the TROSS™ for each condition were replicated on the laboratory setup by tuning impact conditions. The laboratory-scale setup utilized a piston-driven linear impactor to propel a stainless steel footplate into the plantar aspect of the Hybrid III lower extremity biomechanical surrogate foot at a targeted velocity. In addition to supplying a desired loading rate, the impactor is designed to simulate floorplate intrusion. A foot displacement of 12 to 27

millimeters was identified during the Hybrid III laboratory-to-bench scale correlation and used for each condition (Barbir, 2005).

After establishing AV landmine parametric loading rates in the laboratory-scale setup, Barbir (2005) ran a series of tests measuring the biomechanical responses of PMHS at two AV blast loading rates. Ten instrumented PMHS lower limbs were axially impacted at two loading rates correlating with Condition 2 and 3 TROSS™ impact severity listed in Table 5. The lower limbs of all specimens were harvested at the femur approximately 20 centimeters from the knee. The specimen was potted into a device designed to interface with the Hybrid III surrogate. A six-axis tibia load cell was implanted into the mid-shaft of the tibia. Five PMHS lower limbs were impacted at Condition 2 loading rates producing an average tibia axial force of 3.2 kN. The tibia axial compression of the five specimens ranged from 2.3 kN to 4.4 kN. The tibia was loaded for approximately ten to 15 milliseconds duration. None of the PMHS specimen sustained skeletal injury (Barbir, 2005).

Similarly, five PMHS lower limbs were impacted at Condition 3 loading rates producing an average tibia axial force of 4.5 kN. The tibia axial compression of the five specimens ranged from 3.3 kN to 6.4 kN. Again, tibia loading last approximately ten to 15 milliseconds. One PMHS specimen, impacted at Condition 3 loading rates, sustained a plafond fracture. A second PMHS specimen sustained a fracture at the tibia pot and was deemed artificial (Barbir, 2005).

The average PMHS lower limb tibia axial force of 4.5 kN was less than the 5.4 kN tolerance limits specified by Yoganandan et al. (1996) foot and ankle injury risk model for 45 year old male subjects. The impact severity utilized by Barbir (2005) was not

severe enough to cause a high probability of lower limb fractures. Further research is needed to evaluate cadaveric lower limb injury risk at more severe AV blast axial impact conditions (Barbir, 2005).

3.5 Currently Utilized Injury Criteria for Blast Injury

Military defense agencies have adopted available lower extremity injury criteria to define axial loading limits for AV blast events. These injury criteria are utilized to design and evaluate military vehicle protection systems. The adopted injury criteria and associated tolerance limits are specified by the country-specific Defense agency. Currently, there is no single accepted lower extremity injury criterion for an axial blast threat. The following sections highlight several conflicting lower extremity injury criteria standards.

3.5.1 North Atlantic Treaty Organization (NATO) Standard

NATO-affiliated military organizations typically qualify the protection level of a vehicle to Standardization Agreement (STANAG) 4569 and NATO Allied Engineer Publication 55 (AEP-55) Volume 2. AEP-55 (volume two) describes test procedures and injury criteria for evaluating military vehicle protection systems against grenade and blast mine threats. The lower extremity injury criterion is specified for peak lower tibia axial compression force. The tolerance value recommended is derived from Yoganandan et al. (1996); 5.4 kN correlating with a 10 percent risk of AIS two injury.

In 2001, the NATO HFM task group (090/TG-25) was established to identify suitable injury risk models to assess occupant injury probability from AV landmine effects (NATO, 2007). The task group reviewed all open source literature, particularly

from the automotive industry, and proposed a first standard on AV blast injury criteria and tolerance levels. Although some body region injury models were deemed appropriate, other were deemed immature for blast loading applications.

The task group thoroughly reviewed currently available lower extremity injury risk models. Yoganandan et al. (1996) and Funk et al. (2002) risk model were considered the most appropriate given their relatively large sample size and ability to factor in age. Age is considered a significant factor as the majority of active military infantry troops are below the age of 35. In contrast, most injury risk models are developed based on PMHS specimen data with an average age generally above 65. Considering bone density and strength strongly correlate with age, the age difference would suggest PMHS injury corridors are largely conservative. Ultimately, the Yoganandan et al. (1996) model was chosen because “it was developed with a larger number of specimens with wider age range” (NATO, 2007).

Finally, the task group outlined the need to (1) define lower leg loading rates typical of AV landmine events; and (2) establish a military-specific lower extremity injury criterion.

3.5.2 United States Standards

In addition to the NATO Standardization Agreement (STANAG) qualification requirements, the U.S. military implements performance requirements and verification procedures to ensure vehicle crashworthiness and mine blast protection. Two documents are most commonly cited by military vehicle system specifications and procurement documents when discussing injury tolerance or underbody protection metrics: (a) Occupant Crash Protection Handbook (Department of Army, 2000); and (b)

Medical Evaluation of Nonfragment Injury Effects in Armored Vehicle Live Fire Tests (Walter Reid Army Institute of Research, 1989).

The Crash Occupant Handbook appears to be utilized extensively across the Department of Defense in procurement documents, vehicle specifications, and testing protocols. However, the handbook is critically flawed with respect to lower extremity injury tolerances for AV mine effects.

The Occupant Crash Protection Handbook specifies two criteria for tibia loading. The first criterion is specified as a “femur or tibia axial compression force” (Department of Army, 2000). A compressive force tolerance value of 9,074 N and 7,562 N is specified for zero and ten millisecond pulse durations respectively. The assessment reference values are derived from Mertz (1994) for potential fracture of the femur, patella, or pelvis. The handbook does not explain why these values are used to assess tibia compression injury tolerance. Furthermore, the tolerance values proposed by Mertz (1994) for the femur, patella, and pelvis were dispelled by the FMVSS in favor of a 10.0 kN tolerance level.

The second criterion is the tibia axial force combined with tibia bending moment (Department of Army, 2000). Again, this criterion is derived from Mertz (1994) and is commonly referred to as the TI criterion. The tolerance value specified is presented in Equation 1. The TI criterion was later revised by Kuppa et al. (2001) after publication of the handbook. As discussed previously, a rotational injury criterion is not appropriate for AV blast impacts considering the loading is predominately axial.

In 1989, Walter Reed Army Institute of Research (WRAIR) issued the Medical Evaluation of Nonfragment Injury Effects in Armored Vehicle Live Fire Tests report

detailing injury criteria for armored vehicle live fire tests. Although the report is not as extensively utilized as the Department of Army Occupant Crash Handbook currently, references to the report are often found in Department of Defense procurement documents and vehicle specifications prior to the year 2000 (Department of Army, Light Tactical Vehicle System Specification, 1997).

Similar to the Occupant Crash Handbook, the WRAIR proposes a single lower extremity injury criterion for both the femur and tibia. The criterion states that the axial compressive force should not exceed 5.6 kN and 4.0 kN for zero and ten millisecond pulse durations respectively. The injury tolerance is “based on the strength of the tibia and femur under various loading modes” (WRAIR, 1989). The report references the work performed by Melvin et al. (1975) and Powell et al. (1975) to define axial compression tolerances of the knee and femur. However, these publications make no mention directly or indirectly of these tolerance limits. Additionally, work performed by Viano et al. (1977) utilized the impact data from Melvin et al. (1975) and Powell et al. (1975) to suggest the femur could tolerate an instantaneous axial load of 23.1 kN.

3.6 Discussion

The injury tolerance of the lower extremity is dependent on a number of variables. Foremost, a specific loading mechanism must be defined and representative of the actual risk. Several loading mechanisms may occur in frontal automotive vehicle collisions. Occupants may be loaded longitudinally by the interior cabin resulting in axial loads to the knee and femur and perpendicular loads to the tibia and fibula. Occupants may also be loaded by the footplate or pedal projecting axial loads to the plantar aspect of the foot. The later, axial loading of the plantar aspect of the foot, is

most representative of an AV explosive device blast. Consequently, injury risk models for the upper leg appear to be inappropriate for a lower extremity injury criterion for military vehicle occupants involved in underbelly explosive blast events.

Following the same rationale, injury models pertaining to the rotational effects of the foot and ankle complex appear to be inappropriate as well. Although some rotational loading may occur from an AV blast impact, the magnitude of rotational loading is minimal in comparison to pure axial loading. Furthermore, Funk et al. (2000) concluded that lower leg fracture patterns that are typical of rotational effects may also occur with high energy pure axial loading. As such, the primary requirement of an AV blast impact injury criterion is the development of an axial loading threshold.

Injury risk models developed by Yoganandan et al. (1996), Begeman et al. (1996), Schueler et al. (1995), Funk et al. (2002), Kitagawa et al. (1998) and Barbir (2005) primarily focus on dynamic axial loading of the foot, ankle, tibia, and fibula. An important methodological difference between these studies is the technique used to measure axial loads. Below knee techniques, such as Yoganandan et al. (1996), Begeman et al. (1996), Roberts et al. (1993), and Kitagawa et al. (1998) potted the tibia and fibula together at the mid-shaft or proximally. Relative motion of the tibia and fibula was not allowed. The combined load transmitted through the tibia and fibula was measured by a load cell mounted to the tibia/fibula pot. The tibia and fibula loading components cannot be decomposed. Furthermore, the knee joint was uninvolved removing any natural motion of the tibia and fibula about the joint. In contrast, Funk et al. (2002) and Barbir (2005) implanted a tibia load cell directly into the mid-shaft of the tibia. The knee joint or fibula was not compromised. Finally, Schueler et al. (1995) did

not measure axial compression through the tibia in any fashion. Generally speaking, these studies observed 20 to 30 percent higher tibia axial force failure loads in below knee impacts than mid-femur or full lower extremity impacts.

Yoganandan et al. (1996), Begeman et al. (1996), Roberts et al. (1993), Kitagaway et al. (1998), Schueler et al. (1995), and Funk et al. (2002) all reported peak axial loads at the impactor footplate-foot interface. However, loads measured at the impactor footplate may exceed loads measured by a tibia load cell by as much as 50 percent (without Achilles tension) (Funk, 2002). Since currently available ATD or biomechanical surrogates cannot measure footplate force, it is not a useful injury parameter in AV mine applications.

Another critical methodological difference between these studies is the magnitude of loading rates (summarized in Table 6 and graphed in Figures 17-18). The peak impact rates used in Yoganandan et al. (1996) and Begeman et al. (1996) were 7.6 and 9.2 m/s (722 and 690 J) respectively. Kitagawa et al. (1998) impact rates were below 4.0 m/s (143 J). Funk et al. (2002) impact rates were held constant at 5.0 m/s. Schueler et al. (1995) impacted at rates ranging from 6.7 to 12.5 m/s (853 and 2969 J). Although the impact conditions utilized by Barbir (2005) were established by simulated AV landmine blasts, the loading rates are relatively low severity when compared to Schueler. Barbir PMHS impacts ranged from 3.8 to 7.1 m/s (265 to 926 J). The minimum kinetic energy utilized by Schueler exceeded the maximum energies of Yoganandan and Begeman. Loading rates utilized by Schueler are more representative of impact energies in AV explosive device impacts per Wang et al. (2001). In

comparison, automotive impacts are typically simulated at 2.0 to 6.0 m/s (Owens, 2001).

Table 6: Comparison of Axial Loading Lower Extremity Injury Risk Models.

	Study	Impactor Velocity (m/s)		Impactor KE (J)		# of PMHS Impacts
		Lower	Upper	Lower	Upper	
Below Knee	Yoganandan (1996)	3.4	7.6	145	722	26
	Begeman (1996)	4	9.2	130	690	17
	Kitagawa (1998)	2.37	3.99	51	143	16
	Roberts (1993)	---	4.6	---	---	9
Mid Femur	Funk (2000)	---	7	---	809	21
	Funk (2002)	---	5	---	413	43
	Barbir (2005)	3.8	7.1	265	926	10
Whole Cadaver	Schueler (1995)	6.7	12.5	853	2,969	24

Furthermore, the 20 to 60 milliseconds duration of tibia axial force utilized in the Yoganandan et al. (1996), Begeman et al. (1996), Roberts et al. (1993), and Funk et al. (2002) is representative of low to high speed automotive impacts. In contrast, the duration of a tibia axial force pulse in an AV explosive device impact is less than ten milliseconds (NATO, 2007). Although Barbir (2005) obtained impact durations lasting between five and 15 ms, the relatively low severity AV landmine impact conditions utilized failed to populate a significant number of injuries to establish a risk model. Additional PMHS impacts are required to establish a lower limb tolerance threshold for military vehicle occupants involved in blast impacts. Hence, the suitability of any of the

aforementioned lower limb risk models for military AV explosive blast impacts is questionable and must be validated.

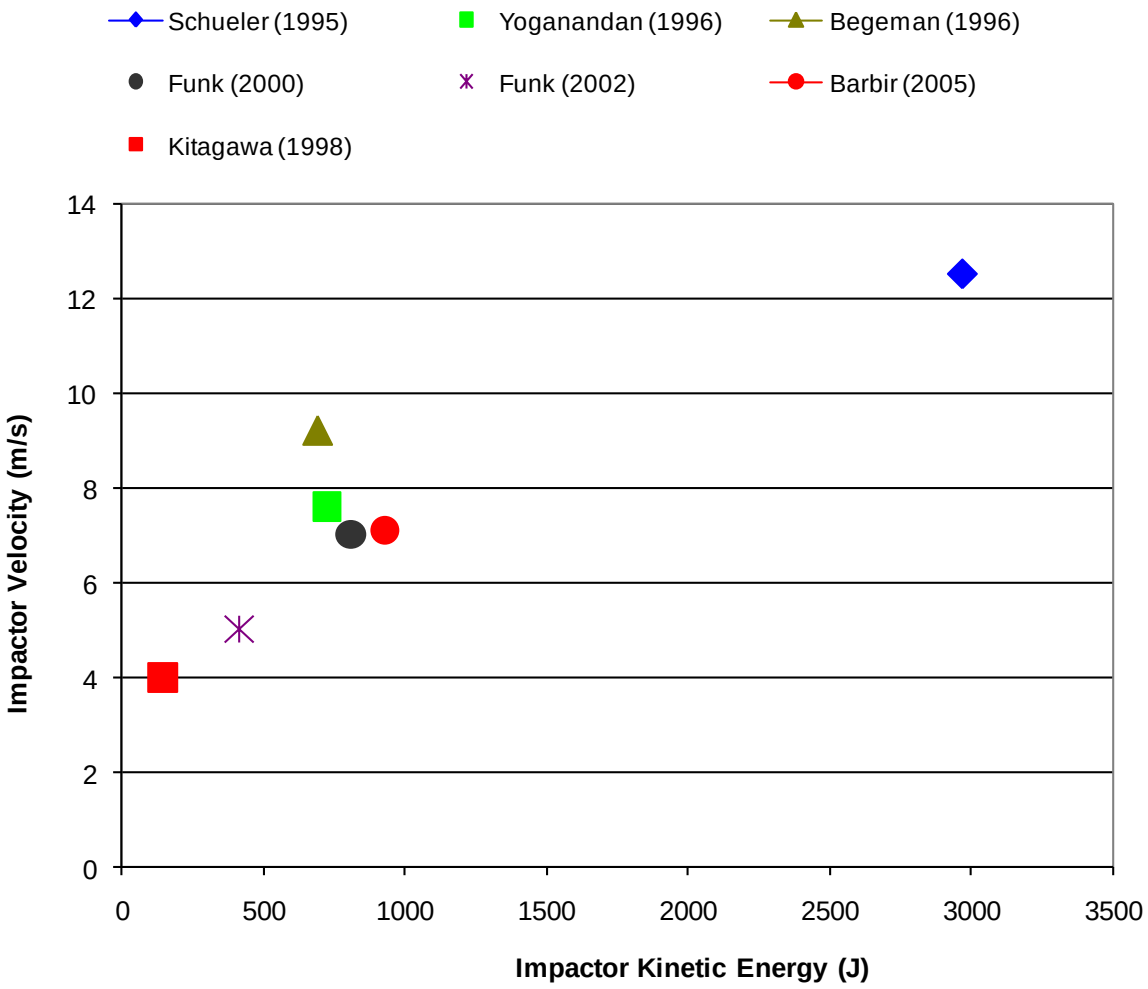

Figure 17: Comparison of Peak Loading Severities Utilized in Lower Extremity Injury Risk Models.

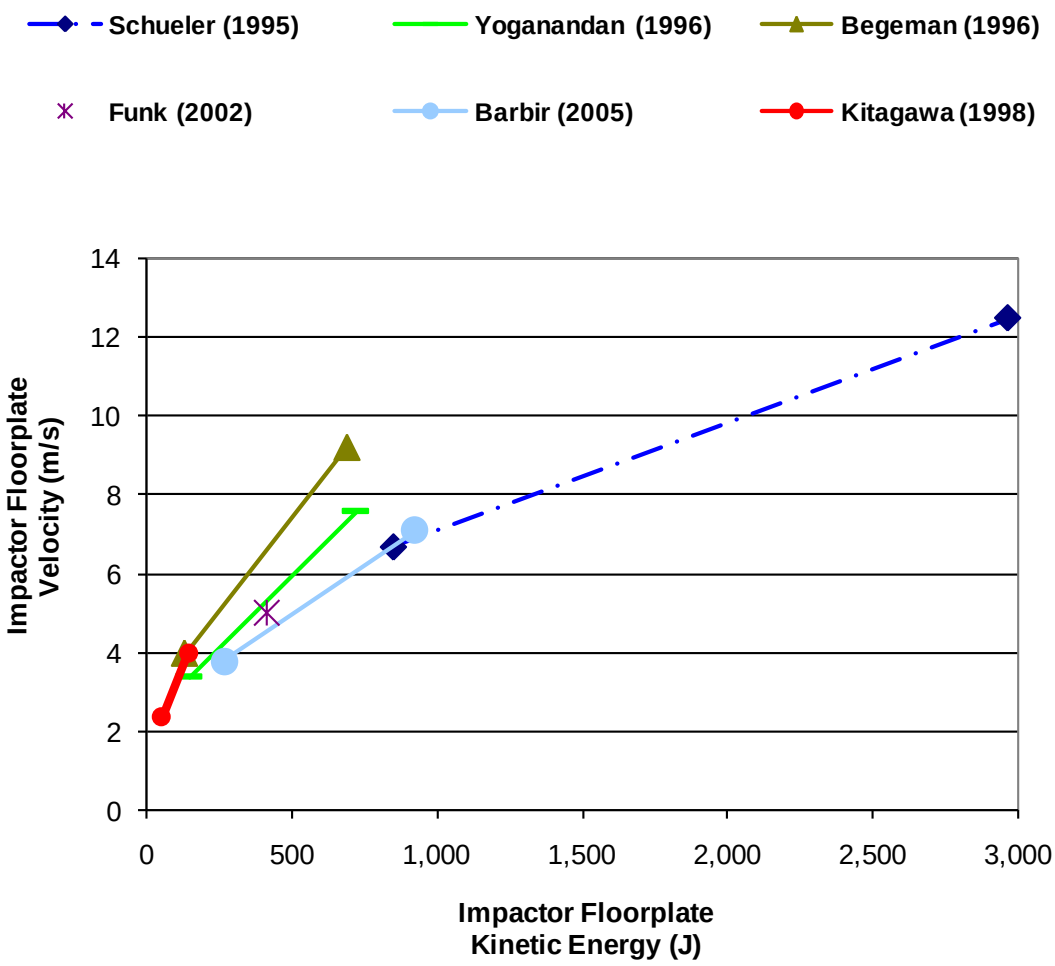

Figure 18: Comparison of Minimum and Maximum Loading Severities Utilized in Lower Extremity Injury Risk Models.

CHAPTER 4

DEVELOPMENT OF LOWER EXTREMITY INJURY CRITERIA UTILIZING CADAVERIC SPECIMEN

Portions of this chapter were published in the Stapp Car Crash Journal:

McKay, B.J. and Bir, C.A. (2009) “Lower Extremity Injury Criteria for Evaluating Military Vehicle Occupant Injury in Underbelly Blast Events,” Stapp Car Crash Journal. Nov; 53: 229-49.

4.1 Introduction

A military vehicle protection system is evaluated in a full-scale landmine blast test to determine the protection afforded to vehicle occupants against a specific threat. The effectiveness of a protection system is determined by comparing the biomechanical response measured by an ATD surrogate to established human injury tolerances. However, neither the currently available lower extremity injury risk models nor the biomechanical surrogates were developed for high rate impact conditions typical of blast events.

Barbir (2005) made the first attempt to impact PMHS lower extremity specimens at AV landmine axial loading rates. However, of the ten PMHS lower limbs impacted only one specimen was injured. Although Barbir (2005) replicated AV landmine floorplate impact conditions, the severity failed to consistently produce injury. Additional PMHS impacts at injurious loading levels are required to establish a lower limb tolerance threshold for military vehicle occupants. This study reports on additional simulated AV blast impact tests using instrumented PMHS.

4.2 Methodology

The current effort was initiated to develop lower extremity injury criteria for a military vehicle occupant involved in an AV underbelly blast impact. This effort focused on populating a PMHS impact dataset using floorplate impact conditions typical of an AV landmine and in excess of those used by Barbir (2005). The study also identified high severity axial blast impact conditions representative of modern combat threats.

4.2.1 Establishment of Blast Impact Severity

In order to establish injurious AV landmine loading levels, full-scale military vehicle blast test data were reviewed for a range of blast magnitudes. Full-scale, live fire military vehicle tests are routinely conducted by the U.S. Military. These tests are utilized to evaluate legacy and novel vehicle protection systems as well as ad-hoc blast mitigation technologies (including armor kits, passenger restraint systems, PPE, etcetera). From 2003 to 2008, U.S. Army Tank-Automotive and Armaments Command (TACOM) and U.S. Army Tank-Automotive Research, Development and Engineering Center (TARDEC), the primary integrators of advanced ground vehicle platform technologies for the U.S. Military, partnered with the U.S. Army Aberdeen Test Center (ATC) to perform a series of full-scale, live fire military vehicle tests to evaluate vehicle protection systems against blast threats typical of OIF and OEF. These blast tests were conducted on U.S. Military vehicles with varying levels of armored protection over a range of blast magnitudes. The vehicles were instrumented with multiple accelerometers strategically mounted to the vehicle cabin, floorboard, hull, and vertical support beams. One or more Hybrid III ATDs were positioned within the vehicle cabin to represent vehicle occupant(s). The number and orientation of HIII ATDs utilized in

the tests were dependent on the vehicle and test protocol. A HIII ATD was equipped with the standard instrumentation required by STANAG 4569 (including tibia load cells). Often, additional accelerometers were mounted to the HIII ATD to collect additional information. Tests conducted at ATC during this program typically utilized an accelerometer mounted at the mid-tibia to monitor the direction of lower extremity movement post impact. Select data collected from vehicle blast tests, particularly vehicle floorplate velocity and ATD Hybrid III biomechanical response data were reviewed. Due to the sensitive nature of the data the information furnished by TARDEC did not contain any information pertaining to the vehicle identity, threat identity, armor system identity, test motives, or vehicle performance. The orientation of the Hybrid III devices within the vehicle and location of the vehicle instrumentation was provided.

Full-scale blast test data furnished by TACOM/TARDEC were thoroughly analyzed. Vehicle accelerometer and mid-tibia accelerometer data were utilized to confirm an axial AV impact. The most accurate indicator of impact severity was shown to be floorboard velocity measured near the primary impact point. Review of the data revealed three distinct levels of impact severity, which correlated with floorplate velocities of 7.0, 10.0, and 12.0 m/s. These velocities reflect the high rate transfer of energy from the vehicle floorplate to the occupant lower extremity producing high amplitude, short duration axial loads.

Similarly, high rate floorplate velocities were also measured by the TROSS™ in high severity explosive blast testing. The two most severe peak floorplate velocities measured by the TROSS™ were 10.4 and 12.3 m/s for TROSS™ condition 5 and 6

respectively (Dosquet, 2008). These velocities produce a kinetic energy of 1920 J (condition 5) and 2765 J (condition 6).

Based on TARDEC and TROSS™ data, three incrementally severe experimental impact conditions were established. The impact conditions, termed WSU Condition 1, 2, and 3 (abbreviated as WSU C1, WSU C2, WSU C3), targeted an impacting floorplate velocity of 7.0, 10.0, and 12.0 m/s respectively (900, 1837, 2645 J). As illustrated in Figure 19, the range of floorplate velocity and kinetic energy furnished by TARDEC and TROSS™ and utilized in this study fall within the lower limb impact conditions utilized by Barbir (2005) and Schueler et al. (1995). Furthermore, the upper floorplate velocity boundary of 12 m/s aligns with Wang et al. (2001) who reported a medium sized armored vehicle floorplate might exceed 12 m/s following an AV landmine underbelly blast.

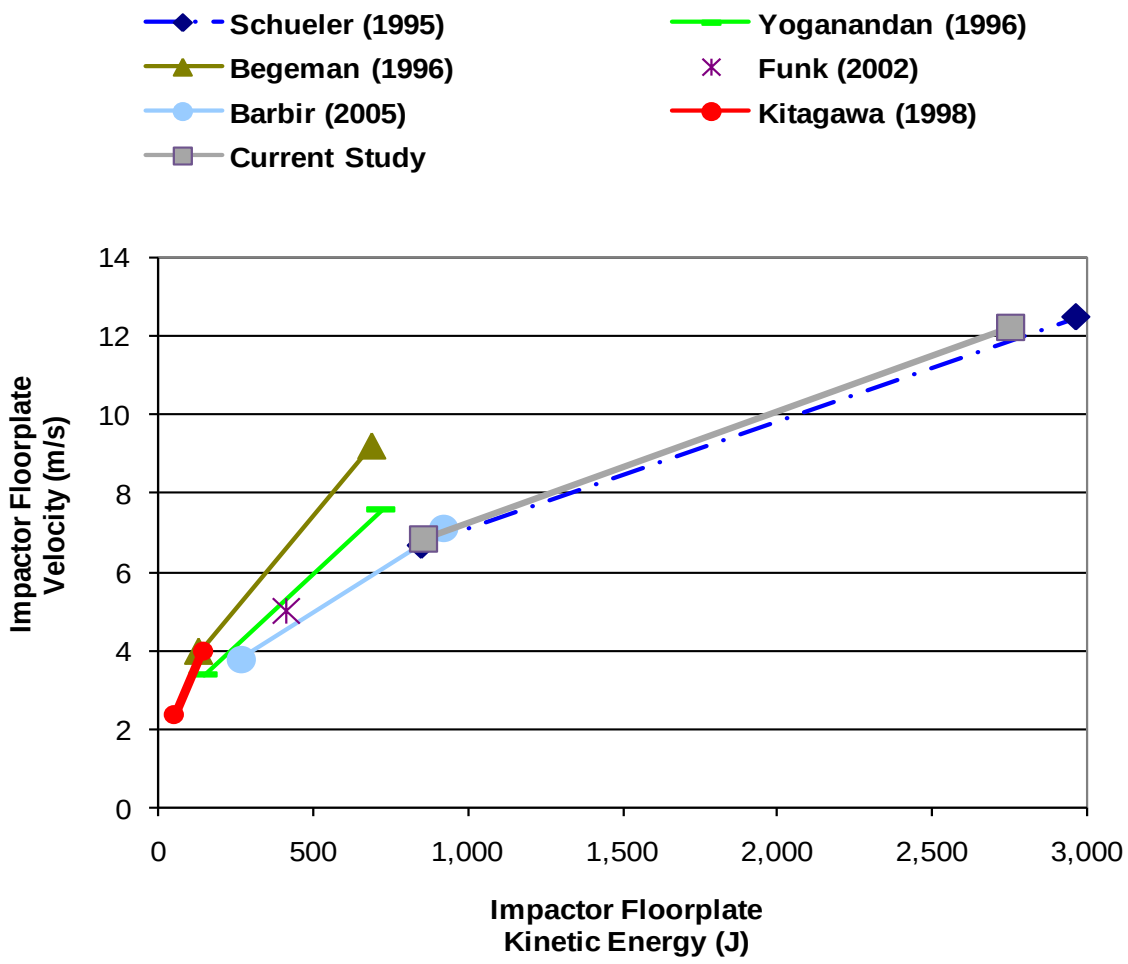

Figure 19: Comparison of Lower Limb Injury Risk Model Loading Rates.

4.2.2 Test Setup

Following an AV underbelly blast, high amplitude and short duration inertial loads are transmitted from the floorplate directly to the foot-ankle-tibia complex of the vehicle occupant loading the lower limb. This transfer of inertial loads to the lower limb was simulated in a laboratory-scale setup using a high rate linear impactor. The impactor was utilized to propel a stainless steel footplate and cylinder shaft into the plantar aspect of a PMHS lower limb at a targeted velocity.

The laboratory-scale setup, shown in Figure 20, simulates a vehicle floorplate using a 30 x 30 x 4.0 cm stainless steel solid mass weighing 7.4 kg. The footplate is fastened to a 29.3 kg cylindrical shaft (10.0 cm outer diameter x 150 cm length) providing a total free body mass of 36.7 kg. The floorplate and shaft are propelled to a targeted velocity by an air operated piston-driven linear impactor. The impactor system is energized by charging helium through a regulator valve into an air piston. After a desired pressure is achieved in the air piston, the piston is fired launching a pendulum into the tail end of the cylindrical shaft. The cylindrical shaft and footplate rapidly accelerate following impact with the pendulum to achieve a targeted velocity. The floorplate/shaft travel up to 140 cm in free flight during a launch.

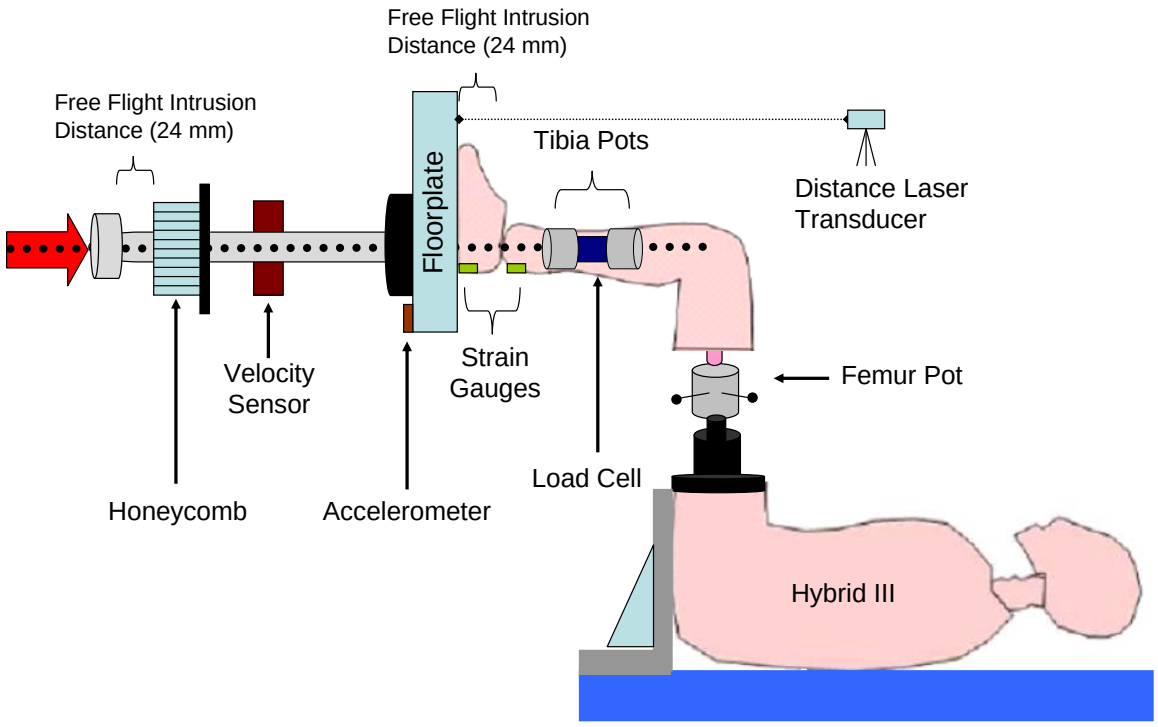

Figure 20: Air Piston Driven Linear Impactor.

WSU Condition 1, 2, and 3 floorplate velocities were achieved by pressurizing the air piston to 90, 180, and 220 psi respectively. In addition to supplying a desired loading rate, the setup simulates the elastic or plastic intrusion of a vehicle floorplate. Footplate intrusion corresponds to the instantaneous displacement of the foot-ankle-tibia from its baseline position. Approximately 24 mm of floorboard intrusion was targeted based on measurements from the TROSS™ simulations for a severe blast charges (Dosquet, 2004). After the targeted intrusion is reached, the impactor is rapidly decelerated using an aluminum honeycomb material. The honeycomb allows a consistent magnitude of plastic compression (or crush), which enables the impactor footplate to drive past the target intrusion displacement at a significantly lower loading rate.

4.2.3 PMHS Preparation

Several techniques have been utilized to measure the axial loading and moment of inertia of a cadaver lower limb. In early lower limb injury risk models, researchers fixed the tibia and fibula together at the mid-shaft using a bone pot. Then a load cell was secured proximal of the pot (Begeman, 1996 and Yoganandan, 1996). Several drawbacks are associated with this technique. Potting the tibia and fibula together restricts the movement and distribution of load during the event. In addition, the knee is completely removed from the loading thereby reducing biofidelity.

More recent lower limb injury risk models implant a load cell at the midshaft of the tibia (Klopp, 1997; Funk, 2000; Funk, 2002; Dean-El, 2003; Barbir, 2005). The knee is left intact. The fibula may be left intact, removed, or instrumented. If a fibula load cell is not implanted, approximately 10 to 15 percent of the total axial loading may be left

unmeasured (as the tibia is responsible for transferring between 85 and 90 percent of the loading depending on the orientation of the extremity; Moore, 2002). A load cell may be carefully implanted at the proximal end of the fibula (Funk, 2002). In practice, it may not be feasible to implant both a tibia and fibula load cell due to the limited surface area of a particular specimen. Due to the confined space limitations, a fibula load cell is typically reserved for inversion and eversion lower limb injury evaluations (Funk, 2002).

Considering the focus of this study is evaluating the human biomechanical response to pure axial loading it was determined measuring load at the mid-shaft of the tibia provided the most valuable data. Tibia load measurements could be collected without jeopardizing the functional anatomy of the knee joint and musculature of the lower limb. Furthermore, measurements at the tibia mid-shaft could be compared to the tibia load cell measurements of the Hybrid III and THOR-Lx biomechanical surrogates.

Eighteen PMHS lower extremities were used in this study. Approval was obtained from the Wayne State University Human Investigation Committee (HIC) review board prior to the commencement of this study. The average age of the PMHS is 68 years old and ranged from 44 to 80 years old. The PMHS were screened for transmissible diseases prior to preparation. The fresh-frozen specimens were allowed to thaw. Bone density dual energy x-ray absorptiometry (DEXA) data were reviewed to screen for osteoporosis. Radiographs of the extremity were taken to screen for pre-existing conditions and included views of the femur, knee, tibia, superior/inferior and anterior/posterior of the foot and ankle. Anthropometry measurements of the PMHS specimens, summarized in Table B1 of Appendix B, were taken before and after instrumentation. PMHS preparation and instrumentation were completed over a three

day period in three to four hour increments. Care was taken to ensure the specimen was properly preserved during the process.

A six-axis tibia load cell (Denton, Inc, model 3786J) was implanted at the mid-shaft of each PMHS lower extremity that was tested using the guidelines of Funk et al. (2002) and Dean-El et al. (2003).

Initially, each lower extremity was removed from the full PMHS by disarticulating the femur from the acetabulum. This was accomplished by making an incision at the medial portion of the pubic tubercle and continuing transversely along the inguinal ligament penetrating all soft tissue. The iliofemoral ligament, pubofemoral ligament, and the ligament at the head of the femur were severed. The lower extremity was weighed to establish a baseline for normalization. Subsequently, an incision was made in the upper leg approximately ten centimeters distal to the knee. All soft tissue proximal to this incision point was removed including the periosteum of the femur. The musculature and functionality of the knee were left intact. The specimen was harvested at the femur approximately 20 cm distal to the knee. Bone marrow from the femur was removed and the bone was dried with the aid of isopropyl alcohol. A specially designed femur pot, designed to interface with the Hybrid III surrogate at the mid thigh, was placed over the distal femur (Figure 21). Four screws were tightened to hold the femur in place. Dyna-Cast, a two part polyurethane casting material was injected into the femur pot using a syringe. The Dyna-Cast was allowed to cure undisturbed for 12 hours to form a secure cast that fixes the bone to the femur pot. The formed cast prevented motion or rotation of the bone within the pot.

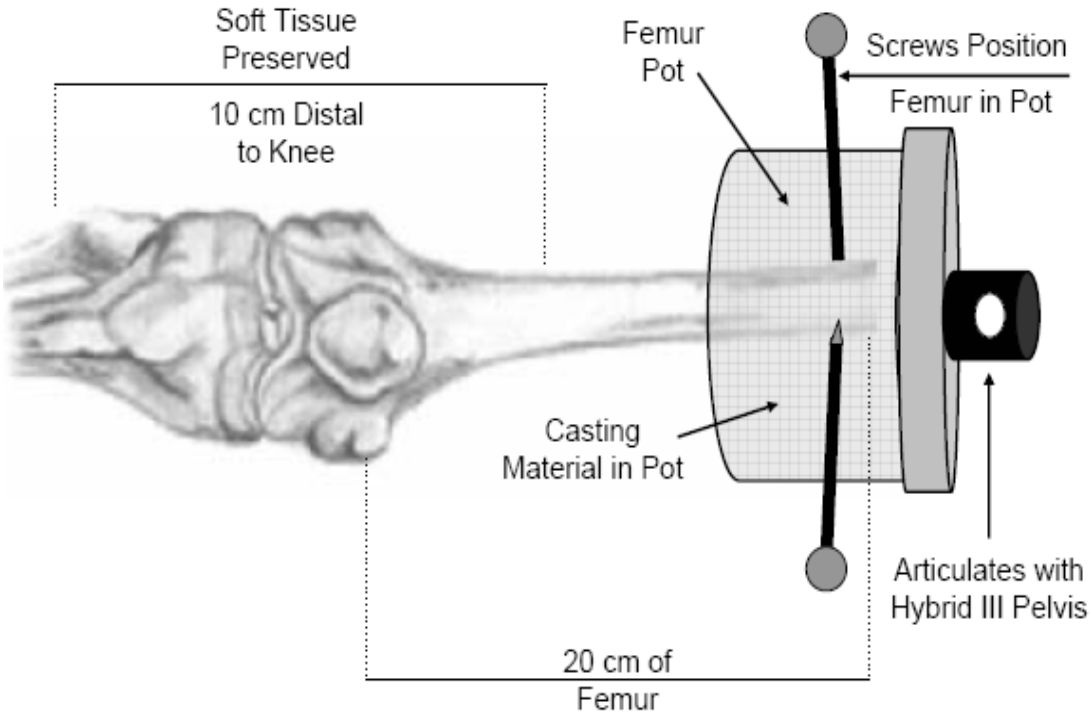

Figure 21: Femur Pot Assembly.

An incision was made in the lower leg along the diaphysis of the tibia. The incision originated and terminated approximately seven to ten centimeters from the proximal and distal ends of the tibia respectively depending on the size of the specimen. A transverse incision was made at the proximal and distal tibia to expose the soft tissue at these locations. The dermis was dissected to create medial and lateral skin flaps (Figure 22). Soft tissue attachments, including the interosseus membrane, to the bone were removed by dissection. Care was taken to minimize the disruption of the leg musculature and functional anatomy.

Figure 22: Exposure of Tibia.

A cylindrical positioning device made of transparent plastic was placed around the exposed tibia. The device was machined with eight holes to accommodate four 0.476 centimeter (3/16 inch) diameter drill bits. Two drill bits were driven through the bone from the medial surface to the lateral surface of the tibia. Similarly, two drill bits were driven through the bone from the anterior surface to the posterior surface of the tibia (Figure 23).

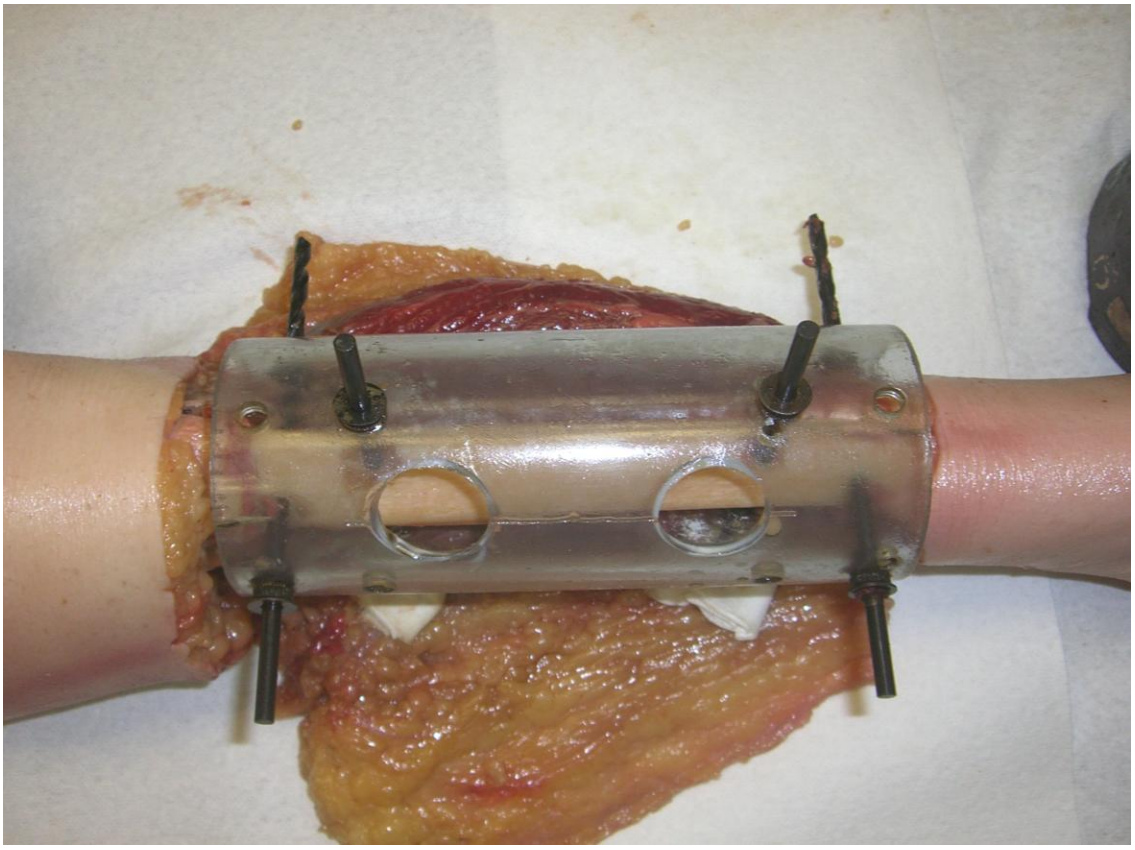

Figure 23: Positioning Jig with Drill Bits through Tibia.

Subsequently, the drill bits and positioning device were removed from the tibia leaving two sets of anterior-posterior holes and medial-lateral holes (Figure 24, Left). A gap osteotomy was performed along the diaphysis of the tibia removing 9.0 centimeter of the tibia and leaving the drilled holes unharmed (Figure 24, Right). The tibia, in essence, was sectioned into the upper and lower tibia. Local bone marrow was removed from the upper and lower tibia and the bone was dried with the aid of isopropyl alcohol. A cylindrical tibia pot, measuring eight millimeter inner diameter and 63.5 milimeter depth, was installed at the distal end of the upper tibia section and the proximal end of the lower tibia section. Holes from the tibia pots were aligned to match

the holes drilled using the positioning device. Two clevis pins, running through the anterior-posterior holes and medial-lateral holes, were inserted through each pot in order to fasten the pot to the tibia. Cotter pins were secured using clevis pins in place. Figure 25 (Left) illustrates the configuration of the cylindrical pots. A six-axis tibia load cell was installed in between the tibia pots. Four screws from the distal portion of the upper tibia pot and proximal portion of the lower tibia pot secured the load cell in place (Figure 25, Right).

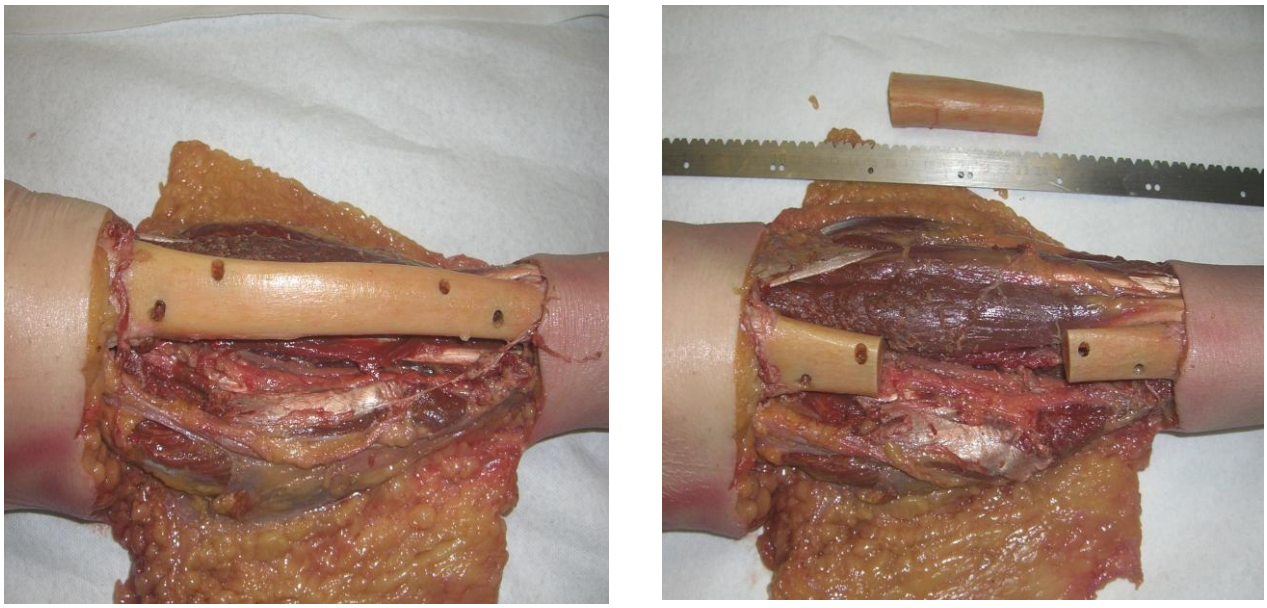

Figure 24: Left: Completion of Load Cell Pre-Positioning. Right: Gap Osteotomy.

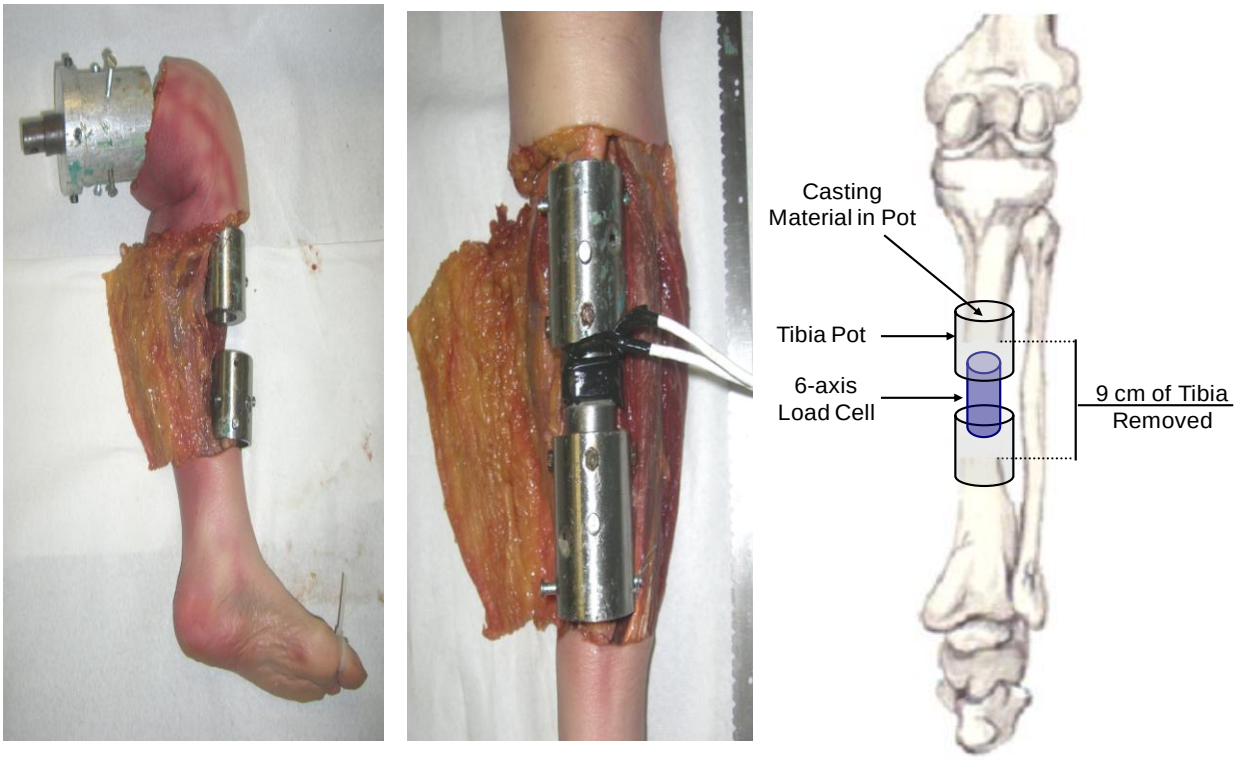

Figure 25: Left: Installation of the Tibia Pots. Middle: Implantation of Six-Axis Tibia Load Cell. Right: Illustration of Tibia Instrumentation.

Dyna-Cast was injected into the upper and lower tibia pot using a syringe. A rubber seal on the tibia pot prevented the Dyna-Cast from contacting the load cell. The Dyna-Cast was allowed to cure undisturbed for 12 hours to form a secure cast that fixes the bone to the tibia pot. The formed cast prevented motion or rotation of the bone within the pot. The tibia pots and the load cell moved as one fixed object similar to an undisturbed tibia.

Two 14 x 8.0 millimeter rosette strain gages were attached to the medial aspect of the calcaneus and to the medial surface of the tibia located proximal to the medial malleolus and distal to the lower tibia pot (Figure 26, Left). Each rosette gauge measures three independent components of plane strain: ε_a, ε_b, and ε_c. The surface of

the bone was exposed by removing a sufficient portion of soft tissue (roughly two to three times the size of the strain gage). The bone was thoroughly dried with the aid of isopropyl alcohol before several drops of cyanoacrylate was used to prepare the surface of the gage attachment. A catalytic adhesive was applied to the strain gage and then pressed against the cyanoacrylate for 60 seconds. Silicone was used to coat the strain gage to further secure and shield the gage mount.

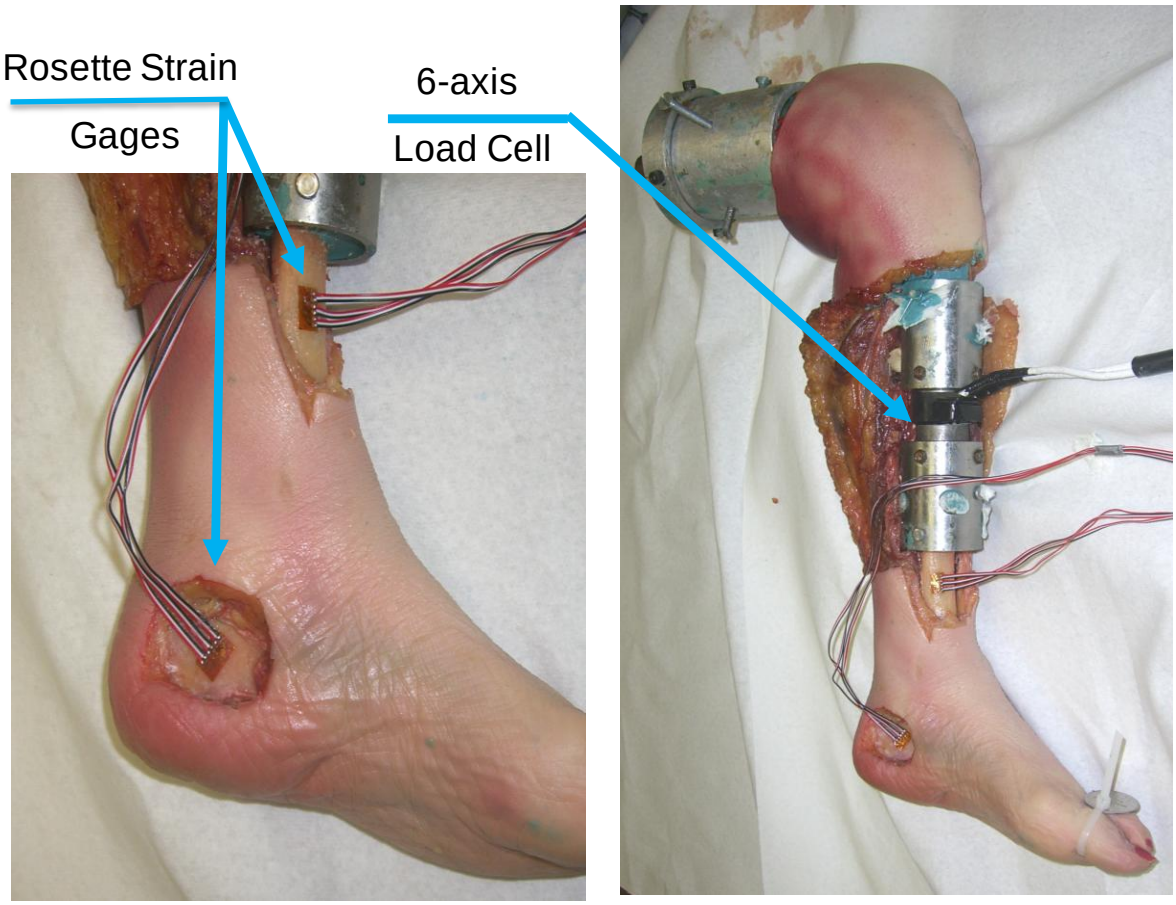

Figure 26: Left: Strain Gage Attachments. Right: Fully Instrumented Left Limb of PMHS.

The skin flaps were sutured together and the leg was wrapped with a flexible bandage. Radiographs of the instrumented lower extremity were taken to confirm the integrity of the fibula and proper alignment of the upper and lower tibia sections. Although great care was taken not to disturb the anatomy and functionality of the PMHS lower limb during the preparation and instrumentation process, the mass of the specimen was affected by the procedure. Soft tissue from the specimen was removed to accommodate the installation of the femur pot and tibia pots. Mass was essentially added to the specimen in the form of equipment, instrumentation, and cast material. The mass of the post-preparation PMHS lower limb increased for smaller specimen and decreased for larger specimen. As a result, the mass differential between the specimens decreased significantly.

The instrumented lower limb specimen was then attached to the Hybrid III surrogate at the mid-thigh using the interface located at the proximal end of the femur pot. The Hybrid III pelvis was configured to allow for free range of motion. As shown in Figure 27, the specimen was held in place at 90 degrees at the knee by a rope attached to a winch above. It was then necessary to further position the foot to neutral position as its natural tendency was towards inversion and plantar flexion. This was achieved using string, one piece just above the ball of the foot in order to dorsiflect it closer to neutral, and another around the three most lateral toes in order to evert the foot closer to its natural position.

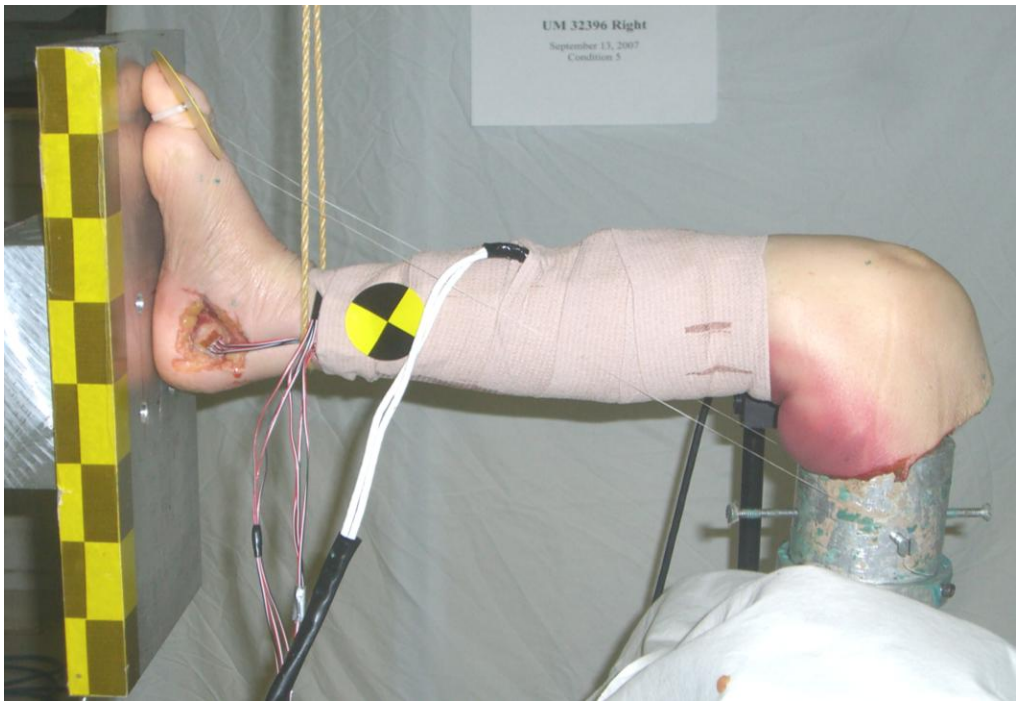

Figure 27: Positioning of Instrumented PMHS Lower Extremity Prior to Impact.

4.2.4 Data Collection and Processing

Six instrumented lower extremity PMHS were impacted at each of the three targeted impact conditions: WSU C1, C2, and C3 (7.0, 10.0, and 12.0 m/s) for a total of 18 specimens. Only one impact per specimen was conducted. High-speed video was collected using a HG 100K Camera (Redlake, Inc) at 10,000 frames per second with a given resolution of 256 by 192 pixels. Data acquisition was conducted at 20,000 Hz using a TDAS Pro System (DTS, Seal Beach, CA). A four-pole Butterworth filter with a cutoff frequency of 4300 Hz was used for anti-aliasing.

Characteristics of the loading environment were measured including impactor floorplate displacement, acceleration, and velocity. The displacement of the impactor floorplate was measured dynamically using a distance laser transducer (Micro-Epsilon Corporation Model number LD 1625-200). The derivative of the displacement was

utilized to calculate impactor velocity at the time of impact. Floorplate displacement data were filtered using a low pass Butterworth filter at 1000 Hz. A non-contact optical velocity sensor was utilized to measure the peak velocity of the cylindrical shaft during free flight. The velocity sensor data, not acquired using TDAS, were measured at 5000 Hz and were not filtered. Floorplate velocity calculated using the distance laser transducer and non-contact optical sensor were in close agreement. Velocity data reported henceforth was measured using the distance laser transducer. A tri-axis accelerometer mounted to the impactor floorplate was utilized to measure floorplate acceleration. Acceleration data were filtered using a CFC 600 filter.

Impactor kinetic energy was calculated using the free body mass of the impactor and the velocity of the floorplate at the point of impact.

Data collected from each specimen include axial force (Fz), the shear forces (Fx and Fy), the fore/aft and lateral bending moments (Mx and My, respectively), and calcaneus and tibia strain. Moment data were filtered using a CFC 180 filter. Tibia load data were filtered using a range of filters to determine the most appropriate filter class for the high rate impact. CFC 600, 1000, 1500, and 2500 filter class were evaluated. Plane strain, ε_a, ε_b, and ε_c, were filtered using a low pass Butterworth filter at 1000 Hz. The principal strain measured by the rosette was computed using strain transformation formulas. The compression data were utilized to calculate the compressive strain (ε) of the lower limb.

Strain gage data were utilized to identify the exact tibia axial force at the initiation of fracture. Analysis of strain gage results demonstrated good correlation between a local peak tibia axial force and peak strain of the injured region. Therefore, the local

peak tibia axial force was assumed to characterize the time of fracture. Data utilized for corridor development were limited up to the time of peak force/strain for tests involving fracture. Strain gage data were also used to identify the exact magnitude of lower limb compression at the initiation of fracture. Compression is defined herein as the magnitude of floorplate intrusion, measured by the laser transducer, while the knee position is fixed. The compression data were utilized to calculate the compressive strain (ε) of the lower limb.

4.2.5 Post Test Assessment

Post impact radiographs were obtained. An autopsy of the lower leg and knee was conducted by an orthopaedic surgeon to identify the incidence of injury. The injuries were ranked based on severity using the AFIS-S injury scale definitions (Levine, 1995). An injury earning an AFIS-S score of four or greater (4+) (severe injury) constitutes an incapacitating injury as mobility is severely jeopardized.

4.2.6 Statistical Analysis

Characteristics of the loading environment, measured stimuli, and calculated criteria were statistically evaluated as incapacitating injury predictors. A parametric distribution analysis was conducted for each predictor variable listed in Table 7 to determine the form of its distribution. Four distributions commonly applied to biomechanic risk functions were evaluated: Weibull, logistic, normal, and log-normal (Kent and Funk, 2004). The adjusted Anderson-Darling (AD*) statistic was calculated from the sample data to compare the fit of the aforementioned parametric distributions. The AD* was calculated using the least squares estimation method.

Table 7: AFIS-4+ Incapacitating Injury Predictor Variables.

Predictor	Decription	Characteristic	Censor Type
V (m/s)	Velocity of the impactor floorplate at time of impact	Extrinsic	Right/Left
KE (J)	Kinetic energy of the impactor floorplate at time of impact. Calculated using the free body mass of impactor and impactor velocity	Extrinsic	Right/Left
Mx (N*m)	Moment measured at X-axis	Intrinsic	Right/Left
My (N*m)	Moment measured at Y-axis	Intrinsic	Right/Left
Fx (N)	Tibia shear force at X-axis	Intrinsic	Right/Left
Fy (N)	Tibia shear force at Y-axis	Intrinsic	Right/Left
Fz (N)	Tibia axial force at Z-axis	Intrinsic	Right/ Uncensored
ε	Compressive strain of the lower limb hard tissue (L-l)/L; where *l* is the compressed length of the limb at the initiation of fracture and L is the original length of the tibia	Intrinsic	Right/ Uncensored

A parametric survival analysis regression was conducted to develop a risk function that defines the probability of AFIS-4+ incapacitating injury in terms of an injury predictor. Survival analysis was chosen as the preferred statistical methodology over standard logistic regression because of its sensitivity to uncensored data (Kent and Funk, 2004).

Two types of survival analysis were conducted based on the nature of the dataset: doubly censored or right-censored/uncensored. Doubly censored data contains right-censored and left-censored data. A data point was classified as right-censored if it was measured in a specimen that did not sustain an incapacitating injury.

A data point was classified as left-censored if it was measured in a specimen that sustained an incapacitating injury and if it could not be determined how much less stimulus would have caused an incapacitating injury (Kent and Funk, 2004). Impactor velocity, impactor kinetic energy, bending moments, and shear forces were considered left-censored stimuli because their magnitudes were independent of the occurrence of injury.

In contrast, if the exact stimulus level for an incapacitating injury is known the data point was classified as uncensored (Kent and Funk, 2004). Uncensored data are critical for evaluating a stimulus-limiting event such as a fracture of a weight-bearing region such as the calcaneus, talus or tibia. These regions are unable to support load following a major fracture and residual stimulus is directed elsewhere. Funk et al. (2002) found that calcaneal and tibia fractures always occurred at the time of peak local tibia axial force using acoustic emission. In this study strain gage data was used to determine that the initiation of fracture occurred at the time of local peak tibia axial force and compressive strain. Therefore, peak axial tibia forces and compressive strain from incapacitating injury tests were considered uncensored predictors of fracture force.

Survival analysis regression coefficients were estimated from the uncensored incapacitating injury data using a least squares estimation method. The overall fit of the survival model and relative improvement were evaluated for each predictor variable using the Pearson correlation coefficient, multiple coefficient determination (R^2), Log-Likelihood, and statistical significance.

4.3 Results

None of the six specimens impacted at the WSU C1 loading rate sustained a skeletal injury. When considering skeletal injuries only, the non-injury constitutes a score of zero on the AFIS-S scale. In contrast, all 12 specimens impacted at the WSU C2 and C3 loading rates sustained at least one skeletal injury. Six of the 12 PMHS skeletal injuries were classified as an AFIS-S 4+ incapacitating injury. A summary of the PMHS lower limb skeletal injuries and associated AFIS-S/AIS scores is displayed in Table 8.

Each of the injured specimens sustained a calcaneal fracture. The severity of the calcaneal fracture varied from a simple, undisplaced, closed fracture to a multi-fragmentary comminuted, displaced, open fracture (Figures 28 and 29).

Table 8: Summary of PMHS Lower Limb Injury Severity and Impairment.

Cadaver ID	Left/ Right	WSU Cond. #	Fractures	Description of Injury	AIS	AFIS-S
UM 32065	Left	1	n/a	No skeletal injury observed.	0	0
UM 32065	Right	1	n/a	No skeletal injury observed.	0	0
UM 32067	Right	1	n/a	No skeletal injury observed.	0	0
UM 32068	Left	1	n/a	No skeletal injury observed.	0	0
UM 32068	Right	1	n/a	No skeletal injury observed.	0	0
WSU 623	Left	1	n/a	No skeletal injury observed.	0	0
WSU 861	Right	2	C, TA	Calcaneal fracture; displaced articular; comminuted. Sub-talar displaced and fractured.	2	5
WSU 863	Left	2	C	Calcaneal fracture; undisplaced articular; oblique.	2	3
UM 32324	Left	2	C	Calcaneal fracture; undisplaced articular; comminuted.	2	3
WSU 709	Right	2	C, TA	Calcaneal fracture; undisplaced articular; comminuted. Fracture of the posterior talocalcaneal articulation.	2	3
UM 32396	Left	2	C, T, F	Calcaneal fracture; undisplaced articular; comminuted. Tibia fracture below tibia pot (transverse). Fibula fracture below pot at epiphysis (oblique).	2	3
UM 32396	Right	2	C, TA	Calcaneal fracture; displaced articular; comminuted. Fracture of the anterior and posterior talocalcaneal articulation.	2	5
WSU 667	Left	3	C, TA, T, F	Calcaneal fracture; displaced articular; comminuted. Talar fracture displaced head, neck, body. Tibia and fibula articular epiphysis fracture.	2	5
WSU 667	Right	3	C, TA, T, F	Calcaneal fracture; displaced articular; comminuted. Talar fracture displaced head, neck, body. Tibia and fibula articular epiphysis fracture. Tri-malleolur fracture.	2	5
UM 32324	Right	3	C, TA	Calcaneal fracture; undisplaced articular; comminuted. Fracture at the trochlea of the tibia.	2	3
WSU 709	Left	3	C, TA	Calcaneal fracture; undisplaced articular; comminuted. Talus fracture head displaced.	2	4
WSU 861	Left	3	C, Cu	Calcaneal undisplaced fracture. Tarsometatarsal fracture (lisfranc).	2	5
WSU 863	Right	3	C, TA, T	Calcaneal fracture; undisplaced articular; comminuted. Talar fracture; undisplaced head, neck, body. Tibia epiphysis fracture; distal articular surface.	2	3

where: C: calcaneus; Cu: cuboid; F: fibula; T: Tibia; TA: talus

Figure 28: Left: Undisplaced, comminuted calcaneal fracture and talar fracture, AFIS-S: 3 (WSU 863 Left). Right: Displaced, comminuted calcaneal fracture, AFIS-S: 5 (UM 32396).

Figure 29: Left: multi-fragmentary comminuted, displaced, open Calcaneus fracture. Right: simple, undisplaced, closed Calcaneus fracture.

The talus bone was the second most frequently injured region of the lower limb occurring in eight specimens. The severity of the talus fractures varied widely and included both undisplaced and displaced fractures. Talar fracture predominately occurred at the anterior and posterior talocalcaneal articulation. Talar fractures also occurred at the trochlea for the tibia and the lateral malleolus articular surface for the fibula articulation. Four lower limb specimens sustained a tibia fracture. It is unknown whether these fractures were influenced by the tibia potting equipment. One tibia fracture was ruled artificial as it was observed at the insertion point of a tibia pot clevis pin. Three of the four tibia fractures occurred at the distal articular epiphyseal plate. One tibia fracture occurred at the medial malleolus. Three specimens sustained a fibula articular epiphysis fracture. Finally, one specimen sustained a Lisfranc fracture of the joints in the midfoot.

Figure 30: Left: Medial Malleolus Fracture. Right: Posterior Calcaneal Articular Surface Fracture.

The WSU C2 impact condition produced a single calcaneal fracture in two specimens and multiple fractures in four specimens. In addition, WSU C2 produced only one instance of tibia and/or fibula fracture. In comparison, the more severe WSU C3 impact condition produced multiple fractures in all six specimens and three instances of tibia and/or fibula fracture. In general, WSU C3 loading generated more severe crush-like fractures than WSU C2 impacts. The fractures contained more bone fragmentation and instances of open fracture than WSU C2.

4.3.2 Transducer Outputs

Table 9 provides a summary of all transducer outputs for the 18 PMHS lower limb impacts. There were three impact conditions (WSU C1, C2, and C3) with average impact velocities of 7.2, 9.9, and 11.8 m/s and kinetic energies of 941, 1802, and 2494 J respectively. Six PMHS lower limbs were impacted at each of the impact condition. For tests that produced fractures, estimates of the tibia axial force at the time of fracture initiation are given. Average and standard deviation values of these measurements for each of the three test conditions are shown in Table 10. No tibia load cell values are given for PMHS WSU 863 Left due to an instrumentation issue. The values for the tibia axial force given in the tables are based on filtering the tibia force versus time curve at CFC 600 since no difference was noted between filtering at CFC 600, CFC 1000, CFC 1500, and CFC 2500 as shown in Figure 31.

Table 9: Summary of Lower Extremity Blast Impact Testing.

Test Cond.	Cadaver ID	Left/ Right	Impactor Velocity (m/s)	Impactor KE (J)	Peak Fz (N)	Fz at Initiation of Fracture (N)	Fx (N)	Fy (N)	Mx (N*m)	My (N*m)	ε
WSU C1	UM 32065	Left	7.1	929	4,789	n/a	261	466	29.8	20.4	0.057
	UM 32065	Right	6.9	875	5,191	n/a	336	635	51.3	22.1	0.057
	UM 32067	Right	6.8	859	5,858	n/a	763	696	33.2	24.9	0.059
	UM 32068	Left	7.7	1,089	5,255	n/a	526	239	25.9	22.3	0.067
	UM 32068	Right	7.3	979	5,340	n/a	544	618	25.4	22.7	0.067
	WSU 623	Left	7.1	913	5,826	n/a	639	356	62.4	24.8	0.053
WSU C2	WSU 861	Right	10.3	1,956	3,829	3,829	380	456	30.5	16.3	0.033
	WSU 863	Left	10.7	2,107	no data	no data	no data	no data	no data	no data	0.045
	UM 32324	Left	10.5	2,006	11,266	3,559	388	714	19.8	55.7	0.036
	WSU 709	Right	9.0	1,491	9,866	9,866	843	791	8.9	24.2	0.043
	UM 32396	Left	9.4	1,637	2,845	2,845	676	508	69.4	59.9	0.046
	UM 32396	Right	9.4	1,616	2,806	2,806	404	555	53.8	10.6	0.042
WSU C3	WSU 667	Left	12.2	2,752	1,360	1,360	402	635	9.1	52.8	0.036
	WSU 667	Right	11.8	2,554	3,357	3,357	334	320	16.9	27.6	0.029
	UM 32324	Right	11.9	2,606	3,700	3,700	336	411	0.1	15.3	0.038
	WSU 709	Left	11.5	2,446	6,940	6,535	171	293	60.0	171.7	0.039
	WSU 861	Left	11.1	2,276	3,937	3,937	400	227	38.8	25.7	0.031
	WSU 863	Right	11.3	2,333	7,624	7,624	436	458	45.5	31.7	0.046

Table 10: Average Lower Extremity Blast Impact Testing.

	Avg. Impactor Velocity (m/s)		Avg. Impactor KE (J)		Avg. Peak Tibia Axial Force, Fz (N)		Avg. Fz at Initiation of Fracture (N)	
	Avg	Std Dev	Avg	Std Dev	Avg	Std Dev	Avg	Std Dev
WSU C1	7.2	0.3	941	84	5,377	408	n/a	n/a
WSU C2	9.9	0.7	1802	252	6,122	4,107	4,581	2,988
WSU C3	11.6	0.4	2494	178	4,486	2,359	4,419	2,280

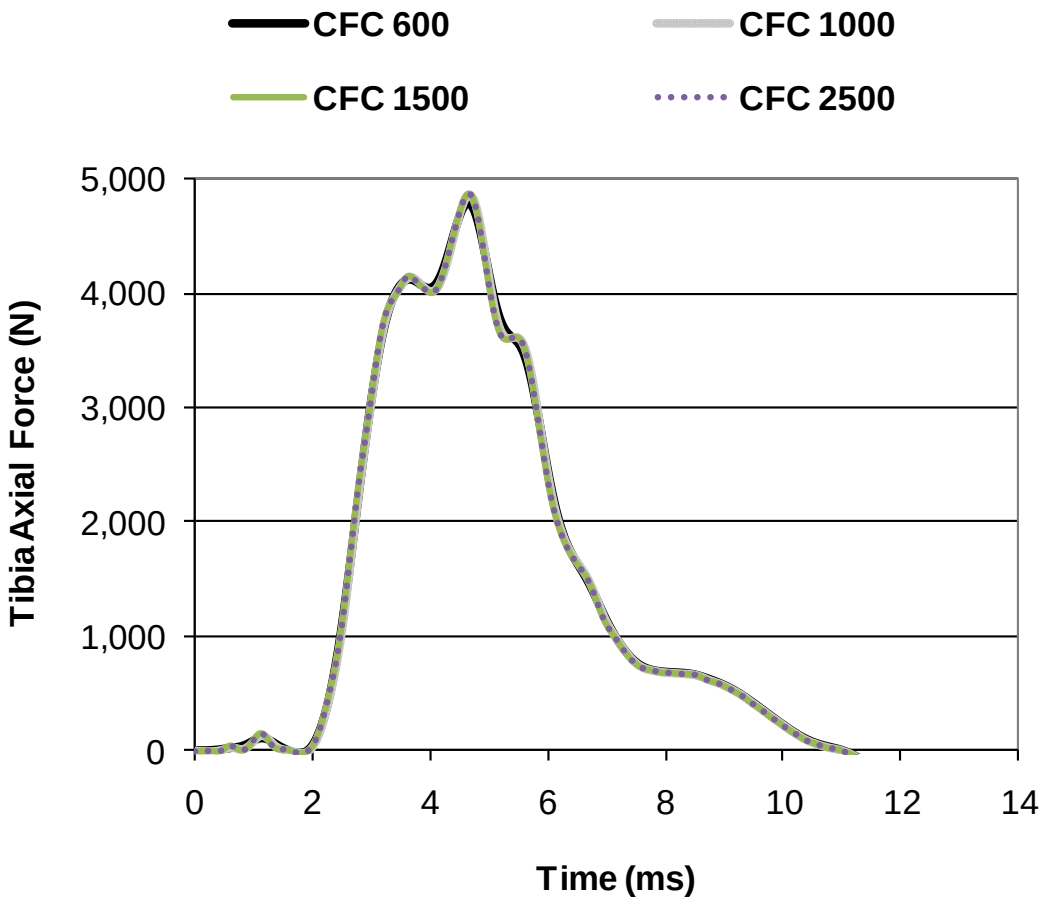

Figure 31: Comparison of CFC 600 to CFC 2500 filter classes for WSU C1 (UM32065 L).

None of the six PMHS sustained a skeletal injury in WSU C1 impacts. Each of the six WSU C1 impacts resulted in similar tibia axial force loading patterns and durations. Time histories for the WSU C1 impacts filtered at CFC 600 are shown in Figure 32. The force-time trajectory of each impact was fairly parabolic. The initiation of tibia axial force occurred within 0.5 millisecond of the floorplate contacting the specimen. Peak tibia axial force was reached at 24 millimeters of floorplate intrusion or approximately three to four milliseconds following the initial impact. The average peak force of a WSU C1 impact was 5,377 N with a standard deviation of 408 N. The loading gradually dropped and returned to its baseline between ten and 15 milliseconds after initial impact. Video analysis of the impact revealed that the position of the knee was fixed during the initial 24 millimeters of floorplate intrusion suggesting the specimen experienced compressive strain. Movement of the knee was initiated after the impactor floorplate was decelerated by the aluminum honeycomb material. The deformation of the honeycomb corresponded with the magnitude of floorplate intrusion. The work performed by the impactor was estimated by the deformation of the honeycomb.

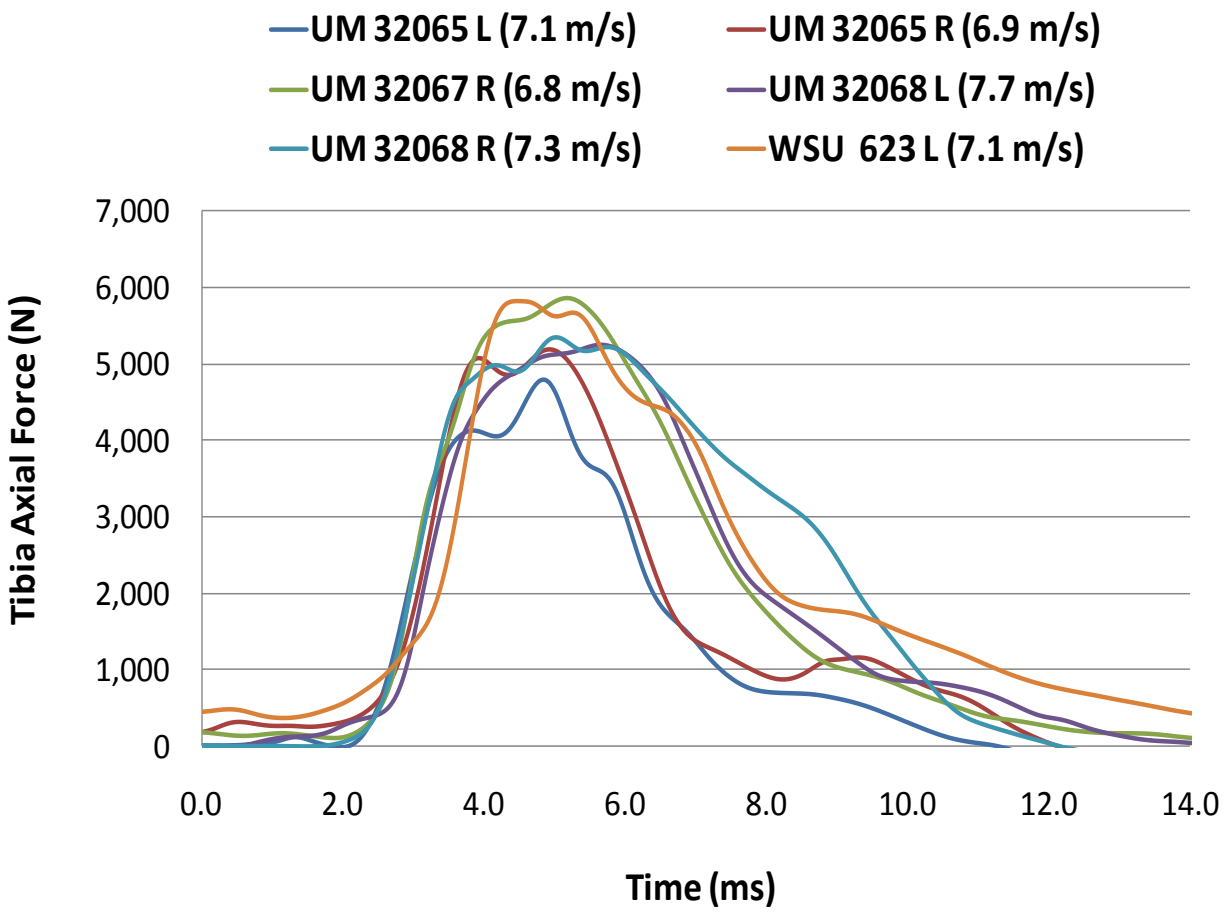

Figure 32: WSU C1 Tibia Axial Force versus Time Trajectories.

The WSU C2 tibia axial force measurements varied significantly based on the occurrence and type of fractures. Time histories for the WSU C2 impacts filtered at CFC 600 are shown in Figure 33. The average peak force of a WSU C2 impact was 6,122 N with a standard deviation of 4,107 N. The average peak force at time of injury was 4,581 with a standard deviation of 2,988. Unlike WSU C1, the force-time trajectory did not follow a parabolic trajectory. An initial peak tibia load was measured within three milliseconds of the impact and occurred prior to the full 24 millimeter floorplate intrusion.

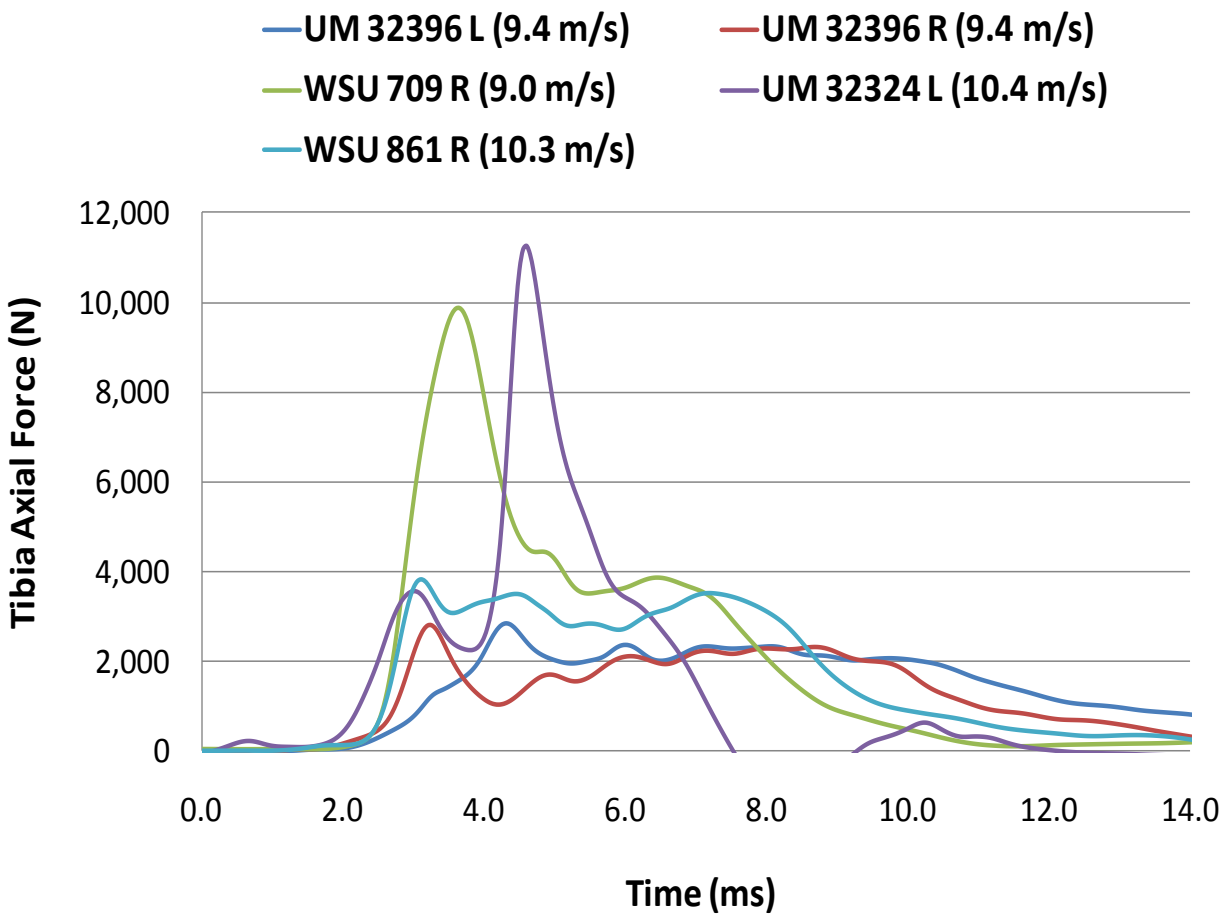

Figure 33: WSU C2 Tibia Axial Force versus Time Trajectories

All six impacts in WSU C3 resulted in fractures with an average impactor footplate velocity of 11.6 m/s (1,802 J). Time histories for the WSU C3 impacts filtered at CFC 600 are shown in Figure 34. The average peak force of a WSU C3 impact was 4,486 N with a standard deviation of 2,359 N. The average peak force at time of injury was 4,419 with a standard deviation of 2,280. WSU C3 impacts produced two or more skeletal injuries in each lower limb specimen and, in general, appeared to cause more catastrophic injuries than WSU C2. Similar to WSU C2, the tibia load data varied significantly based on the occurrence and type of fractures.

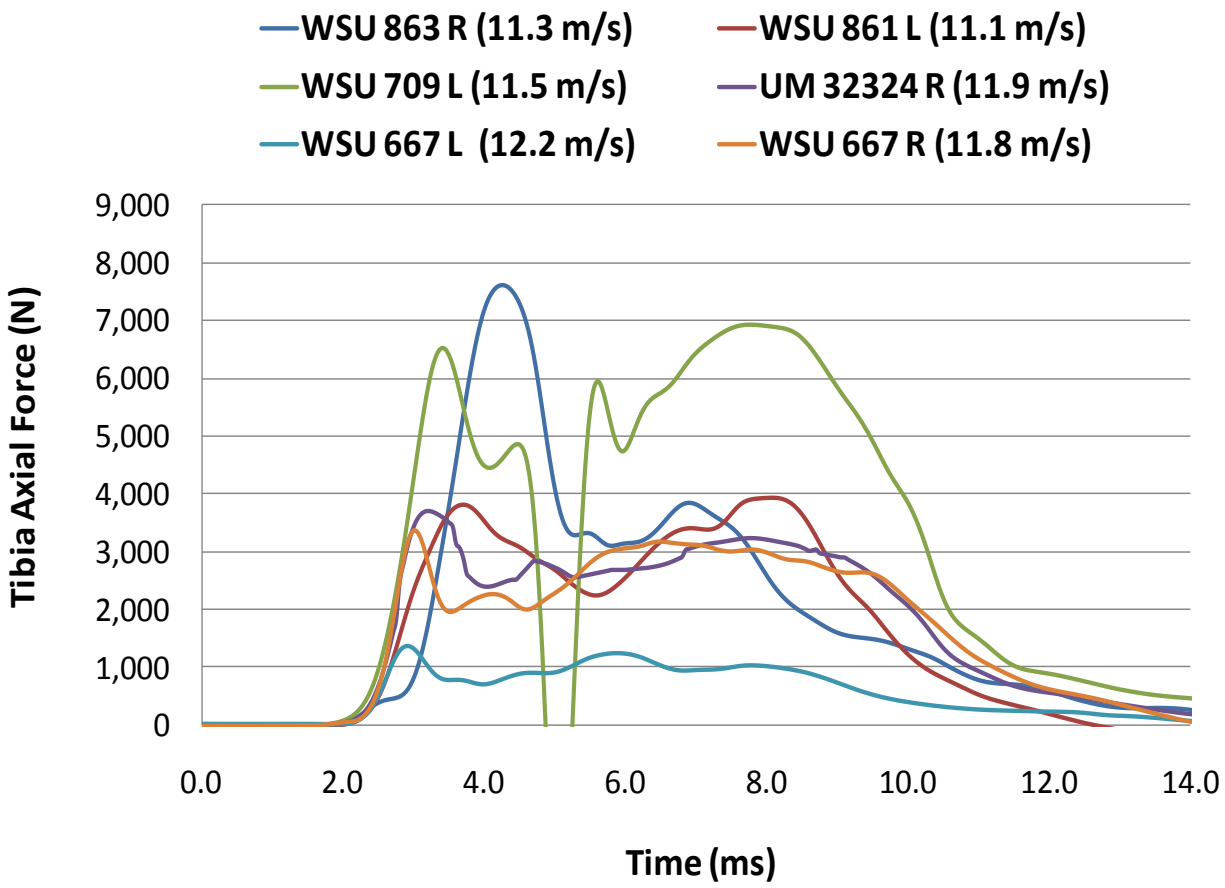

Figure 34: WSU C3 Tibia Axial Force versus Time Trajectories.

In all injurious impacts peak principal strain, measured by the rosette strain gages, corresponded with the first peak tibia axial force. The initial strain and axial force peaks occurred between 15 and 18 millimeters of compression. The first peak tibia axial force was followed by a sharp momentary decrease in stimulus. This activity in conjunction with strain data indicated the occurrence of fracture. Subsequent tibia axial forces and strain were measured until the stimulus gradually dropped to its baseline between ten and 15 milliseconds after initial impact. In one case, the subsequent tibia axial force exceeded the first peak axial force (WSU 709L). Figure 35 illustrates a typical force-time and plane strain-time trajectories for a calcaneal fracture.

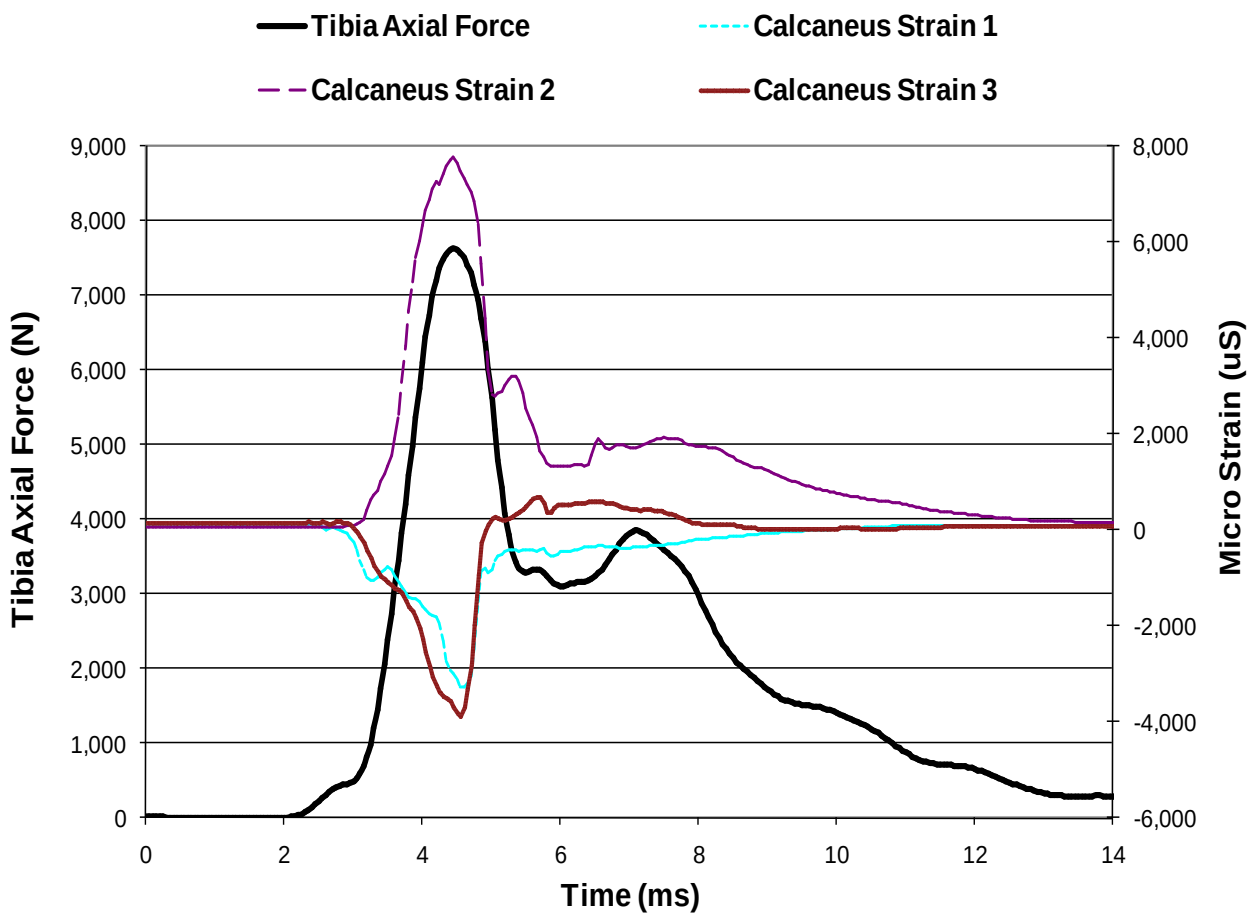

Figure 35: Peak Force and Peak Strain Relationship (WSU 863 Right, WSU C3).

4.4 Injury Mechanism and Probability

Tibia fracture force and compressive strain data from six PMHS sustaining AFIS-S 4+ incapacitating injury were classified as uncensored data. All other injury data were classified as left-censored.

A parametric distribution analysis was conducted for each incapacitating injury predictor variable to determine the form of its distribution. Tables 11 and 12 list the AD* value of each injury predictor. A smaller AD* value indicates a specific distribution is a relatively better fit. Overall, the Weibull distribution was consistently the best fit

parametric distribution for all injury predictors. However, only minor differences in the AD* statistic were observed when comparing a Weibull, logistic, normal, and lognormal distribution for each injury predictor. This suggests the behavior of each distribution is similar near the predicted median probability of injury. Kent and Funk (2004) noted a similar trend for biomechanical studies without large sample populations.

Table 11: Adjusted Anderson-Darling Statistic Value for Right/Left-Censored Predictors.

	Anderson-Darling Statistic Value					
Parametric Distribution	**Impactor Velocity**	**Impactor KE**	**Mx**	**My**	**Fx**	**Fy**
Weibull	11.46	11.46	25.88	25.73	55.50	47.53
Logistic	11.47	11.47	25.90	25.75	55.50	47.53
Normal	11.46	11.46	25.90	25.74	55.50	47.53
Lognormal	11.46	11.46	25.87	25.73	55.50	47.53

Table 12: Adjusted Anderson-Darling Statistic Value for Right-Censored/ Uncensored Predictors.

	Anderson-Darling Statistic Value	
Parametric Distribution	**Fz**	**ε**
Weibull	41.63	66.65
Logistic	41.75	66.65
Normal	41.69	66.65
Lognormal	41.63	66.65

A survival analysis was conducted using a Weibull distribution for doubly censored injury predictors and right-censored and uncensored injury predictors. The Weibull regression model is shown in Equation 4. Table 13 lists the estimated Weibull regression model coefficients and describes the overall fit for each predictor variable. Impactor velocity, impactor kinetic energy, tibia axial force, and compressive strain were found to be statistically significant at the α = 0.05 level.

$$P(x) = 1 - e^{-(x/\lambda)^{\kappa}} \quad \textbf{(Equation 4)}$$

where P is the probability of injury, x is the predictor variable, and λ and κ are the corresponding coefficients associated with each predictor variable.

Table 13: Weibull Regression Model for Extrinsic and Intrinsic Incapacitating Injury Predictors.

Predictor	Shape (κ)	Scale (λ)	Model p-value	AD*	Pearson Correlation Coefficient	R^2	Log-Likelihood	50% POI	Standard Error
V (m/s)	6.98	11.3	0.012	11.46	n/a	n/a	-7.46	10.8	0.666
KE (J)	3.49	2,361	0.012	11.46	n/a	n/a	-7.46	2,126	263
Mx (N*m)	0.316	218	0.921	25.88	0.900	0.810	-11.0	68.4	84.4
My (N*m)	1.10	51.4	0.219	25.81	0.867	0.752	-11.6	36.8	12.8
Fx (N)	3.07	575	0.466	55.50	0.903	0.815	-51.1	509	60.6
Fy (N)	2.47	757	0.313	47.53	0.964	0.929	-47.4	653	99.4
Fz (N)	1.940	7,766	0.010	41.63	0.976	0.953	-62.3	6,429	1,195
ε	6.7	0.0453	0.016	66.65	0.939	0.882	-29.16	0.043	0.003

Impactor velocity was selected as the best extrinsic model candidate for the doubly censored analysis as kinetic energy was not directly measured. Figure 36 illustrates the impactor velocity risk function and associated 95 percentile confidence intervals. An impactor velocity of 8.2 m/s corresponds with a 10 percent probability of incapacitating injury. An impactor velocity of 10.8 m/s corresponds with a 50 percent probability of incapacitating injury.

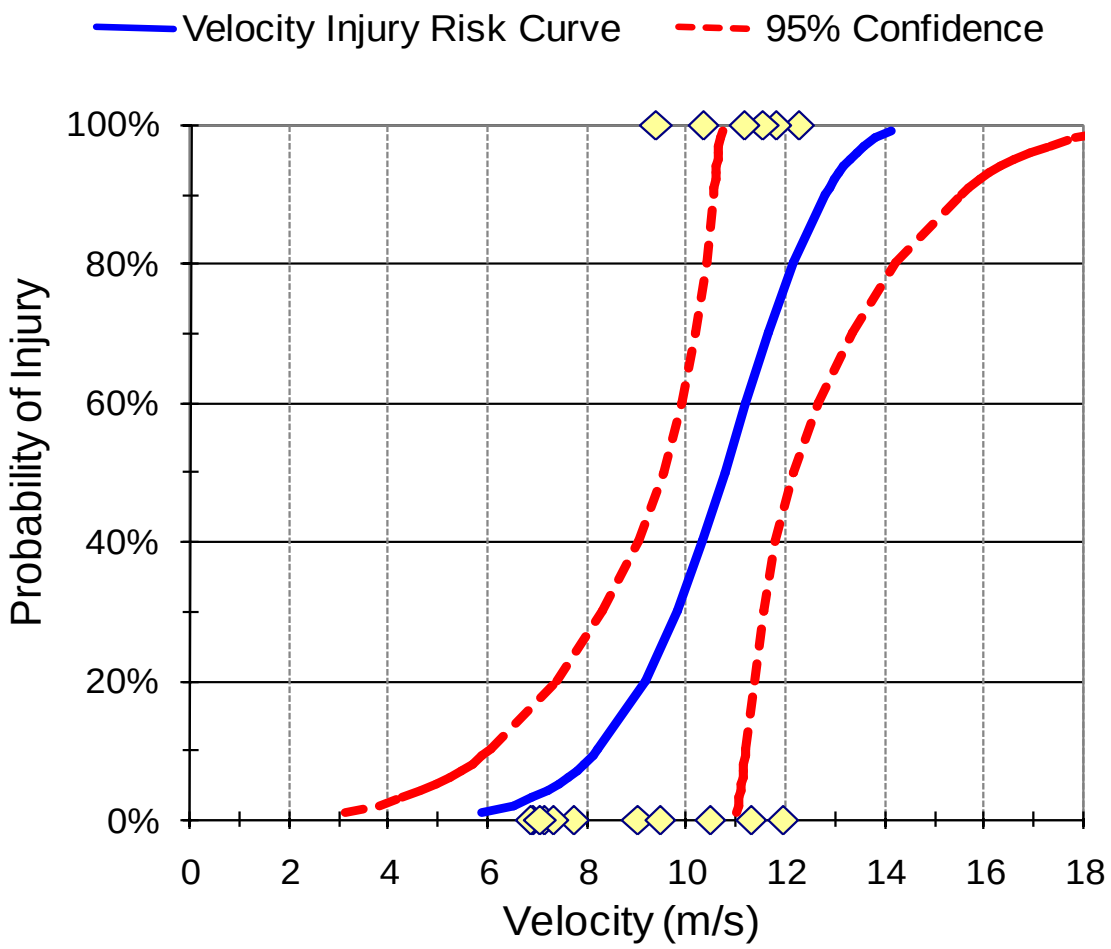

Figure 36: Impactor Velocity Injury Risk Curve by Weibull Regression.

Tibia axial force was selected as the best intrinsic model candidate for right-censored and uncensored analysis. The axial force model proved to be the best overall fit of the data (R^2 = 0.953 and α = 0.01). A tibia axial force of 6,429 N corresponds with a 50 percent probability of incapacitating injury. The standard error at the median is 1,195 N. Figure 37 illustrates the tibia axial force risk function and 95 percentile confidence intervals.

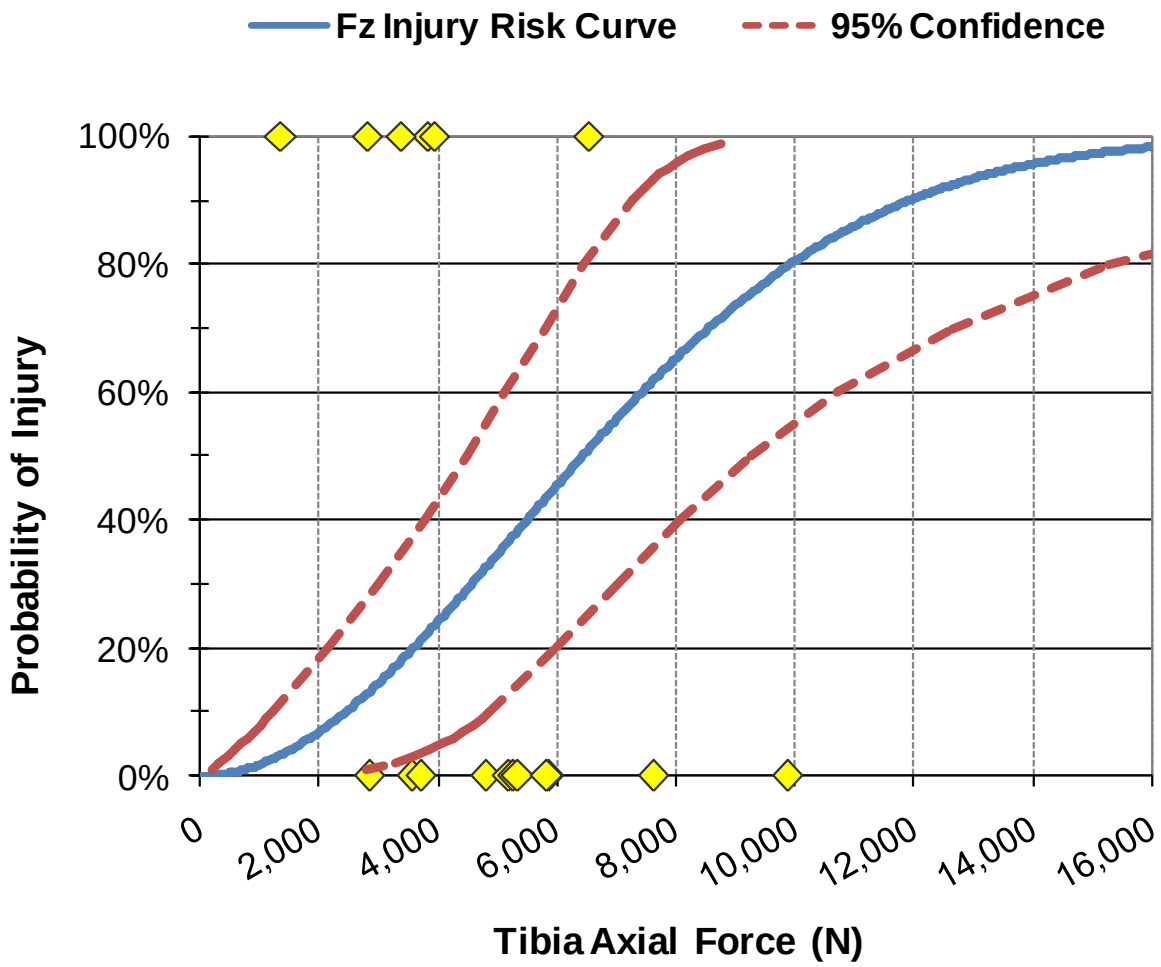

Figure 37: Tibia Axial Force Injury Risk Curve by Weibull Regression.

Although the AD* statistic suggests the overall fit of axial force is comparable across the parametric distributions, the tibia axial force injury risk function is strongly dependent on the parametric distribution selected. Figure 38 compares the tibia axial force injury risk function for each type of parametric distribution. As indicated, the behaviors of the tibia axial force injury risk functions are fairly consistent up to the 40 percent probability of injury. Following this point, the curves diverge. This divergence may be attributed to the limited population of data measured at the more severe axial loads. Considering the nature of the divergence and limited sample population it is common practice to select an injury risk function using the most conservative parametric distribution. The logistic regression distribution risk function and associated 95 percentile confidence interval provide the most conservative estimate of axial force and probability of injury. Therefore, the most appropriate risk function is described by a logistic regression distribution.

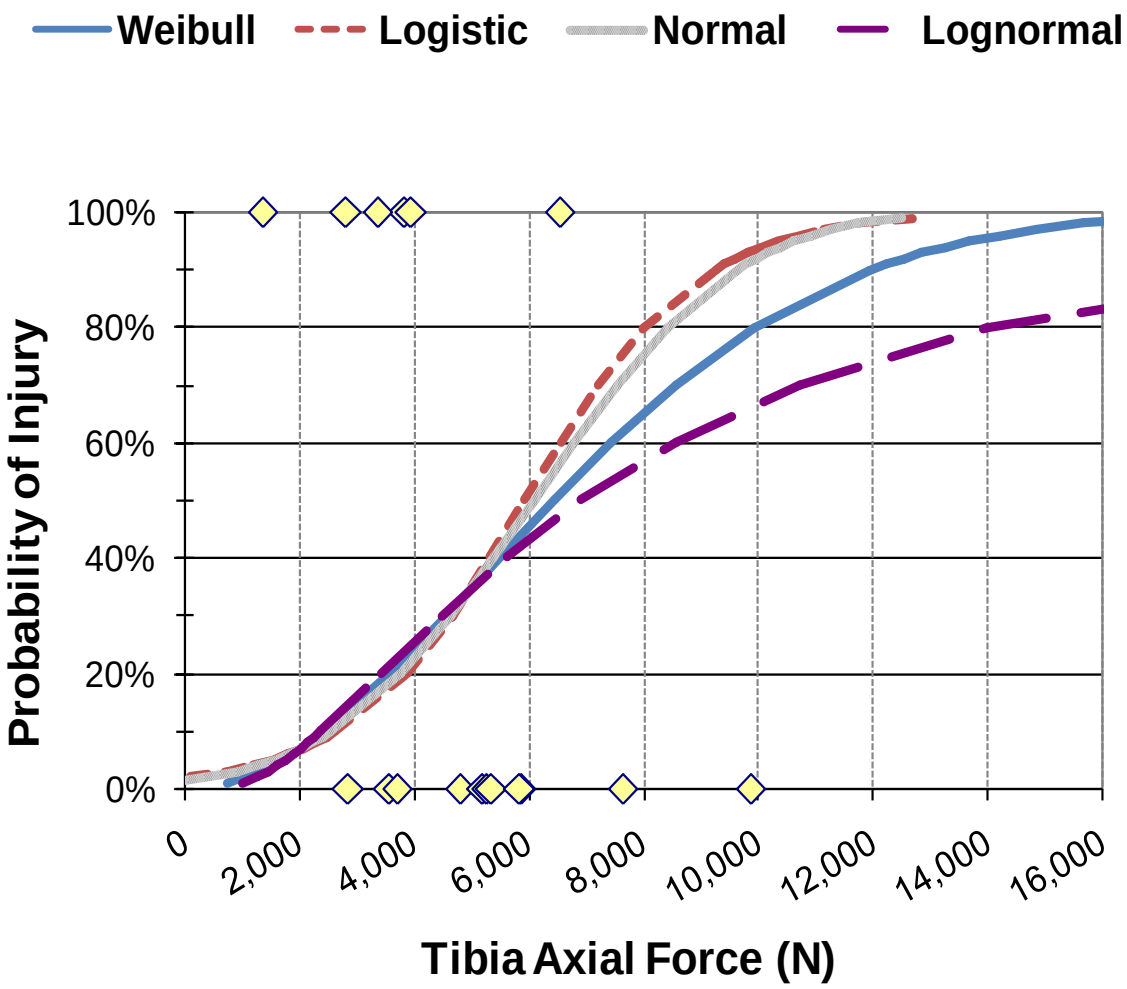

Figure 38: Parametric Distribution Analysis of Tibia Axial Force.

Table 14 lists the estimated logistic regression model coefficients derived from right-censored/uncensored survival analysis and describes the overall fit for the tibia axial force predictor variable. A logistic plot illustrating the probability of an incapacitating lower limb injury and associated 95 percentile confidence intervals is shown in Figure 39. The probability of the incapacitating injury risk function is defined in Equation 5. Axial tibia force was found to be statistically significant at the $\alpha = 0.05$ level.

According to the analysis, the tibia axial force model proved to be a good fit of the data (R^2 = 0.916). A tibia axial force of 2,650 corresponds with a 10 percent probability of incapacitating injury. A tibia axial force of 5,931 corresponds with a 50 percent probability of incapacitating injury. The standard error at the median is 786 N.

Table 14: Logistic Regression Model for Tibia Axial Force.

Predictor	Location (μ)	Scale (σ)	Model p-value	AD*	Pearson Correlation Coefficient	R^2	Log-Likelihood	50% POI	Standard Error
Injury Risk Curve	5931.42	1499.36	0.012	41.8	0.957	0.916	-64.3	5931	786

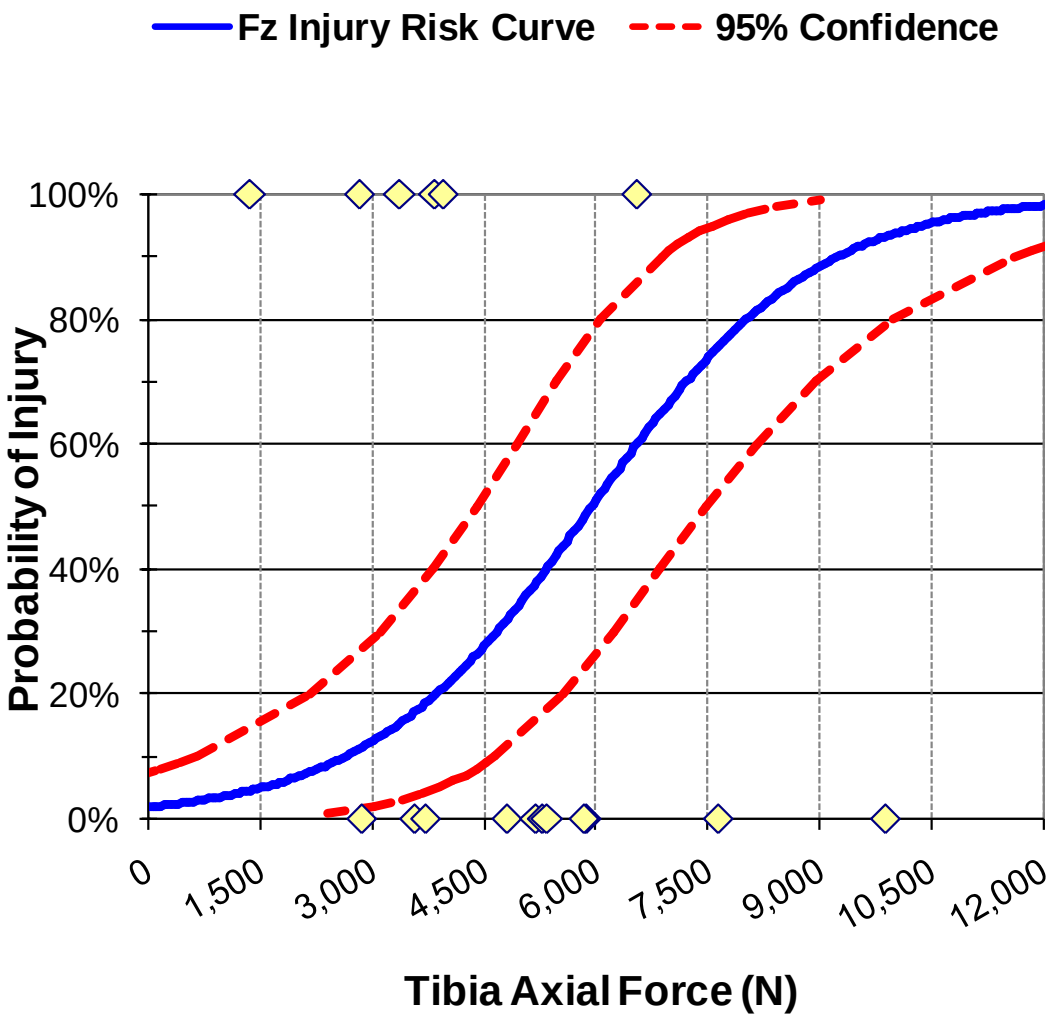

Figure 38: Tibia Axial Force Injury Risk Curve by Logistic Regression.

$$P(F_z) = 1 \Big/ \left(1 + e^{-(F_z - 5931.42)/1499.36}\right) \quad \textbf{(Equation 5)}$$

where P is the probability of injury, Fz is the predictor variable peak tibia axial force.

Characteristics of the specimen including age and gender were evaluated as factors and covariates. A multivariate discriminant analysis was performed on each

characteristic. It was it was determined that gender and age had statistically insignificant effects on probability of injury. This is likely due to the limited sample population and age distribution.

4.5 Discussion

The lower extremity is the principal injury of the U.S. military in combat operations. AV explosive devices pose a ubiquitous threat to military vehicle occupants and are capable of inflicting injury to the lower extremity. Although lower extremity injuries may not be an immediate threat to life, many are immediately incapacitating and require long term rehabilitation to decrease impairment. In order to reduce lower limb injuries to mounted soldiers, the injury tolerance of the lower extremity must be defined for blast impact conditions.

Impact data collected from instrumented PMHS were utilized in this study to establish conservative injury criteria for mounted soldiers in underbelly blast impacts. Eighteen instrumented PMHS were impacted at three incrementally severe impact conditions. Twelve of 18 PMHS in this study sustained hard tissue injury. The distribution of injuries generated in this study accurately depict the type and severity of injuries observed in recent armed conflicts including OIF and OEF. High energy and velocity impact conditions produced numerous complex open fractures with severe levels of comminution. As impactor velocity increased the level of comminution and frequency of tibia and fibula injuries increased. Six of the twelve injuries were classified as an incapacitating injury. All twelve injured specimen in this study sustained a calcaneal fracture; however, only six of the 12 calcaneal fractures were classified as incapacitating.

4.5.1 Tibia Axial Force Injury Risk Function

Right-censored and uncensored tibia axial forces were found to be the most accurate predictor of incapacitating injury according to survival analysis. The tibia axial force risk function model was shown to be an excellent fit of the dataset possessing a R^2 of 0.916. Modeling the risk function with a logistic distribution enabled the selection of the most conservative parametric distribution. As a result, the 95 percentile confidence intervals do not diverge thereby ensuring confidence in the injury probability predictions.

The right-censored/uncensored incapacitating injury risk function formulated in this study compares favorably with the injury risk function proposed by Yoganandan et al. (1996) but more liberal than the risk function proposed by Funk et al. (2002). Figure 40 compares the proposed risk function to the Yoganandan et al. (1996) and Funk et al. (2002) risk functions adjusted for a 67 year old subject (the average age used in this current study) (Note: the Achilles tension value was set to 0.0 N for the Funk et al (2002) curve).

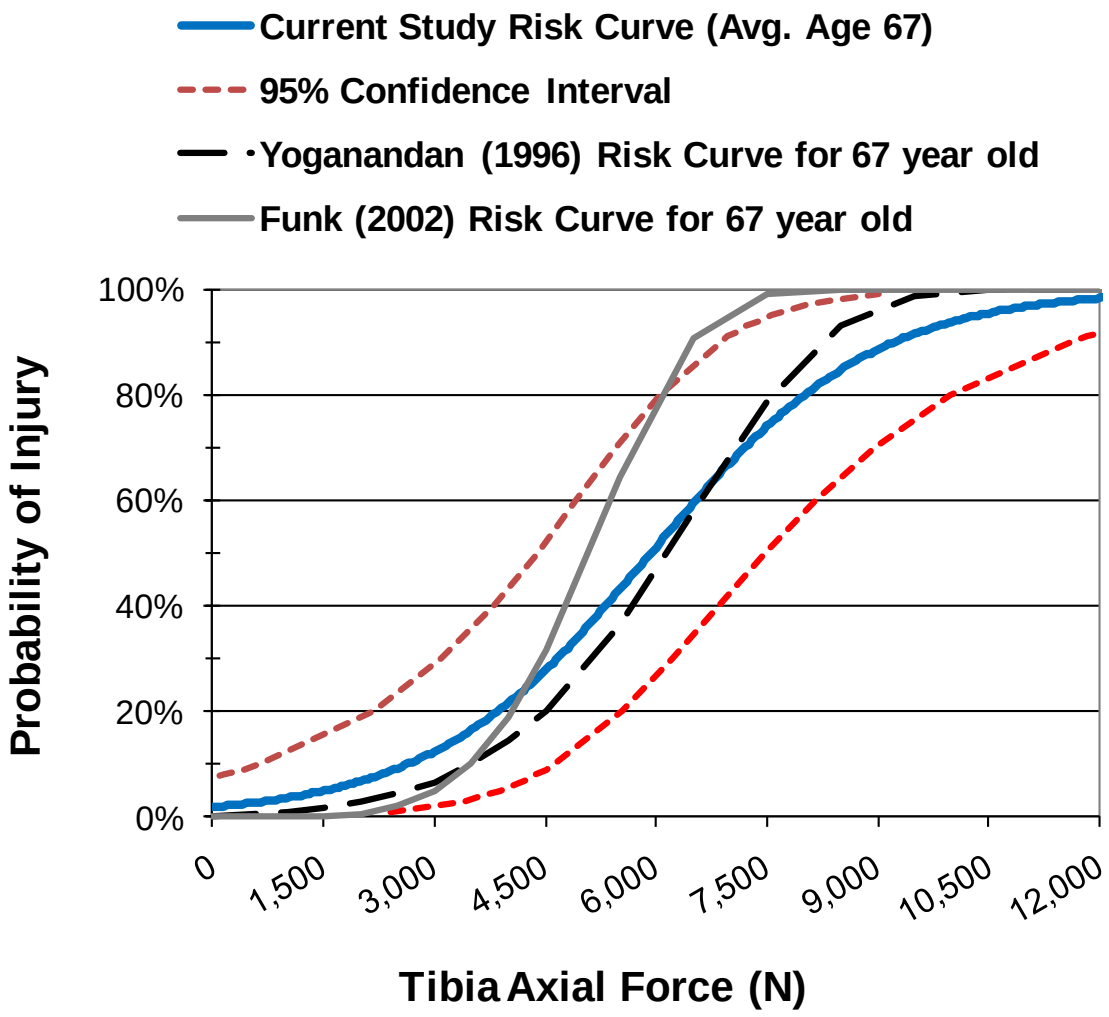

Figure 40: Comparison of Proposed Injury Risk Function with Yoganandan et al. (1996) and Funk et al. (2002) 67 year old Risk Functions.

The risk function proposed in this study appears to be more conservative than the Yoganandan et al. (1996) risk function before the 60 percent probability of injury and less conservative after. As shown in Figure 41, when the Yoganandan et al. (1996) and Funk et al. (2002) risk functions are adjusted for a 45 year old subject, as done by the NATO AEP-55 standard (to be more representative of a combat soldier), the risk curve proposed in this current study is far more conservative (Note: the Achilles tension value

was set to 0.0 N for the Funk et al (2002) curve). Clearly, this outcome is due to the age (correction) bias of the Yoganandan et al. (1996) and Funk et al. (2002) studies.

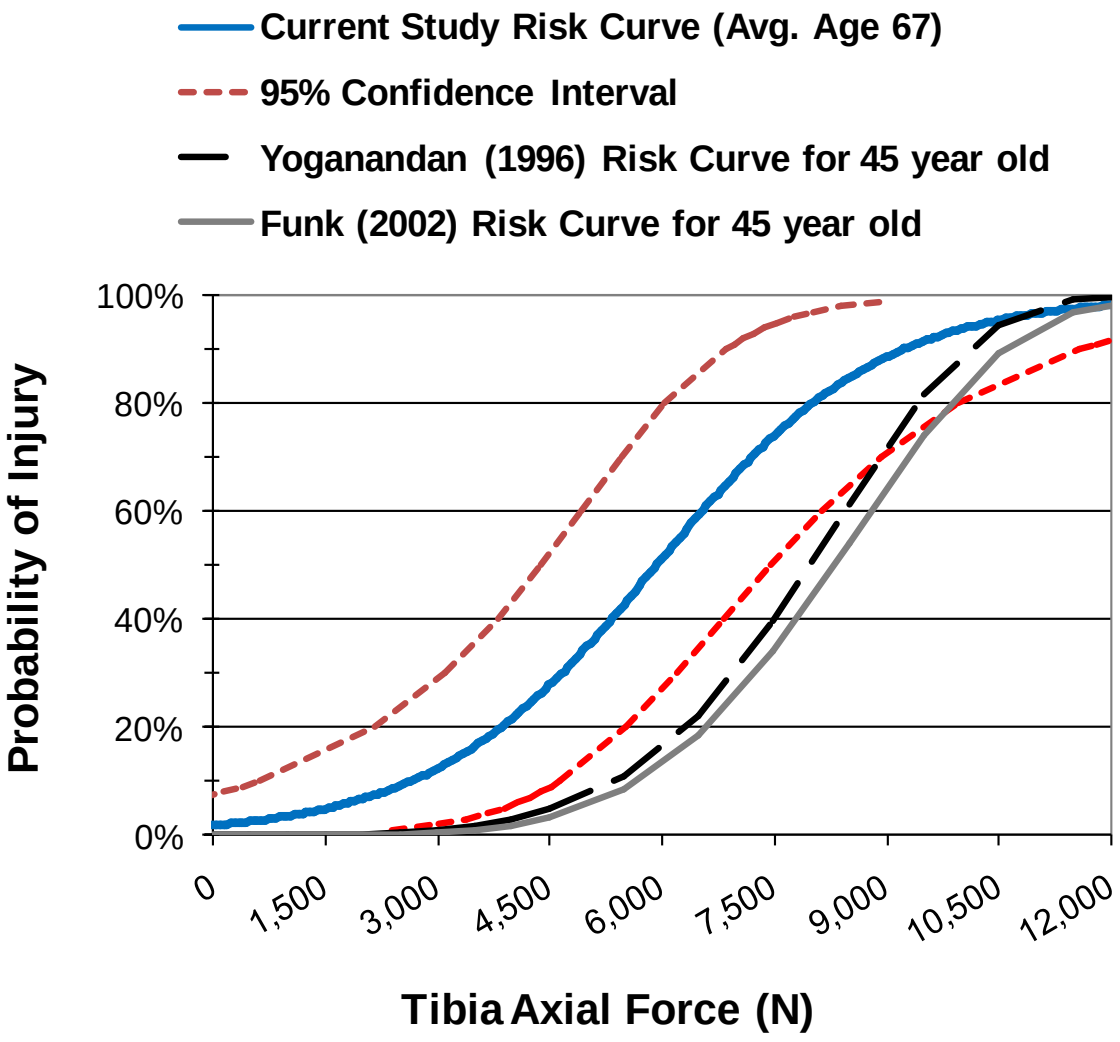

Figure 41: Comparison of Proposed Injury Risk Function with Yoganandan et al. (1996) and Funk et al. (2002) 45 year old Risk Functions.

The limited population size and diversity in this study prevents such corrections for age based on its lack of statistical significance. The upper bound 95 percentile confidence interval of the current study injury risk curve, which would represent the most injury resistant portion of the population, compares favorably with the 45 year old

risk curves of Yoganandan et al. (1996) and Funk et al. (2002). This favorable comparison suggests the upper bound 95 percentile confidence interval may be a satisfactory representation of a younger population. The equation governing the upper bound 95 percentile confidence interval is shown in Equation 6.

$$P(F_z) = 1 \Big/ \left(1 + e^{-(F_Z - 7472.73)/1499.36} \right) \quad \textbf{(Equation 6)}$$

where P is the probability of injury, Fz is the predictor variable peak tibia axial force.

The proposed injury risk function offers several advantages over the age adjusted Yoganandan et al. (1996) and Funk et al. (2002) risk functions for predicting the probability of an incapacitating injury in underbelly blast impacts. First, the proposed risk function and risk function proposed by Funk et al. (2002) were developed using uncensored data measured at the mid tibia. Uncensored data inherently provides more information than censored data. The time of fracture is known thereby improving the reliability of the parametric distribution selection, model confidence and overall fit. Tibia axial force measured at the mid-tibia should compare more favorably to data collected from biomechanical surrogates. The Yoganandan et al. (1996) risk function utilized doubly censored data collected at the proximal tibia. Secondly, because of the inherent surprise nature of an AV explosive device blast, PMHS in the current study were not subjected to Achilles tensioning, to simulate an occupant bracing for impact, like the risk function proposed by Funk et al. (2002). The methodology also accounted for the dynamic behavior of the knee and pelvis whereas Yoganandan et al. (1996) was generated using below knee PMHS only. Thirdly, the impact conditions utilized in this

study were modeled from actual full-scale blast tests, in particular, impactor velocity and kinetic energy, loading duration, and magnitude of intrusion. The impactor kinetic energy utilized in this study ranged from 859 to 2,752 J and was significantly greater than the 130 to 722 J range used by Yoganandan et al. (1996). Peak tibia axial force was reached within three milliseconds in the current study. Automotive loading impacts typically reach peak tibia axial force within five to ten milliseconds depending on the magnitude of intrusion. Finally, the injury risk function proposed in this study is specifically designed to predict incapacitating injury for military applications. Only half of the specimen that sustained skeletal injury was classified as incapacitating.

4.5.3 Impactor Velocity Injury Risk Function

Due to the violent and destructive nature of military vehicle blast testing, a biomechanical surrogate may not always be utilized to collect anthropometric data in blast test events. A velocity risk function may serve as a suitable barometer to evaluate the probability of an incapacitating injury when only vehicle floorplate kinematic measurements are available.

Despite the inherent limitations of an extrinsic and censored injury predictor, impactor velocity was found to be a strong predictor of incapacitating injury in the doubly censored survival analysis. A Weibull distribution of the risk curve was found to be the most conservative risk function at the median and demonstrated the highest level of confidence. The confidence of each parametric distribution appeared to diverge above and below the median probability of injury due to the limited population of velocity impact data.

The velocity that corresponds with the median probability of injury in this study, 10.8 m/s, compares reasonably well with the impactor velocity threshold proposed by Schueler et al. (1995) of 9.7 m/s.

4.5.4 Limitations

The assumption made regarding data censoring were critical in the development of the injury risk functions. The experimental design targeted the collection of uncensored data based on a priori knowledge of the potential use of tibia axial force as an injury metric. The technique used to collect uncensored data (utilization of strain gages) was modeled after Funk et al. (2002).

Analysis of the uncensored tibia axial force data using a standard logistic regression technique that assumes doubly censored data would incorrectly indicate an inverse relationship between stimulus and injury (Kent and Funk, 2004). As shown in Figure 42, a standard logistic regression would suggest injury probability decreases as tibia axial force increases.

Another potential limitation of this study is the influence of the implanted tibia load cell and associated equipment on the biofidelity of PMHS tibia. Fractures occurring near the interface of the tibia and potting equipment were considered artifactual and eliminated. Similarly, the lack of Achilles tensioning used in the testing methodology may have contributed to the large predominance of calcaneal injuries (Kitagawa et al, 1998). Due to the relative unavailability of actual military combat injury distribution data, it is difficult to compare the injuries observed in this study with actual combat injury.

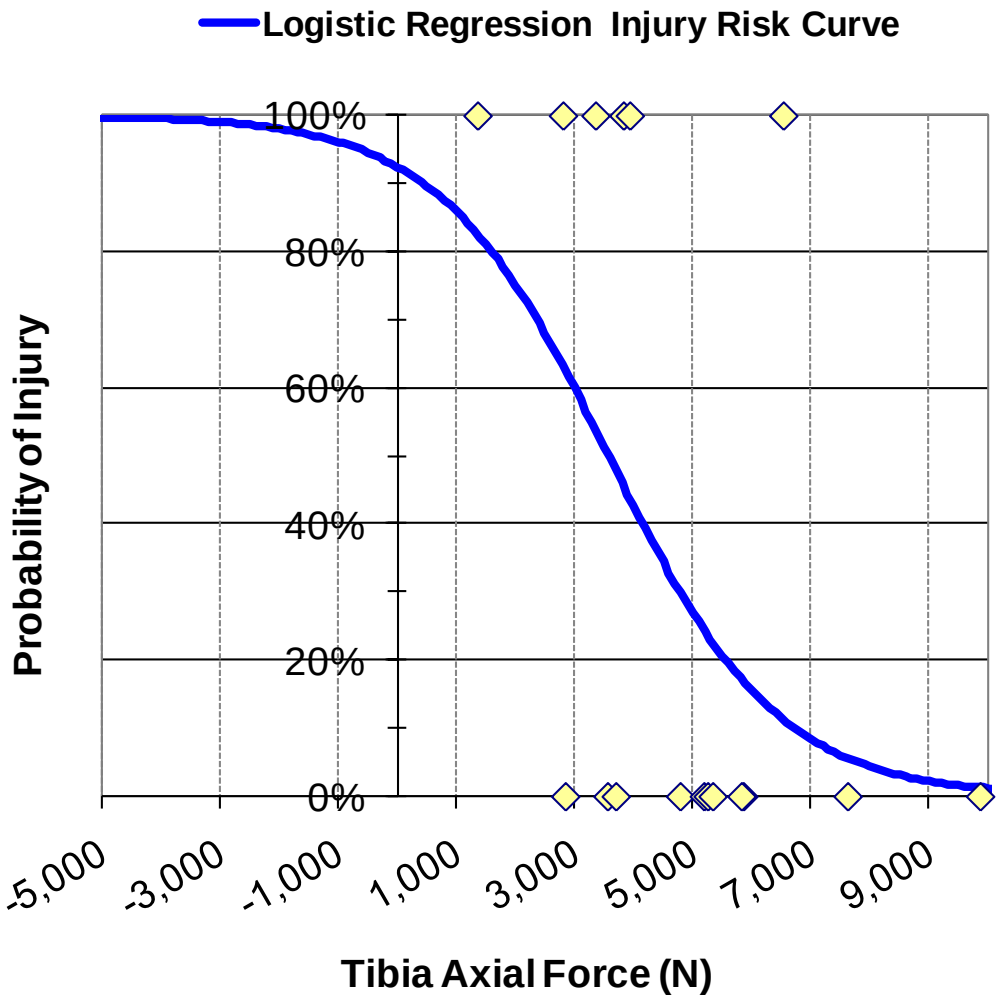

Figure 42: Logistic Regression Injury Risk Curve Assuming Censored Data

Furthermore, the methodology does not consider the load attenuation and distribution effect of a military boot. Barbir (2005) stated a military boot may decrease peak tibia compressive loads by as much as 50 percent. The use of a boot may change the distribution of axial force through the lower leg. The boot may factor in the protection of the calcaneus.

The Yoganandan et al. (1996) tibia axial force risk function offers several advantages over the proposed tibia axial force risk function including a larger data population (52 specimens versus 18), lower average age (56 versus 67), and wider age range (27 to 85 versus 44 to 80). The average age of an active combat soldier is far less than the 67 year old average utilized in this study. Therefore, the proposed risk function is considered conservative.

Finally, currently available lower extremity biomechanical surrogates utilized by the military to assess occupant protection are unable to simulate the biomechanical response of the human tibia to blast impact conditions. The surrogates and have been shown to overestimate tibia axial force by 300 percent (Barbir, 2005). As such, the tibia axial force incapacitating injury risk function proposed in this study is likely not applicable to currently available biomechanical surrogates. A biofidelic surrogate is required that is sensitive to blast impact conditions.

CHAPTER 5

DEVELOPMENT OF A LOWER EXTREMITY BIOMECHANICAL SURROGATE TO ASSESS VEHICLE PROTECTION SYSTEMS IN BLAST IMPACTS

5.1 Introduction

Military organizations utilize standard test methodologies for evaluating the protection level of military vehicles against kinetic energy, artillery, grenade, and mine blast threats. These methodologies standardize test conditions, define threat levels, describe measuring devices and ATD, and specify crew casualty and injury criteria (NATO AEP-55, Procedures for Evaluating the Protection Level of Logistic and Light Armoured Vehicles, 2005). An accurate evaluation of a protection system is dependent on the availability of a biofidelic ATD and accurate injury criteria.

NATO affiliated military organizations typically qualify the protection level of a vehicle to Standardization Agreement (STANAG) 4569. NATO AEP-55 (volume two), *Procedures for Evaluating the Protection Level of Logistic and Light Armoured Vehicles*, describes test procedures and injury criteria for evaluating military vehicle protection systems against grenade and mine blast threats.

The protection level of a military vehicle is determined in full-scale blast tests. A representative military vehicle is subjected to one of four increasingly severe blast mine threats (Table 15). A vehicle that can tolerate a specific threat shall earn a corresponding protection level grade defined in STANAG 4569. Each blast mine threat is detonated under the center of the vehicle or under the wheel or tracks. The vehicle must contain at least one occupant biomechanical surrogate—a standard Hybrid III 50th

percentile male ATD. Additional biomechanical surrogates may be utilized to evaluate injuries to other crew members.

Table 15: Mine Threat Level Definitions (NATO AEP-55, 2006).

Mine Blast Threat Level	Description	Size (kg of TNT)
1	AP fragmentation device	0.55
2	AV blast landmine	6.0
3	AV blast landmine	8.0
4	AV blast landmine	10.0

At minimum, the ATD must be instrumented with a lower tibia load cell, pelvis accelerometer, and upper neck load cell. AEP-55 recommends the ATD include a five-axis load cell for the upper and lower tibia, tri-axial accelerometer located on the tibia mid shaft, shear-axis femur load cell, tri-axial accelerometers in the pelvis, thorax, and head, five-axis load cell in the lumbar spine, and six-axis load cell in the upper neck. The ATD is placed in a realistic position and orientation (seated or standing). The ATD dons the typical military attire and PPE of the test country including military issued boots.

In addition, the vehicle must be instrumented with pressure measurement devices to monitor internal blast overpressure. Although not required by STANAG 4569, additional measuring tools are highly recommended by AEP-55 for collecting additional data to better understand vehicle and biomechanical responses to blast threats. These tools include displacement, acceleration, and force sensors mounted to vehicle structures, foot rests and seating systems, and video data to monitor inside and outside of the vehicle.

National authorities and vehicle designers often deviate from the standard AEP-55 test procedure. These deviations are often implemented to simulate more severe threats, collect more data or evaluate experimental technology and techniques. Various ATD and biomechanical surrogates are utilized to evaluate the effect of passenger size or surrogate biofidelity.

Post-detonation, the vehicle is inspected to rate structural integrity and fragment penetration. Any evidence of vehicle hull rupture, fragment penetration, or potentially injurious loose equipment will result in immediate failure at the tested threat level. An occupant safety evaluation is conducted based on the biomechanical response recorded by the ATD. To earn a passing grade for the tested threat level, the ATD measurements must meet the mandatory performance requirements listed in Table 16.

Table 16: Mandatory Injury Criteria and Tolerance Limits (reprinted from NATO AEP-55, 2006).

Body region	Criteria	Tolerance value	Signification
Lower leg	Peak lower tibia axial compression force (-Fz)	5.4 kN	10% risk of AIS 2+
Thoraco-lumbar spine	Dynamic Response Index (DRIz), calculated with pelvis Az	17.7	10% risk of AIS 2+
Cervical spine (neck)	Upper neck axial compression force (-Fz)	4.0 kN @ 0 ms, 1.1 kN @ 30 ms (see curve in Figure E2.1)	Serious (AIS 3) injuries are unlikely*
	Upper Neck Moment:		Significant (AIS 2+)
	Flexion (+My)	190 Nm	injuries are
	Extension (-My)	57 Nm	unlikely*
Non-auditory internal organs	Chest Wall Velocity Predictor (CWVP)	3.6 m/s	No injury*

The lower extremity injury criterion is specified for peak lower tibia axial compression force. STANAG 4569 references the 45-year old adjusted Yoganandan et

al. (1998) risk function, which specifies a maximum tibia axial force limit of 5.4 kN correlating with a 10 percent risk of AIS two injury. As discussed in Chapter 3, Defense agencies may designate a substitute criterion.

5.1.1 Evaluation of Lower Extremity Biomechanical Surrogates

The responses of the Hybrid III and THOR-Lx biomechanical lower extremity surrogates have been validated for automotive impact conditions. The surrogates were not validated for high amplitude, short duration axial loading typical of an AV explosive blast.

The NATO Research and Technology Organization/ Human Factors Panel (HFM) 090 Task Group 25 Group initiated a multidisciplinary effort to identify an ATD capable of simulating the biomechanical response of a human occupant under blast impact conditions. In an effort to characterize the floorplate loading experienced during an AV landmine blast, Dosquet et al. (2004) performed scaled blast testing using the TROSS™. As described in Chapter 4, scaled charges, ranging from two to ten kilograms of trinitrotoluene (TNT), were detonated under a military vehicle floorplate. The energy emitted from the blast propelled the floorplate axially into the lower limb of a Hybrid III biomechanical surrogate. The floorplate velocity, acceleration, and dynamic displacement, and tibia axial force of the Hybrid III were measured.

Barbir (2005) replicated the TROSS™ parametric floorplate impact conditions in a laboratory-scale setup using a high rate linear impactor. Force-time trajectories measured by a Hybrid III during the TROSS™ evaluations were reproduced in the laboratory setup by tuning impactor floorplate velocity, mass, and length of intrusion. Barbir impacted instrumented PMHS lower limbs at two relatively low severity AV

landmine axial impact conditions (the impact conditions shall be annotated as Barbir C2 and C3) (see Chapter 5 for more details on PMHS impacts). The PMHS lower limbs were instrumented with a tibia load cell at the mid-shaft. Five impacts were conducted at each impact condition. Tibia axial compression data from the PMHS testing were utilized to develop two cadaveric non-injury corridors corresponding to the AV impact impact conditions. Barbir C2 non-injury corridor is shown in Figure 43.

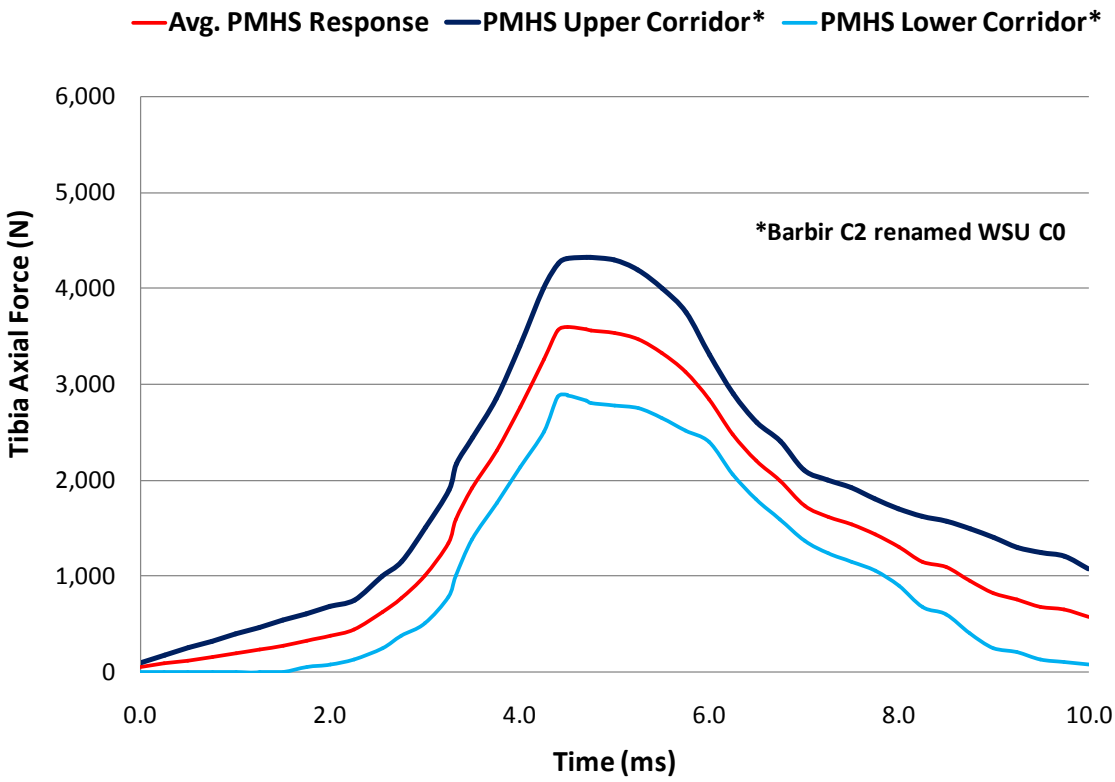

Figure 43: Barbir (2005) PMHS Non-Injury Corridor at Condition 2 Loading.

Utilizing the same high rate linear impactor and simulated AV landmine axial impact conditions, Barbir (2005) evaluated the biomechanical response of a Hybrid III and THOR-Lx lower limb. The biomechanical responses of the surrogates were

compared to the response of instrumented PMHS lower limbs impacted at equivalent impact conditions.

At relatively low severity simulated AV impact conditions, Barbir C2, the tibia axial force of the THOR-Lx compared favorably with the PMHS lower limbs (Barbir, 2005). Figure 44 compares the PMHS tibia axial force non-injury corridor with measurements from six THOR-Lx impact tests at Barbir C2 impact condition.

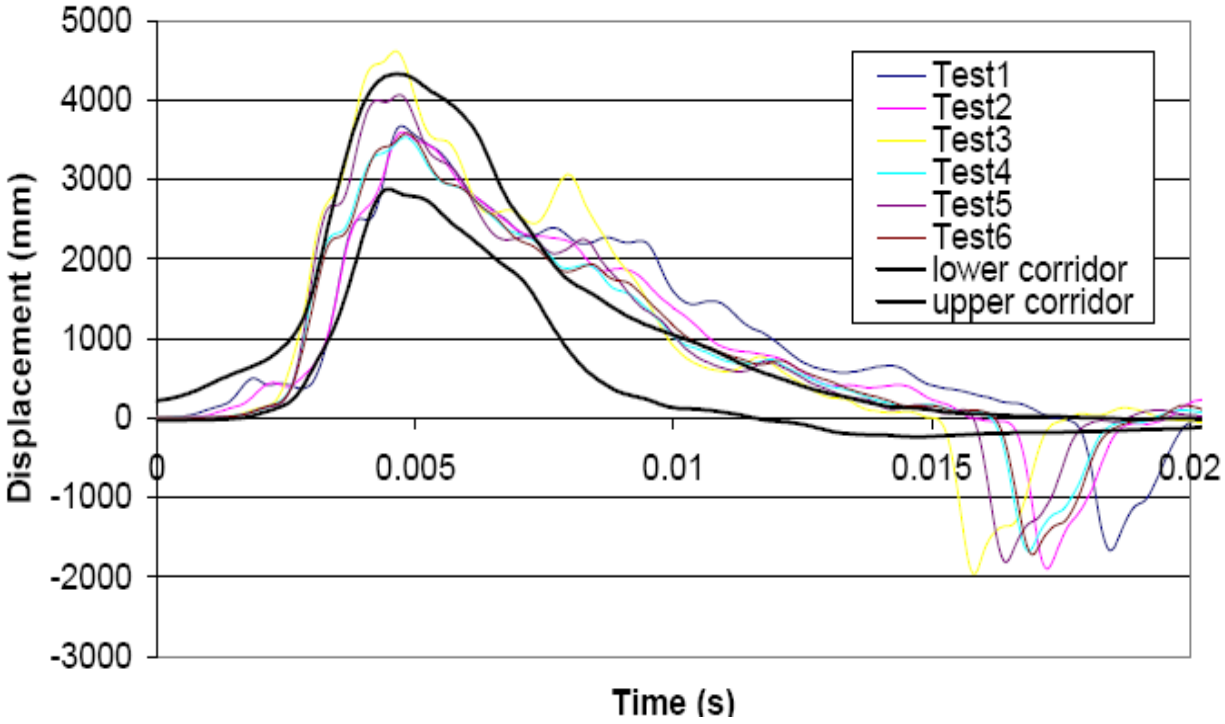

Figure 44: Comparison of Tibia Axial Force at Low Severity Simulated AV Impacts—PMHS Non-injury Corridor and THOR-Lx. (reprinted from Barbir, 2005).

In contrast, the Hybrid III lower limb measured peak tibia axial force nearly three times greater than the PMHS and THOR-Lx (Barbir, 2005). Figure 45 compares the PMHS tibia axial force non-injury corridor with measurements from five Hybrid III impact tests at Barbir C2 impact condition

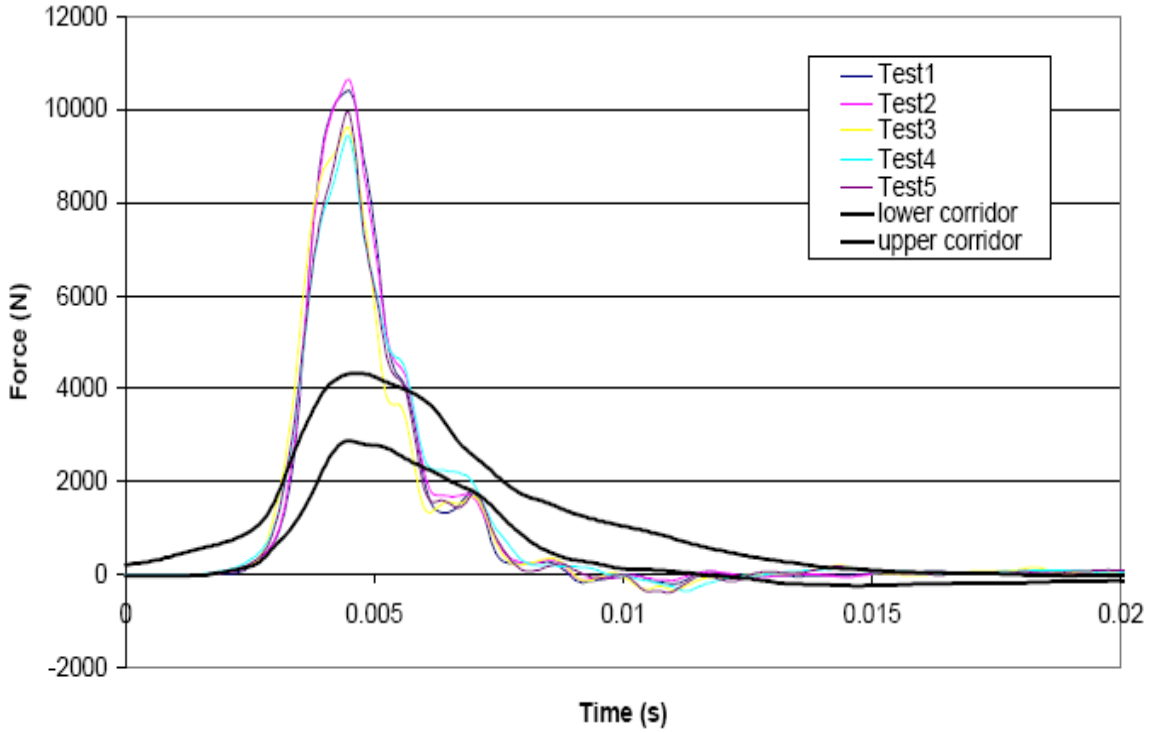

Figure 45: Comparison of PMHS and Hybrid III Tibia Axial Compression at Low Severity Loading (Condition 2) (reprinted from Barbir, 2005).

As simulated AV blast impact severity increased, Barbir C3, the THOR-Lx measured a peak tibia axial force 62 percent larger than the PMHS (Figure 46). Figure 46 compares the PMHS tibia axial force non-injury corridor with measurements from five THOR-Lx impact tests at Barbir C3 impact condition. Hence, the THOR-Lx and Hybrid III lower limb biomechanical surrogates failed to produce a biofidelic response for AV landmine blast loading rates.

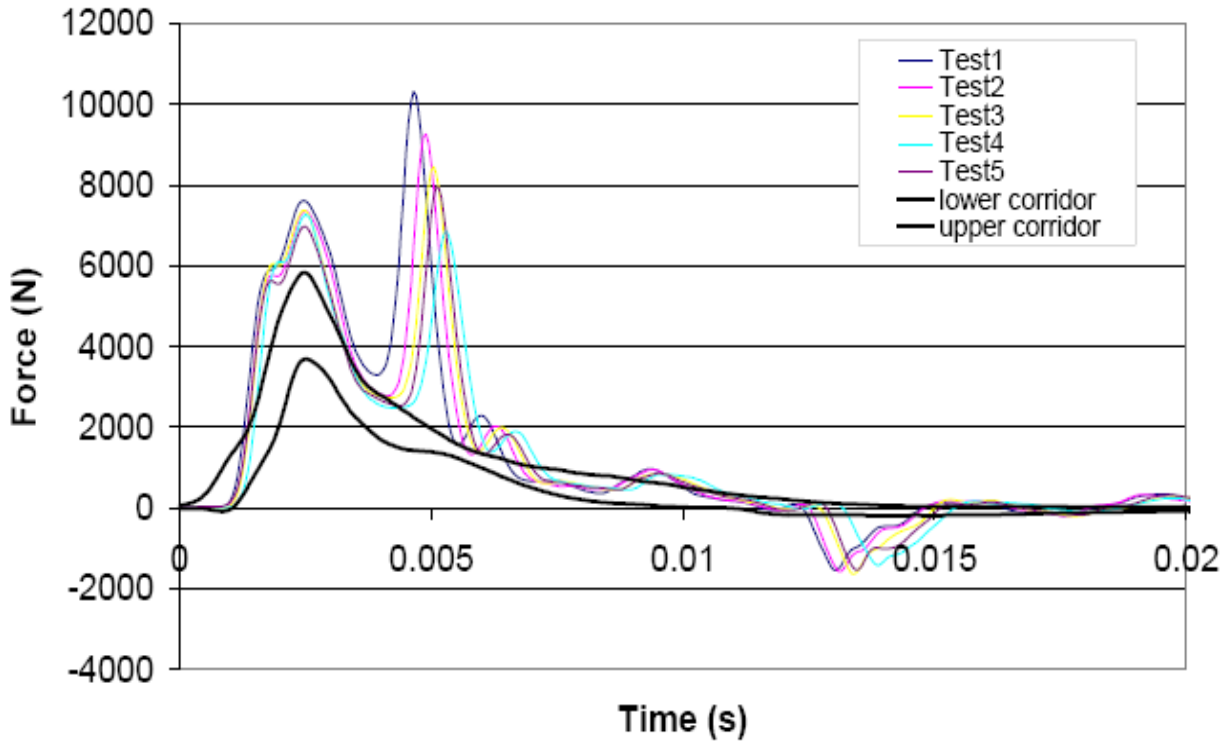

Figure 46: Comparison of PMHS and THOR-Lx Tibia Axial Compression at Increased Severity Loading (Condition 3) (Barbir, 2005).

The simulated AV blast impacts of the Hybrid III and THOR-Lx conducted by Barbir (2005) revealed severe shortcomings in the design of each biomechanical surrogate. The biofidelity of each surrogate decreased substantially when impact severity was increased resulting in an overestimation of peak tibia axial force. This trend suggested the surrogates are too rigid in comparison to a human lower limb. The performance variability between the Hybrid III and THOR-Lx indicated improvements in biofidelity could be achieved by modifying surrogate geometry, components and materials.

5.1.2 Lower Extremity Biomechanical Surrogate Design Objectives

The lack of biofidelity of lower extremity biomechanical surrogates for AV blast impact conditions jeopardizes the validity and accuracy of military vehicle protection system evaluation methodology. A more biofidelic biomechanical surrogate is needed to enable more accurate full-scale vehicle blast test injury assessments and facilitate a means to evaluate blast mitigation systems, personal protective equipment (PPE), materials and structures.

The research presented in this study offers a more biofidelic lower extremity biomechanical surrogate, nicknamed MiL-Lx (military lower extremity), to evaluate the probability of injury resulting from simulated AV blast impacts. A biofidelic surrogate is capable of simulating a biomechanical response of a PMHS under similar impact conditions. Secondly, the surrogate must be capable of distinguishing between a range of impact conditions. More specifically, the surrogate must be able to distinguish between an under-match impact (impact severity that would be unlikely to cause injury) and an over-match impact (impact severity that would likely cause injury). The sensitivity to distinguish between impact severities is needed to evaluate the protective capabilities of PPE, such as military footwear, or blast mitigation materials.

5.1.3 Establishment of PMHS Non-Injury Corridor

The surrogate was developed based on the non-injurious (under-match) biomechanical response of PMHS impacted at WSU C1 loading condition. A lower limb non skeletal injury corridor for axial impacts is presented in Figure 47. The corridor was developed using the force-time trajectories of each WSU C1 impact. The trajectory of each impact was aligned using the peak tibia axial force and a mean average PMHS

response was calculated. The corridor reflects the average peak tibia axial force response at WSU C1 (5,377 N) plus and minus the standard deviation of the peak loads (408 N). The corridor may be utilized to compare the biomechanical response of other surrogates when subjected to similar impact conditions.

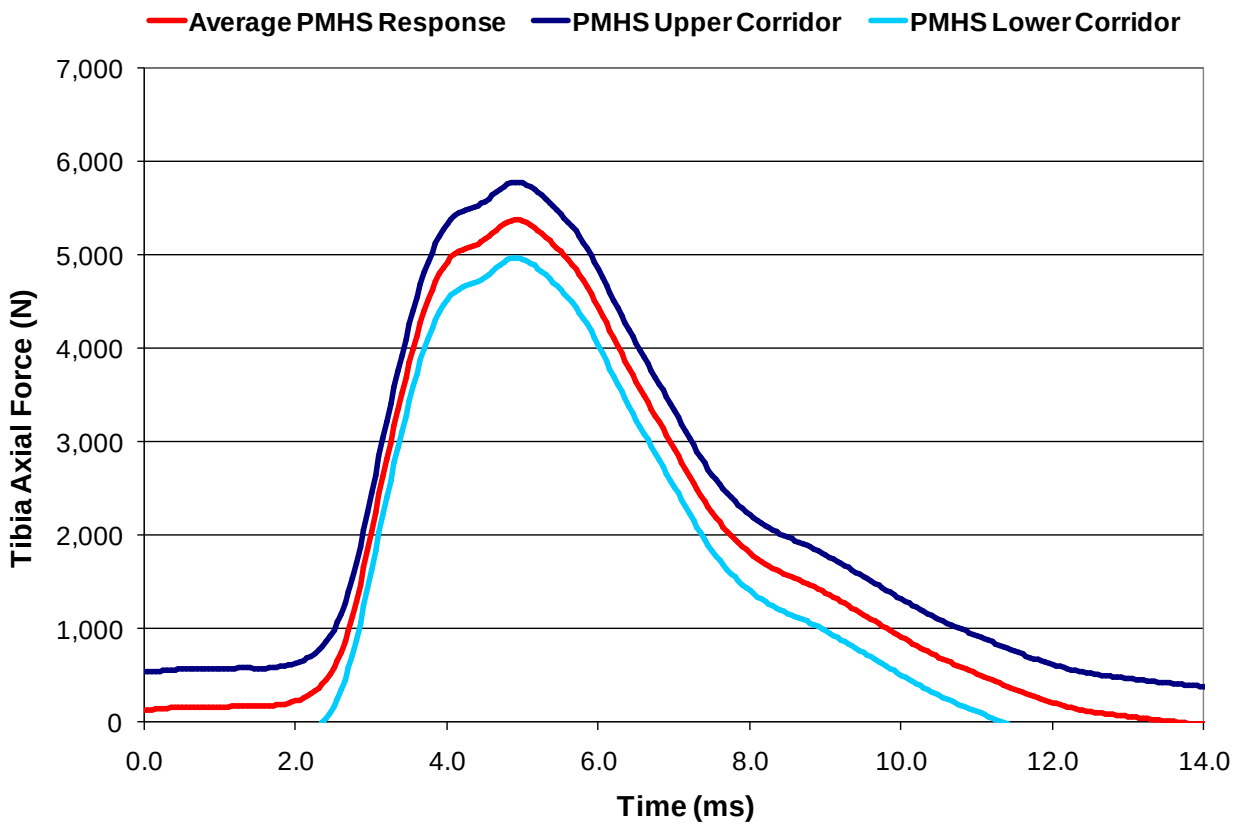

Figure 47: Non-Injury Corridor for Lower Limb Axial Impacts – WSU C1 Impact.

5.2 Surrogate Design

The MiL-Lx was designed and constructed under the scope of this study with the partnership of Denton, ATD INC ®/Humanetics®. The core components of the THOR-Lx were utilized in the construction of the MiL-Lx. The THOR-Lx tibia shaft was incorporated into the design of the MiL-Lx because of its human-like geometry. Unlike the Hybrid III tibia, the THOR-Lx ankle joint and knee clevis are connected by a straight

tibia shaft. The Hybrid III tibia is offset from the line of action between the knee and ankle joint due to a protruding rigid knee clevis (Olson, 2007). Consequently, axial loading of the Hybrid III tibia is not distributed uniformly to the knee joint and may result in high tibia moment of inertia (Zuby, 2001). The THOR-Lx tibia shaft is preferred and has been demonstrated to behave in a biofidelic manner when loaded axially (Zuby, 2001).

In addition, the THOR-Lx tibia compliant element was also adopted into the MiL-Lx design. The compliant element was doubled in length from five to ten centimeters in the MiL-Lx to enable additional room for compression. The longer tibia compliant element was selected to prevent the full compression (often described as “bottoming out”) of the elastomer element at AV blast loading rates. A fully compressed element would often generate two tibia axial force peaks. The first peak was formed as a product of the initial impact. Subsequently, fully compressed compliant element would recoil producing a sudden tension force. The remaining loading from the footplate would then generate a second compressive force on the element.

The compliant element enables the tibia shaft to provide an attenuated force transmission from the heel to the knee complex (National Highway Traffic Safety Administration Vehicle Safety Research, 2000). The compliant element rests between the upper and lower tibia tubes, which hold the upper and lower tibia load cells respectively. The MiL-Lx tibia shaft includes an accelerometer mounting site distal of the compliant element. Figure 48 displays the tibia shaft and associated components.

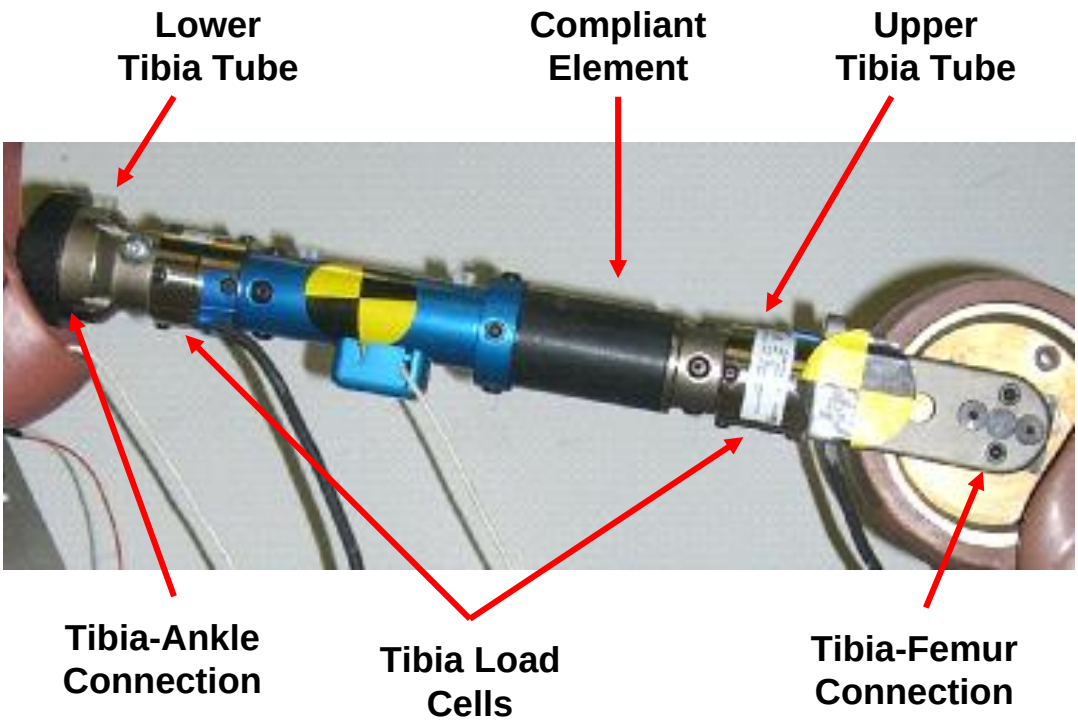

Figure 48: MiL-Lx Tibia Shaft.

The MiL-Lx foot and ankle closely resembles the structure of the Hybrid III and includes several improvements. The MiL-Lx incorporates a more durable polyurethane foot cover than the THOR-Lx and Hybrid III. The cover is expected to enhance the recovery of the elastomer from compression impact to ensure repeatable performance for a longer duration. The cover also includes a slot to install a replaceable compliant footpad. Similar to the tibia compliant element, the footpad dampens or tunes the force transmission from the heel to the ankle joint and tibia shaft (Figure 49). The bones of the foot are simulated by a carbon fiber plate extending from the heel to the foot. An accelerometer mounting site is located at the mid-foot of the MiL-Lx assembly.

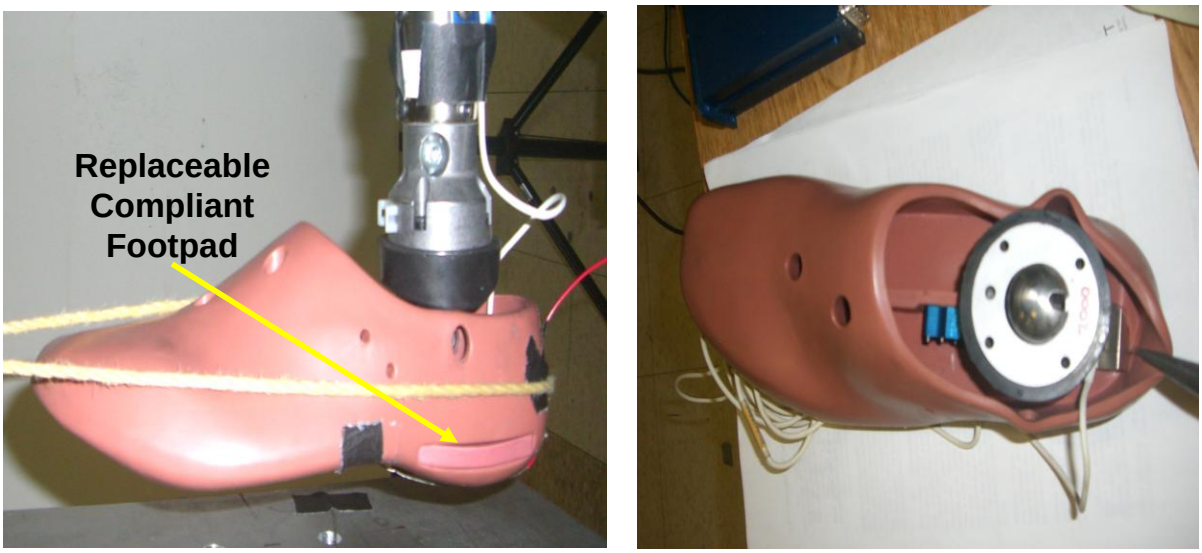

Figure 49: MiL-Lx Foot and Ankle.

The Hybrid III ankle ball joint is utilized in the MiL-Lx to simulate the articulation of the foot and ankle. The ankle joint rotates about the x and y-axes providing inversion/eversion and dorsiflexion/plantarflexion. The joint moment characteristics are controlled by Rosta devices, which increase resistive torque as the joint rotates (National Highway Traffic Safety Administration Vehicle Safety Research, 2000). The ankle joint was designed to reproduce the static and dynamic moment-angle response characteristics in flexion and inversion/eversion measured by Portier et al. (1997) and Petit et al. (1996) in PMHS lower limb studies (Olson, 2007). Similarly, the THOR-Lx ankle joint was designed to produce a biofidelic response to axial loading at the heel Kuppa et al. (1998).

The THOR-Lx contains an Achilles tendon assembly to simulate the passive resistance of the gastrocnemius and soleus muscles to resist rotational energy. In AV blast impacts the magnitude of rotational loading is negligible in comparison to axial

loads generated by the blast. The mechanism of PMHS lower limb skeletal injuries observed in this AV explosive blast study was symptomatic of axial loading only. Furthermore, the unexpected nature of a mine blast likely prohibits the occupant from initiating a bracing motion triggered by the compression of the Achilles tendon. As such, the Achilles tendon assembly was not adopted in the design of the MiL-Lx. In addition to simplifying the overall design, the elimination of the Achilles tendon assembly significantly reduced the cost of the MiL-Lx in comparison to the THOR-Lx.

The finalized MiL-Lx biomechanical surrogate design in shown in Figure 50.

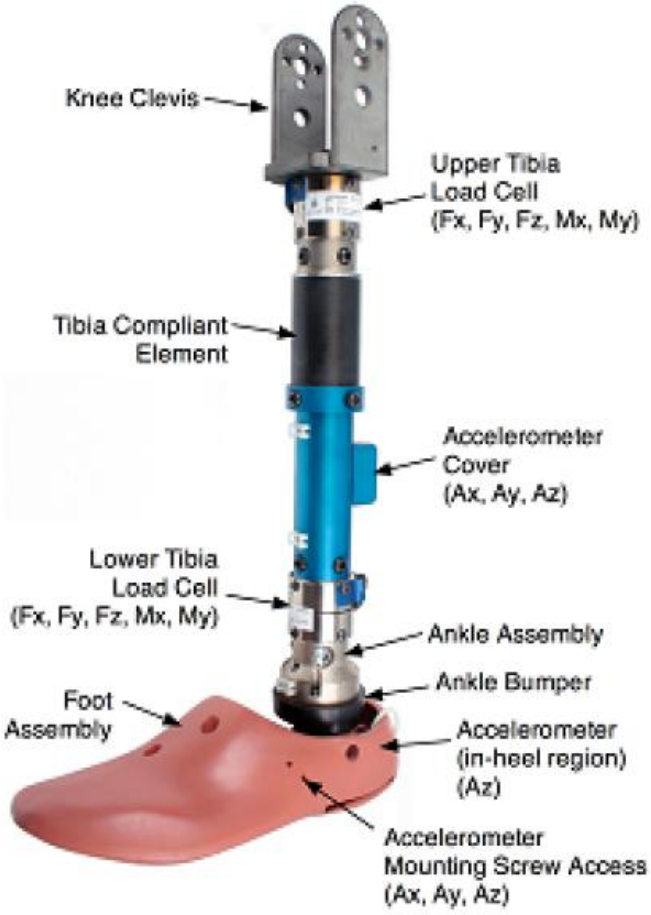

Figure 50: MiL-Lx biomechanical surrogate.

5.3 Methodology

With the core components and instrumentation of the MiL-Lx finalized three categories of testing were defined to critically evaluate the MiL-Lx design: (1) compliant element selection and validation testing; (2) sensitivity evaluation; and (3) out-of-position mechanical durability evaluation.

5.3.1 Material Properties Selection and Validation Testing

A comprehensive evaluation was conducted to identify the optimal material properties of the compliant footpad and tibia compliant element. The compliant materials are responsible for attenuating the peak tibia compressive loads measured by the MiL-Lx during an axial impact. The objective of the material property evaluation is to identify compliant materials that can tune the tibia compressive loads measured by the MiL-Lx when impacted at WSU C1 axial impact condition. As such, the material's stiffness and compressive modulus were the primary properties of interest.

In order to evaluate the effect of the materials' compressive modulus, the material was installed in the MiL-Lx and loaded axially at WSU C1 impact condition. A MiL-Lx lower limb surrogate was connected at the mid-femur to a Hybrid III full body surrogate. An air piston driven linear impactor was utilized to axially load the plantar aspect of the MiL-Lx surrogate at the targeted impact condition. The linear impactor and impact condition utilized in the MiL-Lx evaluation were the same as that utilized in the lower limb PMHS evaluation detailed in Chapter 4. The impactor propelled a steel floorplate and its shaft, weighing a combined 36.7 kg, up to the target impact velocity. The floorplate was allowed to travel a short distance (24 millimeters) after contacting the surrogate to simulate the plastic intrusion of a vehicle floorplate following an explosive

blast. Once the target intrusion was achieved, the linear impactor was rapidly decelerated.

High-speed video was collected using a HG 100K Camera (Redlake, Inc) at 10,000 frames per second with a given resolution of 256 by 192 pixels. The displacement of the impactor floorplate was measured dynamically using a distance laser transducer (Micro-Epsilon Corporation Model number LD 1625-200). The derivative of the displacement was utilized to calculate impactor velocity at the time of impact. A non-contact optical velocity sensor was utilized to measure the peak velocity of the cylindrical shaft following take-off. An accelerometer was mounted to the impactor.

A select tibia compliant element was installed in the MiL-Lx prior to each test. The surrogate is impacted at least two times at WSU C1 impact conditions to establish a repeatable biomechanical response. A minimum of 30 minutes is reserved between impacts to allow the elastomer components to recover from impact. To minimize the degrees of freedom only one compliant material, footpad or tibia compliant element, is varied per impact. Figure 51 shows the test setup and surrogate positioning.

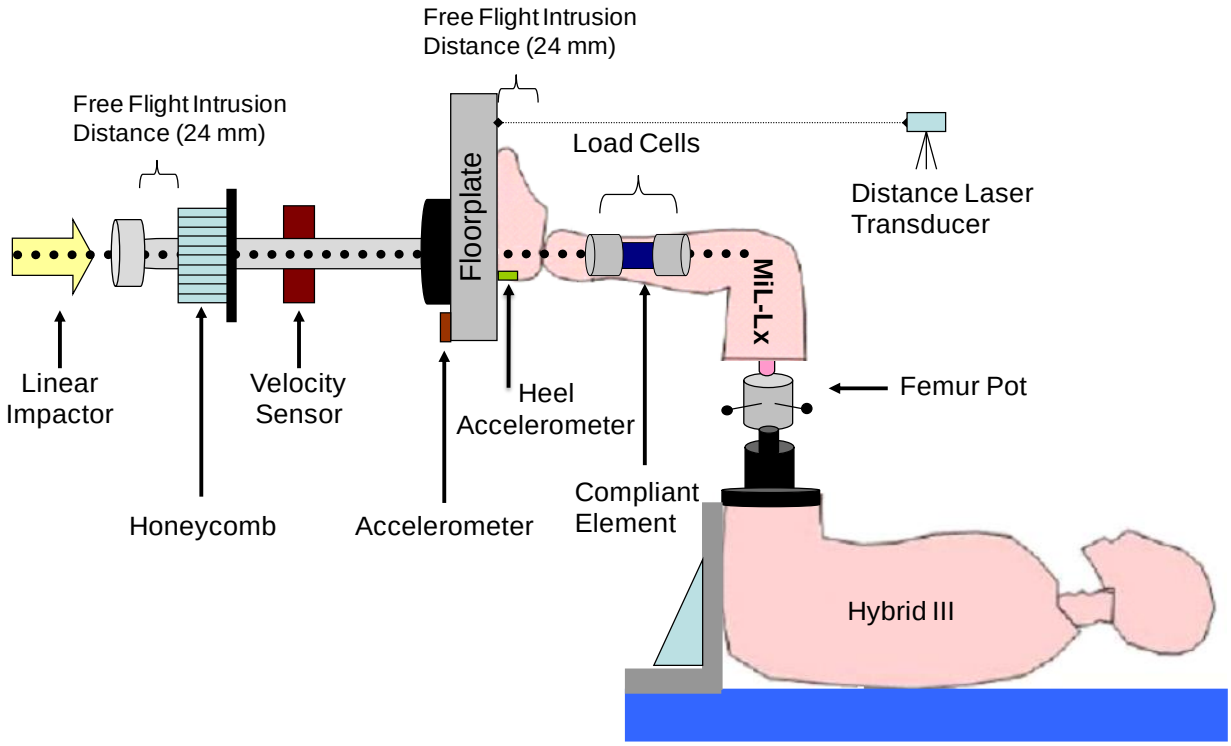

Figure 51: MiL-Lx Impacts using Air Piston Linear Impactor.

Seven levels of footpad stiffness were evaluated to determine the ability of the footpad to attenuate axial loads prior to reaching the lower tibia load cell. The footpad elastomer materials ranged from soft foam rubber to hard neoprene. A compliant footpad possessing similar stiffness properties as a Hybrid III rubber foot cover was utilized as the baseline foot pad stiffness. Figure 52 present these materials utilized in the study and their relative stiffness. Each impact was conducted utilizing the same baseline tibia compliant element to minimize the degrees of freedom.

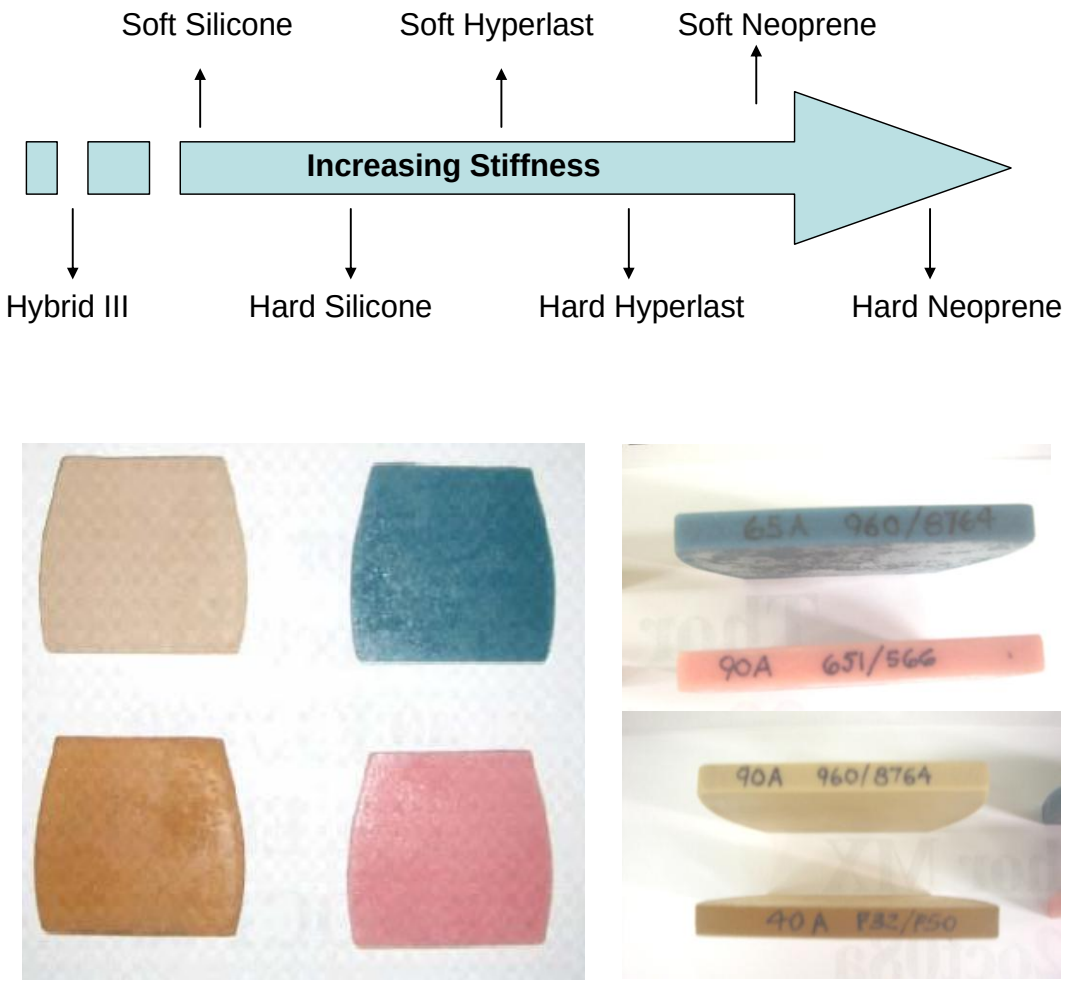

Figure 52: Top: Footpad Stiffness. Bottom: Compliant Footpad Material Samples.

Similarly, 16 levels of tibia compliant element stiffness were evaluated to determine ability of the element to attenuate axial loads prior to reaching the upper tibia load cell. A compliant element possessing similar stiffness properties as the THOR-Lx element was utilized as the baseline stiffness. Three element diameters were evaluated: 3.8, 4.4, and 5.0 centimeters (Figure 53). Each impact was conducted utilizing the same baseline footpad compliant material to minimize variables.

Figure 53: Tibia Compliant Element Material Samples.

Following the identification of suitable compliant material, the repeatability of the finalized MiL-Lx biomechanical response was evaluated. The MiL-Lx was impacted four times at the WSU C1 impact condition. The peak tibia axial force, force loading rate, loading pattern and duration and standard deviation of the data were compared with the PMHS response.

5.3.2 Sensitivity Evaluation

After a suitable combination of compliant element and footpad stiffness was identified to match the non-injury PMHS corridor, the materials were evaluated at incrementally more severe loading rates abbreviated as WSU C2 and C3. An additional low severity loading rate was introduced, WSU C0, to simulate a less severe loading

rate than WSU C1. WSU C0, modeled after Barbir (2005) “Condition 2” (Figure 43), has a launch velocity of 5.5 m/s and a kinetic energy of 555 J.

The objective of the impact testing was to determine whether the surrogate could demonstrate sensitivity to distinguish between AV landmine loading severities. The validated MiL-Lx was impacted at WSU C0, C2 and C3 to determine if the surrogate is capable of distinguishing incrementally severe impact conditions. The sensitivity of the surrogate was evaluated by comparing the peak tibia axial compression, loading pattern, and duration measured by the upper tibia for each loading rate.

5.3.3 Out-of-Position Durability Evaluation

Currently available lower extremity biomechanical surrogates are occasionally destroyed in military full-scale, live fire blast tests. Many of the surrogate losses occur in out-of-position (OOP) testing. The validated MiL-Lx was impacted at two OOP surrogate arrangements at WSU C1, C2, and C3 to determine its mechanical durability under stress. The performance objective of the surrogate is to withstand the loading without mechanical or instrumentation failure. Considering the loading is not purely axial, the biomechanical response data collected could not be translated to human lower limb injury data for AV blast impact severity.

The MiL-Lx was impacted three times at each OOP. The OOP testing was designed to subject the surrogate to a range of radial, oblique, and axial loads. The orientation of the first OOP test, abbreviated OOP-A, was used to mimic the position of a relaxed passenger. The surrogate was positioned with the lower limb flexed to 54 degrees about the knee instead of at 90 degrees in the PMHS lower limb study (Figure

54, Left). The orientation of the second OOP test, abbreviated OOP-B, was used to mimic the position of a driver. The surrogate was positioned with the lower limb flexed to 45 degrees about the knee and the foot dorsiflected to 45 degrees (Figure 54, Right).

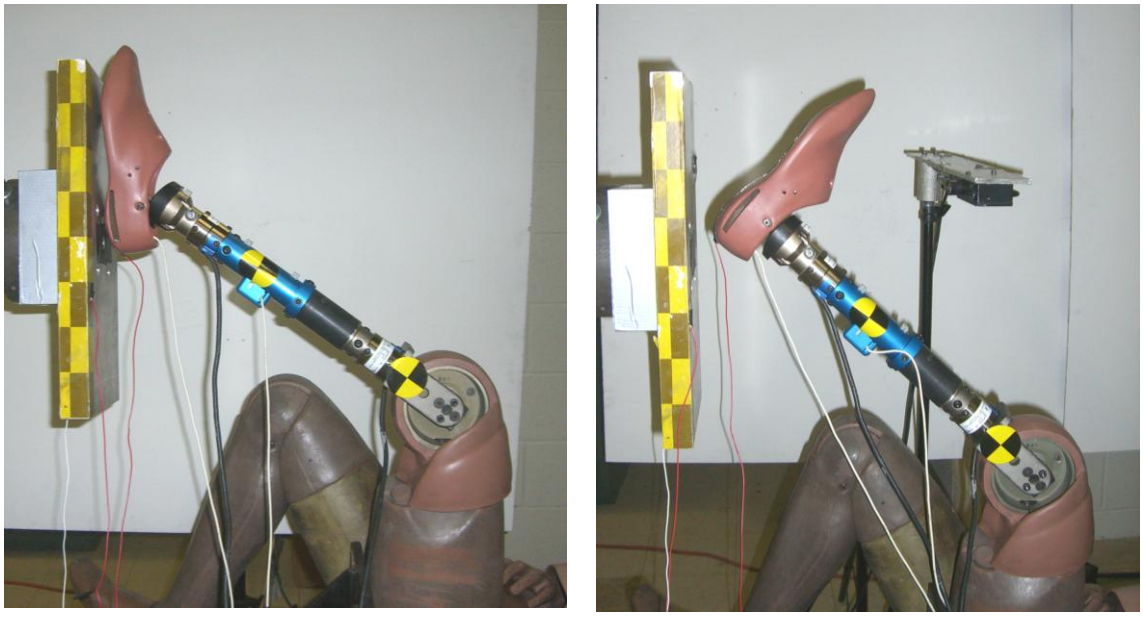

Figure 54: Left: Orientation of OOP-A. Right: Orientation of OOP-B.

5.3.4 Data Collection and Processing

Data acquisition was conducted at 20,000 Hz using a TDAS Pro System (DTS, Seal Beach, CA). A four-pole Butterworth filter with a cutoff frequency of 4300 Hz was used for anti-aliasing. The MiL-Lx surrogate upper and lower tibia load cells measured axial force (Fz), the shear forces (Fx and Fy), the fore/aft and lateral bending moments (Mx and My, respectively). Mid-foot and mid-tibia accelerations were recorded using a tri-axial accelerometer. Extrinsic stimuli including floorplate displacement and acceleration were measured. Acceleration and tibia load data were filtered using a CFC 600 filter. Moment data were filtered using a CFC 180 filter. Floorplate displacement data were filtered using a low pass Butterworth filter at 1000 Hz.

5.4 Results

A series of impact tests were conducted to (1) identify a suitable compliant element and finalize the MiL-Lx design; (2) determine the sensitivity of the MiL-Lx to distinguish loading severity; and (3) evaluate the durability to withstand out-of-position impacts.

5.4.1 Compliant Element Material Selection

A series of impact tests were conducted to identify a suitable combination of footpad and compliant element compression stiffness to enable the MiL-Lx to match the PMHS non-injury corridor.

Initially, the baseline performance of the MiL-Lx was established using the baseline compliant footpad and tibia compliant element (3.8 centimeter diameter) stiffness. The combination of these compliant materials produced a lower and upper peak tibia axial force of 7,225 N and 8,053 N respectively. The peak tibia force far exceeded the average non-injury peak tibia axial force of 5,377 N. A comparison of the baseline MiL-Lx biomechanical response and PMHS upper and lower non-injury corridor is presented in Figure 55.

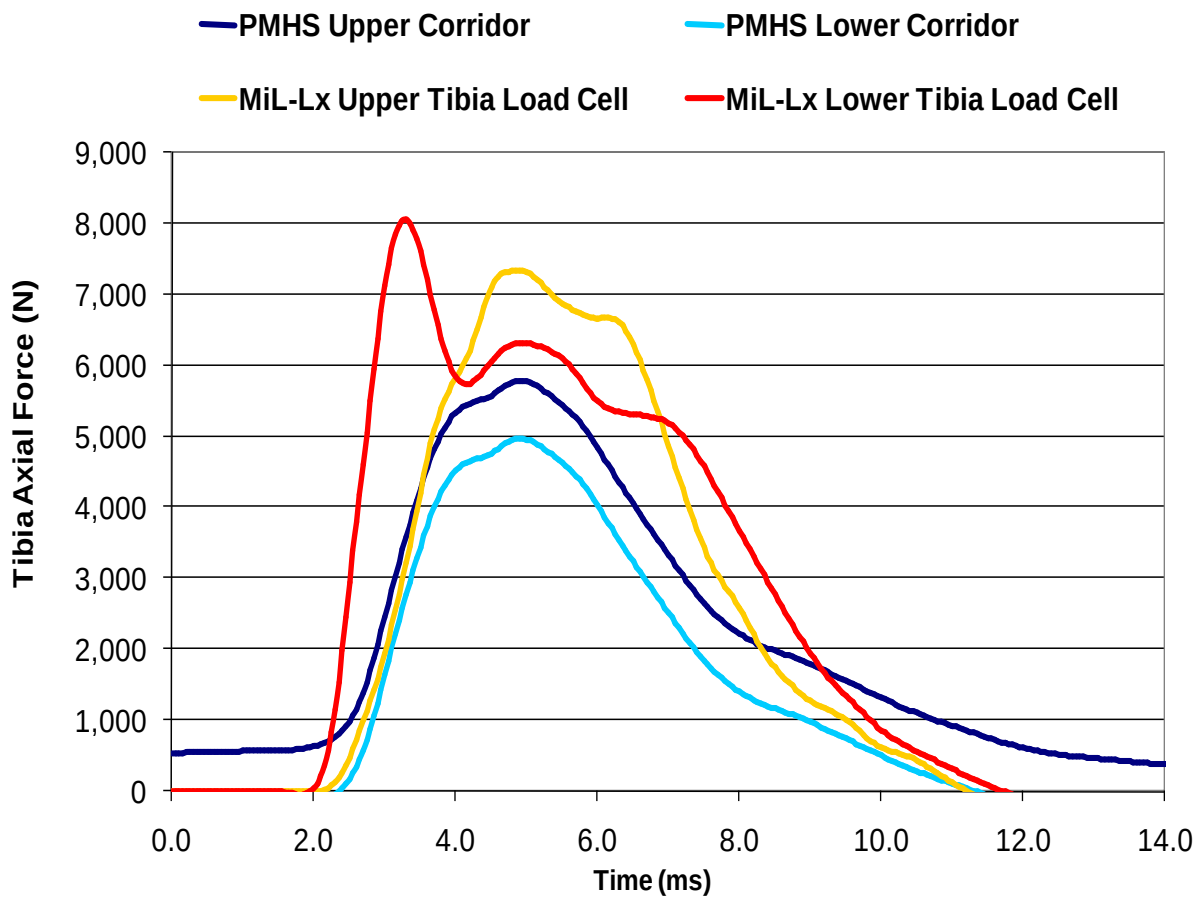

Figure 55: MiL-Lx Baseline Compliant Material Performance.

Unlike the tibia axial force response measured by the PMHS non-injury lower limb and MiL-Lx upper tibia load cell at WSU C1 impacts, the MiL-Lx lower tibia load cell does not follow a parabolic axial force loading pattern. Initially, the impactor footplate transmits high amplitude inertial loads through the foot, footpad, and ankle joint onto the lower tibia tube. The lower tibia load cell reaches its peak axial force as the tibia compliant element, located proximal to the load cell, reaches maximum compression. As the element recovers from the inertial load a tension force drives the tibia shaft away from the axial loading direction. This tension effect is responsible for the sudden drop in

axial force. The compression and subsequent tension of the elastomer generate the first tibia axial force peak. After the element returns to its baseline state additional loads are transmitted through the lower tibia. The subsequent loading often produces a second tibia axial force peak.

Varying the stiffness of the compliant footpad material had minor impact in reducing the initial inertial peak measured by the lower tibia load cell. For example, a softer footpad material was able to reduce the peak axial tibia force by 534 N from the baseline figure of 8,053 N to 7,519 N. Figure 56 illustrates the effect of footpad material on tibia axial force attenuation as measured by the lower tibia load cell (Figure 58). Although the compliant footpad material stiffness had a negligible impact the peak tibia compression measured by the upper tibia load cell, the softer footpad appeared to reduce the vibration or noise measured at the upper tibia load cell.

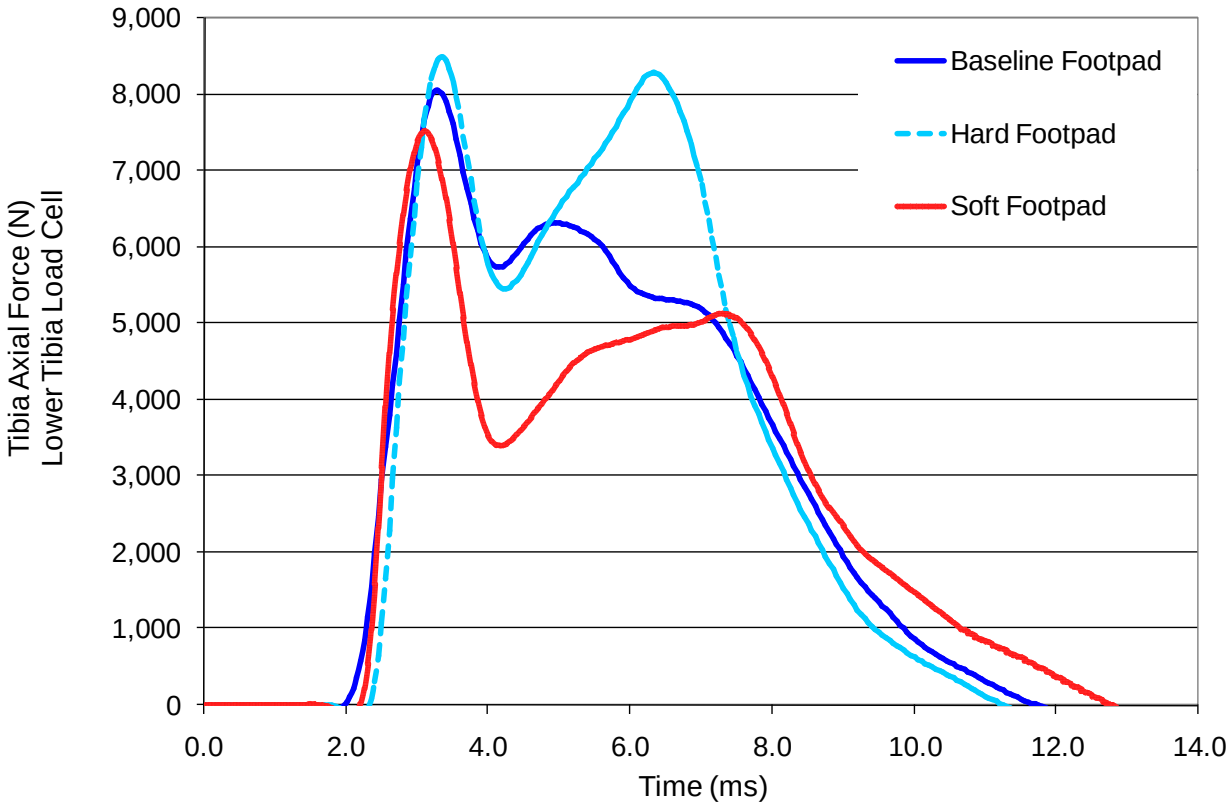

Figure 56: Comparison of Footpad Material Attenuation (Lower Tibia Load Cell).

The upper tibia load cell is loaded immediately as the tibia compliant element begins its compression. The upper tibia reaches its peak axial tibia compressive force after the tibia compliant element completes it return to its baseline state. The upper tibia generates a parabolic loading pattern and loading duration comparable to a PMHS lower limb non-injury response. Since the upper tibia load cell is located proximal of the tibia compliant element the initial inertial peak loads measured by the lower tibia load cell are completely attenuated.

Varying the stiffness of the tibia compliant element produced dramatic improvements in tibia axial force attenuation for the upper tibia load cell. The

attenuation of force is proportional to the energy needed to compress the elastomer material. Figure 57 illustrates the reduction in peak tibia axial force using two softer compliant elements. The utilization of a soft compliant element reduced the peak tibia axial force measured by the upper tibia load cell by 1,943 N from the baseline peak load of 7,331 N to 5,388 N. The average non-injured PMHS lower limb generated a peak tibia axial force of 5,377 N at the same WSU C1 impact condition. Further attenuation may be achieved by utilizing even softer elastomer materials for the compliant element. A very soft compliant element was able to reduce the peak tibia axial force by 3,504 N to achieve a peak force of 3,828 N.

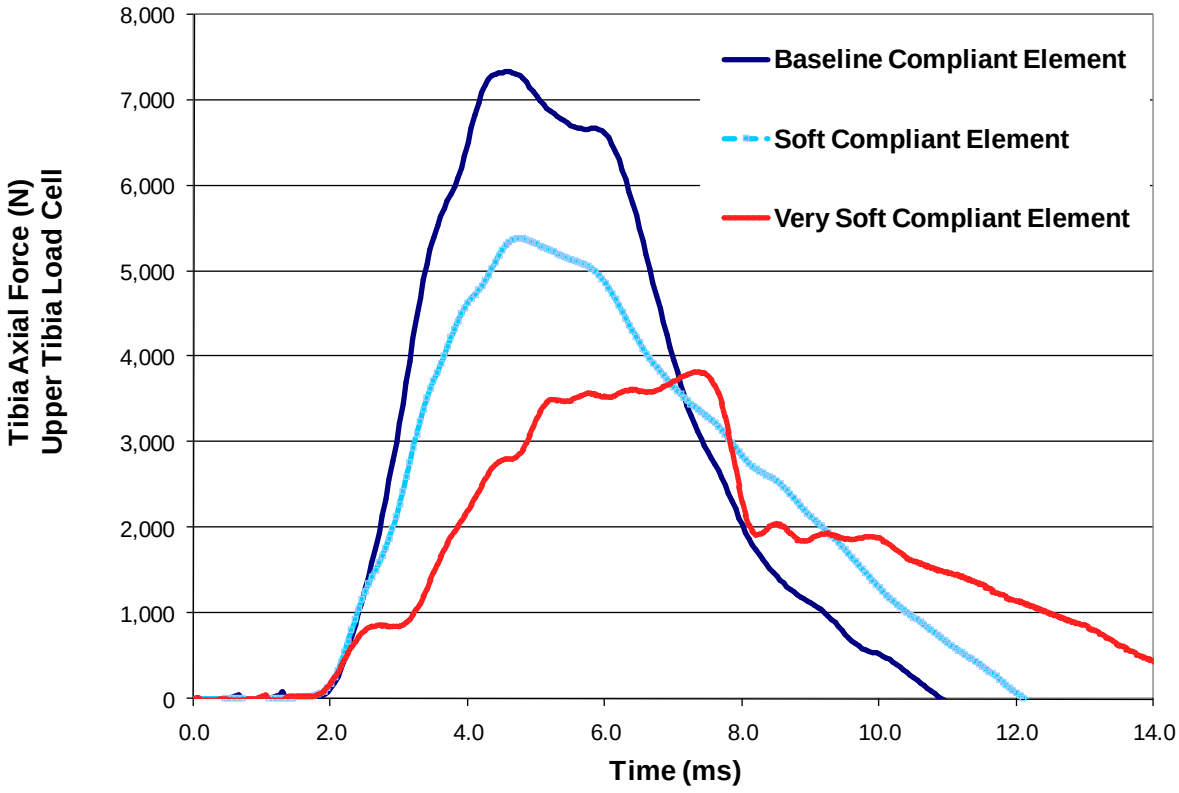

Figure 57: Comparison of Tibia Compliant Element Material Stiffness Attenuation (Upper Tibia Load Cell).

Tibia axial force was also effectively attenuated by increasing the diameter of the tibia compliant element and maintaining baseline stiffness. Increasing from a 2.5 centimeter baseline diameter to a 3.8 and 5.0 centimeters reduced the peak tibia axial force measured by the upper tibia load cell by 367 N and 2,050 N respectively (Figure 58). The upper tibia load cell measured a peak tibia axial force of 5,282 N when using a 5.0 centimeters diameter compliant element. The attenuation of force is proportional to the additional volume of elastomer material participating in the compression.

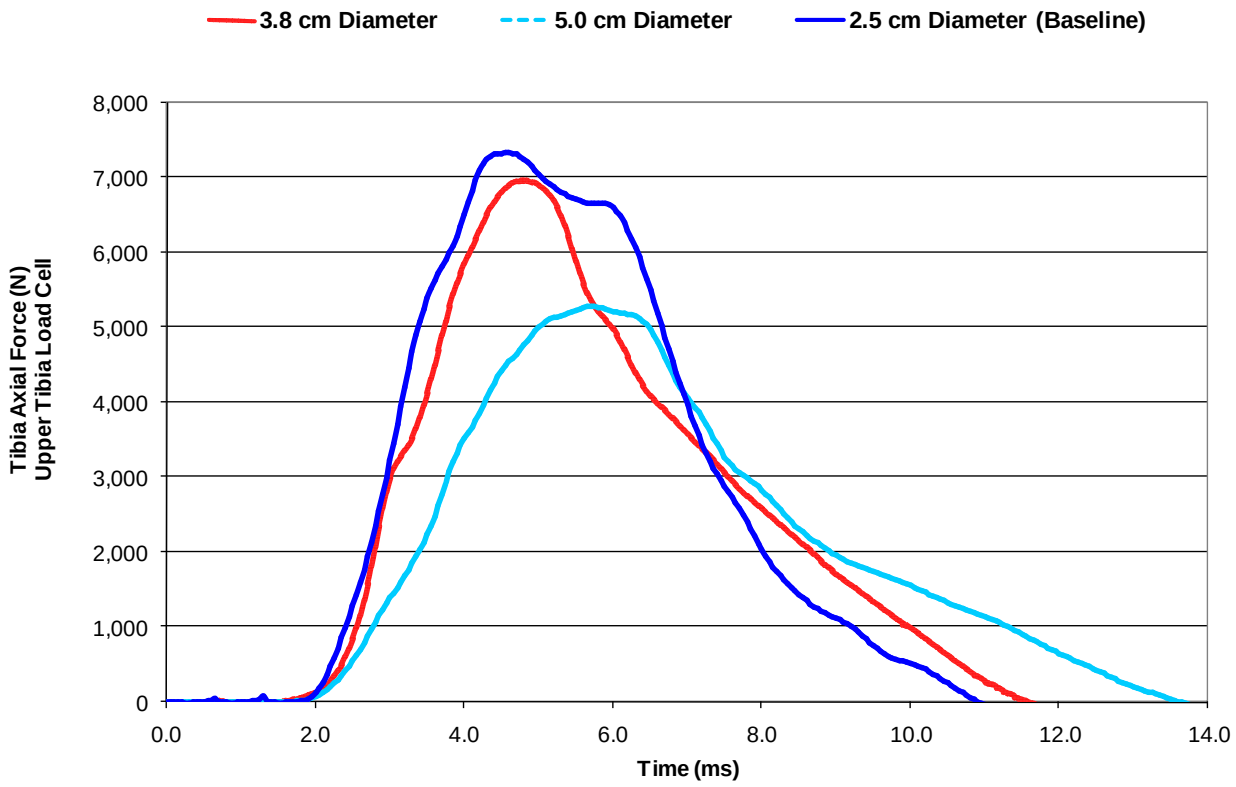

Figure 58: Comparison of Tibia Compliant Element Material Diameter Attenuation (Upper Tibia Load Cell).

Over 100 impact tests were conducted on the MiL-Lx to identify the optimal combination of compliant material stiffness and diameter to produce a biofidelic

biomechanical response to simulated AV landmine impacts. The identified combination of compliant material underwent a series of four validation impacts at WSU C1 impact condition. Table 17 provides a summary of upper tibia transducer outputs and impactor kinematic data for WSU C1 MiL-Lx validation test impacts. The average impact velocity and kinetic energy of the impacts were 7.1 m/s and 933 J respectively. The force-time trajectories measured by the MiL-Lx upper tibia load cell are shown in Figure 59. The MiL-Lx peak upper tibia axial force averaged 5,377 N and ranged from 5,190 to 5,528 N. The MiL-Lx biomechanical response demonstrated high repeatability with a standard deviation of 181 N for peak tibia load.

Table 17: MiL-Lx WSU C1 Validation Testing.

Test Condition	Test	Impactor Velocity (m/s)	Impactor KE (J)	Peak Fz (N)	Fx (N)	Fy (N)	Mx (N*m)	My (N*m)
WSU C1	Impact 1	6.9	875	5,190	456	439	20	82
	Impact 2	7.3	979	5,534	596	541	22	126
	Impact 3	7.2	952	5,499	566	483	22	98
	Impact 4	7.1	926	5,219	520	597	28	34

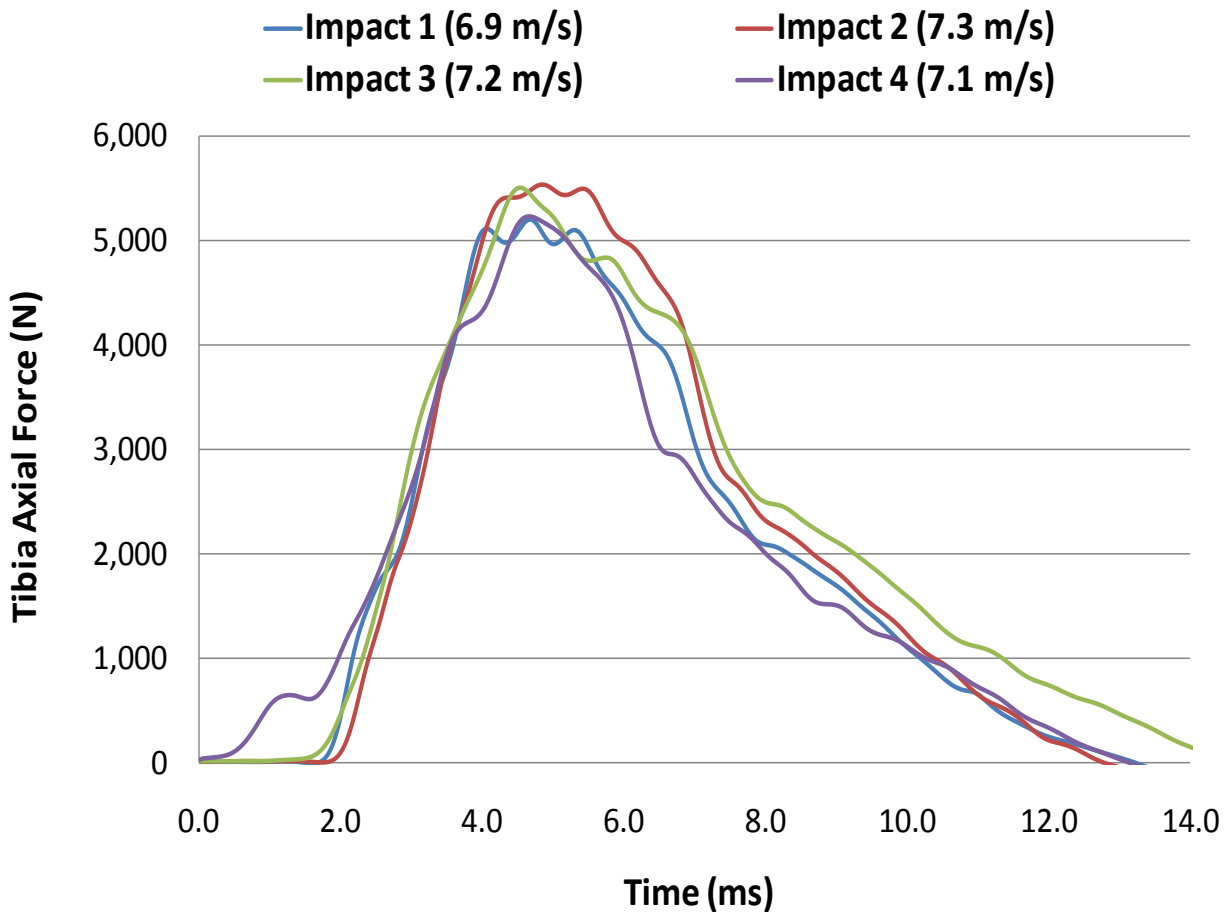

Figure 59: MiL-Lx Response to WSU C1 Loading.

The trajectory of each impact was aligned using the peak tibia axial force and a mean average MiL-Lx response was calculated. Figures 60 and 61 compare the average MiL-Lx response with the PMHS non-injury corridor with respect to duration and intrusion respectively. The biomechanical response of the MiL-Lx compares favorably with the PMHS non-injury corridor with respect to peak tibia axial force, loading rate, loading duration, and intrusion.

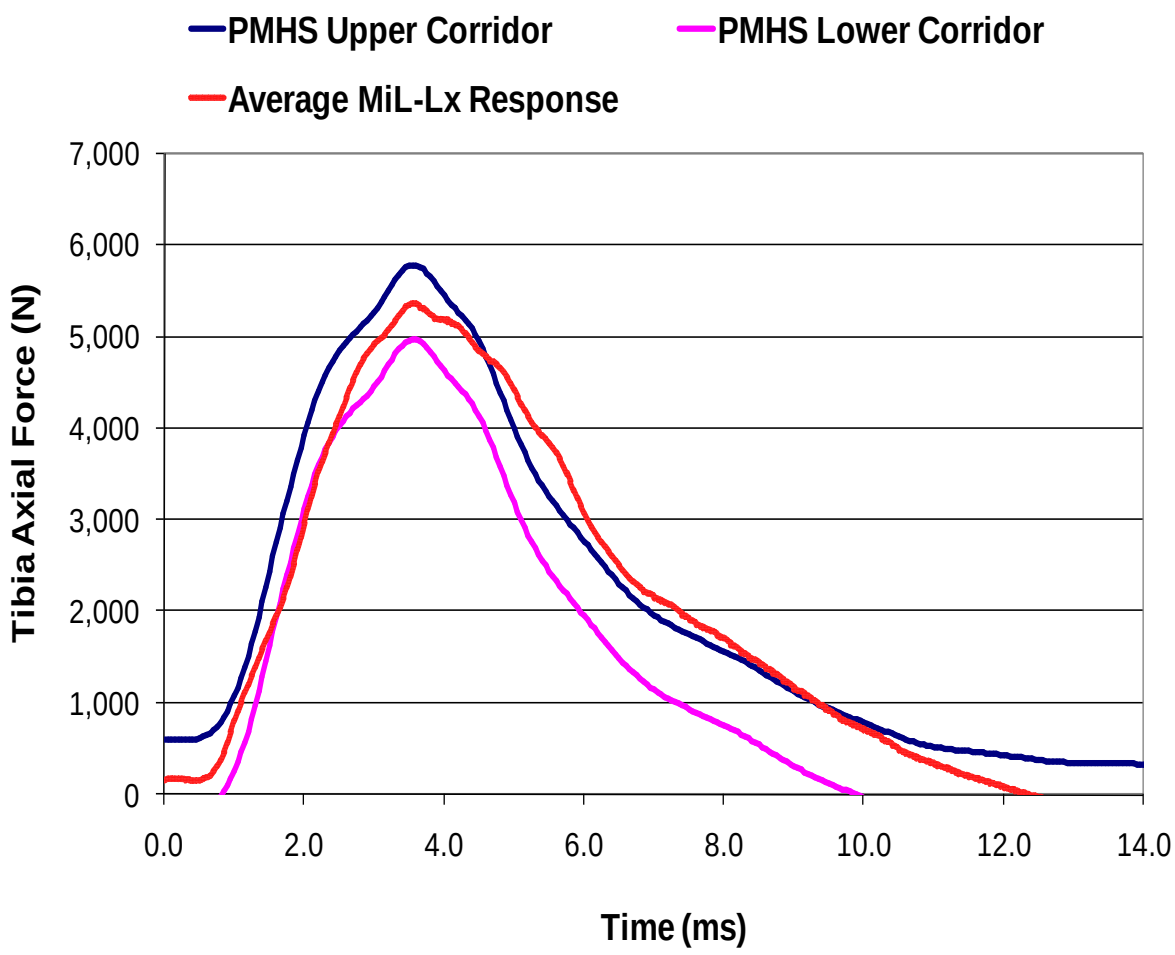

Figure 60: Comparison of PMHS and MiL-Lx Tibia Axial Force-Time Response.

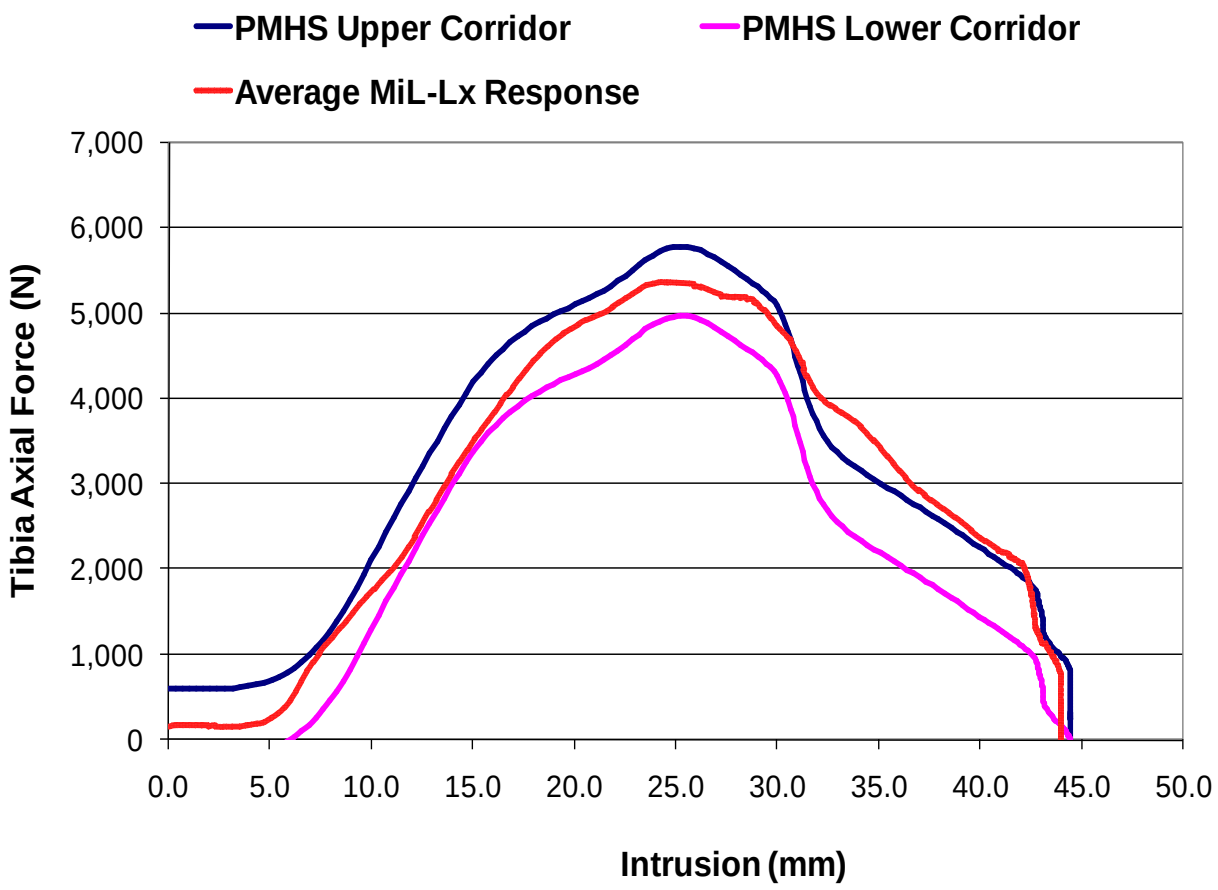

Figure 61: Comparison of PMHS and MiL-Lx Tibia Axial Force-Intrusion Response.

5.4.2 Sensitivity Evaluation

Following the validation testing, the MiL-Lx was impacted at WSU C0, C2, and C3 to determine if the surrogate was capable of distinguishing incrementally severe impact conditions. Four impacts were conducted at each impact condition. Table 18 provides a summary of upper tibia transducer outputs and impactor kinematic data for each impact condition. Table 19 compares the average biomechanical response of the MiL-Lx at each impact severity.

Table 18: Summary of MiL-Lx Response.

Test Condition	Test	Impactor Velocity (m/s)	Impactor KE (J)	Peak Fz (N)	Fx (N)	Fy (N)	Mx (N*m)	My (N*m)
WSU C0	Impact 1	5.6	576	3,724	283	246	33	61
	Impact 2	5.5	556	3,642	299	204	28	51
	Impact 3	5.0	459	3,251	308	228	34	57
	Impact 4	5.3	516	3,354	317	267	38	67
WSU C1	Impact 1	6.9	875	5,190	456	439	20	82
	Impact 2	7.3	979	5,534	596	541	22	126
	Impact 3	7.2	952	5,499	566	483	22	98
	Impact 4	7.1	926	5,219	520	597	28	34
WSU C2	Impact 1	9.8	1,764	6,539	435	518	89	64
	Impact 2	9.6	1,693	6,648	443	456	64	100
	Impact 3	10.1	1,874	6,987	430	441	62	87
	Impact 4	10.5	2,025	7,060	388	290	24	83
WSU C3	Impact 1	10.9	2,183	7,695	738	335	42	66
	Impact 2	11.2	2,304	8,105	711	424	99	80
	Impact 3	11.8	2,558	8,334	518	509	69	87
	Impact 4	12.1	2,690	8,391	397	648	48	91

Table 19: Mean Response of MiL-Lx.

Impact Severity	Impactor Velocity (m/s)		Tibia Axial Force (N)	
	Average	Std Dev	Average	Std Dev
WSU C0	5.4	0.3	3,493	226
WSU C1	7.1	0.2	5,361	181
WSU C2	10.0	0.4	6,809	254
WSU C3	11.5	0.6	8,131	316

Force-time trajectories for the MiL-Lx WSU C0 impacts are shown in Figure 62. The average peak tibia axial force of the MiL-Lx at WSU C0 impact was 3,493 N with a standard deviation of 226 N.

The trajectory of each impact was aligned using the peak tibia axial force and a mean average MiL-Lx response was calculated. The average MiL-Lx response when impacted at WSU C0 compares favorably with the PMHS response observed by Barbir (2005) using a similar impact severity. Figure 63 compares the average MiL-Lx response at WSU C0 impact condition with the Barbir C2 PMHS non-injury corridor previously shown in Figure 43.

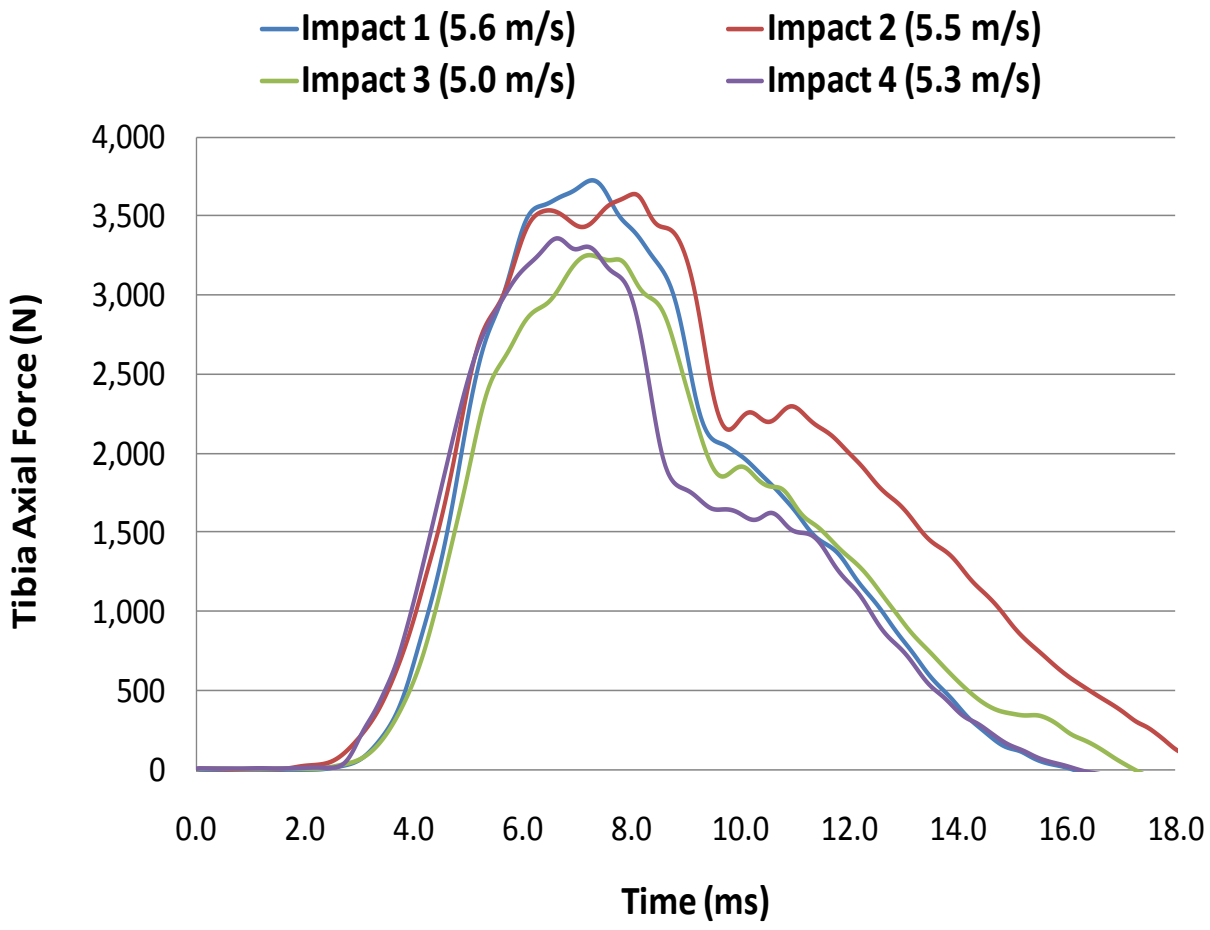

Figure 62: MiL-Lx Response to WSU C0 Loading Severity

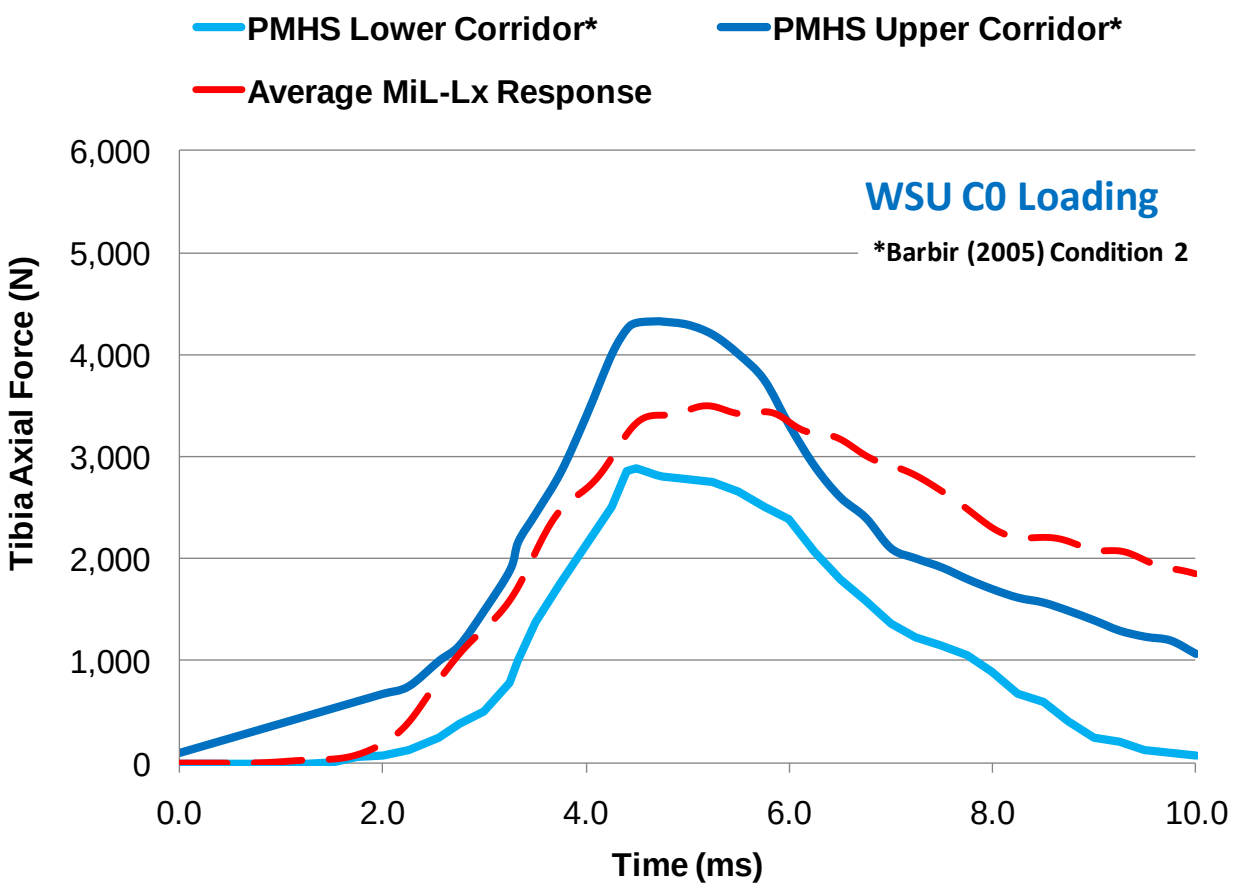

Figure 63: Comparison of PMHS and MiL-Lx at WSU C0 Impact Severity.

Force-time trajectories for the MiL-Lx WSU C2 impacts are shown in Figure 64. The average peak tibia axial force of the MiL-Lx at WSU C2 impact was 6,809 N with a standard deviation of 254 N.

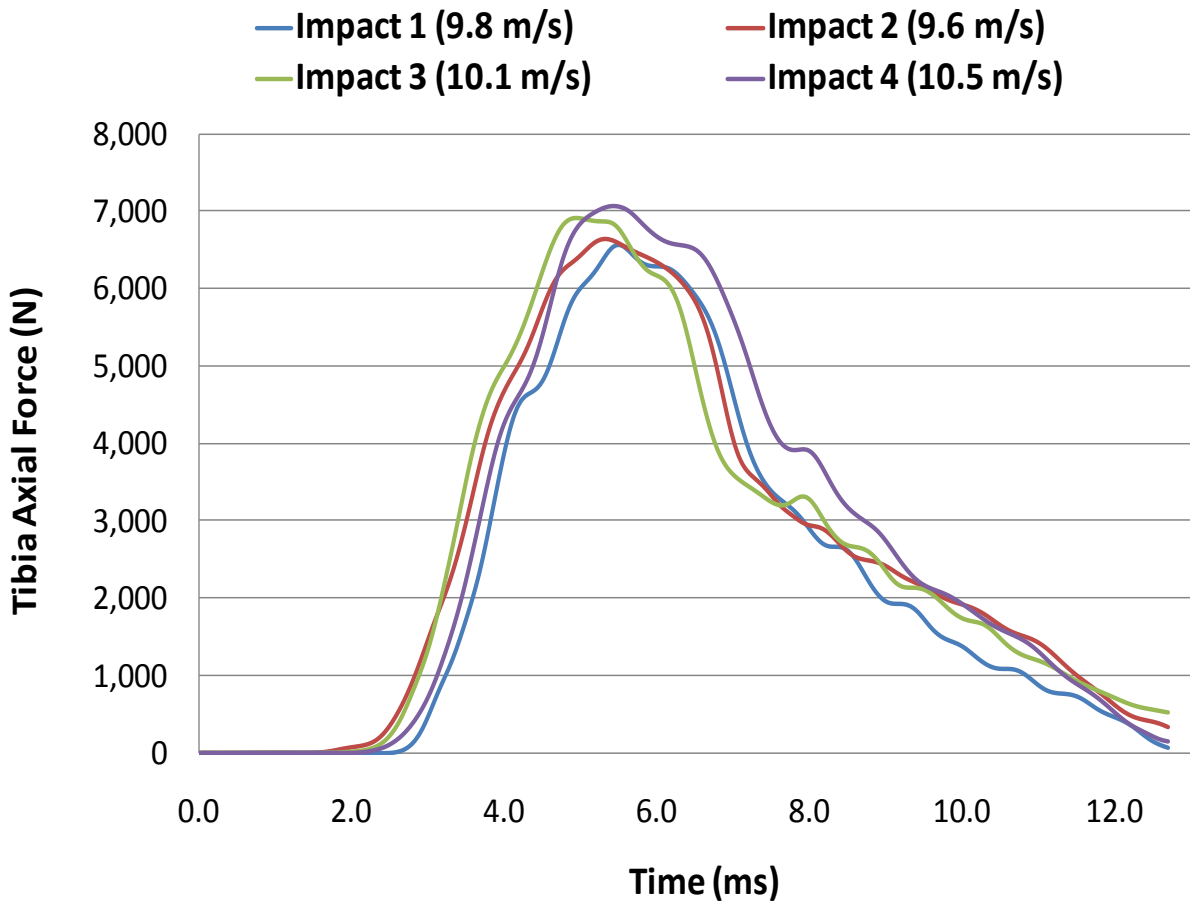

Figure 64: Comparison of PMHS and MiL-Lx at WSU C2 Impact Severity.

Force-time trajectories for the MiL-Lx WSU C3 impacts are shown in Figure 65. The average peak tibia axial force of the MiL-Lx at WSU C3 impact was 8,131 N with a standard deviation of 316 N.

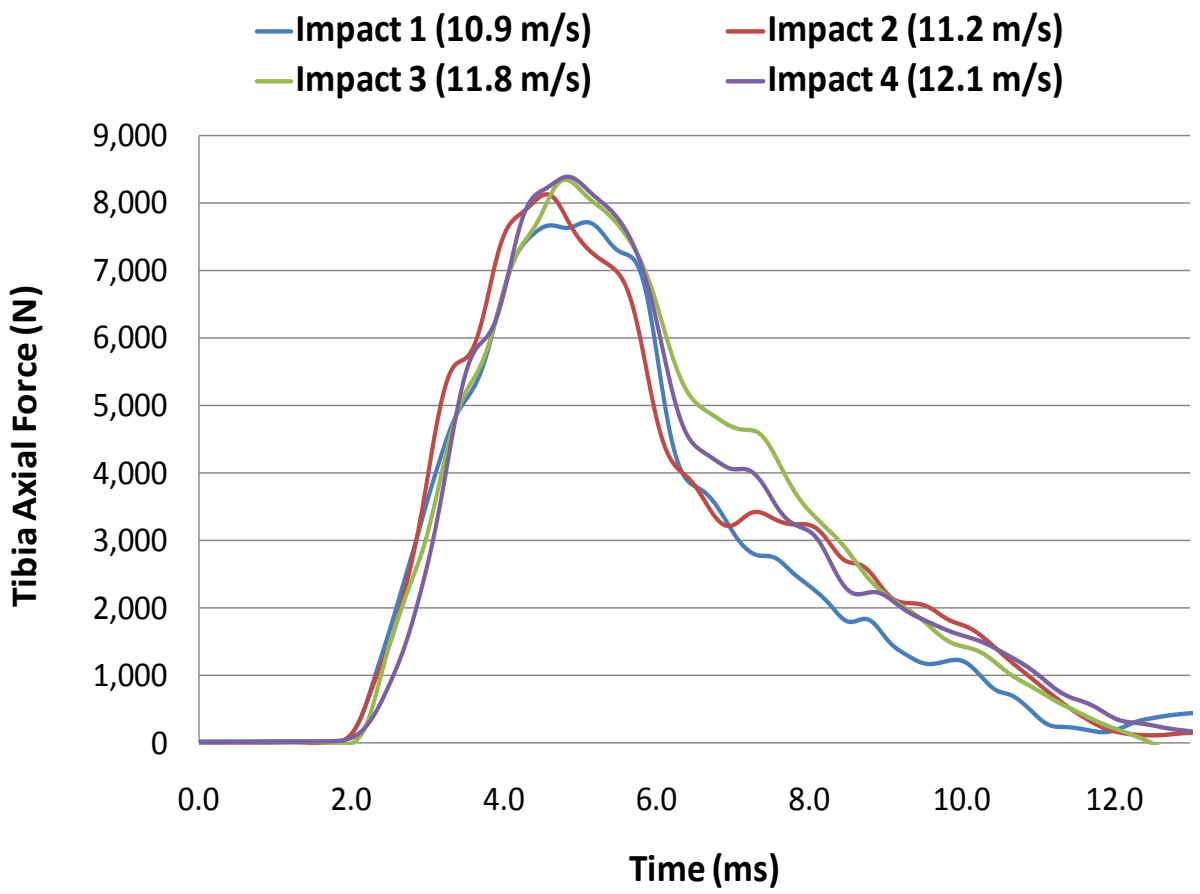

Figure 65: Comparison of PMHS and MiL-Lx at WSU C3 Impact Severity.

A mean average MiL-Lx tibia axial force response was calculated for each impact severity by aligning the individual force-time trajectories of each impact by peak tibia axial force. Figure 66 plots the average force-time trajectory for each impact severity. According to the observed data, the MiL-Lx was capable of distinguishing between impact severity based on peak tibia axial force and tibia compression force loading rate.

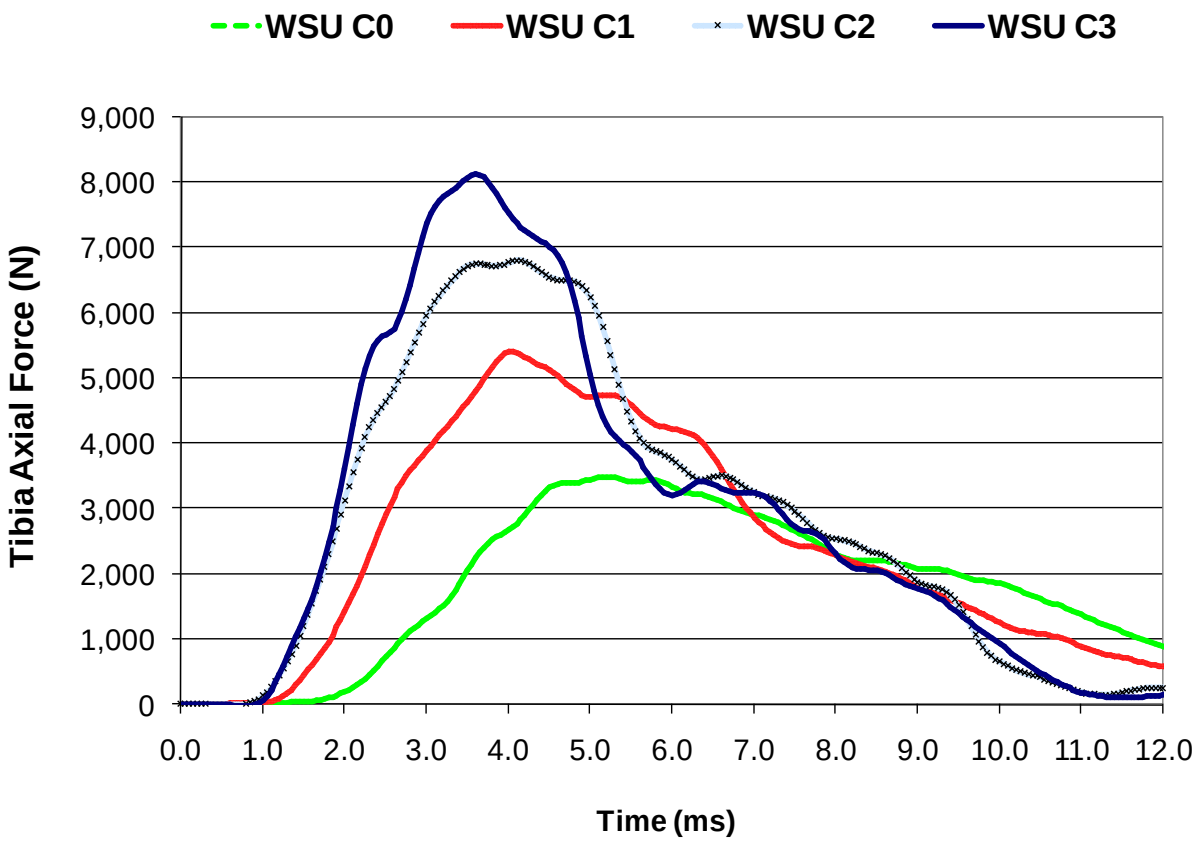

Figure 66: MiL-Lx Response for a Range of AV Landmine Loading Rates.

Tables 20 and 21 compare the biomechanical response of the MiL-Lx to the PMHS under comparable axial loading conditions.

Table 20: Comparison of PMHS and MiL-Lx Tibia Axial Force Response

Tibia Axial Force (N)

	Avg PMHS	Std Dev PMHS	Avg MiL-Lx	Std Dev MiL-Lx
WSU C0	3,605*	724*	3,493	226
WSU C1	5,377	408	5,361	181
WSU C2	4,581	2,988	6,809	254
WSU C3	4,419	2,280	8,131	316

*Barbir (2005) "Condition 2" Results

Table 21: Comparison of PMHS and MiL-Lx Loading Rate Response

Loading Rate (N/ms)

	Avg PMHS	Std Dev PMHS	Avg MiL-Lx	Std Dev MiL-Lx
WSU C0	890*	197*	921	40
WSU C1	1,593	111	1,439	67
WSU C2	2,632	1,506	2,702	89
WSU C3	3,533	1,645	3,295	91

*Barbir (2005) "Condition 2" Results

5.4.3 OOP Durability Evaluation

A series of impact tests were conducted to evaluate the mechanical durability of the MiL-Lx. The validated MiL-Lx was impacted in two out-of-position (OOP) surrogate arrangements: OOP-A and OOP-B. After each impact, the MiL-Lx was inspected to identify mechanical integrity of the components and operability of the instrumentation.

The MiL-Lx was able to withstand WSU C1, C2, and C3 loading without any ill effects in OOP-A. The MiL-Lx did not sustain any identifiable physical damage. The instrumentation recorded data for each impact. Instrumentation was found to be in working condition after the test was completed. A summary of OOP-A tibia axial force data is shown in Table C1 of Appendix C.

The MiL-Lx was able to withstand WSU C1 impact severity only without any ill effects in OOP-B. When impact severity increased to WSU C2 the MiL-Lx foot/calcaneus structure suffered damage. The posterior portion of the calcaneus was sharply bent. Figure 67 illustrates the damage resulting from a WSU C2 impact in OOP-B. The accelerometer mounted on the dorsal portion of the posterior calcaneus was not damaged.

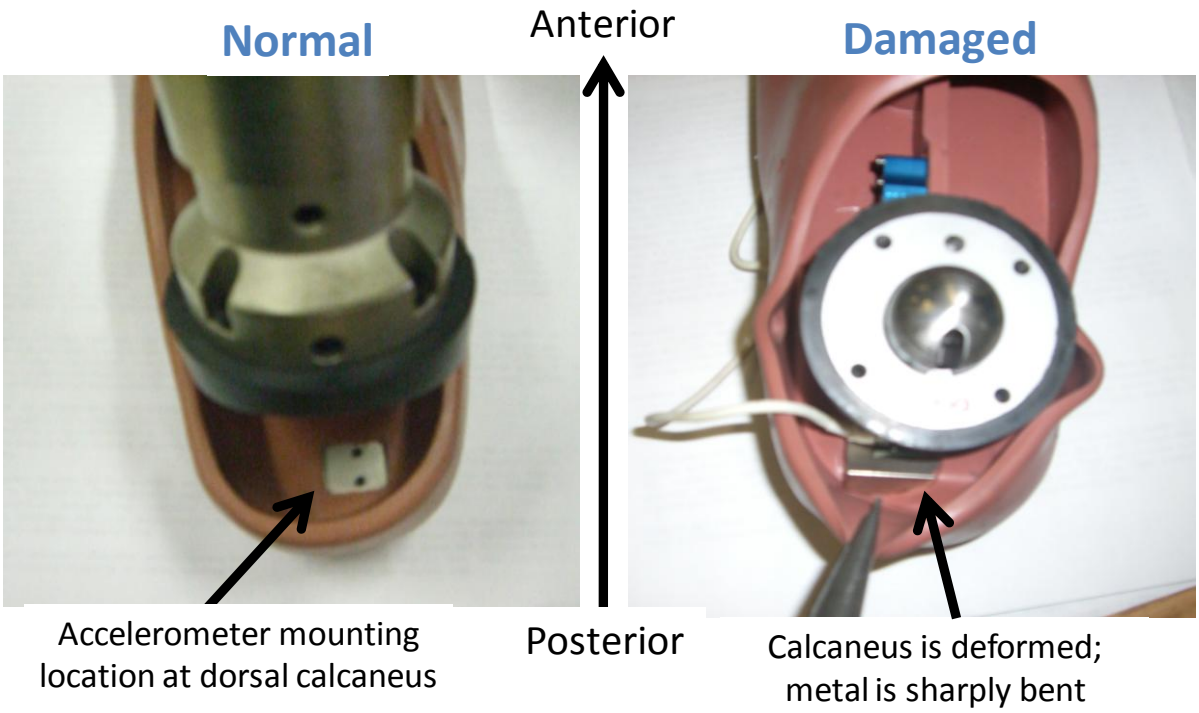

Figure 67: Damaged Calcaneus Resulting from OOP-B Impact.

The damage to the MiL-Lx calcaneus was clearly caused by the angle position of the calcaneus with respect to the impacting footplate. The impactor introduced enough shear force to the plantar aspect of the calcaneus to cause a bending moment. In order to protect against the bending moment, a support bracket, similar to the bracket used to protect the Hybrid III ribs from damage, was installed on the plantar aspect of the foot. The mass added by the support bracket, shown in Figure 68, was removed from the distal tibia resulting in neutral net mass.

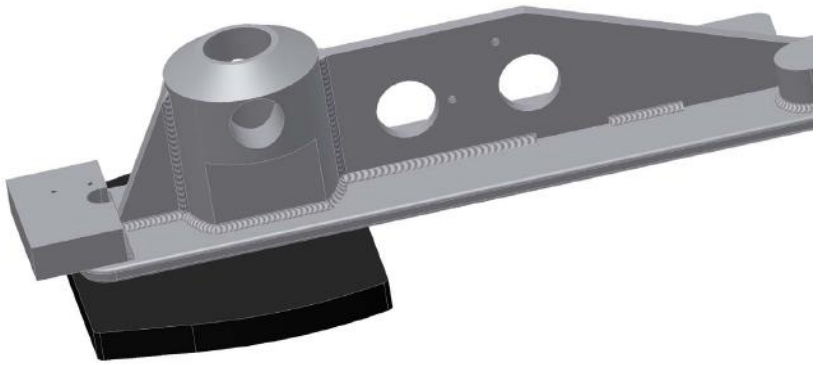

Figure 68: MiL-Lx Calcaneus Support Bracket.

Following the installation of the support bracket, baseline validation tests were conducted to verify the biomechanical response of the MiL-Lx was not changed by the bracket. Subsequently, the modified MiL-Lx was placed in OOP-B and impacted at WSU C2 and C3 impact severities. The improved MiL-Lx was able to withstand WSU C2 and C3 loading without any ill effects in OOP-B. The bracket appeared to work effectively as the MiL-Lx did not sustain any identifiable physical damage. The

instrumentation recorded data for each impact. Instrumentation was found to be in working condition after the test was completed. A summary of OOP-B tibia axial force data is shown in Table C2 of Appendix C.

5.5 Discussion

The human lower extremity injury tolerance to an AV blast explosive device has been established. Current commercially available biomechanical surrogates developed by the automotive industry, THOR-Lx and Hybrid III lower extremity surrogates, are incapable of producing a biofidelic response to simulated AV blast impacts. The materials used in the construction of the surrogates are not sensitive to the short duration (less than 10 milliseconds) and high amplitude loads that characterize explosive blast events. As a result, the surrogates measured loads up to 150 to 200 percent greater than an instrumented PMHS lower extremity.

The current effort was to modify the existing THOR-Lx to accurately simulate the post mortem human specimen (PMHS) lower extremity response to AV axial loading (McKay and Bir, 2009). The THOR-Lx underwent a series of modifications intended to reduce the overall stiffness of the surrogate. After core components of the MiL-Lx were selected from the THOR-Lx, it was necessary to modify the compliant element properties to achieve a desired biomechanical response to a specific impact severity. Modification of footpad was found to have small effects on the biomechanical response of the lower and upper tibia load cell. The combination of the footpad and ankle bumper provided little attenuation and lacked the ability to tune the lower tibia load cell. In contrast, the tibia compliant element, located distal to the upper tibia load cell, was found to have the greatest effect on the forces measured by the upper tibia load cell.

The tibia compliant element attenuated axial forces prior to reaching the upper tibia load cell. The mechanical properties of the tibia compliant element elastomer, specifically its dynamic compressibility, were tuned to achieve a desired tibia axial force response, loading rate, loading pattern, and duration. The tibia compliant element was doubled in length to enable additional clearance for compression.

The modified surrogate, MiL-Lx (military lower extremity), was loaded axially at three simulated AV axial loading rates using a piston driven linear impactor. The diameter and compressive modulus of the tibia compliant element was varied until the axial force measured by the surrogate was equivalent to the PMHS response in magnitude and duration. Over 100 impact tests were conducted to identify an elastomer with suitable dynamic compression properties. Once identified, the MiL-Lx was able to simulate the PMHS response to non-injurious simulated AV blast impact conditions with high repeatability.

Impact testing conducted over a range of non-injurious and injurious simulated AV blast impact conditions revealed the MiL-Lx possessed sufficient sensitivity to distinguish under-match and over-match impact severity.

The MiL-Lx surrogate foot was found to susceptible to high shear forces from OOP impacts. A reinforcement bracket was installed to provide support. The modified surrogate was found to be tolerant to high severity OOP loading conditions.

CHAPTER 6

EVALUATION OF MILITARY FOOTWEAR AND KINETIC ENERGY ABSORBING MATERIALS

6.1 Introduction

Military vehicle occupant protection systems are needed to reduce the injury potential caused by an underbelly blast event. The injury criteria developed in this research effort suggest these objectives may be achieved by reducing the peak tibia axial force experienced by the occupant or reduction of the vehicle floorplate velocity prior to impact. The development of the MiL-Lx surrogate (Chapter 5) showcased the value of material selection to achieve a desired peak tibia axial force. These principals may be applied in the development of occupant PPE and vehicle armor.

Footwear may be utilized to safeguard military occupants involved in explosive blast events. Barbir (2005) showed that a standard issue U.S. Army combat boot may decrease peak tibia axial force in a lower extremity biomechanical surrogate by as much as 35 percent. Whyte (2007) measured the static elastomer properties of numerous military combat boots from several NATO countries revealing a broad range of boot padding properties including stiffness. The variance among elastomer properties suggests that each boot has the potential to provide a different level of protection to the user.

Military vehicle occupant protection systems are evaluated in full-scale, live fire AV blast tests using a Hybrid III biomechanical surrogate. STANAG 4569 specifies the surrogate don standard military occupant PPE including military footwear. As such, the biomechanical response data collected from the surrogate inherently contains the

influence of the footwear. Surrogate data from these live fire tests may be biased depending on the type of footwear used in the evaluation.

Traditionally, military vehicles utilize advanced armor materials to deflect and attenuate kinetic energy to protect vehicle occupants from ballistic or blast threats. These materials, like iron, are typically rigid and heavy. More advanced armor materials including aluminum, steel, titanium and uranium provide similar protection while reducing vehicle weight. More recently ceramics and composite materials have been utilized in modern combat vehicles.

Kinetic energy absorbing materials are being evaluated for application in military vehicle systems, particularly legacy vehicle retrofits, to complement traditional armor and enhance occupant protection systems. Kinetic energy absorbing materials are lightweight and require small clearances to be effective. These materials are typically installed between a rigid vehicle structure (vehicle hull, support beams) and the vehicle occupant.

Kinetic energy absorbing materials protect a vehicle occupant by intercepting kinetic energy propagating from the vehicle hull to the vehicle occupant cabin. The kinetic energy transferred from the blast and through the hull performs mechanical work on the energy absorbing material resulting in elastic or plastic deformation of the material. Residual kinetic energy is transferred to the vehicle cabin and loads the occupant.

Despite advances in civilian automotive vehicle padding, few military vehicles feature soft interior padding for vehicle occupants. A military vehicle occupant cabin will often utilize the same metallurgy as the external armor. This stiff internal metallurgy is

typically selected to defeat the threat of fragments and projectiles. However, these stiff materials may not provide the attenuation required to reduce the potential of lower extremity injury in an underbelly blast event. The potential exists to design vehicles with specialized materials capable of reducing axial forces before they reach the occupant.

6.2 Methodology

The following effort was initiated to evaluate the ability of military footwear and kinetic absorbing materials to reduce peak tibia axial force to vehicle occupants. This effort focused on populating biomechanical response data from a MiL-Lx surrogate that is protected by footwear or kinetic energy absorbing material. The study also established a test methodology from which to evaluate PPE and materials for application in underbelly blast protection system.

6.2.1 Military Footwear Evaluation

A series of impact tests were conducted to quantify the protective capability of military footwear to attenuate axial blast threats. Three military combat boots were evaluated in the study (Figure 69).

I. U.S. Army and Marine Infantry Combat Boot (ICB) [national stock number: 8430-01-516-1506].
II. U.S. Army Desert Combat Boot (DCB) [national stock number: 8430-01-514-5161].
III. AP Mine Protective Over Boot (MOB) [build specification: FQSE/PD-93-06].

The combination of the ICB and MOB was also tested.

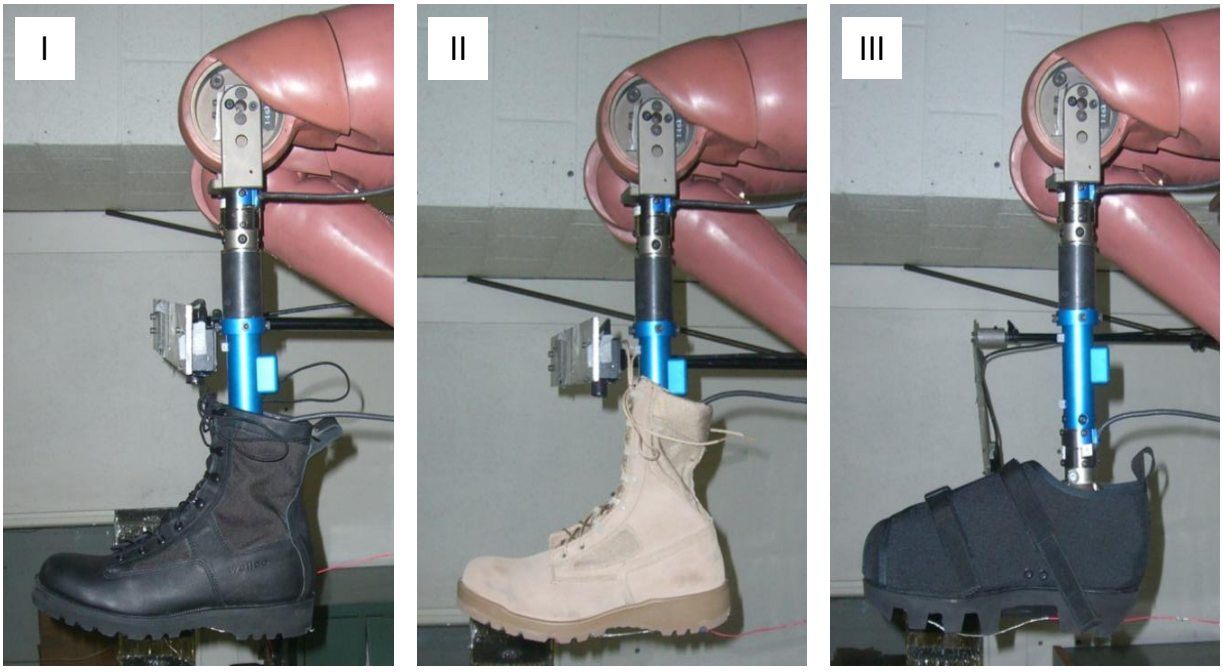

Figure 69: Military Combat Boots. Left: Infantry Combat Boot. Middle: Desert Combat Boot. Right: Mine Over Boot.

Three types of footwear were tested in the evaluation and a combination of boot and over boot were tested. The internal padding of each combat boot varied. The ICB padding was the found to be the softest in bench-top testing followed by the DCB. The MOB was the stiffest boot. The MOB is designed for protection against AP landmines and contains a Kevlar sole to protect against projectiles.

The protective capability of the combat boot was evaluated in simulated AV axial blast tests using the same test setup shown in Figure 50 (Chapter 5). The validated MiL-Lx was dressed in each combat boot or combination of boots and impacted at the plantar aspect of the boot under WSU C1, C2, and C3 impact conditions. Each boot was impacted two times at each impact condition.

6.2.2 Kinetic Energy Absorbing Material Evaluation

The MiL-Lx was utilized to study the ability of kinetic energy absorbing material to reduce the probability of lower limb injury from AV blast loading. Five commercially available kinetic energy absorbing materials were evaluated to determine its effectiveness at reducing lower extremity injuries (Figure 70). These materials include:

I. Collapsible steel plate (CSP) (furnished by U.S. Army TARDEC).

II. Aluminum commercial grade (ACG) honeycomb. Crush strength: 414 kPa (60 psi).

III. ACG honeycomb. Crush strength: 827 kPa (120 psi).

IV. ACG honeycomb. Crush strength: 1689 kPa (245 psi).

V. Aluminum foam (furnished by U.S. Army TARDEC). Crush strength: 9,308 kPa (1350 psi).

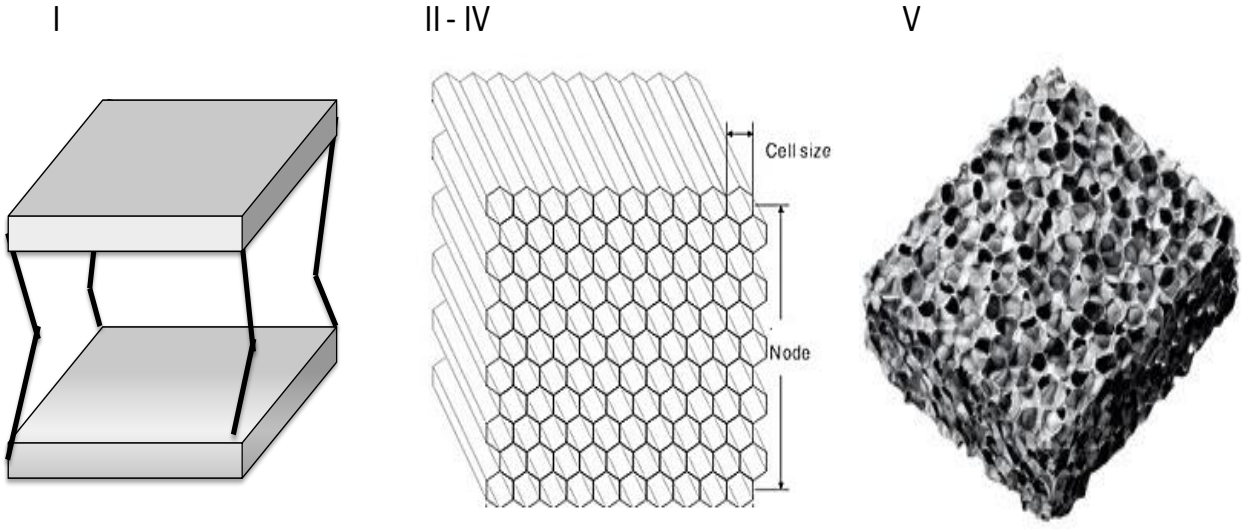

Figure 70: Illustration of Kinetic Energy Absorbing Material. Left: Collapsible Steel Plate. Middle: Aluminum Honeycomb. Right: Aluminum Foam.

The CSP was chosen to represent an elementary protection system whereby support beams are corrugated to provide some resistance to an impacting force. Three ACG materials were selected to provide a range of crush strengths for the evaluation. The crush strength is the amount of resistance the material can sustain before it is compressed. Finally, an Aluminum foam material was selected to compare a very stiff material with high crush strength. The Aluminum foam, or other composite/ceramic materials with similar crush strength, is often used to protect vehicles from ballistic threats.

The protective capability of the kinetic energy absorbing material was evaluated in simulated AV axial blast tests using an air piston driven linear impactor. A 25 x 25 x 10 centimeter section of material was securely fixed to the impactor footplate. Figure 71 shows the positioning of the kinetic energy absorbing material. The kinetic energy absorbing material is launched by impactor into the plantar aspect of the validated MiL-Lx foot (without boot) at WSU C1, C2, and C3 impact conditions. Each material was impacted two times at each impact condition. The tibia axial force reduction of each material was calculated based on the magnitude of peak tibia axial force attenuation.

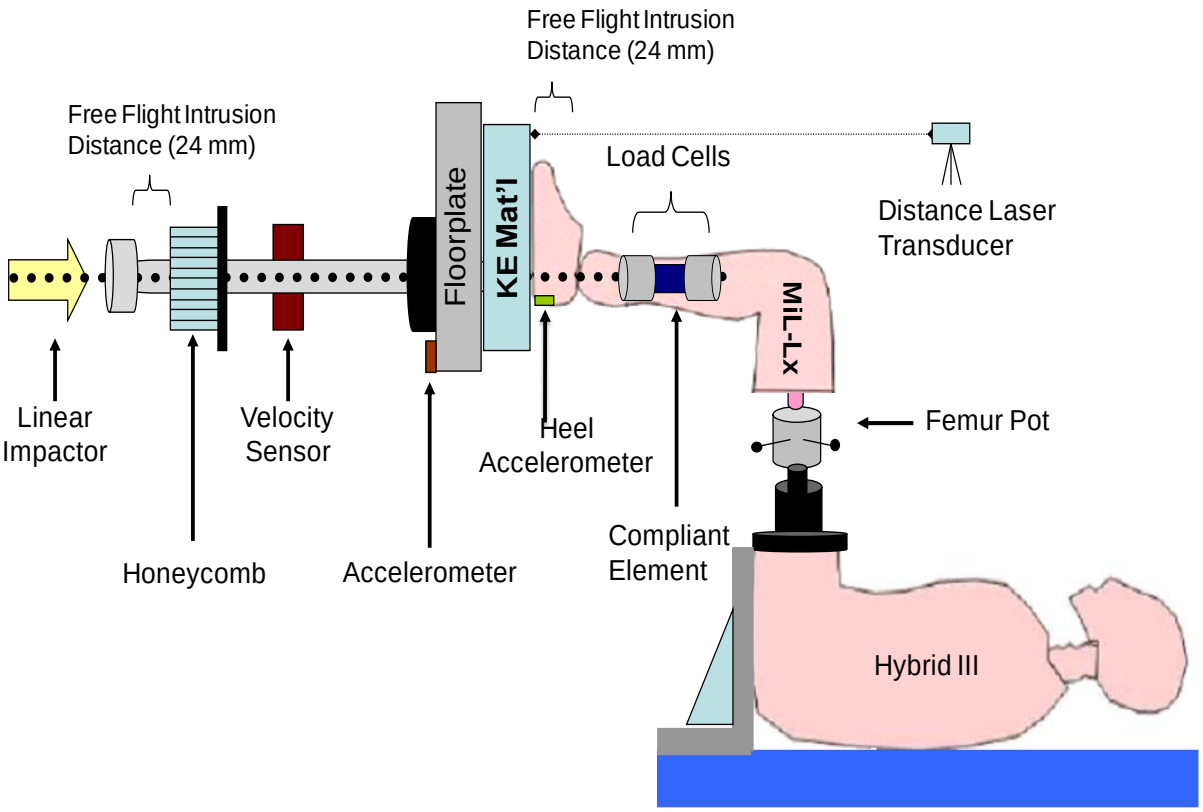

Figure 71: Test Setup to Evaluate Kinetic Energy Absorbing Material.

6.2.3 Data Collection and Processing

High-speed video was collected using a HG 100K Camera (Redlake, Inc) at 10,000 frames per second with a given resolution of 256 by 192 pixels. Data acquisition was conducted at 20,000 Hz using a TDAS Pro System (DTS, Seal Beach, CA). A four-pole Butterworth filter with a cutoff frequency of 4300 Hz was used for anti-aliasing. The MiL-Lx surrogate upper and lower tibia load cells measured axial force (Fz), the shear forces (Fx and Fy), the fore/aft and lateral bending moments (Mx and My, respectively). Mid-foot and mid-tibia accelerations were recorded using a tri-axial accelerometer. Extrinsic stimuli including floorplate displacement and acceleration were measured. Acceleration and tibia load data were filtered using a CFC 600 filter. Moment data were

filtered using a CFC 180 filter. Floorplate displacement data were filtered using a low pass Butterworth filter at 1000 Hz.

6.3 Results

A series of impact tests were conducted to (1) evaluate three types of military footwear; and (2) evaluate the protective capability of select blast mitigation materials.

6.3.1 Military Footwear Evaluation

A summary of the footwear impact data is shown in Tables 22-25. Force-time trajectories for the impacts are shown in Figures 72-75. The average peak tibia axial force for WSU C1 ranged from 3,859 N to 4,865 N. The average peak tibia axial force for WSU C2 ranged from 6,128 N to 7,387 N. The average peak tibia axial force for WSU C3 ranged from 7,325 N to 8,320 N. The ICB was found to provide (alone or in combination with MOB) the lowest peak tibia axial force.

Table 22: MiL-Lx with Infantry Combat Boot Performance Summary.

Infantry Combat Boot (ICB)

Test Condition	Test	Impactor Velocity (m/s)	Impactor KE (J)	Peak Fz (N)	Average Peak Fz (N)	Std Dev Fz (N)
WSU C1	Impact 1	7.0	900	3,584	3,859	389
	Impact 2	7.1	926	4,135		
WSU C2	Impact 1	10.1	1,874	6,358	6,128	325
	Impact 2	9.6	1,693	5,898		
WSU C3	Impact 1	11.3	2,346	7,598	7,520	111
	Impact 2	11.0	2,223	7,441		

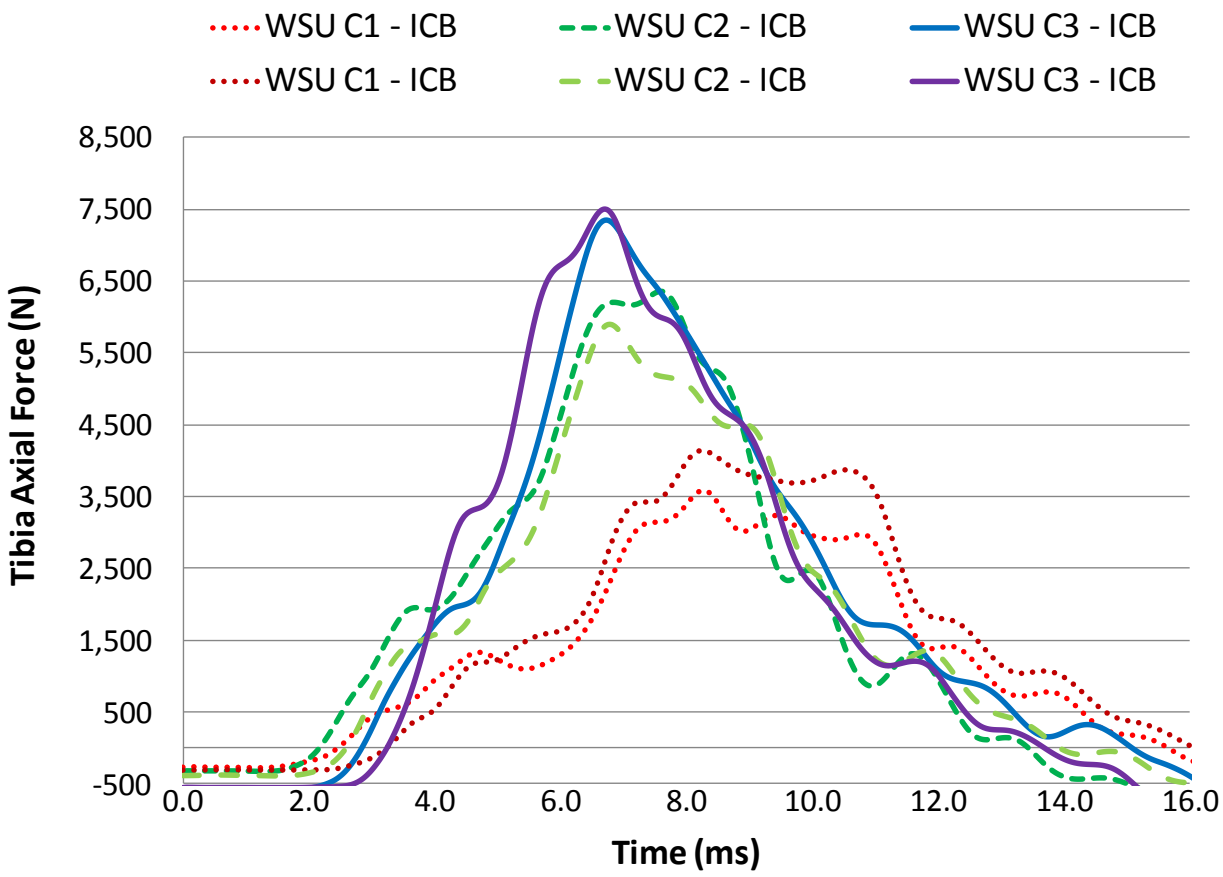

Figure 72: Biomechanical Response of MiL-Lx with Infantry Combat Boot.

Table 23: MiL-Lx with Desert Combat Boot Performance Summary.

Desert Combat Boot (DCB)

Test Condition	Test	Impactor Velocity (m/s)	Impactor KE (J)	Peak Fz (N)	Average Peak Fz (N)	Std Dev Fz (N)
WSU C1	Impact 1	6.9	875	4,356	4,290	93
	Impact 2	7.0	900	4,224		
WSU C2	Impact 1	10.2	1,911	7,593	7,387	292
	Impact 2	9.8	1,764	7,180		
WSU C3	Impact 1	10.9	2,183	8,009	8,119	155
	Impact 2	11.2	2,304	8,228		

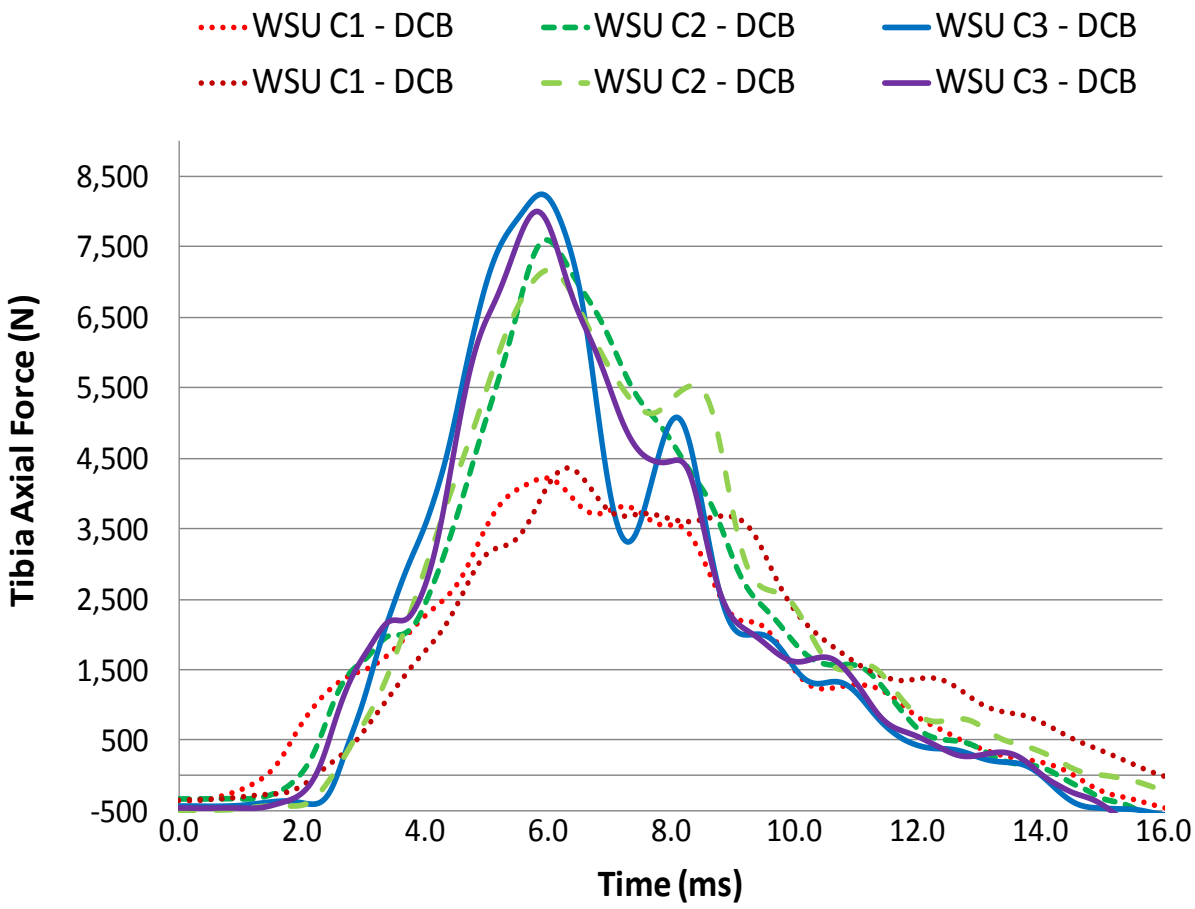

Figure 73: Biomechanical Response of MiL-Lx with Desert Combat Boot.

Table 24: MiL-Lx with Mine Over Boot Performance Summary.

Mine Over Boot (MOB)						
Test Condition	**Test**	**Impactor Velocity (m/s)**	**Impactor KE (J)**	**Peak Fz (N)**	**Average Peak Fz (N)**	**Std Dev Fz (N)**
WSU C1	Impact 1	7.1	926	4,779	4,865	121
	Impact 2	7.1	926	4,950		
WSU C2	Impact 1	9.6	1,693	6,562	6,819	363
	Impact 2	9.9	1,800	7,076		
WSU C3	Impact 1	11.0	2,223	8,059	8,320	369
	Impact 2	11.4	2,387	8,581		

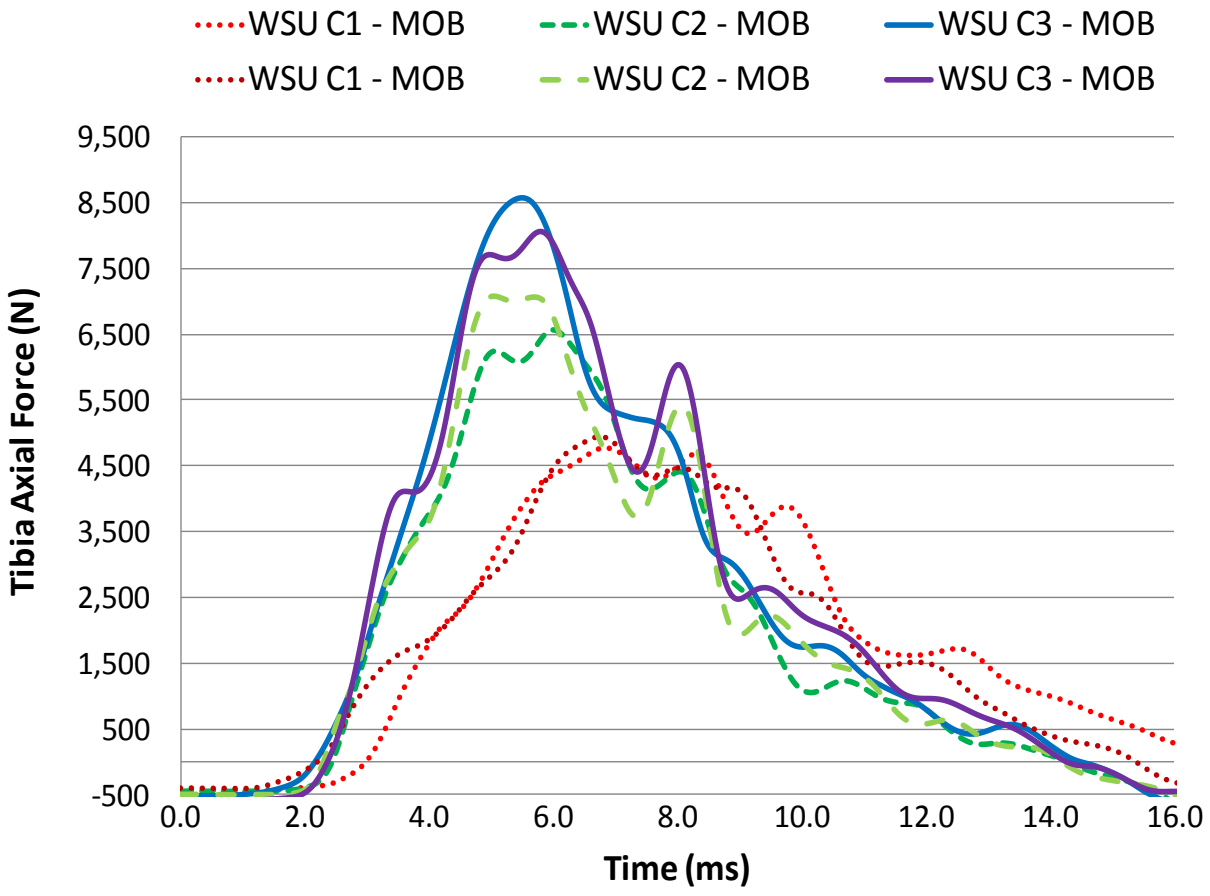

Figure 74: Biomechanical Response of MiL-Lx with Mine Over Boot.

Table 25: MiL-Lx with Infantry Combat Boot and Mine Over Boot Performance Summary.

Infantry Combat Boot (ICB) & Mine Over Boot (MOB)

Test Condition	Test	Impactor Velocity (m/s)	Impactor KE (J)	Peak Fz (N)	Average Peak Fz (N)	Std Dev Fz (N)
WSU C3	Impact 1	11.3	2,346	7,264	7,325	86
	Impact 2	11.2	2,304	7,386		

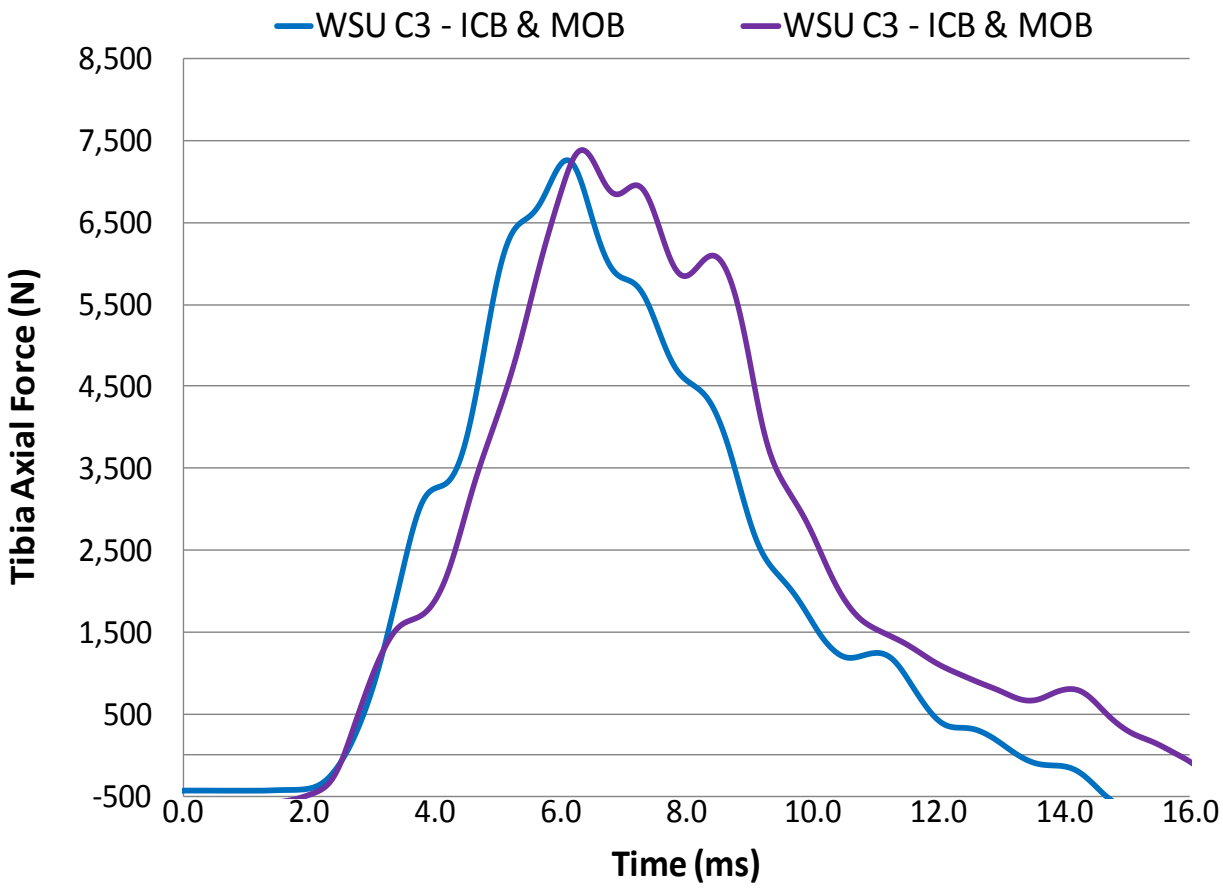

Figure 75: Biomechanical Response of MiL-Lx with Infantry Combat Boot and Mine Over Boot.

6.3.2 Kinetic Energy Absorbing Material

A summary of the kinetic energy absorbing material impact data is shown in Tables 26-30. Force-time trajectories for the impacts are shown in Figures 76-80. The average peak tibia axial force for WSU C1 ranged from 4,610 N to 5,789 N. The average peak tibia axial force for WSU C2 ranged from 5,357 N to 7,409 N. The average peak tibia axial force for WSU C3 ranged from 5,586 N to 8,508 N. The ACG honeycomb, 414 kPa, was found to provide the lowest peak tibia axial force at each impact condition.

Table 26: Collapsible Steel Plate Performance Summary.

Collapsible Steel Plate						
Test Condition	Test	Impactor Velocity (m/s)	Impactor KE (J)	Peak Fz (N)	Average Peak Fz (N)	Std Dev Fz (N)
WSU C1	Impact 1	6.9	875	5,745	5,629	165
	Impact 2	7.1	926	5,512		
WSU C2	Impact 1	9.9	1,800	7,290	7,409	168
	Impact 2	10.0	1,837	7,528		
WSU C3	Impact 1	11.1	2,263	8,104	7,963	199
	Impact 2	10.8	2,143	7,822		

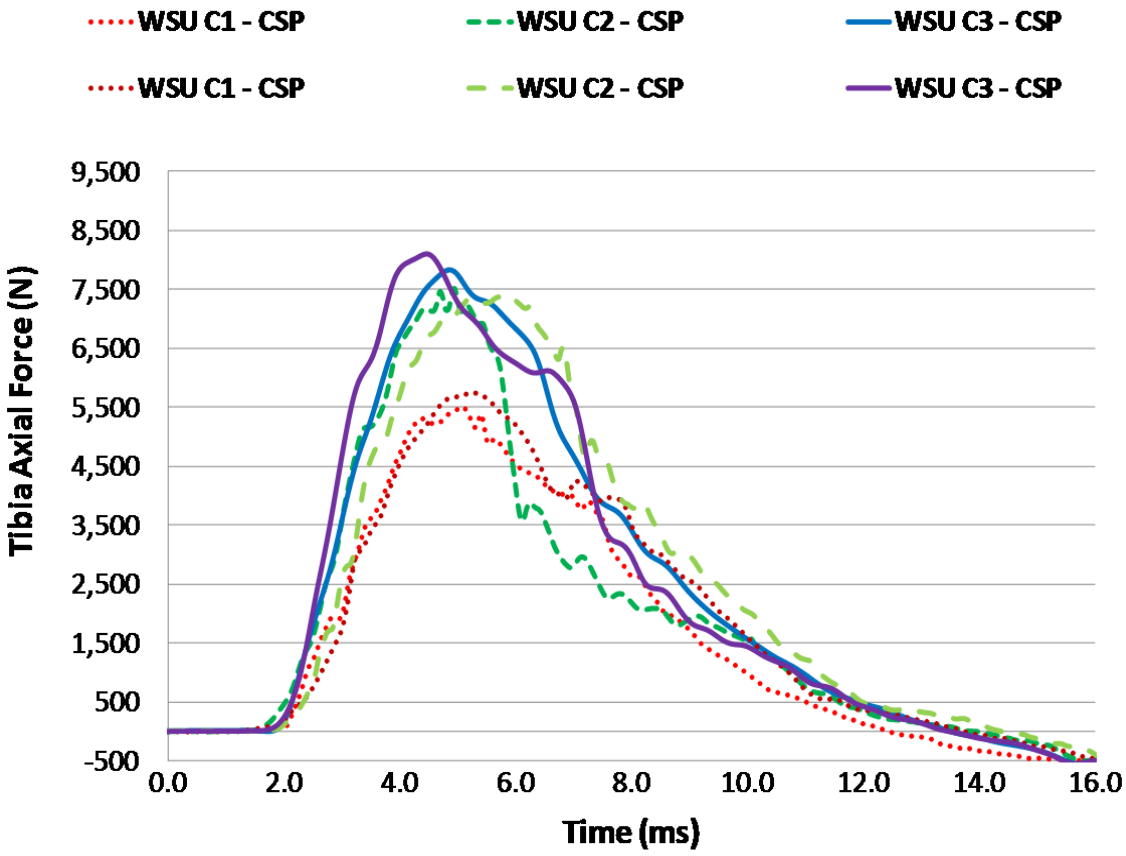

Figure 76: Biomechanical Response of MiL-Lx Impacted with a Collapsible Steel Plate.

Table 27: ACG Honeycomb 414 kPa Performance Summary.

ACG Honeycomb: 414 kPa

Test Condition	Test	Impactor Velocity (m/s)	Impactor KE (J)	Peak Fz (N)	Average Peak Fz (N)	Std Dev Fz (N)
WSU C1	Impact 1	7.0	900	4,731	4,610	172
	Impact 2	7.1	926	4,488		
WSU C2	Impact 1	10.2	1,911	5,504	5,357	208
	Impact 2	10.2	1,911	5,210		
WSU C3	Impact 1	11.1	2,263	5,496	5,586	127
	Impact 2	11.2	2,304	5,676		

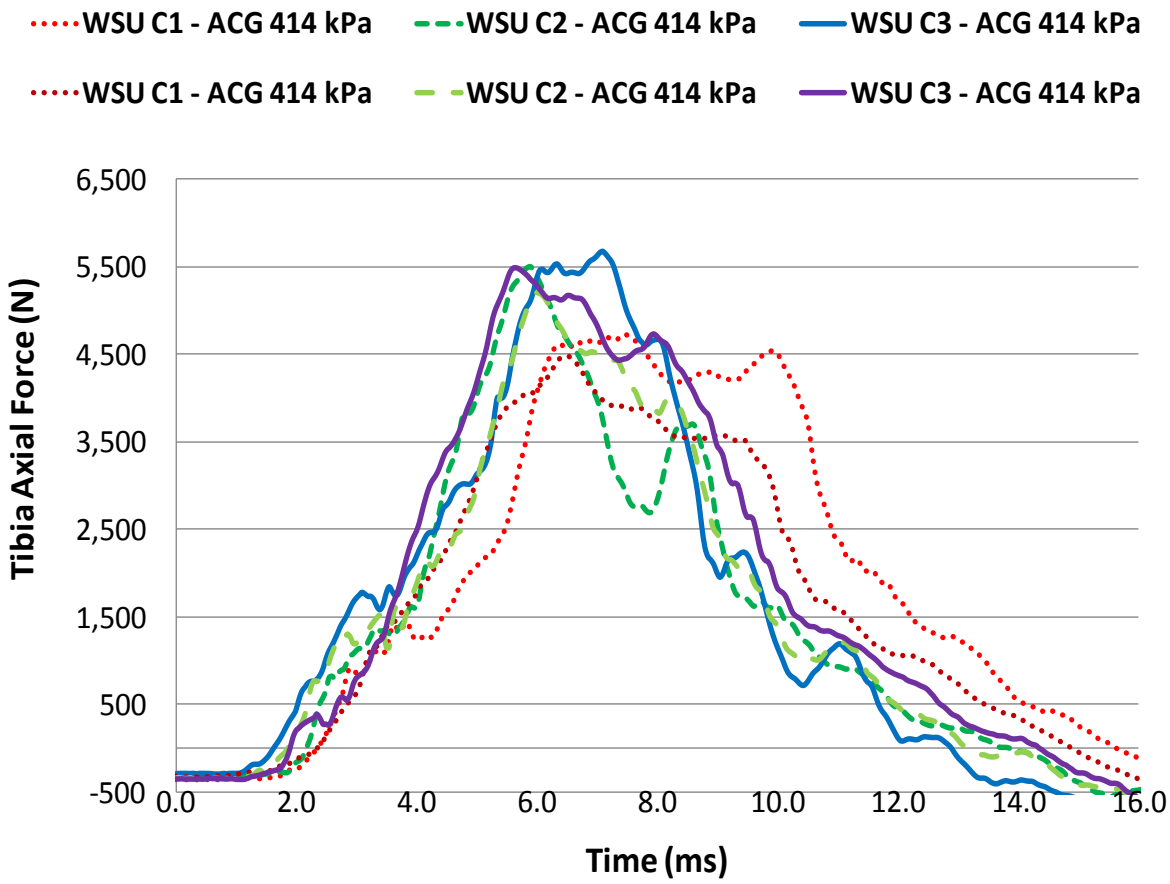

Figure 77: Biomechanical Response of MiL-Lx Impacted with ACG Honeycomb, 414 kPa.

Table 28: ACG Honeycomb 827 kPa Performance Summary.

ACG Honeycomb: 827 kPa

Test Condition	Test	Impactor Velocity (m/s)	Impactor KE (J)	Peak Fz (N)	Average Peak Fz (N)	Std Dev Fz (N)
WSU C1	Impact 1	6.9	875	4,813	4,664	211
	Impact 2	7.1	926	4,515		
WSU C2	Impact 1	9.7	1,728	6,356	6,153	288
	Impact 2	10.0	1,837	5,949		
WSU C3	Impact 1	11.1	2,263	6,562	6,638	107
	Impact 2	11.0	2,223	6,714		

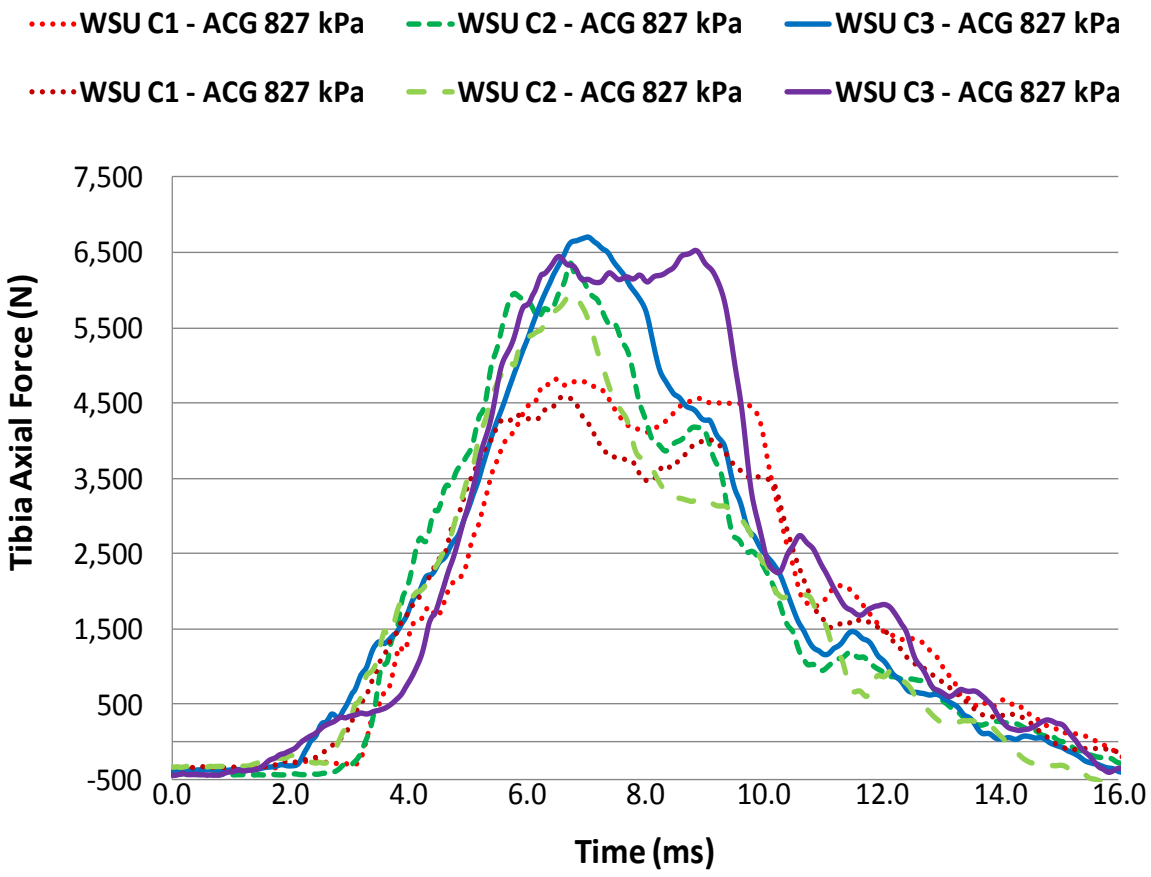

Figure 78: Biomechanical Response of MiL-Lx Impacted with ACG Honeycomb, 827 kPa.

Table 29: ACG Honeycomb 1,689 kPa Performance Summary.

ACG Honeycomb: 1,689 kPa						
Test Condition	**Test**	**Impactor Velocity (m/s)**	**Impactor KE (J)**	**Peak Fz (N)**	**Average Peak Fz (N)**	**Std Dev Fz (N)**
WSU C1	Impact 1	7.1	926	5,224	5,511	406
	Impact 2	7.4	1,006	5,798		
WSU C2	Impact 1	9.9	1,800	7,024	6,913	157
	Impact 2	10.2	1,911	6,802		
WSU C3	Impact 1	11.4	2,387	8,282	8,508	319
	Impact 2	11.1	2,263	8,733		

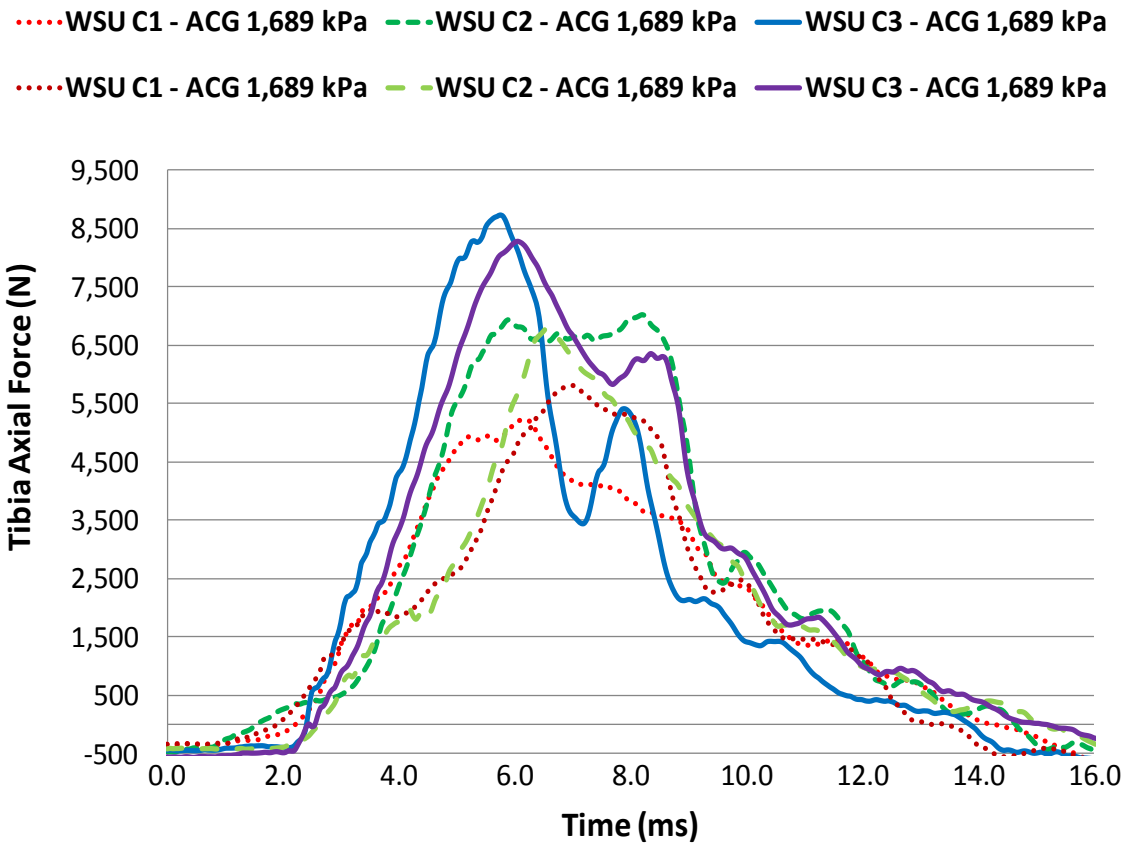

Figure 79: Biomechanical Response of MiL-Lx Impacted with ACG Honeycomb, 1,689 kPa.

Table 30: Aluminum Foam Performance Summary.

Aluminum Silicon Foam: 9,308 kPa						
Test Condition	**Test**	**Impactor Velocity (m/s)**	**Impactor KE (J)**	**Peak Fz (N)**	**Average Peak Fz (N)**	**Std Dev Fz (N)**
WSU C1	Impact 1	6.9	875	5,668	5,789	170
	Impact 2	6.9	875	5,909		
WSU C2	Impact 1	9.9	1,800	7,311	7,111	284
	Impact 2	10.1	1,874	6,910		
WSU C3	Impact 1	11.6	2,472	8,782	8,508	388
	Impact 2	11.4	2,387	8,233		

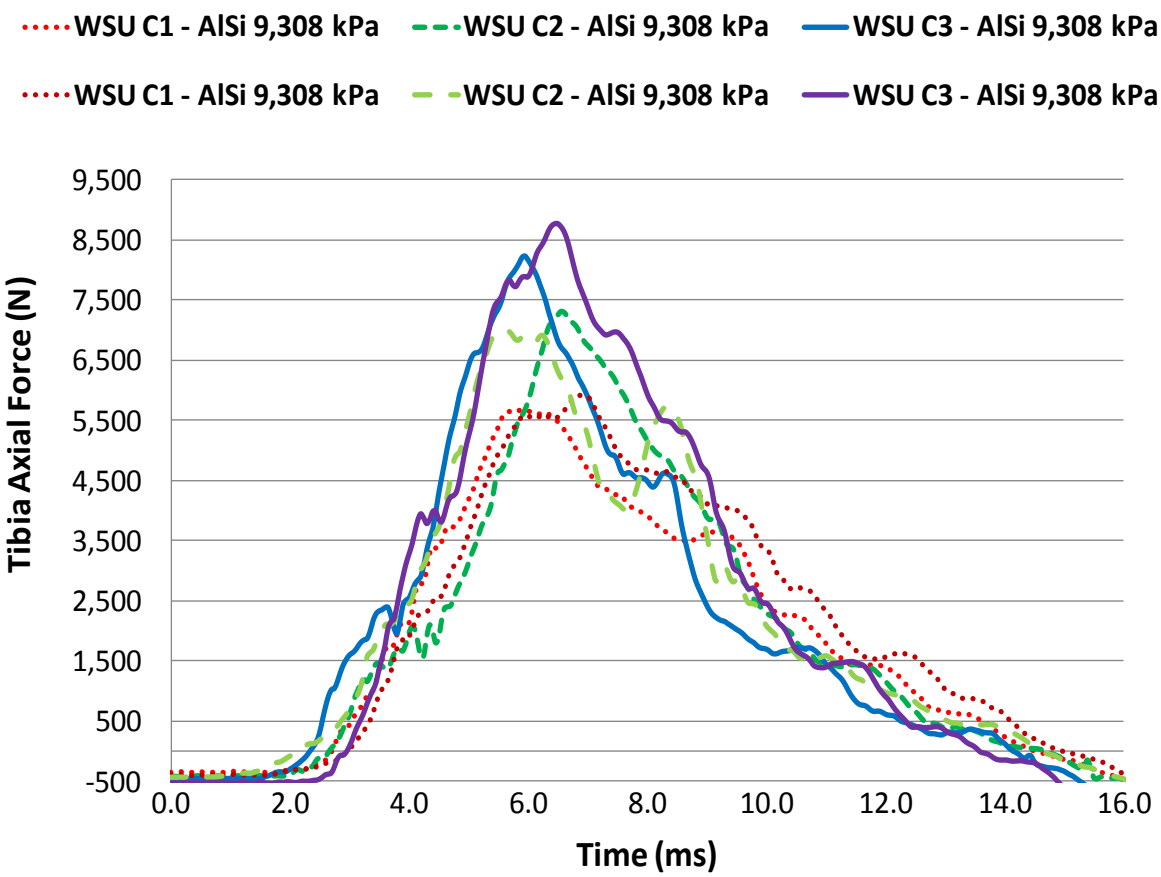

Figure 80: Biomechanical Response of MiL-Lx Impacted with Aluminum Foam, 9,308 kPa.

6.4 Discussion

A series of impact tests were conducted to evaluate the protective capability of military footwear and select blast mitigation materials. Table 31 summarizes the percent attenuation provided by each boot or combination of boots with respect to the baseline MiL-Lx. The MiL-Lx with ICB provided the greatest average reduction in peak tibia axial force at 28, 15, and eight percent at WSU C1, C2, and C3 impact severity respectively. The MiL-Lx with MOB and MiL-Lx with DCB generated the least amount of peak tibia axial force reduction when exposed to WSU C2 and C3 loading severity.

Table 31: Summary of Boot Attenuation Capacity.

	Percent from Baseline		
Specimen	WSU C1	WSU C2	WSU C3
MIL-Lx w/ ICB	-28%	-15%	-8%
MIL-Lx w/ DCB	-20%	2%	0%
MIL-Lx w/ MOB	-9%	-6%	3%
MIL-Lx w/ ICB & MOB	---	---	-10%

ICB: Infantry Combat Boot
DCB: Desert Combat Boot
MOB: Mine Over Boot

As impact severity increased, the effectiveness of each boot to reduce peak tibia axial force lessened. This reduction is likely a function of the elastomer's inherent dynamic compression behavior. Essentially, each elastomer exhibits a specific

behavior to the rate of compression. Elastomers that are more tolerant of dynamic compression are likely to provide the most protection against blast impacts.

In low severity impacts, the force of the impactor does not fully compress the padding material. The padding provides a level of resistance against the impactor and results in the attenuation of tibia axial force measured by the surrogate. This resistance force produced by the elastomer's ability to resist compression (compressive modulus) and recoil following the release of loading. In high severity impacts, the impacting floorplate may fully compress the elastomeric material. Once fully compressed, the elastomer is unable to provide additional resistance. Subsequent force applied by the floorplate would not be attenuated and transferred to the surrogate.

Footwear with soft plantar cushioning, ICB, was found to attenuate peak tibia axial forces by a greater magnitude than footwear with stiffer materials of construction, MOB. The data collected in this study suggests the ICB and DCB possess satisfactory padding material properties to attenuate WSU C1 loading severity. However, as severity increases, only ICB is able to continue providing attenuation. The DCB padding was unable to attenuate the higher severity impact. At WSU C3, the attenuating ability of the ICB is significantly reduced. This suggests the padding is unable to tolerate the severe loading rate and was fully compressed.

The MOB provided negligible protection at each loading severity. The padding material was unable to absorb or resist the kinetic energy applied by the impactor to significantly reduce tibia axial force. The combination of the MOB and ICB produced the highest level of attenuation at WSU C3. The complimentary improvement is likely

related to the increase volume of padding material. The additional volume provided capacity to better handle the rate of compressive loading than the ICB alone.

Other than the CSP, the kinetic energy absorbing material utilized in this evaluation possessed a constant capacity to resist compression. Of the five types of kinetic energy absorbing materials tested in the evaluation, the MiL-Lx protected with a 414 kPa crush strength material experienced the lowest average peak tibia axial for WSU C1, C2, and C3 impact conditions measuring 4,610 N, 5,357 N, and 5,568 N respectively. The MiL-Lx protected with CSP, 1,689 kPA, and 9,308 kPa materials respectively experienced the greatest average peak tibia axial force.

Table 32: Summary of Kinetic Energy Absorbing Material Attenuation Capacity.

	Percent from Baseline		
Specimen	WSU C1	WSU C2	WSU C3
MIL-Lx w/ CSP	-5%	-2%	2%
MIL-Lx w/ 414 kPa	14%	26%	31%
MIL-Lx w/ 827 kPa	13%	15%	18%
MIL-Lx w/ 1,689 kPa	-3%	5%	9%
MIL-Lx w/ 9,308 kPa	-8%	2%	-5%

CSP: Collapsible steel plate

The CSP did not provide a significant reduction in tibia axial force. Upon impact, the CSP immediately collapsed. These results suggest the compressive modulus of the MiL-Lx surrogate, namely the tibia compliant element, was greater than the CSP.

Similarly, the Aluminum foam material did not provide a significant reduction in tibia axial force. The Aluminum foam did not deform or crush in any of the impact tests. These results suggest the compressive modulus of the MiL-Lx surrogate was less than the Aluminum foam. Materials that are stiffer than the lower extremity of the occupant are more likely to transfer the bulk of the energy to the occupant.

The ACG 1,689 kPa was unable to provide any force attenuation at WSU C1. The material did not deform and virtually all of the impactor force was transferred to the surrogate. This suggests the compressive modulus of the surrogate was less than that of the material. However, as loading severity increased the material did provide some minimal level of kinetic energy attenuation. The deformation/crush of the material increased as impact severity increased. This suggests the compressive modulus of the surrogate is loading rate dependent (as the ACG is designed to deform consistently).

The ACG 414 and 827 kPa material provided a significant reduction in peak tibia axial force to the MiL-Lx surrogate at each impact severity. The ACG 414 was found to provide the greatest reduction in forces. Unlike the footwear, the axial force attenuation provided by ACG 414 and 827 kPa improved with impact severity. This is likely due to the consistent deformation of this material versus the dynamic response of an elastomer, which changes with the degree of compression

Figures 81 to 83 compare the baseline MiL-Lx response with the ACG 414 kPa and ICB at WSU C1, C2 and C3 impact severities.

The evaluation of kinetic energy absorbing materials demonstrated the benefits of selecting appropriate materials of construction to achieve an optimum level of protection. Conventional armor and other stiff materials provided virtually no capability to attenuate axial force. Similarly, materials that possess a high bare compressive strength but minimal crush strength are unable to attenuate a sufficient proportion of energy to significantly reduce axial force. The material properties that offer the most protective capability possessed optimal crush strength.

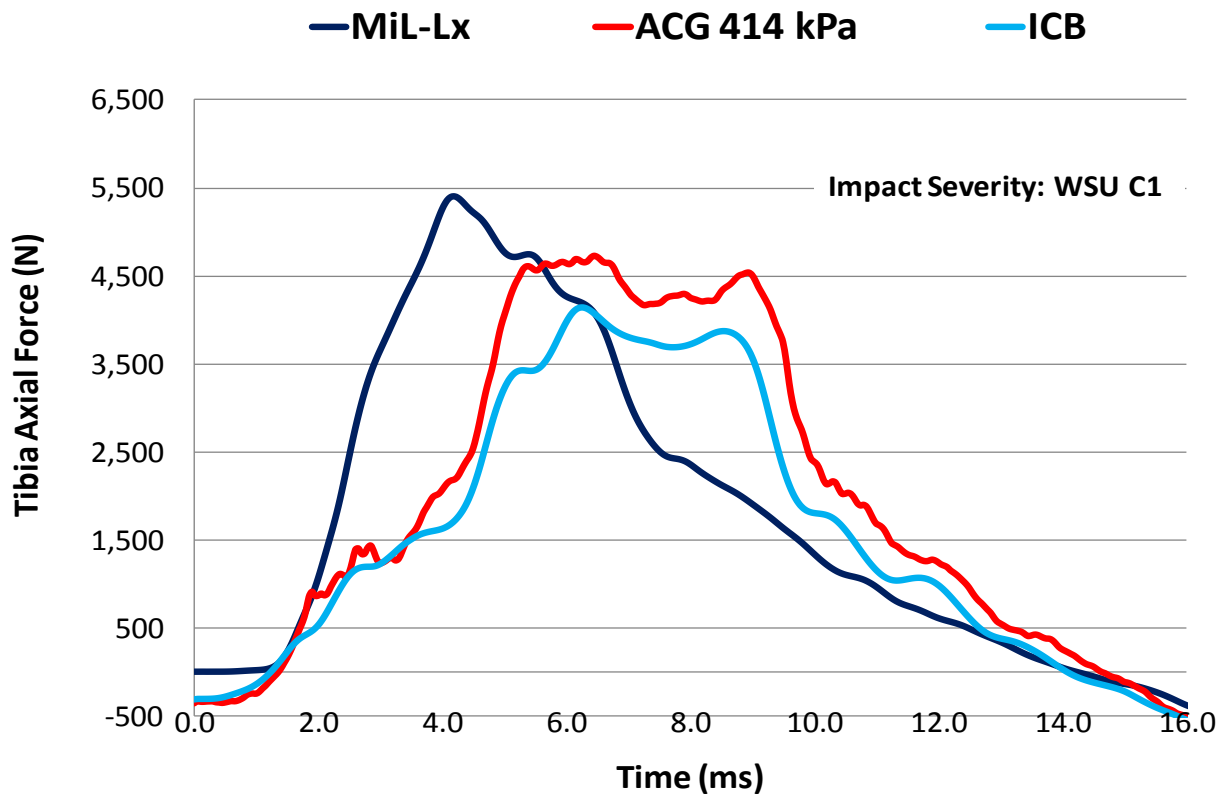

Figure 81: Attenuation Performance at WSU C1.

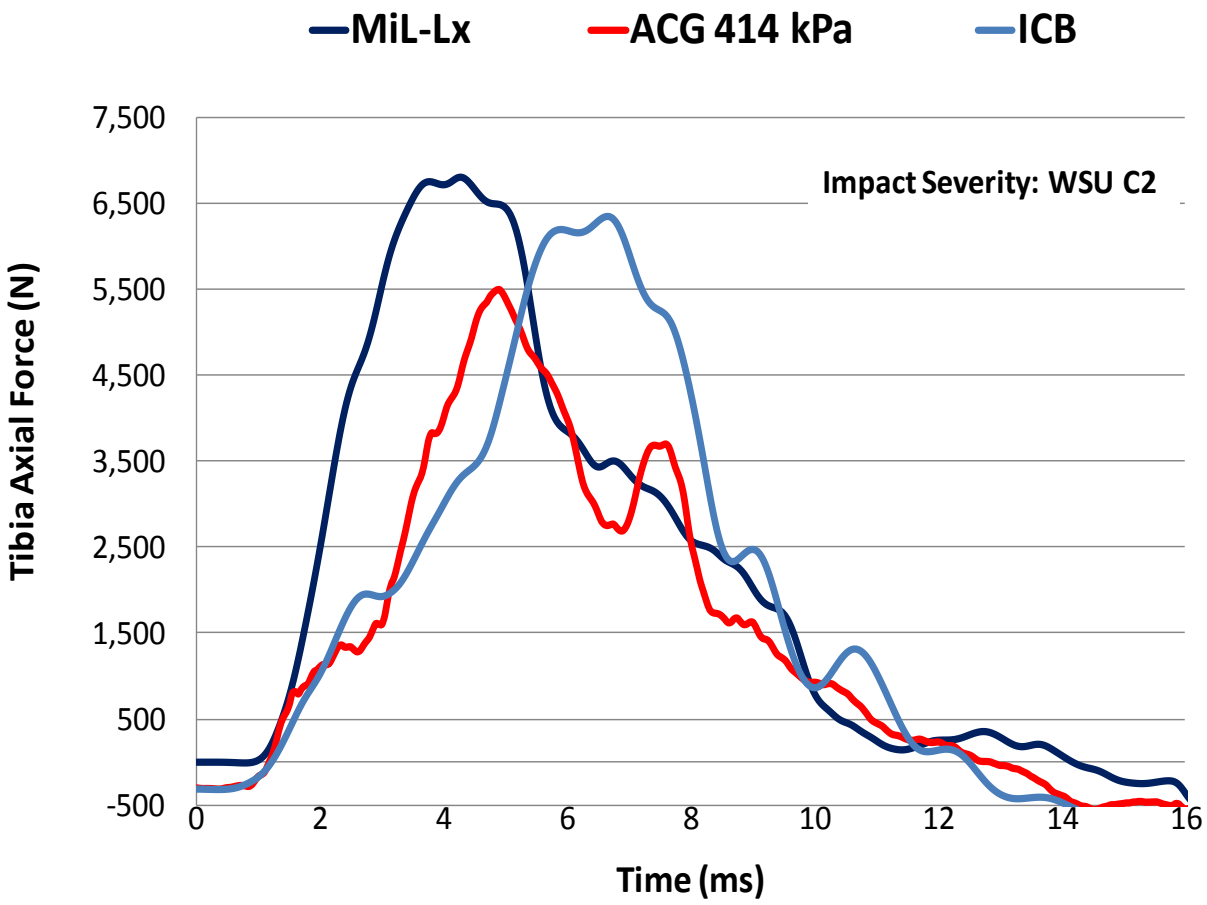

Figure 82: Attenuation Performance at WSU C2.

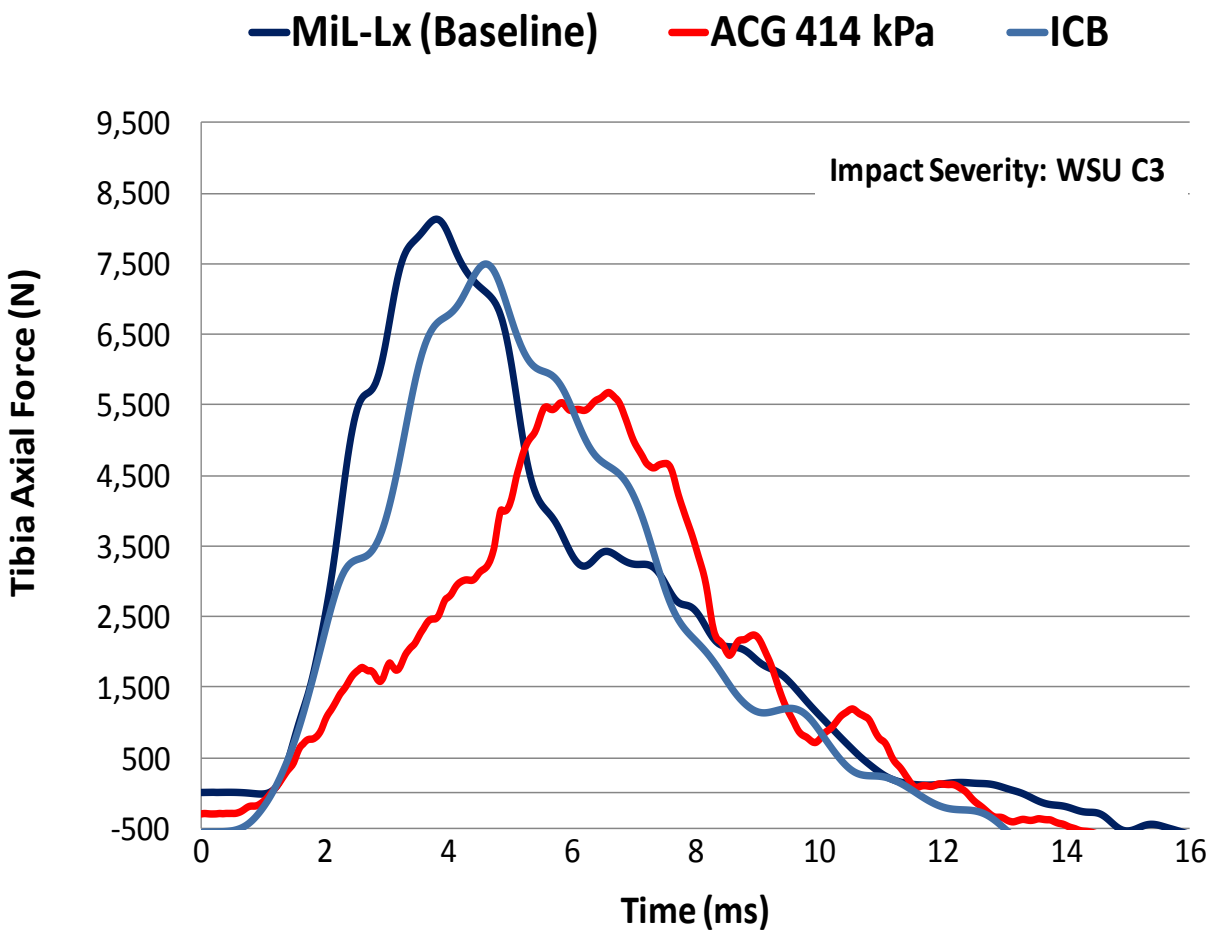

Figure 83: Attenuation Performance at WSU C3.

CHAPTER 7

CONCLUSIONS AND RECOMMENDATIONS

The lower extremity is the principal injury of the U.S. Military. AV explosive devices pose a ubiquitous threat to mounted soldiers and have the potential to inflict damage to an occupant's lower extremity. In addition to accruing significant long term rehabilitation costs, lower extremity injuries may be immediately incapacitating to a soldier.

This study investigated the injury tolerance of the lower extremity to an underbelly AV blast impact. Eighteen lower extremity PMHS were instrumented with an implantable load cell and strain gages and impacted at one of three axial impact conditions. Twelve of 18 PMHS in this study sustained hard tissue injury. The initiation of skeletal injury was precisely detected by strain gages and showed to occur at the local peak tibia axial force.

A right-censored/uncensored survival analysis identified peak tibia axial force as the best predictor of an incapacitating injury. The proposed risk function compares favorably with published literature when adjusted for age. When applying the risk function to the military it is recommended that the upper bound 95 percentile confidence interval curve be utilized to describe the probability of injury as it best represents the age and health of a soldier. When tibia axial force is not measured, a velocity injury risk function may be utilized as a barometer to evaluate probability of incapacitating injury when vehicle floorplate kinematics is known.

The tibia axial force and velocity risk functions may be utilized to evaluate the probability of incapacitating injury to military vehicle occupants in underbelly AV blast

impacts. It is recommended defense agencies and STANAG 4569 adopt the proposed tibia axial force injury risk function where a ten percent probability of AFIS 4+ injury is 2,650 N. If tibia axial force is not available, a velocity risk function may be utilized where a ten percent probability of AFIS 4+ injury is 8.2 m/s.

Military vehicle protection systems are evaluated in full-scale blast tests using an anthropomorphic test device (ATD) to simulate the biomechanical response of occupants. The effectiveness of a protection system is determined by comparing the biomechanical response measured by the ATD to established human injury tolerances. However, currently available lower extremity surrogates fail to accurately simulate the biomechanical response of a human lower extremity to axial blast loading (Bir et al., 2006). A more biofidelic surrogate is needed to enable more accurate injury assessment for evaluating blast mitigation systems, materials, and structures.

An effort was made to modify the existing THOR-Lx surrogate to improve biofidelity. After core components of the MiL-Lx were selected from the THOR-Lx, it was necessary to modify the compliant element properties to achieve a desired biomechanical response to a specific impact severity. The tibia compliant element, located distal to the upper tibia load cell, was found to have the greatest affect on the forces measured by the upper tibia load cell. The tibia compliant element attenuated axial forces prior to reaching the upper tibia load cell. The mechanical properties of the tibia compliant element elastomer, specifically its dynamic compressibility, were tuned to achieve a desired tibia axial force response, loading rate, loading pattern, and duration. Over 100 impact tests were conducted to identify an elastomer with suitable dynamic compression properties. Once identified, the MiL-Lx was able to simulate the

PMHS response to non-injurious simulated AV blast impact conditions with high repeatability.

The Mil-Lx was utilized to evaluate the protective capability of military footwear and kinetic energy absorbing materials. The MiL-Lx demonstrated sufficient sensitivity to distinguish the protective capability based on peak tibia axial force measurements. The impact data revealed the importance of selecting appropriate materials of construction for the threat and application. It is recommended that defense agencies and STANAG 4569 adopt the MiL-Lx surrogate and replace the Hybrid III lower extremity for full-scale vehicle impact tests

Footwear with soft plantar cushioning was found to attenuate peak tibia axial forces by a greater magnitude than footwear with stiffer materials of construction. Similarly, kinetic energy absorbing materials that possess a high bare compressive strength but minimal crush strength are unable to attenuate a sufficient proportion of energy to significantly reduce axial force. The material properties that offer the most protective capability possessed optimal crush strength. The opportunity exists to research and develop material technologies that reduce the risk of lower extremity injury in underbelly blast events. It is recommended the methodology utilized in this study be used to evaluate footwear and kinetic energy attenuating material.

The capabilities provided by the developed Mil-Lx will result in the development of new test standards for evaluating the occupant protection against AV blast threats. In addition, the MiL-Lx will enable the evaluation and development of blast mitigation technologies including PPE, floor board materials, and vehicle structure.

APPENDIX A – HIC APPROVAL

WAYNE STATE UNIVERSITY

HUMAN INVESTIGATION COMMITTEE
4201 St Antoine Boulevard - UHC-6G,
Detroit Michigan 48201
Phone: (313) 577-1628
FAX: (313) 993-7122
www.hic.wayne.edu

Concurrence of Exemption

TO: Cynthia Bir
Biomedical Engineering
818 W. Hancock

FROM: Francis G. LeVeque, D.D.S. Francis G. LeVeque
Chairman, Human Investigation Committee

DATE: April 6, 2005

RE: **HIC#:** 044805MP2X
Study Title: Validation of Lower Limb Surrogates as Assessment Tools for Floor Impacts in Army Vehicles Experiencing Anti-Vehicular Blast Land Mine Explosions
Sponsor: U.S. Army TACOM

The above named protocol has been reviewed and found to qualify for **Exemption** according to paragraph **#4** of 45 CFR 46.101(b) of the Code of Federal Regulations of the Department of Health and Human Services.

As this proposal has not been evaluated for scientific merit, except to weigh the risk to the human subjects in relation to the potential benefits, this approval does not replace, or serve in place of, any departmental or other approvals that may be required.

EXEMPT PROPOSALS DO NOT REQUIRE ANNUAL REVIEW BY THE IRB.

PLEASE SUBMIT AN AMENDMENT FORM IF THERE ARE ANY CHANGES TO THE PROTOCOL WHILE THE STUDY IS BEING CONDUCTED.

ONCE THE PROTOCOL HAS BEEN COMPLETED, PLEASE SUBMIT A CLOSURE FORM TO THE HIC.

APPENDIX B – PMHS DATA

Table B1: Anthropometry Measurement of Impacted PMHS.

Cadaver ID	Left/ Right	Sex	Age	Full Specimen Mass (kg)	Instrumented Lower Limb Mass (kg)	Femur Circum. (cm)	Tibia Circum. (cm)	Length of Tibia (cm)
UM 32065	Left	M	67	76.0	7.5	9.2	11.0	42
UM 32065	Right	M	67	76.0	7.2	9.5	11.5	42
UM 32067	Right	M	56	61.2	8.7	11.5	10.5	41
UM 32068	Left	F	68	61.2	7.6	10.25	8.0	36
UM 32068	Right	F	68	61.2	8.3	10.1	7.8	36
WSU 623	Left	M	45	78.7	7.7	10.5	12.0	45
WSU 861	Right	M	72	---	15.9	13.5	12.0	46
WSU 863	Left	M	80	62.1	15.3	13.5	11.0	37
UM 32324	Left	M	44	56.7	7.0	9	8.5	46
WSU 709	Right	M	75	95.3	8.3	9.5	9.3	40
UM 32396	Left	F	80	63.5	13.8	8	7.5	39
UM 32396	Right	F	80	63.5	14.2	8	7.5	39
WSU 667	Left	F	74	45.4	12.5	10.5	10.0	36
WSU 667	Right	F	74	45.4	13.2	10.5	10.0	36
UM 32324	Right	M	44	56.7	6.9	8.75	8.5	46
WSU 709	Left	M	75	95.3	9.0	9.5	9.3	40
WSU 861	Left	M	72	---	15.9	13.5	12.0	46
WSU 863	Right	M	80	62.1	15.3	13.5	11.0	37

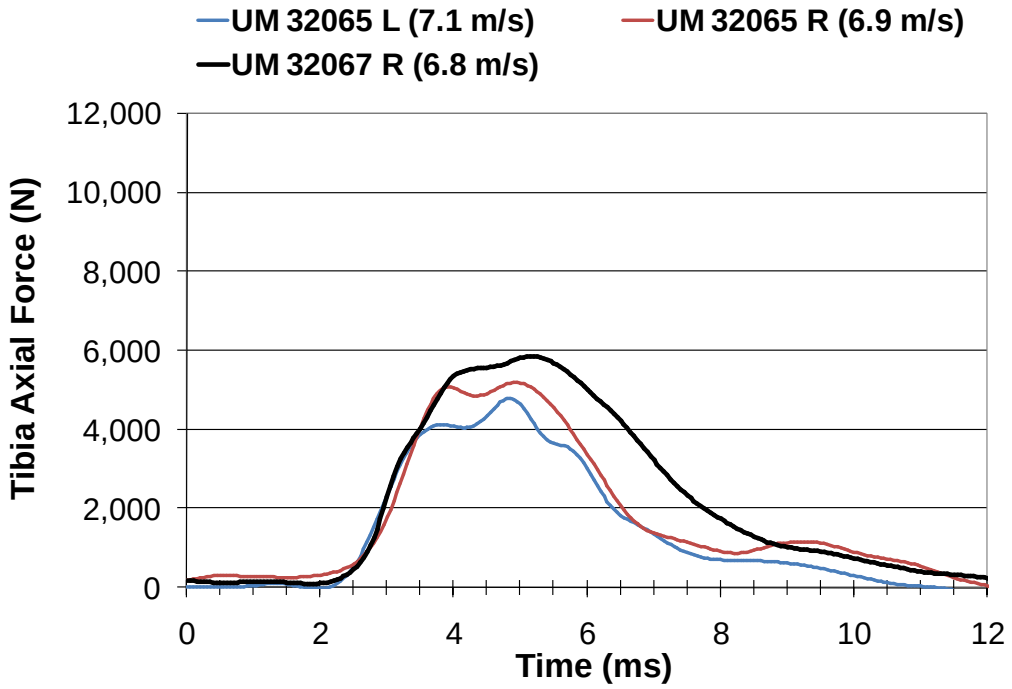

Figure B1: WSU C1 Force versus Time Trajectories (1 of 2).

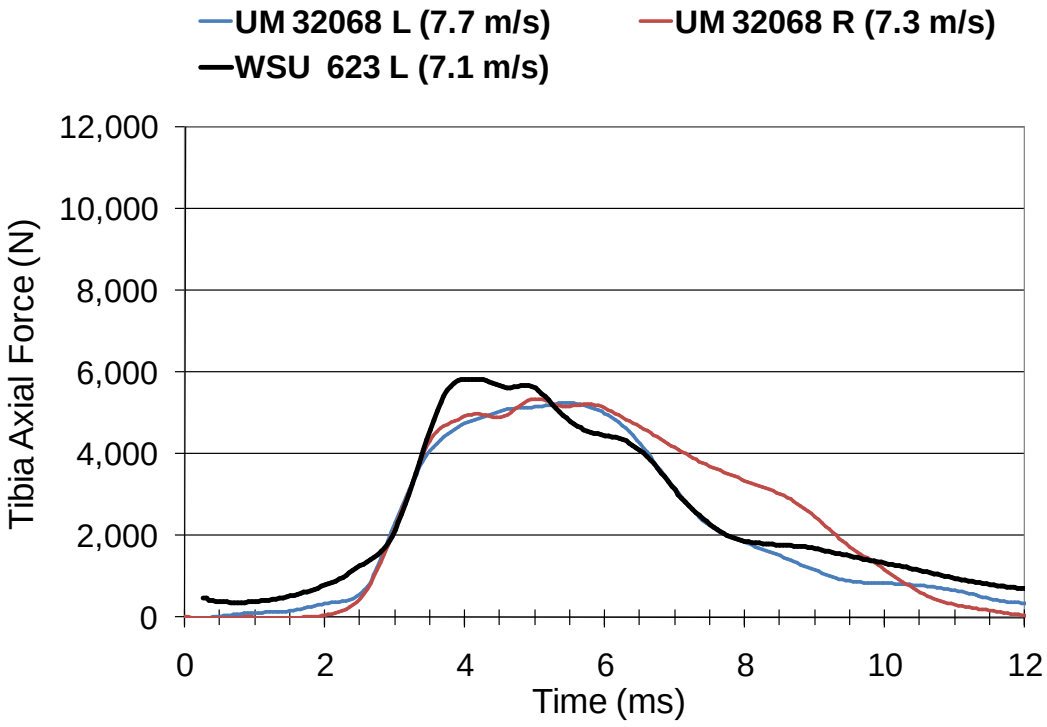

Figure B2: WSU C1 Force versus Time Trajectories (2 of 2).

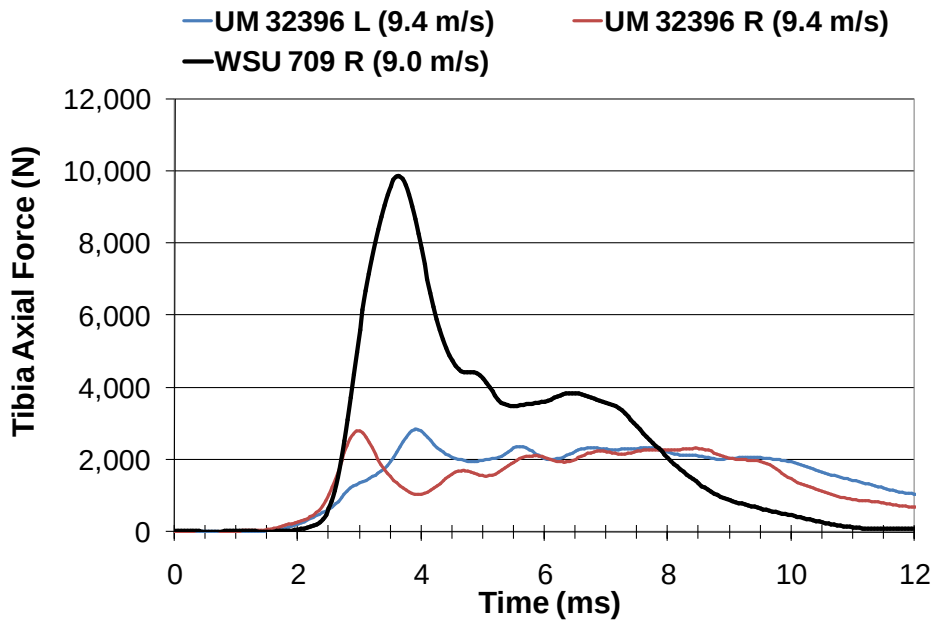

Figure B3: WSU C2 Force versus Time Trajectories (1 of 2).

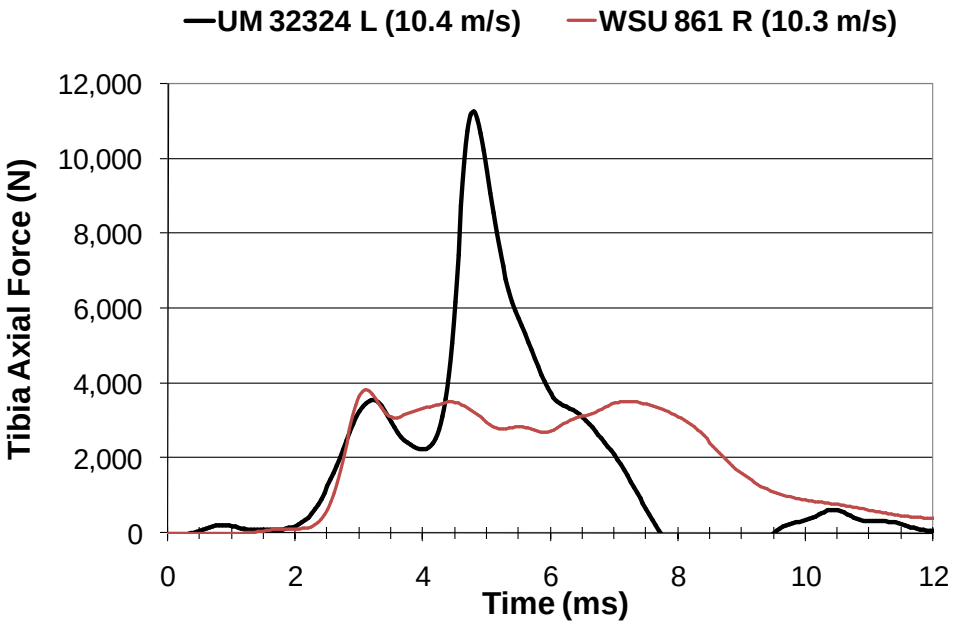

Figure B4: WSU C2 Force versus Time Trajectories (2 of 2).

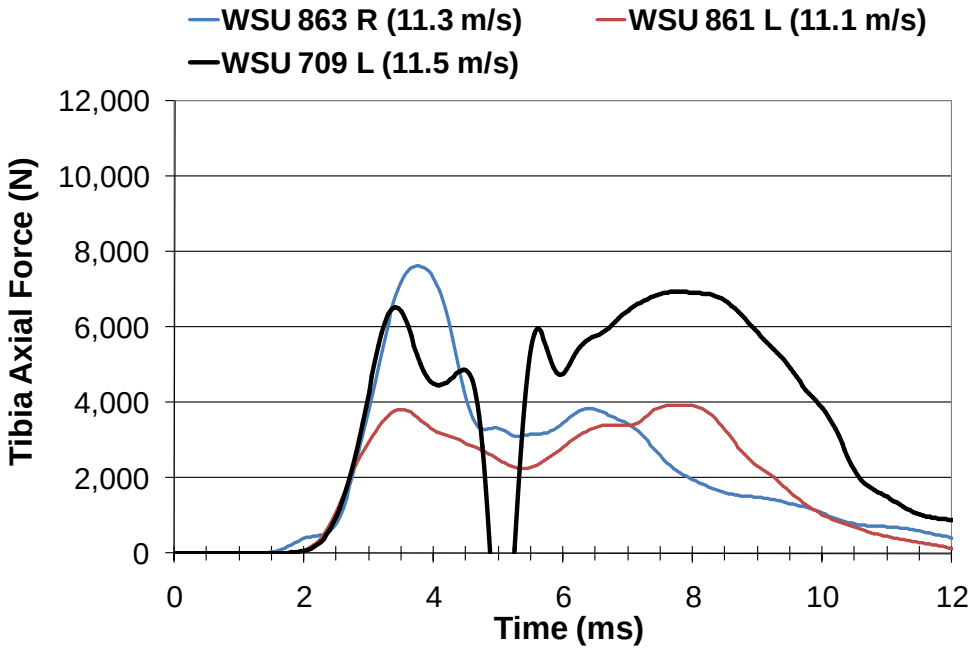

Figure B5: WSU C3 Force versus Time Trajectories (1 of 2).

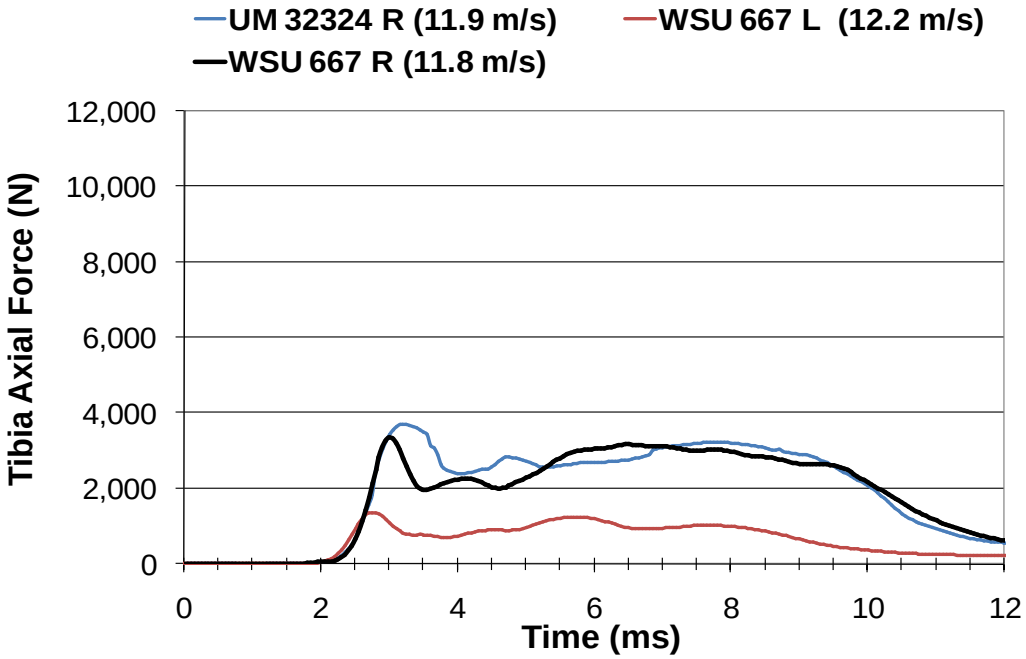

Figure B6: WSU C3 Force versus Time Trajectories (2 of 2).

APPENDIX C – MIL-LX DATA

Table C1: Summary of OOP-A Impact Test Results.

	Peak Tibia Axial Force (N)					
Loading Severity	**Impact 1**	**Impact 2**	**Impact 3**	**Impact 4**	**Average**	**Std Dev**
WSU C1	3,979	3,709	4,138	4,190	4,004	216
WSU C2	5,039	4,672	5,221	4,955	4,972	228
WSU C3	6,025	6,241	5,452	5,573	5,823	372

Table C2: Summary of OOP-B Impact Test Results.

	Peak Tibia Axial Force (N)					
Loading Severity	**Impact 1**	**Impact 2**	**Impact 3**	**Impact 4**	**Average**	**Std Dev**
WSU C1	4,002	4,124	4,466	4,220	4,203	197
WSU C2	5,195	5,317	5,382	5,408	5,326	95
WSU C3	6,311	6,434	5,771	5,615	6,033	401

REFERENCES

25th Infantry Division. (2004). OIF deployment photos. Retrieved Jan. 25, 2008, from http://www.25idl.army.mil/deployment/OIF%20Iraq/Deployment/29Nov04pictures.htm.

Association for the Advancement of Automotive Medicine. (1990). The abbreviated injury scale: 1990 revision. Des Plaine, IL: Association for the Advancement of Automotive Medicine.

Barbir, A. (2005). Validation of lower limb surrogates as injury assessment tools in floor impacts due to anti-vehicular landmine Explosions, Master Thesis, Wayne State University, Detroit, USA.

Begeman, P., Prasad, P. (1990). Human ankle impact response in dorsiflexion. Society of Automotive Engineers, Paper 902308.

Begeman, P. and Aekbote, K. (1996). Axial load strength and some ligament properties of the ankle joint; Injury Prevention though Biomechanics Symposium.

Bergeron, D.M., Coley, C.G., Rountree, M.S., Anderson, I.B. and Harris, R.M. (2001). Assessment of foot protection against anti-personnel landmine blast using a frangible surrogate leg, Proceedings of the 2001 UXO Conference, New Orleans, USA.

Bir, C., Barbir, A., Wilhelm, et al. (2006). Validation of lower limb surrogates as injury assessment tools in floor impacts due to anti-vehicular landmine explosions. In Proceedings of International conference of biomechanics of impact (IRCOBI), September, Madrid, Spain.

Bird, R. (2001). Protection of vehicles against landmines. Journal of Battlefield Technology 4(1), 14-17.

Cavanaugh, J.M., R.S., Nahum, A.M., Melvin, J.W. (2003). Accidental injury: biomechanics and prevention [Biomechanics of Thoracic Trauma]. New York, NY: Springer-Verlag.

Champion, H. R., Bellamy, R. F., Roberts, C. P., et. Al. (2003). A profile of combat injury. Journal of Trauma, 54(5), S13-S19.

Dean, E.I., Boyse, H. (2003). Implantation design guidelines for instrumenting the cadaveric lower extremity to transducer femur loads and tibial forces and moments. Society of Automotive Engineers, Paper 2003-01-0162.

Department of Army. (1997). Light Tactical Vehicle System Specification. Retrieved November 12, 2007, from http://www.fas.org/man/dod-101/sys/land/docs/LTVSPEC3.PDF

Department of Army. (2000). Occupant crash handbook for tactical ground vehicles (light, medium, and heavy duty).

Department of Defense Personnel & Procurement Statistics. (2008). Global War on Terrorism by Reason. Retrieved March 14, 2008, from http://siadapp.dmdc.osd.mil/personnel/CASUALTY/castop.htm.

Dischinger, P. C., Read, K. M., Kufera, J. A., et al. (1994). Consequences and costs of lower extremity injuries. Association for the Advancement of Automotive Medicine, 48, 339-353.

Dosquet, F., Nies, O., Lammers, C. (2004), Test methodology for protection of vehicles occupants against IED. Proceedings of 18th Symposium of Military Aspects of Shock and Blast, Bad Reichenhall, Germany.

Feickert, A. (2006). U.S. Army and Marine Corps equipment requirements: background and issues for Congress. 2-40.

Funk, J.R., Tourret, L., George, S., et al. (2000). Role of axial loading in malleolar fractures. Society of Automotive Engineers, Paper 2000-01-0155.

Funk, J.R., Crandall, J.R., Tourret, L.J., et al. (2002). The axial injury tolerance of the human foot/ankle complex and the effect of achilles tension, Journal of Biomechanical Engineering, 24, 750-757.

Galaneau, M.R., Hancock, W.C., Konoske, P., et al. (2006). The Navy-Marine Corps combat trauma registry. Military Medicine, 171(8), 691-697.

Gray, H. (2000). Anatomy of the human body. Philadelphia: Lea & Febiger. Bartleby.

Gregory, G.T., Peclet, R.J., et al. (1985). The mangled extremity syndrome (MES): a severity grading system for multisystem injury of the lower extremity. Journal of Trauma, 25, 1147-1150.

Gondusky, J.S., Reiter, M.P. (2005). Protecting military convoys in Iraq: an examination of battle injuries sustained by a mechanized battalion during Operation Iraqi Freedom II. Military Medicine, 170(6), 546-550

Horst, M. J. van der, Simms, C.K., Maasdam, R. van, et al. (2005). Occupant Lower Leg Injury Assessment in Landmine Detonations under a Vehicle. IUTAM Symposium on Biomechanics of Impact: From Fundamental Insights to Applications, Dublin.

Huelke, D.F. (1986). Anatomy of the lower extremity – an overview. Society of Automotive Engineers, Paper 861921.

Kitagawa, Y., Ichikawa, H., King, A.I., et al. (1998). A severe ankle and foot injury in frontal crashes and its mechanism. Society of Automotive Engineers, Paper 983145.

Kitagawa, Y., Ichikawa, H., King, A.I., et al. (2000). Finite element simulation of ankle/foot injury in frontal crashes. Society of Automotive Engineers, Paper 2000-01-0456.

Kuppa, S., Klopp, G.S, Crandall, J.R, et al. (1998). Axial impact characteristics of dummy and cadaver lower limbs, 16th International Technical Conference on the Enhanced Safety of Vehicles in Windsor, Ontario.

Kuppa, S.M., Wang, J., Haffner, M., et al. (2001), Lower Extremity Injuries and Associated Injury Criteria. 17th International Technical Conference on the Enhanced Safety of Vehicles in Amsterdam, The Netherlands, National Highway Traffic Safety Administration, Washington, D.C., Paper 457.

Leerdam, P.J.C. (2002). Research experiences on vehicle mine protection, First European Survivability Workshop (ESW), February, 2002, Germany.

Levine, R.S., Nahum, A.M., Melvin, J.W. (2003). Accidental injury: biomechanics and prevention [Injury to the extremities]. New York, NY: Springer-Verlag.

Levine, R.S., Manoli, A., Prasad, P. (1995). Ankle and foot injury scales: AFIS-S & AFIS-I. American Orthopaedic Foot and Ankle Society Trauma Committee.

Melvin, J. W., Stalnaker, R. L., Alem, N. M., et al. (1975). Impact response and tolerance of the lower extremities. Society of Automotive Engineers, Paper 751159.

Mertz, H.J. (1984). Injury assessment values used to evaluate Hybrid III response measurements. NHTSA Docket 74-14, Notice 32, Enclosure 2 of Attachment I of Part III of General Motors Submission USG 2284.

Mertz, H. J., & Backaitis, S. H. (1994). Hybrid III: The first human-like crash test dummy. Warrendale, PA: Society of Automotive Engineers, Inc.

Moore, K. L., & Agur, A. M. (2002). Essential clinical anatomy. Baltimore, MD: Lippincott Williams & Wilkins.

Nechaev, E.A., Gritsanov, A.I., Fomin, N.F., et al. (1995). Mine blast trauma: Experience from the war in Afghanistan. Khlunovskaya GP, translator. Varnamo (Sweden): Russian Ministry of Public Health and Medical Industry; 1995. p. 463.

Netter, F. H. (2006). Atlas of human anatomy. St. Louis: W. B. Saunders.

North Atlantic Treaty Organization AEP-55. (2005). Procedures for evaluating the protection level of logistic and light armoured vehicles. Volume 1, Edition 1: Allied Engineering Publication.

North Atlantic Treaty Organization AEP-55. (2006). Procedures for evaluating the protection level of logistic and light armoured vehicle: for mine threat.. Volume 2, Edition 1: Allied Engineering Publication.

North Atlantic Treaty Organization TR-HFM-090. (2007), Test methodology for protection of vehicle occupants against anti-vehicular landmine effects, Final Report of the Human Factors and Medicine Task Group 090 (HFM-090).

Nyquist, G.W., Cheng, R., El-Bohy, A., et al. (1985). Tibia bending strength and response. Society of Automotive Engineers, Paper 851728.

Olson, C., Rouhana, S., Spahn, B., et al. (2007). Comparison of the THOR and Hybrid III lower extremities in laboratory testing. Society of Automotive Engineers, Paper 2007-01-1168.

Owens B.D., Kragh J.F., Macaitis J., Svoboda S.J., et al. (2007). Characterization of extremity wounds in Operation Iraqi Freedom and Operation Enduring Freedom. Journal of Orthopaedic Trauma, 21, 254-257.

Pilkey, W.D., Sieveka, E.M., Crandall, J.R., et al. (1994). The influence of foot placement and vehicular intrusion on occupant lower limb injury in full-frontal and frontal-offset crashes. Proceedings of the 14th International Technical Conference on Enhanced Safety Vehicles, Munich, Germany. Paper Number 94S4W31.

Petit, P. (1996). Quasistatic characterization of the human foot-ankle joint in a simulated tensed state and updated accidentological data. International conference of biomechanics of impact (IRCOBI), 363-376.

Portier, L. (1997). Dynamic biomechanical dorsiflexion responses and tolerances of the ankle joint complex. Proceedings of the 41st Stapp Car Crash Conference.

Powell, W.R., Ojala, S.J., Advani, S.H., et al. (1975). Cadaver Femur responses to longitudinal impacts. Society of Automotive Engineers, Paper 751160.

Radonić, V., Giunio, L., Biočić, M., et al. (2004). Injuries from Antitank Mines in Southern Croatia. Military Medicine, 169, 320-324.

Roberts, D., Donnelly, B., Severin, C., et al. (1993). Injury mechanisms and tolerance of the human ankle joint. Centers for Disease Control,

Rush, R. M., Kjorstad, R., Starnes, B. W., et al. (2007). Application of the Mangled Extremity Severity Score in a combat setting. Military Medicine, 172(7), 777-782.

Schneck, W. C. (1998). The origins of military mines: Part II. Engineer Bulletin

Schueler, F., Mattern, R., Zeidler, F., et al. (1995). Injuries of the lower legs –foot, ankle joint, tibia; mechanisms, tolerance limits, injury-criteria evaluation of a recent biomechanic experiment-series; International Research Council on the Biomechanics of Injury, 33-45.

Viano, D.C. (1977). Considerations for a femur injury criterion. Society of Automotive Engineers, Paper 770925.

Walter Reed Army Institute of Research. (1989), Medical evaluation of nonfragment injury effects in armored vehicle live fire tests. Instrumentation Requirements and injury criteria. Department of Respiratory Research Division of Medicine. Washington, D.C. AD-A233058.

Wang, J., Bird, B., Swinton, B., and Krstic, A. (2001). Protection of lower limbs against floor impact in army vehicles experiencing landmine explosion, Journal of Battlefield Technology, 4(3), 8-12.

Whyte, T. (2007), Investigation of factors affecting surrogate limb measurements in the testing of landmine protected vehicles. MS thesis, University of Cape Town, South Africa.

Yoganandan, N., Pintar, F., Boynton M. et al (1996). Dynamic Axial Tolerance of the Human Foot-Ankle Complex, Society of Automotive Engineers, Paper 962426.

Zouris, J.M., Walker, J.G., Dye, J., et al. (2006). Wounding patterns for U.S. Marines and Sailors during Operation Iraqi Freedom, major combat phase. Military Medicine, 171(3) 246-252.

Zuby, D.S., Farmer, C.M., Lund, A.K. (1995). Intrusion and lower extremity injury risk in offset frontal test crashes. Society of Automotive Engineers, Paper 950500.

Zuby, D.S., Nolan, J.M., Sherwood, C.P. (2001). Effect of Hybrid III leg geometry on upper tibia bending moments. Society of Automotive Engineers, Paper 2001-01-0169.

ABSTRACT

DEVELOPMENT OF LOWER EXTREMITY INJURY CRITERIA AND BIOMECHANICAL SURROGATE TO EVALUATE MILITARY VEHICLE OCCUPANT INJURY DURING AN EXPLOSIVE BLAST EVENT

by

BRIAN JOSEPH MCKAY

December 2010

Advisor: Dr. Cynthia Bir

Major: Biomedical Engineering

Degree: Doctor of Philosophy

Anti-vehicular (AV) landmines and improvised explosive devices (IED) have accounted for more than half of the United States military hostile casualties and wounded in Operation Iraqi Freedom (OIF). The lower extremity is the predominantly injured body region following an AV mine or IED blast accounting for 26 percent of all combat injuries in OIF (Owens et al., 2007). Detonations occurring under the vehicle transmit high amplitude and short duration axial loads onto the foot-ankle-tibia region of the occupant causing injuries to the lower leg. The current effort was initiated to develop lower extremity injury criteria and biofidelic biomechanical surrogate to evaluate military occupant injury during an AV (axial) blast event.

Eighteen lower extremity post mortem human specimens (PMHS) were instrumented with an implantable load cell and strain gages and impacted at one of three incrementally severe AV axial impact conditions. Twelve of the 18 PMHS specimens sustained fractures of the calcaneus, talus, fibula and/or tibia. A tibia axial

force of 2,650 N and impactor velocity of 8.2 m/s corresponds with a ten percent risk of an incapacitating injury.

Currently available lower extremity biomechanical surrogates were shown to lack biofidelity when impacted at simulated AV blast severities. A THOR-Lx underwent a series of modifications intended to reduce the overall stiffness of the surrogate. Its tibia compliant element was doubled in length to enable additional clearance for compression. The modified surrogate, MiL-Lx (military lower extremity), was loaded axially at three simulated AV axial loading rates using a piston driven linear impactor. The diameter and compressive modulus of the tibia compliant element was varied until the axial force measured by the surrogate was equivalent to the PMHS non-injury response in magnitude and duration. The MiL-Lx surrogate was capable of distinguishing between incrementally severe loading rates using tibia axial force. The MiL-Lx improves the accuracy and sensitivity needed to evaluate blast mitigation technologies designed to reduce injury to occupants of vehicles encountering AV landmines. The use of the MiL-Lx shall result in the development of new standards for the testing of blast mitigation technologies including underbelly protection, floor board materials, and vehicle structure.

AUTOBIOGRAPHICAL STATEMENT

BRIAN JOSEPH MCKAY

EDUCATION:

2010	PhD	Biomedical Engineering	Wayne State University
2005	MS	Biomedical Engineering	Wayne State University
2003	BS	Chemical Engineering	Wayne State University

PROFESSIONAL EXPERIENCE:

2010 to Date	Marathon Oil Company	Operations Supervisor
2008 to 2010	Marathon Oil Company	Technical Services Engineer
2006 to 2008	U.S. Army TARDEC	Research Engineer, Blast Mitigation
2003 to 2006	U.S. Army TARDEC	Project Engineer, Force Projection

NOTABLE PUBLICATIONS:

McKay, B.J., Foster, C., Depinet, P., Bir, C.A. (2010) "A Biofidelic Lower Extremity Surrogate for Evaluating Military Vehicle Occupant Injury in Underbelly Blast Impacts," Proceedings of the Personal Armour Systems Symposium (PASS), Quebec City, Canada, September 13-17.

McKay, B.J. and Bir, C.A. (2009) "Lower Extremity Injury Criteria for Evaluating Military Vehicle Occupant Injury in Underbelly Blast Events," Stapp Car Crash Journal. Nov; 53: 229-49.

McKay, B.J. and Bir, C.A. (2008) "Development of a Lower Extremity Injury Criterion for Military Vehicle Occupants Involved in Explosive Blast Events," Proceedings of the Personal Armour Systems Symposium (PASS), Brussels, Belguim, October 7-10.

McKay, B.J. and Bir, C.A. "The Development of an Injury Corridor to Assess Lower Extremity Injuries Resulting from Anti-Vehicular (AV) Landmine/Improvised Explosive Device (IED) Blasts in Military Vehicles", Paper No. 2007-176666. Proceedings of the ASME Summer Bioengineering Conference, Keystone, Colorado, June 20-24.

NOTABLE ACHIEVEMENTS:

2009 – Awarded the Engineering Society of Detroit (ESD) Alpha Award for Innovation in Engineering and Technology for the development of the MiL-Lx Biomechanical Surrogate.

2008 – Awarded an honorary coin from General Richard A. Cody, Vice Chief of Staff, U.S. Army, in appreciation of research efforts promoting military crew protection.

2000 – Recipient of the Wayne State University Presidential Scholarship Award.